THERMODYNAMIC ARTIFACTS IN LIQUID ALLOYS

A THESIS SUBMITTED TO THE

CENTRAL DEPARTMENT OF PHYSICS

INSTITUTE OF SCIENCE AND TECHNOLOGY

TRIBHUVAN UNIVERSITY

NEPAL

FOR THE AWARD OF

DOCTOR OF PHILOSOPHY

IN PHYSICS

By

RAMESH KUMAR GOHIVAR

FEBRUARY 2023

THERMODYNAMIC ARTIFACTS IN LIQUID ALLOYS

A THESIS SUBMITTED TO THE

CENTRAL DEPARTMENT OF PHYSICS

INSTITUTE OF SCIENCE AND TECHNOLOGY

TRIBHUVAN UNIVERSITY

NEPAL

FOR THE AWARD OF

DOCTOR OF PHILOSOPHY

IN PHYSICS

BY

RAMESH KUMAR GOHIVAR

FEBRUARY 2023

DECLARATION

Thesis entitled **"Thermodynamic Artifacts in Liquid Alloys"** which is being submitted to the Central Department of Physics, Institute of Science and Technology (IOST), Tribhuvan University, Nepal for the award of the degree of Doctor of Philosophy (Ph.D.), is a research work carried out by me under the supervision of Prof. Dr. Devendra Adhikari of Department of Physics, Mahendra Morang Adarsh Multiple Campus, Tribhuvan University, Biratnagar, Nepal and co-supervised by Dr. Ram Prasad Koirala of Department of Physics, Mahendra Morang Adarsh Multiple Campus, Tribhuvan University, Biratnagar, Nepal.

This research is original and has not been submitted earlier in part or full in this or any other form to any university or institute, here or elsewhere, for the award of any degree.

.....

Ramesh Kumar Gohivar

RECOMMENDATION

This is to recommend that **Ramesh Kumar Gohivar** has carried out research entitled **"Thermodynamic Artifacts in Liquid Alloys"** for the award of Doctor of Philosophy (Ph.D.) in **Physics** under our supervision. To our knowledge, this work has not been submitted for any other degree.

He has fulfilled all the requirements laid down by the Institute of Science and Technology (IOST), Tribhuvan University, Kirtipur for the submission of the thesis for the award of Ph.D. degree.

. . . . . .

Dr. Devendra Adhikari
Supervisor
(Professor)
Department of Physics
Mahendra Morang Adarsh Multiple Campus
Tribhuvan University
Biratnagar, Nepal

. . . . . .

Dr. Ram Prasad Koirala
Co-Supervisor
(Associate Professor)
Department of Physics
Mahendra Morang Adarsh Multiple Campus
Tribhuvan University
Biratnagar, Nepal

February 2023

LETTER OF APPROVAL

[Date: 05/02/2023]

On the recommendation of Prof. Dr. Devendra Adhikai and Dr. Ram Prasad Koirala, this Ph.D. thesis submitted by **Ramesh Kumar Gohivar**, entitled **"Thermodynamic Artifacts in Liquid Alloys"** is forwarded by Central Department Research Committee (CDRC) to the Dean, IOST, T.U.

.....

Dr. Om Prakash Niraula
(Professor)
Head
Central Department of Physics,
Tribhuvan University
Kirtipur, Kathmandu
Nepal

ACKNOWLEDGMENTS

I offer my sincere reverence and indebtedness to my respected supervisor Professor Dr. Devendra Adhikari for his guidance, support, fruitful suggestions, critical remarks and affectionate encouragement. I am truly thankful and obliged to him for introducing me to the research community.

I express my sincere gratitude to my co-supervisor Dr. Ram Prasad Koirala for his continuous inspiration and valuable suggestions on my research.

I am thankful to Dr. Shashit Kumar Yadav of the Department of Physics, Mahendra Morang Adarsh Multiple Campus, Biratnagar, Tribhuvan University, Nepal for his continuous advice, cooperation and help during my Ph.D. research work.

I express my humble token of regards to Prof. Dr. Om Prakash Niraula, Head of the Central Department of Physics, Tribhuvan University, Kirtipur, Nepal for his guidelines and help to complete this work.

My sincere reverence goes to Prof. Dr. Binil Aryal, Dean, IOST, T.U. for his constant motivation during the work.

I am thankful to Prof. Dr. Narayan Prasad Adhikari, Prof. Dr. Raju Khanal, Prof. Dr. Ishwar Koirala, Prof. Dr. Hari Prasad Lamichhane and Dr. Balram Ghimire of the Central Department of Physics, Tribhuvan University, Kirtipur, Nepal for their support, continuous encouragements and inspirations during the work. I also appreciate all the faculty members and non-teaching staffs of the department for their support.

I record my immense gratitude to Prof. Dr. Ashok Kumar, Head of the Department of Physics, Mahendra Morang Adarsh Multiple Campus, Biratnagar, Tribhuvan University, Nepal for his valuable suggestions and constant encouragement.

I am also thankful to my colleagues and fellow workers Upendra Mehta and Arjun Dhungana for their cooperation and help.

For continuous encouragement and good wishes, I would like to thank Dr. Indu Shekhar Jha, Mr. Jamil Akhter and all the teaching and non-teaching staff of the Department of Physics, Mahendra Morang Adarsh Multiple Campus, Biratnagar, Tribhuvan University, Nepal.

I am thankful to Tribhuvan University, Nepal for granting me the study leave to pursue Ph.D. research.

I am thankful to Research Management Cell, Mahendra Morang Adarsh Multiple Campus, T.U. Biratnagar, Nepal for providing me partial financial support to pursue my research work.

I am thankful to Mrs. Sarita Adhikari and Tanka Devi Lamichhane for their encouragement, compassion and good wishes.

This thesis is dedicated to my beloved parents, Harihar Prasad Gohivar and Khusita Devi. They have raised me with unconditional love and instilled a passion of science in me and always support in every way to achieve my success.

For their love, inexplicable patience and continuous support, I thank my beloved wife Mamta and sons Ayush and Raunak. I would also like to thank my elder brother Mithilesh, his wife Rashmilata and nephew Aadesh and nice Ananya for their love, support and good wishes for this work.

. . . . . .

Ramesh Kumar Gohivar

February 2023

ABSTRACT

The experimental and literature values of the excess free energy of mixing of Al–Fe, Al–Mn, Al–Ti, and Li–Mg binary and Al–Li–Zn ternary liquid alloys were modeled in terms of self-consistent interaction energy parameters within the framework of Redlich-Kister (R-K) polynomials. Initially, these parameters were assumed to be linearly dependent on temperature (T-dependent). The linear T-dependent interaction parameters were used to study various thermodynamic properties, such as free energy of mixing, enthalpy of mixing, activity, and concentration fluctuation in long wavelength limit of the aforementioned liquid alloys at various temperatures. At temperatures close to the melting point, it was found that the thermodynamic properties of the liquid alloys agree well with the corresponding experimental values. However, at higher temperatures, thermodynamic properties of the liquid alloys showed unusual phase equilibrium conditions. These conditions were referred to be artifacts or artificial inverted miscibility gaps because they were only observed in theoretical calculations and not in experimental measurements. The linear T-dependent optimised parameters of R-K polynomials were, therefore, considered inadequate at higher temperatures to account for the presence of such artifacts in the thermodynamic properties of liquid alloys. Consequently, it became clear that the interaction energy parameters must be re-optimized in order to produce parameters appropriate throughout a broad range of T-dependence.

The interaction parameters for the respective excess free energy of mixing of the aforementioned liquid alloys were then re-optimized within the R-K polynomial framework, considering the exponential T-dependence of the parameters. Again, the optimized exponential T-dependent interaction parameters were utilized to assess the thermodynamic properties of the liquid alloys. As in the prior case, the thermodynamic properties of the alloys were found to agree well with the corresponding experimental values at temperatures close to the melting point. In addition, the thermodynamic properties of the liquid alloys computed at higher temperatures with T-dependent exponential parameters were free of artifacts. This study, thus, shows clearly that the poor modelling of interaction energy parameters is responsible for the appearance of artifacts in the properties of liquid alloys. It was also found that the exponential T-dependent parameters can be used over a wide temperature range for the evaluation of the thermodynamic properties of liquid alloys without producing artifacts. In addition, the ternary Al–Li–Zn liquid alloy showed the critical mixing behaviour at a Li concentration of 0.3 and a temperature of 973 K at the $x_{Al} : x_{Zn} = 1 : 1$ cross section from the Li corner. This interesting behaviour in the ternary Al–Li–Zn liquid alloy is recommended for further investigation.

LIST OF ACRONYMS AND ABBREVIATIONS

CALPHAD	: Calculation of Phase Diagram
CFM	: Compound Formation Model
LET	: Linear and Exponential Temperature-Dependent
LE	: Lupis and Elliott
R-K	: Redlich-Kister
R-K-M	: Redlich-Kister-Muggianu

LIST OF SYMBOLS

a_k : Activity of Component (k = A, B)
E_{AA} : Bond Energy Between A and A
E_{AB} : Bond Energy Between A and B
E_{BB} : Bond Energy Between B and B
k_B : Boltzmann's Constant
$S_{CC}(0)$: Concentration Fluctuation in Long Wavelength Limit
x_k : Concentration of Component (k = A, B)
h_i : Contribution of Enthalpy of Mixing
τ_i : Contribution of Excess Entropy of Mixing
$S^{id}_{CC}(0)$: Ideal Concentration Fluctuation in Long Wavelength Limit
H_M : Enthalpy of Mixing
G^{xs}_M : Excess Free Energy of Mixing
$(G^{xs}_M)^{A-B}$: Excess Free Energy of Mixing of Sub-binary Liquid A-B Alloy
$(G^{xs}_M)^{B-C}$: Excess Free Energy of Mixing of Sub-binary Liquid B-C Alloy
$(G^{xs}_M)^{C-A}$: Excess Free Energy of Mixing of Sub-binary Liquid C-A Alloy
S^{xs}_M : Excess Entropy of Mixing
G^{ter} : Free Energy Associated with Ternary Interaction Parameters
G_M : Free Energy of Mixing
G^{ϕ}_k : Free Energy of Components (k=A, B, C) in ϕ Phase
G^{ϕ}_M : Free Energy of Mixing of ϕ Phase
L_i : Interaction Parameters
δ_{kj} : Kronecker Delta Function
G^{xs}_k : Partial Excess Free Energy of Mixing of Component (k = A, B)
R : Universal Gas Constant

LIST OF TABLES

LIST OF FIGURES

TABLE OF CONTENTS

Page No.

CHAPTER 1

1. INTRODUCTION

1.1 Prologue

In the present world, more new materials surround us than ever before. There is still a growing demand for new materials. Much attention has been devoted to the research and development of new materials through rapid industrialisation process to meet growing demand. Material properties must be studied in order for them to be useful for specific purposes. Metallic materials, in particular, have wide-range applications in a variety of industries, including the automobile industry, aerospace, power plants, civil construction, and medical instrumentation (Singh & Sommer, 1997).

Pure metals have very few desirable properties. Therefore, in metallurgical science, metals are alloyed together to obtain new materials. Metal alloys are generally more beneficial than pure metals for their various improved properties, such as increased mechanical strength, heat resistance, electrical properties, and other features such as decreased production costs and a wider range of colour not found naturally (Sarmiento-Pérez et al., 2015; Anusionwu, 2006). Alloys have tremendous use in almost entire fields. Brass (an alloy of copper and zinc) is used in musical instruments and decorative items; bronze (an alloy of copper and tin) is used in making statues, bearings, and coins; duralumin (an alloy of aluminum, copper, magnesium, and manganese) is used as a material in aircraft and bicycles; and nichrome (an alloy of nickel and chromium) is used as electrical heating elements. Similarly, steel (an alloy of iron and carbon) is used as a material in construction, tools, and vehicles; stainless steel (an alloy of iron, chromium, and carbon) is used in kitchen fixtures, cutlery, and surgical equipment; solder (an alloy of lead and tin) is used in joining metals, etc. Materials with a good balance of mechanical characteristics, microstructural stability, and corrosion resistance at relatively high temperatures are needed for high temperature applications, such as those found in aircraft and land-based turbine engines as well as boilers (Basuki et al., 2017).

Alloys are formed by combining metals or metal with nonmetals. Commercial alloys, which are used in the solid state, are formed from the cooling of their initial melts. An understanding of the mixing behaviour of liquid alloys may provide useful information on the metallurgical process and on the energetics of the formation of solid alloys. A knowledge of the thermo-physical and electrical properties of the liquid alloys helps to understand the stability of the metallic glasses (Ramachandrarao et al., 1984; Singh,

1987). The study of the mixing properties of liquid alloys is essential for producing new materials required at normal and especially for high temperature applications. In order to understand the mixing behaviour of alloys, it is thus important to study their properties in the liquid state.

Mixing properties of a liquid alloy include mainly the thermodynamic properties, microscopic properties, surface properties and transport properties. The mixing properties of the liquid alloys often show deviations from ideal behaviour and the study of alloys has always been a subject of challenge to researchers. The mixing thermo-physical properties of binary liquid alloys can be studied by both experimental and theoretical methods. Experimental methods (Ishiguro et al., 1982; Harada et al., 1988; Bergman et al., 1994; Feufel et al., 1997; Kanibolotsky et al., 2002; Kehr et al., 2008; Gancarz et al., 2011; Yakymovych et al., 2014; Gasior et al., 2016; Debski & Terlicka, 2016) have several limitations, such as the fact that they provide only a few properties, often limited to temperature changes, and are still not sufficient to fulfil the ever-increasing demand for accurate data in technology and research.

As an alternative to the experimental methods of determining the mixing properties, theoretical methods have been developed to fill the gaps in the data on binary and multi-component alloys required for particular applications. The theoretical methods so far developed over years are broadly classified into two major classes: electronic models of mixing (Faber, 2010; Stroud, 1973) and statistical models of mixing (Butler, 1932; Darken, 1950; Bhatia et al., 1973; Lele & Ramachandrarao, 1981; Bhatia & Singh, 1982; Singh, 1987; Kaptay, 2004). Theoretical studies (Bhatia et al., 1973; Lele & Ramachandrarao, 1981; Bhatia & Singh, 1982; Singh, 1987; Prasad & Singh, 1991; Singh & Sommer, 1997; Anusionwu, 2000; Novakovic et al., 2002; Prasad & Jha, 2005; Adhikari, Jha, & Singh, 2010) based on statistical consideration are beneficial as they can be used to extrapolate data on various properties of mixing at relevant temperatures of interest.

Alloying of metals is a complex phenomenon. In statistical view, this may be understood in terms of the atomic arrangements. Basically, during mixing of metals, inter-atomic arrangements may take place in different ways such as like atoms pairing, unlike atoms pairing and complex formation. The bonding of atoms in the arrangements is due to the inter-atomic forces. The energy associated with bonding or interaction between like atoms is not always the same as that associated with unlike atoms. The magnitude of the inter-atomic force of attraction between the two distinct species in the solution must be greater than that of like species in order to form complexes. There is link between the nature of atomic arrangements in an alloy and its mixing properties, which mainly include thermodynamic, microscopic, surface and transport properties. The major thermodynamic properties of alloys are the excess free energy of mixing (G_M^{xs}),

enthalpy of mixing (H_M) and entropy of mixing (S_M). The microscopic properties are the structural functions namely concentration fluctuation in the long wavelength limit ($S_{CC}(0)$) and short-range parameter (Bhatia & Singh, 1982; Singh, 1987). The surface properties of liquid alloy are the surface tension and surface concentration (Butler, 1932; Prasad & Singh, 1991; Kaptay, 2015) and the transport properties are diffusion and viscosity (Singh & Sommer, 1997; Kaptay, 2005; Iida et al., 2007).

1.2 Thermodynamic properties

The mixing properties of binary metal alloys vary as a function of composition, temperature, and pressure. As the study of the liquid alloys is usually carried out at the fixed pressure, most likely, the atmospheric pressure, the thermo-physical properties of a binary liquid alloy at a given temperature vary with the composition of the alloy and often show an interesting behaviour as a function of composition. In most alloys, interactions or bond energies between like atoms and unlike atoms are different, and the property of mixing cannot be expressed as the concentration average of the properties of the constituent metals, i.e., they exhibit non-ideal mixing behaviour. From the viewpoint of theoretical modelling, the binary molten alloys may be broadly grouped into two categories: symmetric and asymmetric alloys. As the name suggests, the properties of mixing, such as excess free energy of mixing (G_M^{xs}), heat of mixing (or enthalpy of mixing, H_M), concentration fluctuation in long wavelength limit ($S_{CC}(0)$) etc. are symmetrical or very close to it about the equiatomic composition in symmetric alloys. Symmetric alloys such as Al–Ga, Bi–Pb and Na–K having their entropy of mixing (S_M) equal to or very close to the ideal values are said to be regular alloys whereas the alloys such as Au–Cu, Cu–Sn and Fe–Mn are asymmetrical in mixing properties about the equiatomic composition.

In order to have comprehensive information regarding the mixing properties of alloys, primarily knowledge of thermodynamic properties is necessary. In thermodynamics, Helmholtz free energy is a thermodynamic potential that measures useful work at a fixed temperature. The Gibbs free energy of mixing (G_M) is the maximum amount of non-expansion work or useful work at constant temperature and pressure. The function G_M provides information about the formation of the nature of the complex and its stiochiometric composition in the metallic solution. Its positive value means the mixing of components cannot be sustained going forward. The considerably high negative value of G_M means that there is a strong mixing tendency in the alloy, and its small negative value indicates a weak mixing tendency. However, based on G_M, one cannot distinguish whether the alloy is ordering or segregating in nature. Therefore, the excess free energy of mixing (G_M^{xs}) is introduced in the study of alloy systems. Its positive value indicates

that the alloy is segregating in nature, which means that there is preferential among the like atoms. The negative value of G_M^{xs} indicates the ordering nature in which unlike atom pairing takes place.

When two pure metals of types A and B are combined to form an alloy, A-B, the chemical bonds between A-A and B-B are broken and the chemical bond between A-B is formed. In this process, energy is either liberated or absorbed from the system, which takes the form of heat. During the mixing process, the entire quantity of heat evolved or absorbed is equal to the system's change in enthalpy under constant pressure, called the enthalpy of mixing (H_M). It can be measured directly from the experiments by the calorimetric and emf methods. It is related to G_M^{xs} by standard thermodynamic relation $H_M = G_M^{xs} - T\partial G_M^{xs}/\partial T$. Its positive and negative values correspond to repulsive and attractive interatomic forces between the atoms of the complex in the initial melt. In an ideal mixture, interchange energy is assumed to be zero.

Systems of non-interacting constituents can be described by ideal models. In an ideal solution A-B, the bond energy between two unlike constituents (A and B) is equal to the average of the bond energies of like constituents (A-A and B-B). For non-ideal solution, the difference in energy E is calculated by the following relation $E = E_{AB} - 0.5(E_{AA} + E_{BB})$ where E_{AB}, E_{AA} and E_{BB} are bond energy of A-B, A-A and B-B. These energies are identified by electronic, vibrational, magnetic, and configurational contribution (Porter & Easterling, 2009). If $E = 0$, then the solution is ideal. In this case, the atoms are randomly arranged in the solutions. If $E < 0$, then atoms are proffered to surround by unlike atoms and this is case of short- and long-range order or clustering. If $E > 0$, there is a tendency for phase separation, in which atoms prefer to be surrounded by like atoms. This is also a case of the miscibility gap.

Activity is an important thermodynamic function that measures the escaping tendency of the component from the complex in the phase. The activity of an alloy is an experimentally observable thermodynamic function. Even though different methods have been used to measure the activity, researchers consider the electromotive force method to be more accurate (Alcock et al., 1973). Other properties such as the free energy of mixing, concentration fluctuation in long wavelength limit ($S_{CC}(0)$) and surface properties may be determined on the basis of experimental activity data. The free energy of mixing (G_M) of a binary liquid alloy is calculated from the activity of individual component (a_k) using the equation $G_M = RT \sum x_k \ln a_k$, where R is the universal gas constant, T is absolute temperature, k = A, B species, and x_k is the mole fraction of the component. The mixing or demixing nature of the alloy components can be examined by comparing one's activity with the ideal values (Raoult's law). The activity depends on the temperature and composition. The activity at a particular composition of the alloy should shift toward the ideal value as the temperature of the system is raised. At a very high temperature, the

alloy behaves like an ideal for which free energy of mixing $G_M^{id} = RT \sum x_k \ln x_k$.

The entropy of mixing (S_M) is another thermodynamic function that measures the number of ways in which components are arranged in a system. In physics, order and disorder refer to whether or not there is any symmetry or correlation in a system of many particles. Systems are usually organised in condensed matter physics at low temperatures; upon heating, they move through one or more phase transitions into less ordered states. Entropy of alloys is calculated from statistical approximation by the relation $S = k_B \ln W$, where k_B is Boltzmann's constant and W is the ways of distribution of components in a system. In an ideal alloy, no interaction is assumed; there is configurational entropy $S_M = -R(x_A \ln x_A + x_B \ln x_B)$. In this case, an increase of the entropy of mixing it leads not to an increase but to decrease (to larger negative values) of the free energy of mixing. In non-ideal alloys, entropy is associated with both interaction and configuration. The entropy of a system represents the sharing of energy among the atoms in the solution. The entropic effect competes with the enthalpic effect to dictate the degree of segregation in the binary liquid alloys (Singh & Sommer, 1997). Even for the positive values of the interaction energy, phase separation may be prevented by the increase in entropy involved in the alloying of metals (Adhikari, 2011). Moreover, high entropy multi-component alloys are prone to phase separation because they include numerous elements in significant amounts (Manzoor et al., 2018). The entropy of a system, which is affected by factors such as vibrational, electronic, and configurational contributions, plays an important role in determining the phase stability of binary alloys. Due to prominent thermal agitation, the liquid alloy has no electronic or magnetic contribution at elevated temperatures. Systems with negative enthalpies of mixing can nevertheless exhibit phase instability, which manifests as a miscibility gap. In contrast, systems with positive enthalpies of mixing might exhibit phase stability because of entropic contributions.

1.3 Structure factor in the long wavelength limit

Crystalline solids have a periodic arrangements of atoms and a defined number of atomic bondings (Sundman et al., 2007). Unlike crystalline materials, the local arrangement of atoms in the liquid state is not periodic. The non-periodicity in the local atomic arrangement causes the disorder in liquid alloys. Because of the strong correlations between the atoms and the lack of long-range structural periodicity, understanding the properties of liquid binary alloys is much more complex than that of crystals. As a result, the binary alloy can be further classified into two types based on the range of bonding or nature of interaction among the atoms: ordering (hetero-coordinating) and segregating (homo-coordinating) alloys (Singh, 1987; Novakovic, 2010). In alloys, ordering or homogeneous atom mixing is possible when the interaction between unlike atoms is

more attractive than that between like atoms. Similarly, when the interaction between unlike atoms is repulsive, the association of like atoms (A-A) or (B-B) is favourable to form the clusters in the binary A-B alloy. The nature of the atomic arrangement in a binary liquid alloy is theoretically observed by calculating concentration fluctuation in the long wavelength limit ($S_{CC}(0)$), which can be calculated directly from the excess free energy of mixing or activity of alloy species (Bhatia & Thornton, 1970; Singh & Sommer, 1997) from the following expressions.

$$S_{CC}(0) = RT\left(\frac{\partial^2 G_M}{\partial x_k^2}\right)^{-1} = \frac{x_A a_B}{(\partial a_B/\partial x_A)_{T,p}} = \frac{x_B a_A}{(\partial a_A/\partial x_A)_{T,p}} \tag{1.1}$$

$S_{CC}(0)$ gives the idea regarding arrangement of atoms in the nearest neighborhood of initial melt. A positive deviation of $S_{CC}(0)$ from the ideal value ($S_{CC}^{id}(0) = x_A x_B$) indicates segregating behaviour, whereas its negative deviation from the ideal value indicates the ordering nature of an alloy.

If the deviations of mixing behaviour of alloys from Raoult's law are considerably large for which ($S_{CC}(0)$) also shows large departure from ideal values,they may lead either to phase separation or compound formation in the binary system. There are liquid alloys such as Au–Ni and Cr–Mo that neither show phase separation nor compound formation but exhibit immiscibility in the solid phase, which is not evidently visible in the corresponding liquid phase. Also, alloys such as Al–Pb, Cd–Ga, Ga–Pb, Pb–Zn, Cu–Pb, etc. show liquid miscibility gaps. In the region of the miscibility gap, $S_{CC}(0)$ increases sharply with the decrease in temperature in Cd–Ga and Bi–Zn alloys. The properties in the liquid phase tend to change markedly as a function of composition, temperature, and pressure. Liquid alloys with a miscibility gap are important for advanced bearing materials (Singh & Sommer, 1997). Thus, it seems instructive to study the miscibility gap in liquid alloys.

1.4 Miscibility gap in alloy

Miscibility is the property of two substances to dissolve into each other in any composition to form a homogeneous mixture or solution. This term is generally used for liquids, but it is also used for solids and gases. Many metals are dissolved in each other at all compositions and temperatures. Alloys cannot be formed by mixing immiscible metals. In some cases, metals mix in their molten state, but on freezing, they separate from each other. For example, when copper and cobalt are mixed in a molten state, they precipitate during solidification (Mallinson, 2001). An eutectic alloy freezes and melts at a single temperature that is lower than the melting temperatures of its constituents (Guthrie, 1884).

This temperature is known as the eutectic temperature of the alloy. A peritectic alloy decomposes into another solid compound and a liquid. Herein, a reaction between a liquid and a solid phase in a given ratio occurs at a given temperature to produce a single solid phase (Nic et al., 2005). Since the solid product develops at the interface of the two reactants, it has the potential to create a diffusion barrier and slow down the reaction process significantly compared to eutectic transformations.

A phase is a portion of a system with homogeneous properties and composition that is physically distinguishable from other portions of the system. Phase transformations are the processes by which one or more phases in an alloy change into a new phase or mixture of phases. The initial state is unstable relative to final state of alloy is reason of phase transformations. The stability state of alloys can be measured by study of their thermodynamics.

Phase separation in certain liquid alloys appears when their temperature is lowered due to nucleation growth or spinodal decomposition. Alloys undergo stable or metastable liquid phase separations, resulting in their having very distinct microstructures. The compositions of these microstructures depend upon the rate of cooling or route preferred for the solidification process. The slow rate of cooling and the static environment are the main causes of liquid-phase separations (Derimow & Abbaschian, 2018).

The calculated phase diagram of some binary systems shows the non-mixing of constituent elements in a certain range of compositions and temperatures, which is identified as the miscibility gap (Chen et al., 2001). A miscibility gap is a region in a phase diagram where two or more phases co-exist. The most common phenomenon in glass-forming alloys is the liquid-liquid phase transition. Such transition is observed in the alloys having the same composition but different crystal structures, densities, and entropies (Xu et al., 2015; Kobayashi & Tanaka, 2016; Zhao et al., 2017; Bo et al., 2018). Also it has been noticed in ternary $Al_{55}Bi_{36}Cu_9$ alloy during the solidification process from 1190 K to 926 K (Bo et al., 2018).

Alloys cannot be directly distinguished as to whether they are ordered or disordered systems. Therefore, it is analysed from thermodynamic functions (heat of mixing, the excess free energy of mixing, activity), structural function (concentration fluctuation in the long wavelength limit), and thermo-physical functions (viscosity, surface tension, diffusivity, electrical resistivity). Liquid-phase separation is observed in alloys due to the heterogeneous mixing of constituent atoms. It can be analysed by positive heat of mixing, considerable positive deviation of activity from Raoult's law, and larger values of concentration fluctuation in the long wavelength limit over its ideal values. It is actually due to the sign of excess free energy of mixing (G_M^{xs}) which has contributions from the heat of mixing (H_M) and excess entropy of mixing (S_M^{xs}). Generally, a system with

a negative value of heat of mixing shows phase stability, whereas one with a positive value shows an unstable phase. But in the case of high entropy systems, alloys having negative heat of mixing show phase unstability, and conversely, systems with positive heat of mixing show stability due to the contribution of entropy of mixing (Manzoor et al., 2018). However, if negative heat of mixing dominates high entropy of mixing of the system in any phase, the phase is super stable. The unstable liquid phase of Cu-Si at

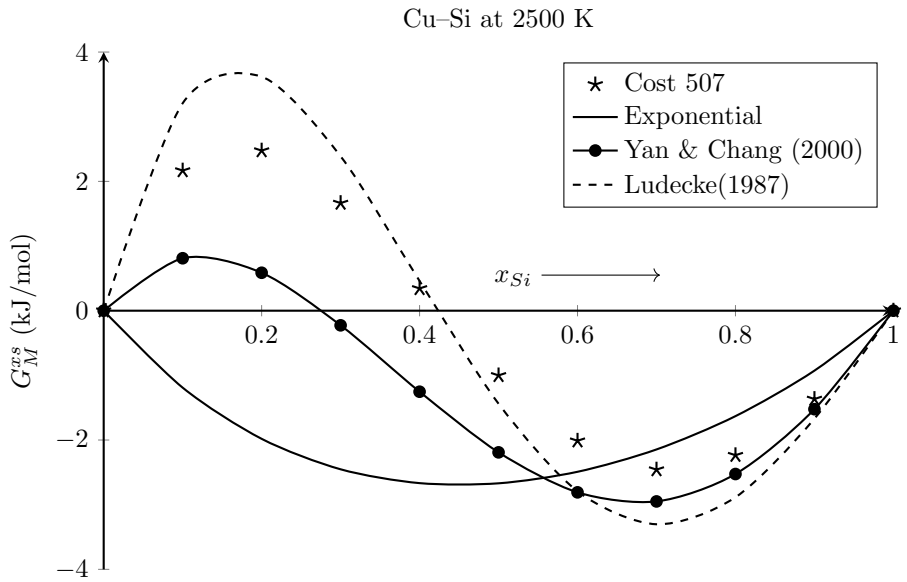

Figure 1: Excess free energy of mixing (G_M^{xs}) of liquid Cu-Si alloy at 2500 K.

temperature 2500 K is observed in the calculated excess free energy of mixing the G_M^{xs} by linear temperature interaction parameters (Yan & Chang, 2000; Lüdecke, 1987) and Cost 507 (Ansara et al., 1998) (Figure 1).

However, this discrepancy has been removed by considering exponential temperature-dependent interaction optimised parameters (R. K. Gohivar, Koirala, et al., 2020). The calculation of the structural properties of the liquid Cu-Si alloy at temperature 2500 K using these linear interaction parameters shows the phase transiton from segregating to ordering whereas the behaviour changes on using the exponential interaction parameters (Figure 2).

1.5 Prediction of properties of alloys at high temperature

The mixing properties of initial melts of different alloys can be determined using different statistical models such as Flory's model (Flory, 1942), R-K polynomial model (Redlich & Kister, 1948), ideal solution model (Hildebrand & Scott, 1950; Prigogine & Defay, 1954; Bhatia & Hargrove, 1974), conformal solution model (Longuet-Higgins, 1951),

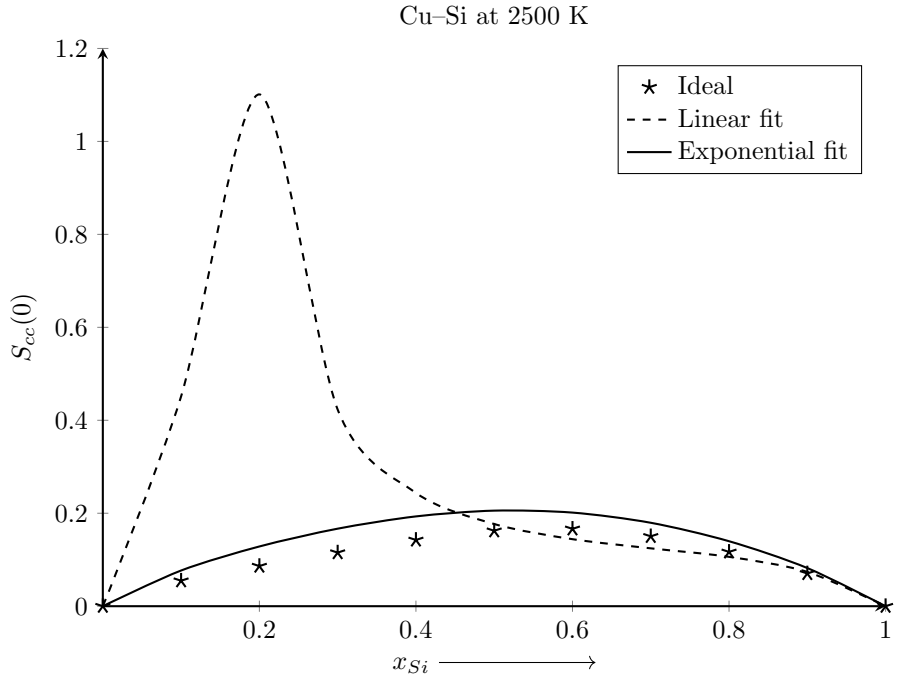

Figure 2: $S_{CC}(0)$ of liquid Cu-Si alloy at 2500 K.

compound formation model (Bhatia & Hargrove, 1974), quasi-chemical model (Bhatia & Singh, 1982), quasi-lattice model (Bhatia & Singh, 1984), regular associated solution model (Lele & Ramachandrarao, 1981; Adhikari, Jha, & Singh, 2010) and quasi-chemical approximation (Singh & Sommer, 1992, 1997). The properties at high temperatures can be predicted theoretically by extrapolating the data from the optimization. Ternary or higher-order alloys are created by melting each constituent element and mixing them in the appropriate proportions. Because each sub-binary alloy has a different melting temperature, the working temperature for multi-component alloys should be higher than that of the individual binary systems. As a result, the temperature-dependent interaction energy parameters of sub-binary systems are required for calculation. When the melting temperatures of sub-binary systems are close to each other, linear temperature-dependent interaction parameters are used to study alloy properties at their melting temperatures. With the linear interaction parameters in some cases at higher temperatures, artificial miscibility gaps may appear in the computed mixing properties. Interaction energy parameters may be assumed to vary exponentially with temperature (Kaptay, 2004) when there is a large difference in melting temperatures of sub-binary alloys or when the mixing properties are computed at higher temperatures using the R-K polynomial framework (L. Zhang et al., 2006; Tang et al., 2011; S. M. Liang et al., 2016; Ghasemi et al., 2019; R. K. Gohivar, Yadav, et al., 2021b). To compute the mixing properties of the alloy systems at different temperatures, the optimised interaction parameters of G_M^{xs} are required. In this work, interaction parameters $L_i = (a_i + b_i T)$

and then $L_i = h_i \exp(-T/\tau_i)$ for G_M^{xs} have been determined using the frame work of R-K polynomial, i.e., $G_M^{xs} = x_k(1 - x_k) \sum_i L_i(1 - 2x_k)^i$ where k= A, B.

However, the properties of an alloy may change at higher temperatures. The quality of an alloy may decrease greatly with rise in temperature and this is referred in literature as degradation of alloy. The amount of vacancies necessary for atom and ion diffusion in alloy increases exponentially with temperature (Basuki et al., 2017). A severe high temperature corrosion mode known as hot corrosion was created as a result of the interaction between high temperature operation and environmental pollutants such sulphur, sodium, halides, and vanadium. The very worst alloy degradation processes are oxidation and hot corrosion because of their close links to environments that are challenging to manage. Protective scales are made of oxides (Al_2O_3, Cr_2O_3, SiO_2) that are thermodynamically stable at high temperatures, have a high melting point, a low vapour pressure, a slow formation rate, a high level of attachment to the surface of the alloy, a low thermal expansion, and good erosion resistance. Aluminum is mostly added to Fe and Ni based alloys to increase alloy strength and provide protective scales (Pettit et al., 1984). Therefore, high temperature alloys are typically designed to minimise this change.

1.6 Thermodynamic artifacts

The excess free energy of mixing of phases of alloy is usually obtained from R-K polynomials in the calculation of phase diagram (CALPHAD). The energy interaction parameters of R-K polynomial are expressed as $L_i = a_i - b_i T$, where both a_i and b_i should have the same signs. The excess free energy changes its sign at a certain temperature and has large value at high temperature. In some cases this can also result in an artificial phase stability at high temperature which is of course an emergence of an artificial miscibility gap in the phase diagram. The appearance of artificial inverted miscibility gap and re-stabilization of liquid phase in solidus region are thermodynamic artifacts. In the calculation of phase diagram, the artifacts were seen as (i) inverted miscibility gap, (ii) re-stabilization of solid phases at high temperature and (iii) inadvertent stability of ordered phases. Many researchers have found such artifacts in the calculated phase diagrams of different systems (Chen et al., 2001; Kevorkov et al., 2004; Kaptay, 2004; Balakumar & Medraj, 2005; Arroyave & Liu, 2006; Schmid-Fetzer et al., 2007; Yuan et al., 2009; Wang, Du, & Liu, 2011; Tang et al., 2011; Abe et al., 2012; S. M. Liang et al., 2016; Ghasemi et al., 2019). Chang et al. (2004) used second generation software (PANDAT) and published binary thermodynamic descriptions. They found unintended phase equilibria in three system namely Sn–Zr, Ni–Ti and Al–Nb. The appearance of such artifacts in study of mixing properties of alloys at higher temperatures are generally

due to the incompetency of modelling parameters in wide temperature range.

In the present work, we have investigated mixing properties of some binary and ternary liquid alloys at different high temperatures on the framework of R-K polynomial using linear temperature dependent interaction parameters. In our calculations for the alloys Al–Fe, Al–Mn, Al–Ti and Li–Mg and Al–Li–Zn, artificial miscibility gaps appear in the alloys. We have next computed the thermodynamic and structural properties of the above mentioned liquid alloys using exponential temperature dependent interaction parameters in the R-K polynomial. The calculations in the latter case show removal of the artificial miscibility gaps for the allows with the prediction of the thermodynamic and structural properties at different high temperatures which may serve as a short database in case unavailability of experimental data.

1.7 Problem statement

As stated in the literature review, numerous efforts have been made over the years by researchers in the field of metallurgical science to understand the mixing properties of binary and ternary liquid alloys. The selection of the micro-ingredients for the formation of alloys in order to get the desired attributes is aided by an understanding of the thermodynamic, structural, and surface properties of liquid alloys. The mixing properties of alloys have been studied in the framework of several models at temperatures near their melting points. Redlick-Kister polynomial was widely used to study the thermodynamics, structural, surface, and transport characteristics of binary and, especially, ternary systems at different temperatures. The appearance of artificial inverted miscibility gaps was observed in some cases when the phase diagrams of these alloys were projected at higher temperatures. Poorly optimised modelling parameters were the most common cause of such artifacts. The available databases of the alloying properties of the initial melts were not enough to comprehend the various studies in depth. Moreover, the datasets produced by different methods may not be in proper consistency with the actual data for the interpolation and extrapolation of these properties at temperatures of interest. Generating a universal method for producing reliable datasets is an important goal for researchers in order to boost the development of modern technologies.

1.8 Objectives

The general and specific objectives of the present work are mentioned as follows:

A. General objective

To study the appearance of thermodynamic artifacts in liquid alloys and use a model to remove them.

B. Specific objectives

i. To study the thermodynamic properties, such as excess free energy of mixing, enthalpy of mixing, activity and concentration structure factor in long wave-length limit of binary Al–Fe, Al–Mn, Al–Ti and Li–Mg and ternary Al–Li–Zn liquid alloys in the Redlich-Kister model at different temperatures.

ii. To re-optimise the model parameters of R-K polynomial assuming them to be exponential T-dependent in order prevent the emergence of artificial inverted miscibilty gaps.

iii. To predict the heat of mixing and other properties at various temperatures using the modified model.

1.9 Plan of Thesis

The work of the present thesis is arranged in different chapters and their subdivision is as follows.:

CHAPTER 1: In this chapter we have presented general introduction about this work. It deals with the thermodynamic properties of mixing, miscibility gap, basic idea about thermodynamic artifacts and problem statement along with objectives of the study.

CHAPTER 2: This chapter contains a brief review of literature survey about study of liquid alloys and also about theoretical models and thermodynamic artifacts.

CHAPTER 3: This chapter presents the necessary background of the Redlich-Kister polynomial model and formulation of analytical expressions for thermodynamic and structural functions of liquid alloys.

CHAPTER 4: This chapter outlines the results of our calculations for thermodynamic and structural properties of binary liquid alloys Al-Fe, Al-Mn, Al-Ti, Li-Mg, and ternary alloy Al-Li-Zn at different temperatures which is followed by the discussion section.

CHAPTER 5: This chapter contains the conclusions of the present work and recommendations for the further work.

CHAPTER 6: This chapter includes a summary about the study of thermodynamic properties and structural properties of selected binary and ternary alloys along with thermodynamic artifacts.

CHAPTER 2

2. LITERATURE REVIEW

For the designing, developing, and fabricating of new metallic materials, many researchers have been working in the fields of material and metallurgical science. There are mainly two types of work: one is experimental work (Feufel et al., 1997; Bergman et al., 1994; Trybula et al., 2014; Gasior et al., 2016; Debski & Terlicka, 2016) , and the other is statistical work (Butler, 1932; Darken, 1950; Bhatia & Singh, 1984; Desai, 1987; Chou & Chang, 1989; Gasior et al., 1996; Chen et al., 2001; Kaptay, 2004; Schmid-Fetzer et al., 2007; Adhikari, Jha, & Singh, 2010; Novakovic et al., 2012), including theoretical modelling and simulation. In the experimental work of alloys, only limited thermodynamic functions can be measured, such as the activity coefficient, enthalpy of mixing, heat capacity, and chemical potential. There are different experimental methods like the calorimetric method, electromotive force (Emf), vapour method, and the Knudsen effusion method, etc. Among them, the calorimetric method is used for the measurement of the enthalpy of mixing and heat capacity of alloys. There are four classes of calorimeter, namely isothermal, adiabatic, heat-flow, and isoperibol calorimeters (Saunders & Miodownik, 1998) . Similarly, the activity can be measured by the electromotive force (Emf) method, the vapour method, or the Knudsen effusion method. On the basis of these experimental data, other properties like free energy of mixing, surface tension, structural and transport properties can be calculated by means of theoretical procedures.

2.1 Theoretical models for liquid alloys

Unlike crystals, liquid alloys are disordered systems whose properties are so varied that single theoretical approach is not sufficient to explain alloying behaviour of different alloys. In order to account the observed behaviour of the alloys, so many researchers have suggested several models over time. Basically, the theoretical study of alloys is carried out in two broad categories: the electronic model of mixing and the statistical model of mixing. With the idea of theoretical models for alloying that primarily stem from binary alloys are being extended for ternary and higher order alloys.

2.1.1 Electronic model of alloys

In an electronic model of mixing, a liquid alloy can be considered as ions of the metals present in the cloud of conduction electrons in which coulomb interaction of electrons and ions is assumed to take place. At a given temperature and pressure, the interactions between ions and electrons give rise to the properties of the alloys in liquid phase (Alblas et al., 1983). The major contributions in the electronic theories are from hard sphere model (Lebowitz, 1964; Carnahan & Starling, 1969; Visser et al., 1980; Singh & Choudhary, 1981; A. K. Mishra et al., 1993; Vora, 2010) and pseudo-potential theory (Harrison, 1966; Heine, 1970; Faber, 2010) In the pseudo-potential theory, the ion-electron interaction in an alloy is expressed in terms of pseudo-potential and partial structure factors. In the hard sphere model, the molecules of the metals in the solution are assumed to be hard spherical cores which have finite configurational internal energy and there is repulsive inter-molecular interactions. It is possible to explain the symmetry of an alloy and the band structure of an ordered alloy using a theory of the electronic structure of alloys, which provides a straightforward framework for a disordered substitutional alloy (Beeby, 1964). The alloys in which strong interaction between the unlike atoms exists leading to compound formation tendency, pseudopotential theory cannot be applied. Therefore, the electronic theories require improvements to yield better results for the properties of binary liquid alloys. The literature (Ashcroft & Mermin, 1976; Kittel & McEuen, 2018) contains more information on the fundamental knowledge of bonding. Furthermore, the stability of an alloy phase can be explained in terms of thermodynamic parameters like free energy of formation, enthalpy of formation, and entropy of formation using statistical theory of alloys.

2.1.2 Statistical model of alloys

Along with electronic theory, statistical models have been used to study the properties of liquid alloys in metallurgical science. Theoreticians have concentrated their efforts on thermodynamic and statistical mechanics-based solution theories. Earlier researchers (Hildebrand & Scott, 1950; Prigogine & Defay, 1954; Bhatia & Hargrove, 1974) described the thermodynamic properties of liquid alloys using the paradigm of a real solutions as ideal ones. The ideal solution model states that the two atomic species are very similar in size, are surrounded by the same number of nearest neighbour atoms, and mix together randomly without any perceptible volume change or heat expulsion or absorption, such as Co and Ni in a Co-Ni alloy (Dinsdale, 1984). In the real solution model, there is no enthalpy change on mixing, but there is an entropic contribution to the Gibbs free of mixing since the mixture has gained some disorder. As a result, configurational entropy, or the total number of alternative distributions over lattice sites, determines the

free energy of mixing (Alblas et al., 1983). The ideal solution model is not a feasible paradigm for explaining observed alloy mixing behaviour. Longuet-Higgins (1951) proposed a conformal solution model that combines the energetic effects and is a theory of small atomic size ratio.

Transport, surface, and thermodynamic properties are associated with an arrangement of species at the micro-and macroscopic level (Alblas et al., 1983; Plevachuk et al., 2014; Adhikari, Jha, & Singh, 2010; Koirala et al., 2013; Yadav, Jha, & Adhikari, 2016; Awe, 2019). Statistical theory deals with the configuration of atoms in a system. The entropy of a system is a measurement of randomness, which is due to thermal contribution and configuration contribution. In a solid, there is thermal energy distribution over atoms, which provides vibrational motion. In solutions, the randomness of atoms depends upon the number of ways in which they are arranged. A theory associated with the electronic structure of alloys is present, which accounts for the symmetry in the alloy and the band structure for an ordered alloy, giving a simple frame for a disordered substitutional alloy.

Several researchers (Bhatia & Thornton, 1970; Lele & Ramachandrarao, 1981; Chou & Chang, 1989; Desai, 1987; Kaptay, 2004; Debski & Terlicka, 2016; Arslan & Dogan, 2022; R. K. Mishra et al., 2023; K. Sun et al., 2023) have long been working on the development of different statistical models. They are: complex formation model (Bhatia & Singh, 1982; Singh et al., 1991; Kumar et al., 2005; Thakur et al., 2005), quasi-chemical model (Cobos, 1997; Pelton et al., 2001; Su & Wang, 2013), regular associated solution model (Lele & Ramachandrarao, 1981; Kelley et al., 1982; Adhikari, Singh, et al., 2010), and quasi-lattice theory (Vera et al., 1977; Singh, 1987; Prasad & Singh, 1990) have been employed to study and explain the mixing properties of binary liquid alloys.

2.1.3 Compound formation model (CFM)

The complex-forming alloys have been thoroughly explored and are known by a variety of names in the literature, including compound-forming solution, complex-forming solution and regular associated solution. These systems have high interactions in general. Even though there aren't many size differences between the constitutent species, G_M and $S_{CC}(0)$ are frequently observed to be asymmetric approximately about the equi-atomic composition. In the compound formation model, alloy is treated as pseudo-ternary mixture of A-atoms, B-atoms and cluster $A_\mu B_\nu$ (μ and ν are small integers). The cluster is a solid-state intermetallic complex that is energetically favoured and is in chemical equilibrium with every other component (Bhatia & Hargrove, 1974; Bhatia & Singh, 1984). The model is reduced to the quasi-chemical approximation for regular solutions assuming the absence of clusters in the melt (Singh, 1987). Bhatia & Singh (1982) developed the complex formation model further by introducing the idea of grand partition

function and taking into account the energy of A-B, A-A, or B-B bond pairs depending on whether the bond is a component of the complex $A_\mu B_\nu$ or not. On the basis of this assumption, they developed the analytical expressions for various thermodynamic functions, and the model was given the name quasi-chemical theory.

2.1.4 Quasi-lattice theory

The fundamental principle is that a binary A-B alloy capable of producing compounds in a liquid state is composed of a specific number of individual A and B atoms as well as chemical complexes $A_\mu B_\nu$ which are all in chemical equilibrium with one another (Bhatia & Singh, 1984). It is assumed that every atom is situated on a lattice site. The closest neighbours of each site are z (co-ordination number). Each atom can be regarded of as a monomer if the size difference between the two types of atoms, A and B, is less than 50%. The complex $A_\mu B_\nu$ is considered as $\mu + \nu$-mer and occupies $\mu + \nu$ lattice sites. Pelton modified quasi-chemical model to allow free choice of the composition of maximum short-range ordering in a binary system, to express the energy of pair formation as a function of composition and to extend the model to multicomponent systems. Since then, the model has been used to evaluate and optimise many liquid oxide, salt, and alloy solutions Pelton et al. (2000).

2.1.5 Redlich-Kister formulation

Among the different statistical models, one of the most widely used models to study mixing properties of an alloy is the Redlich-Kister polynomial(Redlich & Kister, 1948). Many researchers (Lüdecke, 1987; Chevalier, 1989; Soon-Don, 1992; Feufel et al., 1997; Yan & Chang, 2000; Chang et al., 2004; Kaptay, 2004; Du et al., 2008; Tang et al., 2012; Abe et al., 2012; Gancarz et al., 2013; Trybula et al., 2018; R. Gohivar et al., 2021; Mehta et al., 2020) have employed this polynomial to explain the properties of binary alloys. Teichert et al. (2017) compared the results of chemical potential obtained using Redlich-Kister polynomial with that from cubic spline. Kohler (1960); Toop (1965); Muggianu et al. (1975); Chou & Chang (1989) developed model under frame work of the Redlich-Kister polynomial in order to apply it to calculate mixing properties of ternary alloys (Du et al., 2008; Tang et al., 2012; Bencze & Popovic, 2013; Trybula et al., 2018; R. K. Gohivar, Yadav, et al., 2021c; Mehta et al., 2020). Du et al. (2007, 2008) have used this polynomial to describe liquid phase of ternary Al–Mg–Mn and Al–Fe–Si system. Tang et al. (2012) described thermodynamic of Al–Mg–Si system in this model. Bencze & Popovic (2013) used Redlich-Kister-Muggianu (RKM) sub-regular solution model to study thermodynamic mixing properties of ternary Cu–In–Sn, Ag–In–Sn, Al–Cu–Sn and

Cu–Sb–Sn liquid alloys. Mehta et al. (2020) have described thermo-physical properties of ternary Al–Cu–Fe system in this frame. This model is extended to calculate mixing properties of multi-components alloy (higher order). In framework of this model, Kaptay (2004) developed exponential interaction parameters for high temperature calculation in place of linear interaction parameters. Besides these, the calculation of phase diagrams (CALPHAD) is a technique to couple all phases (stable and metastable phases at a wide range of composition, temperature, and pressure), stoichiometric compounds, intermetallic compounds, and thermochemicals of a system.

2.1.6 Calculation of phase diagram (CALPHAD)

Phase diagrams are widely used as an initial roadmap in material science and engineering. It displays the phase stability of an alloy with respect to different parameters, such as composition, temperature, and rarely pressure. Calculation of phase diagram (CALPHAD) is a technique based on the least square optimization procedure to evaluate values of model parameters by taking into account different phases and experimental values. In other words, thermodynamic software packages are used for the optimization, which assure only the accuracy of phase models within the region where experiments were carried out. Kattner (1997) have described a thorough explanation of Calphad method. When excess free energy in liquid phase is modeled such that interaction parameters depend linearly on temperature then in some cases inverted miscibility gap appears (Chen et al., 2001; Kevorkov et al., 2004; Kaptay, 2004; Balakumar & Medraj, 2005; Arroyave & Liu, 2006; Malakhov & Balakumar, 2007; Schmid-Fetzer et al., 2007; Yuan et al., 2009; Wang, Du, & Liu, 2011; Tang et al., 2011; Kaptay, 2012; Abe et al., 2012; Kaptay, 2014; S. M. Liang et al., 2016; Liu et al., 2016; Kaptay, 2017; Ghasemi et al., 2019). Chen et al. (2001) had used the PANDAT computer-based software package and prior published model parameters to calculate phase-diagrams of some binary alloy systems. The phase diagram for the Si–Ta system, Al–Nb system, and Co–Si system were calculated by Chen et al. (2001) using respective modelling parameters from (Vahlas et al., 1989; Soon-Don, 1992) and Cost 507. Chen et al. (2001) had found that an inverted miscibility gap appeared in these calculated phase diagrams due to poor modelling parameters. Kevorkov et al. (2004) had also detected the appearance of an artificial inverted miscibility gap in Mg–Si system at higher temperatures. Therefore, this system was remodelled and these parameters were then used in the Mg-Si-Li system, which supported the experimental results. Kaptay (2004) developed a new modelling equation to remove the artifacts that appeared due to poor modelling rather than developing software by Chen et al. (2001). In this new equation, he made the assumption that in the Redlich-Kister (R-K) polynomial model, the interaction energy parameters were exponentially temperature dependent. Balakumar and Medraj (2005) optimised the model parameters for liquid

sub-binaries Al-Sb and Mg-Sb of the ternary Mg–Al–Sb system following this process. To test the validity of optimised parameters, thermodynamic functions were calculated and compared with experimental results. When these parameters were used for the ternary system, miscibility gap appeared in the calculated mixing properties (Balakumar & Medraj, 2005).

Arroyave & Liu (2006) used three models, namely, linear and exponential temperature dependence interaction parameters and an associated model to calculate the phase diagram and thermodynamic properties of the Zn–Zr system. There were unstable liquid phases in the range T > 2973 K when linear-T model parameters were used. Further, the excess free energy of mixing of liquid phases was found to decrease exponentially with temperature when exponential temperature-dependent parameters were used. But the results of associated model showed ideal behaviour at higher temperatures.

Schmid-Fetzer et al. (2007) used corrected parameters of the Mg–Si system from Kevorkov et al. (2004) to calculate the phase diagram and found that artifacts appeared at higher temperatures. In order to avoid the artifacts at high temperatures, they re-modelled the system by considering exponential temperature-dependent interaction parameters, which were proposed in (Kaptay, 2004). On using these parameters, artifacts (re-stabilization of liquid phase below solidus) were observed at low temperatures. Further, they pointed out that the presence of the low-temperature artifact was due to the exponential temperature-dependent parameters which exaggerate negative values of excess Gibbs energy of mixing at the very low temperature. According to Yuan et al. (2009), the presence of liquid phase at low temperatures is most likely due to the fact that they (Schmid-Fetzer et al., 2007) accomplished a simplified evaluation of the Mg–Si system without considering all of the experimental data. In addition, to assess the full thermodynamics of the Mg-Si system, the exponential parameters were optimised by using the PARROT module of Thermo-Calc. When these parameters were used to calculate the phase diagram, no any high-temperature or low-temperature artifacts appeared in the calculations (Yuan et al., 2009). Wang, Zhou, et al. (2011) introduced thermodynamic constraints to remove the artifacts in the Cu—Nd system by using density functional theory. The thermodynamic constraint was that the second derivative of the Gibbs energy of the phase with respect to the concentration of constituents of the system should be greater than zero. In the liquidus region of the Cu–Nd system, where the unrealistic miscibility gap appeared, a negative value of the second derivative of Gibbs energy was found. When the thermodynamic constraints were introduced, it was found that there was no such gap. Tang et al. (2011) used exponential model without introducing any thermodynamic constraint to eliminate the presence of an artificial miscibility gap in the phase diagram of the Fe-Zn system at higher temperatures. The presence and elimination of the gap was also shown in the plot of the enthalpy of mixing (Tang et al., 2011). For high temperature study of binary alloys,

Kaptay (2012) reformulated the rule of Lupis and Elliott (LE), and he further checked the validity of the new formulations by considering twelve different binary systems. He also showed that when exponential temperature-dependent parameters for excess Gibbs free energy of mixing were computed based on the LE rule, no artifacts were observed at elevated temperatures. But when linear temperature-dependent parameters (contrary to the LE rule) were considered, artificial inverted miscibility appeared in the phase diagram. The interaction parameters of the sub-binary Al–Mg, Mg–Si, and Al–Si systems were optimised as exponential temperature-dependent to remove the artificial inverted miscibility gap caused by the linear model in excess Gibbs energy of mixing of ternary Al–Mg–Si system (Tang et al., 2012). Abe et al. (2012) analyzed linear temperature-dependent interaction parameters $L_i = a_i + b_i T$ of Redlick-Kister polynomial for binary systems and concluded that no miscibility gap appears at high temperatures when $-2R \leq b_i \leq 2R$, where R is universal gas constant. Liu et al. (2016) found inverted miscibility gap in Zn–P system by using linear temperature-dependent interaction $L_0 = -125601.92 - 248.0033T$ and $L_1 = 324677.14 - 385.3940T$ (Tu et al., 2009) and so he optimized interaction parameters exponentially to study thermodynamics of ternary Zn–Si–P system.

Kaptay (2014) put forwarded the combination of linear and exponential temperature-dependent LET model to explain the re-stabilization liquid phase in "exceptional systems" seen by using exponential model. S. M. Liang et al. (2016) proposed new temperature function for interaction parameters L_i which was inherently consistent. The new function excluded both the exaggerated negative values and positive values of L_i for low temperature and high temperature respectively. Kaptay (2017) revisited the exponential model and suggested that the combined linear-exponential model should be used when the excess free energy of mixing changes sign with the change of temperature. Further, Kaptay used an exponential model for the reassessment of the Mg–Si system and it was shown that no low-temperature artifact appeared as claimed in (Schmid-Fetzer et al., 2007). Ghasemi et al. (2019) reassessed the Zn–P system by using exponential model (Kaptay, 2004) and combined model (S. M. Liang et al., 2016) to solve the problem of artifact found in the excess Gibbs energy of mixing, entropy of mixing, enthalpy of mixing and specific heat capacity at elevated temperatures. Artifacts are known to appear when thermodynamic functions do not shift towards ideal values at extremely high temperatures due to inadequacy of the interaction parameters.

CHAPTER 3

3. MATERIALS AND METHODS

The physics of many phenomena can be understood through relevant mathematical analysis. Analytical expressions are essential tools for easy understanding of physical quantities. Experimentally observed data for liquid alloys are interpreted in many ways with the help of different models. This section deals with the detailed mathematical formulation necessary in the framework of Redlich-Kister (R-K) polynomials for studying the thermodynamic and structural properties of some liquid alloys. In the R-K polynomial, the interaction parameters for liquid alloys are needed to explain the properties of mixing. The procedure for optimising the required interaction parameters is described in detail below.

3.1 Thermodynamic properties

In general, the mixing behaviour of liquid alloys can be characterised by the temperature, pressure, and composition. As the study of the liquid alloys is usually carried out at the fixed pressure, most likely, the atmospheric pressure, the thermo-physical properties of a binary liquid alloy at a given temperature vary with the composition of the alloy and often show an interesting behaviour as a function of composition. It is convenient to take relative composition, i.e., mole fraction concentrations of components, in the analysis of binary mixtures than to use the actual amount present in the combination. The mole fraction x_k of component k of a binary mixture A-B is calculated as $x_k = n_k / \sum n_k$ where n_k is the number of moles of component k.

The necessary mathematical formulation for thermodynamic properties such as excess free energy of mixing (G_M^{xs}), partial excess free energy of mixing (G_k^{xs}), excess entropy of mixing (S_M^{xs}), enthalpy of mixing (H_M) and activity (a_k) of alloy is described in the following sections.

3.1.1 Free energy of mixing (G_M) of binary A-B liquid alloy

The stability of solutions can be comprehended in terms of their thermodynamic function namely the free energy of mixing. Atoms of components A and B of mole fraction x_A and x_B are mixed to form one mole of a binary solution. The free energies of components A and B are G_A and G_B, respectively, and the initial total free energy before mixing is

given as

$$G_1 = x_A G_A + x_B G_B \tag{3.1}$$

The free energy of an alloy in a phase is related to the free energies of its components and the energy associated with interaction terms in that phase. After mixing the atoms A and B, the free energy of solution becomes

$$G_2 = G_1 + G_M \tag{3.2}$$

where G_M is the change in free energy on mixing.The values of free energy of mixing (G_M) of liquid alloys determines the bonding strength between atoms. At a given temperature T, the free energy of mixing is expressed in terms of enthalpy of mixing (H_M) and entropy of mixing (S_M) through the standard thermodynamic relation $G_M = H_M - TS_M$. The free energy should always be negative in all cases for the spontaneous process of mixing to occur. The free energy of mixing of a solution in phase (ϕ) may be expressed as

$$G^{\phi} = x_A \, G_A^{\phi} + x_B \, G_B^{\phi} + G_M^{xs} + G_M^{id} \tag{3.3}$$

where G_A^{ϕ} and G_B^{ϕ} are free energy of components A and B in pure state; G_M^{xs} is excess free energy of mixing and G_M^{id} is the ideal free energy of mixing of the A-B alloy in the phase ϕ.

The excess free energy of mixing of alloys is the excess amount of integral free energy of mixing from its ideal value at a given temperature. In ideal case, the constituent atoms are supposed to be distributed randomly in solutions. However, in real solutions, there are some specific atomic arrangements. For the change from random to particular distribution, some work should be performed which is known as excess free energy of mixing. This function at a temperature may be expressed in terms of the excess entropy of mixing (S_M^{xs}) as $G_M^{xs} = H_M - TS_M^{xs}$.

The excess free energy of mixing may be positive or negative depending on the nature alloy.The conditions for $G_M^{xs} < 0$ may be mentioned as follows:

i. $H_M << 0$ and $S_M^{xs} < 0$, ordering nature of alloy (Ag-Au, Ag-In, Al-Au, Al-Fe, Al-Mg, Au-Cd, Au-Zn, Cd-Hg, Cd-Mg, Cd-Na, Fe-Si, Ga-Mg, Hg-Na, In-Na, K-Pb, Mg-Tl, Pb-Tl, etc.)

ii. $H_M < 0$ and $S_M^{xs} > 0$, ordering nature of alloy (Ag-Al, Ag-Ga, Al-Cu, Al-Ge, Au-Cu, Au-Pb, Au-Sn, Bi-Hg, Bi-In, Bi-Mg, Bi-Pb, Cu-Sn, In-Mg, In-Sb, In-Sn, Li-Mg, Pb-Sb, etc.)

iii. $H_M > 0$ and $S_M^{xs} >> 0$, ordering nature of alloy (Au-Bi, Au-Tl, Bi-Cd, Bi-Sb, etc.)

On the other hand, the conditions for $G_M^{xs} > 0$ may be summarised as below:

i. $H_M > 0$ and $S_M^{xs} < 0$, segregating nature of alloy (Al-Cd, Bi-Sn, Cu-Ni, Fe-Pd, Hg-Pb, In-Tl, Ni-Pd, Pb-Sn, etc.)

ii. $H_M >> 0$ and $S_M^{xs} > 0$, segregating nature of alloy (Ag-Cu, Ag-Pb, Ag-Tl, Al-Ga, Al-In, Al-Sn, Al-Zn, Au-Fe, Bi-Zn, Cd-Ga, Cd-In, Cd-Pb, Cd-Sn, Cd-Tl, Cd-Zn, Cu-Fe, Cu-Pb, Cu-Tl, Ga-Zn, In-Pb, In-Zn, etc.)

iii. $H_M < 0$ and $S_M^{xs} << 0$, segregating nature of alloy (Co-Fe)

In the most of cases, the sign of G_M^{xs} is similar to sign of H_M for low entropy alloy and their signs differ for only some alloys of high entropy or low enthalpy of mixing.

The excess free energy of mixing (G_M^{xs}) is calculated in the framework of Redlich-Kister (R-K) polynomials (Redlich & Kister, 1948) by the following relation

$$G_M^{xs} = x_A x_B \sum_{i=0}^{n} L_i \, (x_A - x_B)^i \tag{3.4}$$

where x_A and x_B are concentration of constituents A and B of the A-B alloy, and L_i are interaction parameters due to all types of bonding between them that are expressed as (Singh & Sommer, 1997)

$$L_i = a_i + b_i T + c_i T \ln T + d_i T^{-2} + \ldots \tag{3.5}$$

where a_i, b_i and c_i are the contributions of the enthalpy of mixing (H_M), excess entropy of mixing (S_M^{xs}) and specific heat capacity (C) respectively and are independent of concentration and temperature.

Considering interaction between components A and B as linear temperature-dependent, the interaction parameter in Equation (3.5) contains only the first two terms as

$$L_i = a_i + b_i T \tag{3.6}$$

The excess free energy of mixing (G_M^{xs}) in Equations (3.4) can then be expressed in terms of linear temperature-dependent interaction parameters as below

$$G_M^{xs} = x_A x_B \sum_{i=0}^{n} (a_i + b_i T) \, (x_A - x_B)^i \tag{3.7}$$

Equations (3.7) suggests the enthalpy of mixing and excess entropy of mixing of the alloys are temperature-independent thermodynamic functions. However, with increasing temperature, the behaviour of all thermodynamic functions should shift toward ideal

behaviour. In order to account this behaviour, Kaptay (2004) considered interaction parameters to depend exponentially on temperature as

$$L_i = h_i \exp\left(-\frac{T}{\tau_i}\right) \tag{3.8}$$

where h_i and τ_i are contribution of enthalpy of mixing and excess entropy of mixing respectively which are independent of concentration and temperature.

On expanding Equation (3.8), we get

$$L_i = h_i[1 + \frac{(-\frac{T}{\tau_i})}{1!} + \frac{(-\frac{T}{\tau_i})^2}{2!} + \dots] \tag{3.9}$$

At lower temperatures, $\frac{T}{\tau_i} << 1$, then Equation (3.9) is reduced in the form

$$L_i = h_i\left[1 - \frac{T}{\tau_i}\right] \tag{3.10}$$

The exponential temperature-dependent excess free energy of mixing (G_M^{xs}) is obtained by using Equations (3.4) in (3.8) as

$$G_M^{xs} = x_A x_B \sum_{i=0}^{n} h_i \exp\left(-\frac{T}{\tau_i}\right) (x_A - x_B)^i \tag{3.11}$$

The ideal value of free energy of mixing of the alloy (G^{id}) at temperature T is calculated from the following relation

$$G_M^{id} = RT\,(x_A \ln x_A + x_B \ln x_B) \tag{3.12}$$

The free energy of mixing of binary A-B alloy (G_M) is given by the relation

$$G_M = G_M^{xs} + G_M^{id} \tag{3.13}$$

Using the Equations (3.4) and (3.12) in Equation (3.13), we get the analytical equation for G_M in the following form

$$G_M = x_A x_B \sum_{i=0}^{n} L_i\,(x_A - x_B)^i + RT\,(x_A \ln x_A + x_B \ln x_B) \tag{3.14}$$

3.1.2 Excess free energy of mixing of ternary A-B-C liquid alloy

The majority of commercial ternary alloys such as Al–Cu–Zn, Cu–Sn–Zn, Ni–Co–Fe, Al–Zn–Mg etc. are formed by combining at least three components. The ternary and higher order systems can be studied by extending the concepts developed for binary systems (Chou & Chang, 1989). The free energy of ternary A-B-C alloy in phase (ϕ) is computed by

$$G^{\phi} = x_A G_A^{\phi} + x_B G_B^{\phi} + x_C G_C^{\phi} + G_M^{xs} + G_M^{id} \tag{3.15}$$

where x_A, x_B and x_C are concentration of constituents A, B and C of ternary A-B-C alloy such that $x_A + x_B + x_C = 1$ and G_A^{ϕ}, G_B^{ϕ} and G_C^{ϕ} are free energy of corresponding constituents and G_M^{xs} is the excess free energy of mixing and G_M^{id} is the ideal free energy of mixing of the alloy in the phase ϕ. The excess free energy of mixing (G_M^{xs}) is calculated in framework of Redlich-Kister-Muggianu (R-K-M) polynomials by the following relation

$$G_M^{xs} = (G_M^{xs})^{A-B} + (G_M^{xs})^{B-C} + (G_M^{xs})^{C-A} + G_M^{ter} \tag{3.16}$$

where the first three terms are from the sub-binary A-B, B-C, and C-A contributions, and the last term arises from the ternary contribution. The analytical expression for G_M^{xs} of the ternary alloy can then be obtained in terms of the interaction parameters in the following form

$$\begin{aligned} G_M^{xs} =& x_A x_B \sum_{i=0}^{n} L_i^{A-B} (x_A - x_B)^i + x_B x_C \sum_{i=0}^{n} L_i^{B-C} (x_B - x_C)^i \\ &+ x_C x_A \sum_{i=0}^{n} L_i^{C-A} (x_C - x_A)^i + x_A x_B x_C (L^0 x_A + L^1 x_B + L^2 x_C) \end{aligned} \tag{3.17}$$

where L_i^{A-B}, L_i^{B-C} and L_i^{C-A} are interaction parameters of respective sub-binary A-B, B-C and C-A systems of ternary A-B-C alloy and L^0, L^1 and L^2 are the ternary interaction terms given as $L^0 = h_0 \exp(-T/\tau_0)$, $L^1 = h_1 \exp(-T/\tau_1)$ and $L^2 = h_2 \exp(-T/\tau_2)$.

The ideal value of free energy of mixing of the ternary alloy (G_M^{id}) at temperature T is calculated from the relation

$$G_M^{id} = RT (x_A \ln x_A + x_B \ln x_B + x_C \ln x_C) \tag{3.18}$$

Similarly, the free energy of mixing of ternary A-B-C alloy (G_M) is obtained from

Equations (3.1.2) and (3.18), in the form

$$\begin{aligned} G_M =& x_A x_B \sum_{i=0}^{n} L_i^{A-B} (x_A - x_B)^i + x_B x_C \sum_{i=0}^{n} L_i^{B-C} (x_B - x_C)^i \\ &+ x_C x_A \sum_{i=0}^{n} L_i^{C-A} (x_C - x_A)^i + x_A x_B x_C (L^0 x_A + L^1 x_B + L^2 x_C) \\ &+ RT (x_A \ln x_A + x_B \ln x_B + x_C \ln x_C) \end{aligned} \tag{3.19}$$

3.1.3 Excess entropy of mixing (S_M^{xs})

The entropy of mixing of a system is carried out by considering equal-priority for constituents in configuration arrangements which is arrangement of ideal case. In a real system, interaction among constituents causes the entropy of mixing to shift from ideal value. The entropy of mixing of the system deviates from ideal value according to nature of interaction (attractive or repulsive). The difference of entropy of mixing from ideal value is termed as excess entropy of mixing. The excess entropy of mixing (S_M^{xs}) of binary A-B alloy is derived from the excess free energy of mixing using the standard thermodynamic relation

$$S_M^{xs} = -\frac{\partial G_M^{xs}}{\partial T} \tag{3.20}$$

Now using Equation (3.4) in Equation (3.20), one can obtain the relation for S_M^{xs} as

$$S_M^{xs} = -x_A x_B \sum_{i=0}^{n} \frac{\partial L_i}{\partial T} (x_A - x_B)^i \tag{3.21}$$

On using linear temperature-dependent interaction parameters of Equation (3.6) in Equation (3.21),the temperature independent S_M^{xs} is obtained as

$$S_M^{xs} = x_A x_B \sum_{i=0}^{n} (-b_i) (x_A - x_B)^i \tag{3.22}$$

Similarly, on using Equation (3.8), Equation (3.21) for the temperature dependent case becomes

$$S_M^{xs} = x_A x_B \sum_{i=0}^{n} \left(\frac{h_i}{\tau_i}\right) \exp\left(-\frac{T}{\tau_i}\right) (x_A - x_B)^i \tag{3.23}$$

3.1.4 Enthalpy of mixing (H_M)

Enthalpy of mixing H_M of binary A-B alloy is calculated from the standard thermodynamic relation

$$H_M = G_M^{xs} + TS_M^{xs} \tag{3.24}$$

Using Equations (3.7) and (3.22) in Equation (3.24) then we obtain a relation for temperature independent H_M as

$$\begin{aligned} H_M &= x_A x_B \sum_{i=0}^{n} (a_i + b_i\, T)\, (x_A - x_B)^i + T x_A x_B \sum_{i=0}^{n} (-b_i)\, (x_A - x_B)^i \\ &= x_A x_B \sum_{i=0}^{n} a_i\, (x_A - x_B)^i \end{aligned} \tag{3.25}$$

Similarly, using Equations (3.11 & 3.23), which incorporate the exponential temperature-dependent interaction parameters, in Equation(3.24), the analytical expression for the enthalpy of mixing of binary alloy is obtained in the form

$$H_M = x_A x_B \sum_{i=0}^{n} (1 + \frac{T}{\tau_i}) h_i \exp\left(-\frac{T}{\tau_i}\right) (x_A - x_B)^i \tag{3.26}$$

3.1.5 Enthalpy of mixing of ternary A-B-C liquid alloy

The enthalpy of mixing (H_M) of ternary A-B-C liquid alloy is computed by taking the contribution of sub-binary A-B, B-C, C-A interactions and the ternary interaction with exponential parameters in R-K-M model.

$$H_M = (H_M)^{A-B} + (H_M)^{B-C} + (H_M)^{C-A} + (H_M)^{ter} \tag{3.27}$$

An analytical expression for H_M may be expressed in the following form

$$\begin{aligned} H_M =& x_A x_B \sum_{i=0}^{n} [L_i(1 + \frac{T}{\tau_i})]^{A-B}\, (x_A - x_B)^i + x_B x_C \sum_{i=0}^{n} [L_i(1 + \frac{T}{\tau_i})]^{B-C}\, (x_B - x_C)^i \\ &+ x_C x_A \sum_{i=0}^{n} [L_i(1 + \frac{T}{\tau_i})]^{C-A}\, (x_C - x_A)^i \\ &+ x_A x_B x_C [L^0(1 + \frac{T}{\tau_0}) x_A + L^1(1 + \frac{T}{\tau_1}) x_B + L^2(1 + \frac{T}{\tau_2}) x_C] \end{aligned} \tag{3.28}$$

L_i^{A-B}, L_i^{B-C} and L_i^{C-A} are interaction parameters of respective sub-binary A-B, B-C and C-A systems of ternary A-B-C alloy and L^0, L^1 and L^2 are the ternary interaction terms

given as $L^0 = h_0 \exp(-T/\tau_0)$, $L^1 = h_1 \exp(-T/\tau_1)$ and $L^2 = h_2 \exp(-T/\tau_2)$

For the comparative study of the enthalpy of mixing of ternary liquid alloy, we have also employed the following expression of Toop model (Toop, 1965)

$$H_M = \frac{x_B}{1-x_A}(H_M)^{A-B} + (x_B + x_C)^2 (H_M)^{B-C} + \frac{x_C}{1-x_A}(H_M)^{C-A} \tag{3.29}$$

where

$$(H_M)^{A-B} = x_A(1-x_A) \sum_{i=0}^{n} [L_i(1 + \frac{T}{\tau_i})]^{A-B} \, (2x_A - 1)^i \tag{3.30a}$$

$$(H_M)^{B-C} = \frac{x_B x_C}{(x_B + x_C)^2} \sum_{i=0}^{n} [L_i(1 + \frac{T}{\tau_i})]^{B-C} \, (\frac{x_B - x_C}{x_B + x_C})^i \tag{3.30b}$$

$$(H_M)^{C-A} = x_A(1-x_A) \sum_{i=0}^{n} [L_i(1 + \frac{T}{\tau_i})]^{C-A} \, (2x_A - 1)^i, \tag{3.30c}$$

3.1.6 Activity

The activity is an experimentally measurable fundamental thermodynamic function. It can be measured directly using a variety of experimental techniques such as electromotive force, vapour pressure, chemical equilibria, and so on. Activity represents the tendency of atoms to leave a solution and it can be used to interpret the stability of complexes in an alloy in terms of its constituents through the study of the thermodynamic and structural functions. Any variation from the ideal behaviour of liquid binary alloys can be integrated into the activity. In theoretical study, it can be determined as function of the alloy composition and temperature.

The general expression for partial excess free energy constituents k (=A,B) of liquid A–B alloy (S. B. Zhang & Li, 1986) is

$$G_k^{xs} = G_M^{xs} + \sum_{j=1}^{k} (\delta_{kj} - x_j) \frac{\partial G_M^{xs}}{\partial x_j} \tag{3.31}$$

where δ_{kj} is Kronecker delta function. On solving Equation (3.31), the expressions for the partial excess free energy of constituents A and B of binary A-B alloy are deduced as

$$G_A^{xs} = G_M^{xs} + (1 - x_A) \frac{\partial G_M^{xs}}{\partial x_A}, \quad G_B^{xs} = G_M^{xs} + (1 - x_B) \frac{\partial G_M^{xs}}{\partial x_B} \tag{3.32}$$

On using Equation (3.4) in Equation (3.32) and solving, we get

$$G_A^{xs} = (1 - x_A)^2 \sum_{i=0}^{n} L_i[(1 + 2i)x_A - (1 - x_A)](2x_A - 1)^{i-1} \tag{3.33}$$

and

$$G_B^{xs} = (1 - x_B)^2 \sum_{i=0}^{n} L_i[(1 + 2i)x_B - (1 - x_B)](2x_B - 1)^{i-1} \tag{3.34}$$

The activity of constituents A and B of binary A-B alloy are computed by using their corresponding values of partial excess free energy from Equations (3.33) and (3.34) in the following expressions

$$a_A = x_A \exp\left(\frac{G_A^{xs}}{RT}\right), \quad a_B = x_B \exp\left(\frac{G_B^{xs}}{RT}\right) \tag{3.35}$$

3.1.7 Activity of ternary A–B–C liquid alloy

For simplicity Equation (3.19) is written in the following form

$$\begin{aligned} G_M = G_M^{xs} + G_M^{id} = {} & x_A x_B Y_{AB} + x_B x_C Y_{BC} + x_C x_A Y_{CA} \\ & + x_A x_B x_C (x_A L^0 + x_B L^1 + x_C L^2) + G_M^{id} \end{aligned} \tag{3.36}$$

where

$$Y_{AB} = L_0^{A-B} + L_1^{A-B}(x_A - x_B) + L_2^{A-B}(x_A - x_B)^2 + L_3^{A-B}(x_A - x_B)^3 + L_4^{A-B}(x_A - x_B)^4 \tag{3.37}$$

$$Y_{BC} = L_0^{B-C} + L_1^{B-C}(x_B - x_C) + L_2^{B-C}(x_B - x_C)^2 + L_3^{B-C}(x_B - x_C)^3 + L_4^{B-C}(x_B - x_C)^4 \tag{3.38}$$

$$Y_{CA} = L_0^{C-A} + L_1^{C-A}(x_C - x_A) + L_2^{C-A}(x_C - x_A)^2 + L_3^{C-A}(x_C - x_A)^3 + L_4^{C-A}(x_C - x_A)^4 \tag{3.39}$$

The first derivative of G_M^{xs} w.r.t. x_A, x_B and x_C from Equation (3.1.7) are expressed in the following expressions

$$\begin{aligned} \frac{\partial G_M^{xs}}{\partial x_A} = {} & x_B Y_{AB} + x_A x_B \frac{\partial Y_{AB}}{\partial x_A} + x_C Y_{CA} + x_A x_C \frac{\partial Y_{CA}}{\partial x_A} \\ & + x_B x_C (x_A L^0 + x_B L^1 + x_C L^2) + x_A x_B x_C L^0 \end{aligned} \tag{3.40a}$$

$$\frac{\partial G_M^{xs}}{\partial x_B} = x_A Y_{AB} + x_A x_B \frac{\partial Y_{AB}}{\partial x_B} + x_C Y_{BC} + x_B x_C \frac{\partial Y_{BC}}{\partial x_B} + x_A x_C (x_A L^0 + x_B L^1 + x_C L^2) + x_A x_B x_C L^1 \tag{3.40b}$$

$$\frac{\partial G_M^{xs}}{\partial x_C} = x_B Y_{BC} + x_B x_C \frac{\partial Y_{BC}}{\partial x_C} + x_A Y_{CA} + x_A x_C \frac{\partial Y_{CA}}{\partial x_C} + x_A x_B (x_A L^0 + x_B L^1 + x_C L^2) + x_A x_B x_C L^2 \tag{3.40c}$$

For the derivative terms of Equations (3.40a-3.40c), one can obtain derivative of Equations (3.37-3.39) w.r.t. x_A, x_B and x_C in the following forms

$$\frac{\partial Y_{AB}}{\partial x_A} = L_1^{A-B} + 2L_2^{A-B}(x_A - x_B) + 3L_3^{A-B}(x_A - x_B)^2 + 4L_4^{A-B}(x_A - x_B)^3 = -\frac{\partial Y_{AB}}{\partial x_B} \tag{3.41a}$$

$$\frac{\partial Y_{CA}}{\partial x_A} = -L_1^{C-A} - 2L_2^{C-A}(x_C - x_A) - 3L_3^{C-A}(x_C - x_A)^2 - 4L_4^{C-A}(x_C - x_A)^3 = \frac{\partial Y_{CA}}{\partial x_C} \tag{3.41b}$$

$$\frac{\partial Y_{BC}}{\partial x_B} = L_1^{B-C} + 2L_2^{B-C}(x_B - x_C) + 3L_3^{B-C}(x_B - x_C)^2 + 4L_4^{B-C}(x_B - x_C)^3 = -\frac{\partial Y_{BC}}{\partial x_C} \tag{3.41c}$$

Moreover, it should be mentioned that in each solution one of the components should be selected as "dependent", while the other components are "independent" and the derivative of excess free energy of mixing by the mole fraction of the dependent must be zero. This will simply the following equations (Hillert & Staffansson, 1970)

$$\begin{aligned} G_A^{xs} &= G_M^{xs} + \frac{\partial G_M^{xs}}{\partial x_A} - \left(x_A \frac{\partial G_M^{xs}}{\partial x_A} + x_B \frac{\partial G_M^{xs}}{\partial x_B} + x_C \frac{\partial G_M^{xs}}{\partial x_C} \right), \\ G_B^{xs} &= G_M^{xs} + \frac{\partial G_M^{xs}}{\partial x_B} - \left(x_A \frac{\partial G_M^{xs}}{\partial x_A} + x_B \frac{\partial G_M^{xs}}{\partial x_B} + x_C \frac{\partial G_M^{xs}}{\partial x_C} \right), \\ G_C^{xs} &= G_M^{xs} + \frac{\partial G_M^{xs}}{\partial x_C} - \left(x_A \frac{\partial G_M^{xs}}{\partial x_A} + x_B \frac{\partial G_M^{xs}}{\partial x_B} + x_C \frac{\partial G_M^{xs}}{\partial x_C} \right) \end{aligned} \tag{3.42}$$

Finally, activity of ternary components can be calculated with aid of Equations (3.42) in the following expressions

$$a_A = x_A \exp\left(\frac{G_A^{xs}}{RT}\right), \quad a_B = x_B \exp\left(\frac{G_B^{xs}}{RT}\right), \quad a_C = x_C \exp\left(\frac{G_C^{xs}}{RT}\right) \tag{3.43}$$

3.2 Structural properties

The study of structural functions helps to understand the complexity of mixing behaviour of liquid alloys. Because the alloys are formed from a liquid state, they are considered as disordered systems having only local interactions. Structural functions such as concentration fluctuation in the long wavelength limit ($S_{CC}(0)$) can be used to interpret the local configurations of atoms in the initial melt.

3.2.1 Concentration fluctuation in long wavelength limit for binary liquid alloy

The stability of a system can be determined by the calculating stability function. It is calculated by taking second derivatives of free energy of mixing with respect to mole fraction. A phase is stable against fluctuations in compositions if this function is greater than zero. In some systems, this function changes its sign and the point where this function becomes zero, is called spinodal (Sundman et al., 2007). Further if the stability function is less than zero then the free energy of mixing is lowered spontaneously and the phase decomposes into two phases of different compositions having same structure. Among the three structure factors in long wavelength limit namely mean square fluctuation in number-number ($S_{NN}(0)$), mean square fluctuation in concentration-concentration ($S_{CC}(0)$) and mean square fluctuation of number-concentration ($S_{NC}(0)$), $S_{CC}(0)$ is commonly used structure factor for binary alloys in literature. An important function that describes the nature of ordering or segregation of mixing behaviour is the concentration fluctuation in the long wavelength limit ($S_{CC}(0)$) of the binary system which is computed from the standard expression (Bhatia & Thornton, 1970)

$$S_{CC}(0) = N \left\langle (\Delta c)^2 \right\rangle$$

The function $\left\langle (\Delta c)^2 \right\rangle$ represents mean square fluctuation in the concentration and N is total number of atoms. It can be derived from the free energy of mixing, G_M (Bhatia & Thornton, 1970) as,

$$S_{CC}(0) = RT \left(\frac{\partial^2 G_M}{\partial x_A^2} \right)^{-1} = RT \left(\frac{\partial^2 G_M}{\partial x_B^2} \right)^{-1} \tag{3.44}$$

The Equation (3.14) can also be expressed in the following form

$$G_M = (x_A - x_A^2) \sum_{i=0}^{n} L_i (2x_A - 1)^i + RT[x_A \ln x_A + (1 - x_A) \ln(1 - x_A)] \tag{3.45}$$

Taking differentiation of Equation (3.45) w.r.t. concentration of component A in liquid A–B alloy twice, we have

$$\frac{\partial G_M}{\partial x_A} = (1-2x_A)\sum_{i=0}^{n} L_i(2x_A-1)^i + (x_A - x_A^2)\sum_{i=0}^{n} 2iL_i(2x_A-1)^{i-1} + RT[1+\ln x_A + 1 - \ln(1-x_A)] \tag{3.46}$$

and,

$$\frac{\partial^2 G_M}{\partial x_A^2} = -2\sum_{i=0}^{n} L_i(2x_A-1)^i + (1-2x_A)\sum_{i=0}^{n} 2iL_i(2x_A-1)^{i-1} + (1-2x_A)\sum_{i=0}^{n} 2iL_i(2x_A-1)^{i-1} + (x_A - x_A^2)\sum_{i=0}^{n} 4i(i-1)L_i(2x_A-1)^{i-2} + RT[\frac{1}{x_A} + \frac{1}{(1-x_A)}] \tag{3.47}$$

or,

$$\frac{\partial^2 G_M}{\partial x_A^2} = \sum_{i=0}^{n}[4i(i-1)x_A(1-x_A)(2x_A-1)^{i-2} - (4i+2)(2x_A-1)^i]L_i + \frac{RT}{x_A(1-x_A)} \tag{3.48}$$

Substituting the value from Equation (3.48) in Equation (3.44), we get the analytical expression for $S_{CC}(0)$ as

$$S_{CC}(0) = RT\left[\sum_{i=0}^{n}(4i(i-1)x_A(1-x_A)(2x_A-1)^{i-2} - (4i+2)(2x_A-1)^i)L_i + \frac{RT}{x_A(1-x_A)}\right]^{-1} \tag{3.49}$$

The ideal value of concentration fluctuation in long wavelength limit ($S_{cc}^{id}(0)$) is calculated by simple relation

$$S_{CC}^{id}(0) = x_A x_B = x_A(1-x_A) \tag{3.50}$$

This ideal value is same for all liquid binary alloys. However, in real case, the value of $S_{CC}(0)$ is either greater or smaller than the ideal value depending on the nature of local arrangement of atoms in the alloys.

3.2.2 Concentration fluctuation in long wavelength limit for ternary liquid alloy

The expressions of concentration fluctuation in long wavelength limit for ternary A–B–C mixture (Bhatia & Ratti, 1977) are given as

$$S_{C_1C_1}(0) = \frac{RTG_{22}}{G_{11}G_{22} - (G_{12})^2}, \quad S^{id}_{C_1C_1}(0) = x_A(1 - x_A) \tag{3.51}$$

$$S_{C_2C_2}(0) = \frac{RTG_{11}}{G_{11}G_{22} - (G_{12})^2}, \quad S^{id}_{C_2C_2}(0) = x_B(1 - x_B) \tag{3.52}$$

$$S_{C_1C_2}(0) = \frac{-RTG_{12}}{G_{11}G_{22} - (G_{12})^2}, \quad S^{id}_{C_1C_2}(0) = -x_Ax_B \tag{3.53}$$

where

$$G_{11} = \frac{\partial^2 G_M}{\partial x_A^2}, \quad G_{22} = \frac{\partial^2 G_M}{\partial x_B^2}, \quad G_{12} = \frac{\partial^2 G_M}{\partial x_A \partial x_B} \tag{3.54}$$

The second derivative of G^{xs}_M are obtained by taking derivative of Equations (3.40a-3.40c) in the following forms

$$\begin{aligned}\frac{\partial^2 G^{xs}_M}{\partial x_A^2} &= 2x_B\frac{\partial Y_{AB}}{\partial x_A} + x_Ax_B\frac{\partial^2 Y_{AB}}{\partial x_A^2} + 2x_C\frac{\partial Y_{CA}}{\partial x_A} + x_Cx_A\frac{\partial^2 Y_{CA}}{\partial x_A^2} \\ &\quad + x_Bx_CL^0 + x_Bx_CL^0 \end{aligned} \tag{3.55a}$$

$$\begin{aligned}\frac{\partial^2 G^{xs}_M}{\partial x_B^2} &= 2x_A\frac{\partial Y_{AB}}{\partial x_B} + x_Ax_B\frac{\partial^2 Y_{AB}}{\partial x_B^2} + 2x_C\frac{\partial Y_{BC}}{\partial x_B} + x_Bx_C\frac{\partial^2 Y_{BC}}{\partial x_B^2} \\ &\quad + x_Ax_CL^1 + x_Ax_CL^1 \end{aligned} \tag{3.55b}$$

$$\begin{aligned}\frac{\partial^2 G^{xs}_M}{\partial x_A \partial x_B} &= Y_{AB} + x_A\frac{\partial Y_{AB}}{\partial x_A} + x_B\frac{\partial Y_{AB}}{\partial x_B} + x_Ax_B\frac{\partial^2 Y_{AB}}{\partial x_A \partial x_B} \\ &\quad + x_C(x_AL^0 + x_BL^1 + x_CL^2) + x_Cx_AL^0 + x_Bx_CL^1 \end{aligned} \tag{3.55c}$$

Now taking derivative of Equations (3.41a & 3.41b) w.r.t. x_A and x_B respectively, we get

$$\frac{\partial^2 Y_{AB}}{\partial x_A^2} = 2L_2^{A-B} + 6L_3^{A-B}(x_A - x_B) + 12L_4^{A-B}(x_A - x_B)^2 = \frac{\partial^2 Y_{AB}}{\partial x_B^2} \tag{3.56a}$$

$$\frac{\partial^2 Y_{BC}}{\partial x_B^2} = 2L_2^{B-C} + 6L_3^{B-C}(x_B - x_C) + 12L_4^{B-C}(x_B - x_C)^2 = \frac{\partial^2 Y_{BC}}{\partial x_C^2} \tag{3.56b}$$

Taking derivative of Equation (3.41b) w.r.t. x_A

$$\frac{\partial^2 Y_{AB}}{\partial x_A \partial x_B} = -2L_2^{A-B} - 6L_3^{A-B}(x_A - x_B) - 12L_4^{A-B}(x_A - x_B)^2 \tag{3.57a}$$

The second derivative of G_M^{xs} are used to obtain G_{11}, G_{22} and G_{12} from the following equations

$$G_{11} = \frac{\partial^2 G_M^{xs}}{\partial x_A^2} + RT\left(\frac{1}{x_A} + \frac{1}{x_C}\right), \tag{3.58}$$

$$G_{22} = \frac{\partial^2 G_M^{xs}}{\partial x_B^2} + RT\left(\frac{1}{x_B} + \frac{1}{x_C}\right), \tag{3.59}$$

$$G_{12} = \frac{\partial^2 G_M^{xs}}{\partial x_A x_B} + \frac{RT}{x_C} \tag{3.60}$$

Finally, the values of $S_{CC}(0)$ of ternary liquid alloys are computed from Equations (3.51).

3.3 Optimization process for linear interaction parameters

The optimization technique is a strong tool for obtaining desirable parameters. Optimization is a mathematical technique in which different model parameters are incorporated to predict various thermodynamic functions at different compositions and temperatures. This would serve as an alternative guide for the experimental work which may assist to reduce the risk and save operating costs.

3.3.1 Least square method

The least square method is used for computation parameters a_i and b_i of linear temperature-dependent interaction parameter ($L_i = a_i + b_i T$) of excess free energy of mixing. In this process, the experimental or literature values of H_M and S_M^{xs} at available concentrations are taken into account to compute fitting parameters a_i and b_i. The enthalpic and entropic contributions in the linear interaction parameters are described below.

Enthalpy of mixing contribution

For optimization of parameters a_i, Equation (3.25) is extended up to 4th power as

$$H_M = x_A x_B[a_0 + a_1(x_A - x_B) + a_2(x_A - x_B)^2 + a_3(x_A - x_B)^3 + a_4(x_A - x_B)^4] \tag{3.61}$$

For simplification, suppose $(x_A - x_B)^i = d_i$.
Taking summation over entire concentration range, we have

$$\sum\left(\frac{H_M}{x_A x_B}\right) = \sum a_0 + a_1 \sum d_1 + a_2 \sum d_2 + a_3 \sum d_3 + a_4 \sum d_4 \tag{3.62}$$

$$\sum\left(\frac{H_M d_1}{x_A x_B}\right) = a_0 \sum d_1 + a_1 \sum d_2 + a_2 \sum d_3 + a_3 \sum d_4 + a_4 \sum d_5 \tag{3.63}$$

$$\sum\left(\frac{H_M d_2}{x_A x_B}\right) = a_0 \sum d_2 + a_1 \sum d_3 + a_2 \sum d_4 + a_3 \sum d_5 + a_4 \sum d_6 \tag{3.64}$$

$$\sum\left(\frac{H_M d_3}{x_A x_B}\right) = a_0 \sum d_3 + a_1 \sum d_4 + a_2 \sum d_5 + a_3 \sum d_6 + a_4 \sum d_7 \tag{3.65}$$

$$\sum\left(\frac{H_M d_4}{x_A x_B}\right) = a_0 \sum d_4 + a_1 \sum d_5 + a_2 \sum d_6 + a_3 \sum d_7 + a_4 \sum d_8 \tag{3.66}$$

Writing Equations (3.61) – (3.66) in matrix form

$$\begin{pmatrix} \sum \frac{H_M}{x_A x_B} \\ \sum \frac{H_M d_1}{x_A x_B} \\ \sum \frac{H_M d_2}{x_A x_B} \\ \sum \frac{H_M d_3}{x_A x_B} \\ \sum \frac{H_M d_4}{x_A x_B} \end{pmatrix} = \begin{pmatrix} \sum 1 & \sum d_1 & \sum d_2 & \sum d_3 & \sum d_4 \\ \sum d_1 & \sum d_2 & \sum d_3 & \sum d_4 & \sum d_5 \\ \sum d_2 & \sum d_3 & \sum d_4 & \sum d_5 & \sum d_6 \\ \sum d_3 & \sum d_4 & \sum d_5 & \sum d_6 & \sum d_7 \\ \sum d_4 & \sum d_5 & \sum d_6 & \sum d_7 & \sum d_8 \end{pmatrix} \begin{pmatrix} a_0 \\ a_1 \\ a_2 \\ a_3 \\ a_4 \end{pmatrix} \tag{3.67}$$

Equation (3.67) is solved for the values of a_i in the following matrix equation

$$\begin{pmatrix} a_0 \\ a_1 \\ a_2 \\ a_3 \\ a_4 \end{pmatrix} = \begin{bmatrix} \sum 1 & \sum d_1 & \sum d_2 & \sum d_3 & \sum d_4 \\ \sum d_1 & \sum d_2 & \sum d_3 & \sum d_4 & \sum d_5 \\ \sum d_2 & \sum d_3 & \sum d_4 & \sum d_5 & \sum d_6 \\ \sum d_3 & \sum d_4 & \sum d_5 & \sum d_6 & \sum d_7 \\ \sum d_4 & \sum d_5 & \sum d_6 & \sum d_7 & \sum d_8 \end{bmatrix}^{-1} \begin{pmatrix} \sum \frac{H_M}{x_A x_B} \\ \sum \frac{H_M d_1}{x_A x_B} \\ \sum \frac{H_M d_2}{x_A x_B} \\ \sum \frac{H_M d_3}{x_A x_B} \\ \sum \frac{H_M d_4}{x_A x_B} \end{pmatrix} \tag{3.68}$$

The experimental values of enthalpy of mixing (H_M) of selected alloy at available concentration and temperature are used in Equation (3.68) and we get value of a_0, a_1, a_2, a_3, a_4.

Excess entropy of mixing contribution

For optimization of excess entropy contribution parameters b_i, Equation (3.22) is extended up to 4th power as

$$S_M^{xs} = x_A x_B[-b_0 - b_1(x_A - x_B) - b_2(x_A - x_B)^2 - b_3(x_A - x_B)^3 - b_4(x_A - x_B)^4] \quad (3.69)$$

For simplification, again suppose $(x_A - x_B)^i = d_i$.
Taking summation over the concentration range, we have

$$\sum\left(\frac{S_M^{xs}}{x_A x_B}\right) = \sum -b_0 - b_1\sum d_1 - b_2\sum d_2 - b_3\sum d_3 - b_4\sum d_4 \quad (3.70)$$

$$\sum\left(\frac{S_M^{xs} d_1}{x_A x_B}\right) = \sum -b_0 d_1 - b_1\sum d_2 - b_2\sum d_3 - b_3\sum d_4 - b_4\sum d_5 \quad (3.71)$$

$$\sum\left(\frac{S_M^{xs} d_2}{x_A x_B}\right) = \sum -b_0 d_2 - b_1\sum d_4 - b_3\sum d_4 - b_3\sum d_5 - b_4\sum d_6 \quad (3.72)$$

$$\sum\left(\frac{S_M^{xs} d_3}{x_A x_B}\right) = \sum -b_0 d_3 - b_1\sum d_4 - b_2\sum d_5 - b_3\sum d_6 - b_4\sum d_7 \quad (3.73)$$

$$\sum\left(\frac{S_M^{xs} d_4}{x_A x_B}\right) = \sum -b_0 d_4 - b_1\sum d_5 - b_2\sum d_6 - b_3\sum d_7 - b_4\sum d_8 \quad (3.74)$$

The parameters b_i are computed similar to Equation (3.68) in the following form

$$\begin{pmatrix} -b_0 \\ -b_1 \\ -b_2 \\ -b_3 \\ -b_4 \end{pmatrix} = \begin{bmatrix} \sum 1 & \sum d_1 & \sum d_2 & \sum d_3 & \sum d_4 \\ \sum d_1 & \sum d_2 & \sum d_3 & \sum d_4 & \sum d_5 \\ \sum d_2 & \sum d_3 & \sum d_4 & \sum d_5 & \sum d_6 \\ \sum d_3 & \sum d_4 & \sum d_5 & \sum d_6 & \sum d_7 \\ \sum d_4 & \sum d_5 & \sum d_6 & \sum d_7 & \sum d_8 \end{bmatrix}^{-1} \begin{pmatrix} \sum \frac{S_M^{xs}}{x_A x_B} \\ \sum \frac{S_M^{xs} d_1}{x_A x_B} \\ \sum \frac{S_M^{xs} d_2}{x_A x_B} \\ \sum \frac{S_M^{xs} d_3}{x_A x_B} \\ \sum \frac{S_M^{xs} d_4}{x_A x_B} \end{pmatrix} \quad (3.75)$$

The experimental values of excess entropy of mixing (S_M^{xs}) of selected alloy at available concentration and temperature are used in Equation (3.75) and we get the value b_0, b_1, b_2, b_3, b_4.

Finally linear temperature-dependent interaction parameters for excess free energy of mixing are obtained from Equation (3.6).

3.4 Optimization of exponential parameters

The optimization procedures for parameters of h_i and τ_i of Equation (3.8) are described below.
At temperature $T = T_1$, Equation (3.8) can be written as

$$L_i = h_i \exp\left(-\frac{T_1}{\tau_i}\right) \tag{3.76}$$

On solving

$$\frac{L_i}{h_i} = \exp\left(-\frac{T_1}{\tau_i}\right)$$

or,

$$\ln\left(\frac{\pm L_i}{\pm h_i}\right) = \exp\left(-\frac{T_1}{\tau_i}\right)$$

or,

$$\ln(\pm L_i) - \ln(\pm h_i) = -\frac{T_1}{\tau_i}$$

or,

$$\ln(\pm L_i) = \ln(\pm h_i) - \frac{T_1}{\tau_i} \tag{3.77}$$

Similarly, at temperature $T = T_2$ the interaction parameters become

$$L_i' = h_i \exp\left(-\frac{T_2}{\tau_i}\right) \tag{3.78}$$

Similar to Equation (3.77), we can obtain

$$\ln(\pm L_i') = \ln(\pm h_i) - \frac{T_2}{\tau_i} \tag{3.79}$$

Writing Equation (3.77) and (3.79) in matrix form, we have

$$\begin{bmatrix} \ln(\pm L_i) \\ \ln(\pm L_i') \end{bmatrix} = \begin{bmatrix} 1 & T_1 \\ 1 & T_2 \end{bmatrix} \begin{bmatrix} \ln(\pm h_i) \\ \frac{-1}{\tau_i} \end{bmatrix} \tag{3.80}$$

The values of L_i are calculated from linear temperature-dependent parameters a_i and b_i at temperatures T_1 and T_2. Then Equation (3.80) is solved for h_i and τ_i in the following

matrix equation.

$$\begin{bmatrix} \ln(\pm h_i) \\ \frac{-1}{\tau_i} \end{bmatrix} = \begin{bmatrix} 1 & T_1 \\ 1 & T_2 \end{bmatrix}^{-1} \begin{bmatrix} \ln(\pm L_i) \\ \ln(\pm L_i') \end{bmatrix} \tag{3.81}$$

Solving Equation (3.81), we obtain the values of h_i and τ_i

During the optimization process, two different temperatures, T_1 and T_2 are selected at which respective interaction parameters L_1 and L_2 should have same sign, otherwise the equations cannot be solved.

CHAPTER 4

4. RESULTS AND DISCUSSION

In chapter 3, we have presented the theoretical foundation in the framework of Redlich-Kister (R-K) polynomial in order to study the thermodynamic and structural properties of a few binary and ternary liquid alloys. The analytical expressions for the excess free energy of mixing (G_M^{xs}), activity of constituents (a_k), enthalpy of mixing (H_M) and concentration fluctuation in long wavelength limit ($S_{CC}(0)$) were derived.

In this chapter, the results and discussion of the present study are outlined. The present work basically stems from the study of excess free energy of mixing of binary liquid alloys. The calculation of G_M^{xs} in the framework of R-K polynomial involves interaction energy parameters defined in Equation (3.5). Thus it is rational to discuss first the role of the parameters on G_M^{xs} for the computation of other thermodynamic and structural properties. For the computation of the mixing properties, we have first optimised the interaction energy parameters of the R-K polynomial for G_M^{xs} for binary Al–Fe, Al–Mn, Al–Ti, and Li–Mg liquid alloys and ternary liquid Al–Li–Zn alloy. The thermodynamic and structural functions of these alloys were then computed at different temperatures and compositions.

4.1 Effect of interaction parameters on G_M^{xs}

The excess free energy of mixing (G_M^{xs}) of alloys is a function of composition and temperature. The interaction energy parameters of R-K polynomials are basically assumed to vary linearly with temperature (Equation (3.6)). The parameters a_i and b_i are considered to arise from the contribution of enthalpy of mixing and excess entropy of mixing respectively. In this formulation, the enthalpy of mixing and excess entropy of mixing are found to be temperature-independent (T-independent) functions. The variation of G_M^{xs} with temperature is due to the energy contribution of excess entropy of mixing. When the values of coefficients $b_i > 2R$, where R is universal gas constant, then artificial inverted miscibility gap may appear at higher temperatures in some alloys (Kaptay, 2004). The large value of b_i means a high contribution of entropy of mixing in the alloys. These coefficients may lead to incorrect predictions when extrapolated to higher-order systems. The contribution of various terms of the interaction parameter (L_0, L_1, L_2 & L_3) with the same typical value of 20000 J/mol in the $G_M^{xs}$are shown in Figure 3. The calculated values of G_M^{xs} with contribution of individual even term (L_0

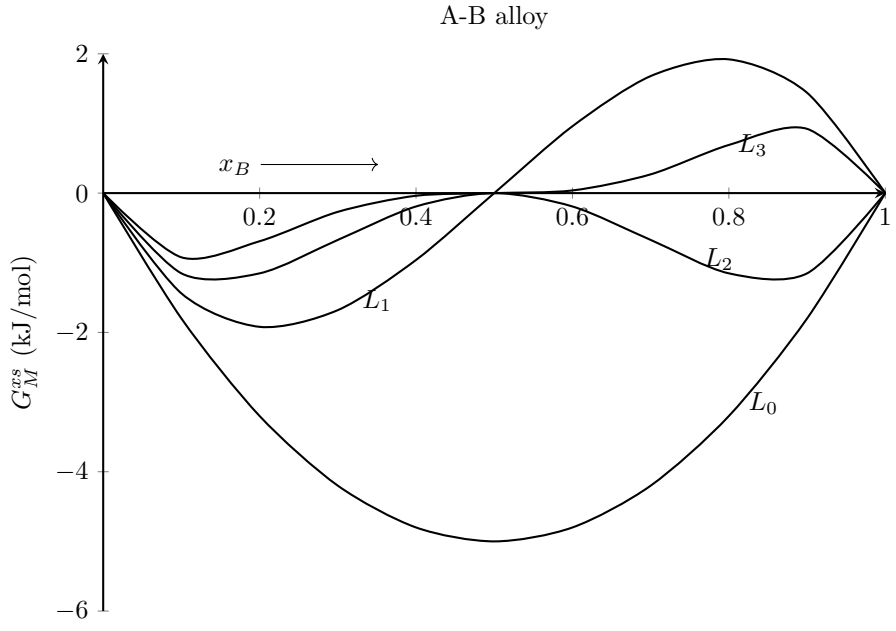

Figure 3: Variation of G_M^{xs} of A–B alloy with interaction parameters L_i = 20000 J/mol.

& L_2) have positive sign throughout whole concentration and that from odd terms (L_1 & L_3) have changed the sign at equi-atomic compositions of the system. The value of G_M^{xs} has been found to decrease on increasing the order of terms L_0, L_1, L_2 & L_3. When the first term L_0 alone is used, the system always exhibits regular-solution behaviour. Symmetric or asymmetric behaviour and the miscibility gap observed in some liquid alloys may be described using at least first two terms of R-K polynomials. To eliminate the artificial miscibility gap, Kaptay (2004) assumed the interaction parameters to be exponential temperature dependent (Equation (3.8)). In this model, τ_i must be positive, so the interaction energy decreases with increase in temperature. Otherwise, the excess free energy of mixing and other thermodynamic functions deviate from ideal behaviour while extrapolating at higher temperatures. As H_M varies with temperature under consideration of exponential parameters, it may be assumed that the mixing properties of alloys are correctly calculated at different temperatures.

The effect of linear (this work and Cost 507) and exponential interaction parameters on G_M^{xs} at $x_{Fe} = 0.5$ for Al–Fe system is observed nearly the same near the melting temperature (Figure 4). It is observed that with use of linear parameters, G_M^{xs} varies more rapidly than with the exponential parameters.

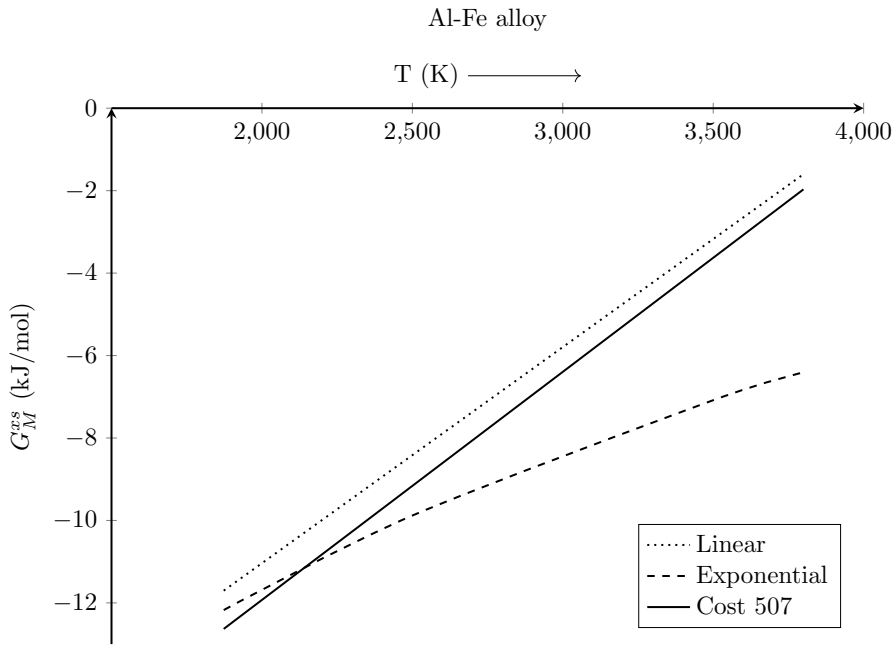

Figure 4: Variation of G_M^{xs} at x_{Fe} = 0.5 of liquid Al–Fe alloy with temperature.

4.2 Thermodynamic properties of binary liquid alloys

In this section, results and discussion associated with the thermodynamic properties, such as the excess free energy of mixing (G_M^{xs}) and activity of constituents (a_k) of binary and ternary liquid alloys are presented. Furthermore, the enthalpy of mixing (H_M) of binary Li-Mg and ternary Al-Li-Zn alloys are also presented in the following sub-sections.

4.3 Excess free energy of mixing (G_M^{xs}) for binary liquid alloys

4.3.1 G_M^{xs} for liquid Al–Fe alloy

The binary Al–Fe and Al–Fe-based higher order alloys can be used in high-temperature appliances as they have superior oxidation resistance, reduced weight, and improved mechanical strength (Basuki et al., 2017). For these favourable qualities, Al–Fe alloys are mixed with various metals (Si, Zn, Mg, Ni, Cr, etc.) at various compositions to produce higher order alloys such as Al–Fe–Si, Al–Fe–Zn, Al–Fe–Mg, Al–Fe–Ni–Cr alloys. In this section, we have investigated the excess free energy of mixing (G_M^{xs}) of Al–Fe system at different temperatures using the R-K polynomial.

The experimental data of H_M and S_M^{xs} for Al–Fe alloy at melting temperature (1873 K) were taken from Hultgren et al. (1973). Using the least square fit technique i.e., the optimization process mentioned in Section 3.3, the linear T-dependent interaction

parameters were calculated for G_M^{xs}. Further, the parameters (h_i & τ_i) of exponential T-dependent interaction parameters were then calculated using these linear T-dependent parameters by following the steps mentioned in the Section 3.4. The optimised interaction parameters of this work and Cost 507 are presented in Table 1. The interaction parameters of Table 1 were utilized in Equation (3.4) to calculate G_M^{xs} of Al–Fe system at 1873 K, 2500 K, 3500 K and 3800 K at various compositions.

Table 1: Optimised coefficients of R-K polynomial for G_M^{xs} of liquid Al–Fe alloy

	Interaction Parameters (J/mol)		
	Exponential fit	Linear fit	Cost 507 (Ansara et al., 1998)
L_0	$-90837.2\exp(-3.33\times10^{-4}T)$	$-86088 + 20.96T$	$-91976.5 + 22.1314T$
L_1	$-32581.6\exp(-7.26\times10^{-4}T)$	$-26415 + 10.65T$	$-5672.58 + 4.8728T$
L_2	$-4458.6\exp(-1.66\times10^{-5}T)$	$-4458 + 0.07T$	121.9

Table 2: G_M^{xs} of liquid Al–Fe alloy at 1873 K and 2500 K

x_{Fe}	G_M^{xs} (kJ/mol)							
	T=1873 K					T=2500 K		
	Linear fit	Exponential fit	Experimental*	Cost 507	Ref.**	Linear fit	Exponential fit	Cost 507
0.1	-4.927	-5.234	-4.866	-4.291	-4.955	-3.260	-4.185	-2.823
0.2	-8.359	-8.843	-8.331	-7.745	-8.747	-5.612	-7.079	-5.232
0.3	-10.519	-11.074	-10.538	-10.316	-11.124	-7.195	-8.889	-7.145
0.4	-11.587	-12.130	-11.625	-11.959	-12.222	-8.110	-9.781	-8.482
0.5	-11.703	-12.174	-11.729	-12.631	-12.250	-8.416	-9.881	-9.162
0.6	-10.966	-11.327	-10.968	-12.290	-11.369	-8.131	-9.272	-9.107
0.7	-9.433	-9.669	-9.430	-10.896	-9.682	-7.231	-7.998	-8.239
0.8	-7.119	-7.238	-7.119	-8.408	-7.210	-5.653	-6.061	-6.482
0.9	-3.997	-4.030	-3.996	-4.789	-4.013	-3.292	-3.422	-3.760

*Hultgren et al. (1973),**Adhikari et al. (2014)

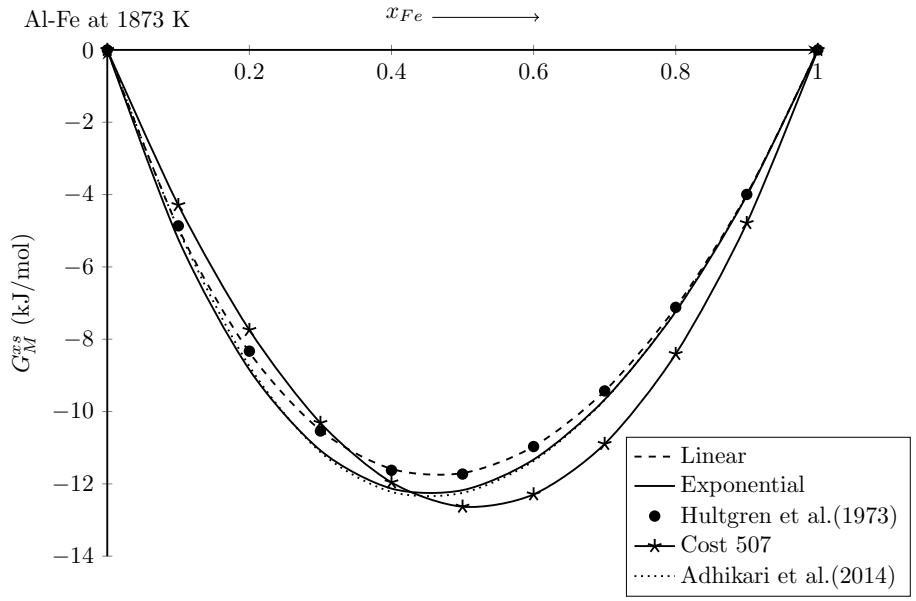

Figure 5: G_M^{xs} of liquid Al–Fe alloy at 1873 K.

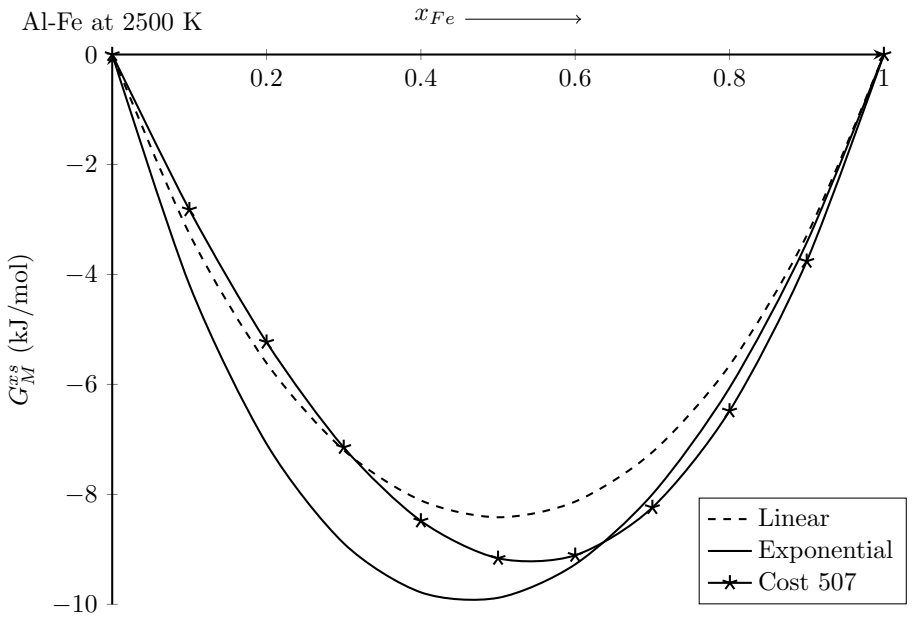

Figure 6: G_M^{xs} of liquid Al–Fe alloy at 2500 K.

These computed values, along with the experimental data of Hultgren et al. (1973) and computed values from Adhikari et al. (2014) are displayed in Tables 2-3 and plotted in Figures 5-8. The computed values of G_M^{xs} at 1873 K are found in good agreement with experimental and literature data, whereas they differ slightly from Cost 507 (Figure 5). At $x_{Fe} = 0.6$ and 1873 K, the experimental and computed values of G_M^{xs} are respectively found to be (-10.968 ± 2.09) kJ/mol (Hultgren et al., 1973), and -10.966 kJ/mol (using linear parameters) and -11.327 kJ/mol (using exponential parameters). These investigations validate the present optimisation procedures and hence these parameters can be used for further computations of thermodynamic and structural functions. At 2500 K, G_M^{xs} computed using exponential T-dependent interaction parameters (exponential parameter) and linear T-dependent interaction parameters (linear parameters) in this work are found to differ from each other at a low concentration of x_{Fe} (Figure 6). At temperatures 3500 K and 3800 K, the plots of the G_M^{xs} using linear parameters are found S-shaped whereas those with exponential parameters are obtained symmetric about the equi-atomic composition (Figures 7 and 8). The value of G_M^{xs} at 3800 K changes from negative to positive in the region $x_{Fe} < 0.2$ while linear parameters are used. In general, as temperature rises, G_M^{xs} should approach the ideal behaviour (Kaptay, 2012). This transition indicates that alloy changes its phase from ordering to segregating at higher temperatures. This unusual tendency is termed as artificial inverted miscibility gap. The value of b_0 for L_0 in the linear model were found to be 20.96 J/(mol K) (linear fit) and 22.1314 J/(mol K) (Cost 507) in Table 1 which are greater than 2R, leading to the artifact. When exponential parameters were used, such transition was not observed. Hence, it can

Table 3: G_M^{xs} of liquid Al–Fe alloy at 3500 K and 3800 K

x_{Fe}	G_M^{xs} (kJ/mol)					
	T=3500 K			T=3800 K		
	Linear fit	Exponential fit	Cost 507	Linear fit	Exponential fit	Cost 507
0.1	-0.602	-2.977	-0.480	0.196	-2.697	0.223
0.2	-1.230	-5.022	-1.223	0.085	-4.542	-0.020
0.3	-1.894	-6.307	-2.088	-0.304	-5.699	-0.571
0.4	-2.565	-6.964	-2.936	-0.902	-6.293	-1.273
0.5	-3.174	-7.083	-3.629	-1.601	-6.410	-1.969
0.6	-3.609	-6.717	-4.029	-2.252	-6.095	-2.506
0.7	-3.720	-5.876	-4.001	-2.667	-5.352	-2.729
0.8	-3.317	-4.529	-3.408	-2.616	-4.146	-2.486
0.9	-2.167	-2.608	-2.119	-1.830	-2.400	-1.627

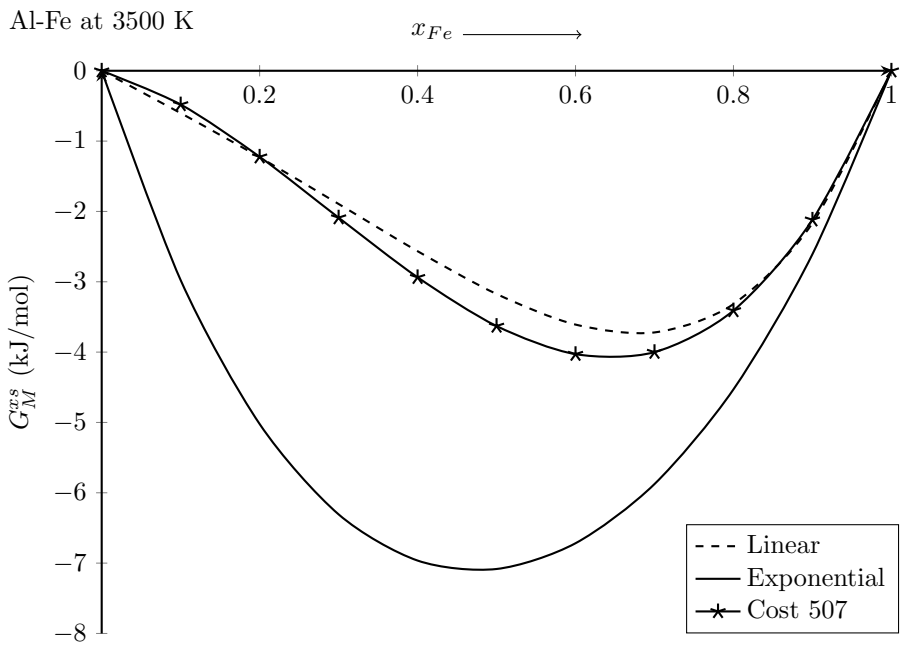

Figure 7: G_M^{xs} of liquid Al–Fe alloy at 3500 K.

be concluded that exponential parameters are more appropriate to explain the mixing behaviour of the system at higher temperatures.

4.3.2 G_M^{xs} for liquid Al–Mn alloy

The Al–Mn system has been a matter of interest for a long time due to its wide range applications, such as in manufacturing foil, roof sheets, cooking utensils, rigid containers, bearing assembly, step soldering, and radiation shielding. So, several researchers (Bergman et al., 1994; Jansson, 1992; Du et al., 2007; Shukla & Pelton, 2009; R. K. Gohivar, Yadav, et al., 2020) have studied the mixing properties of the

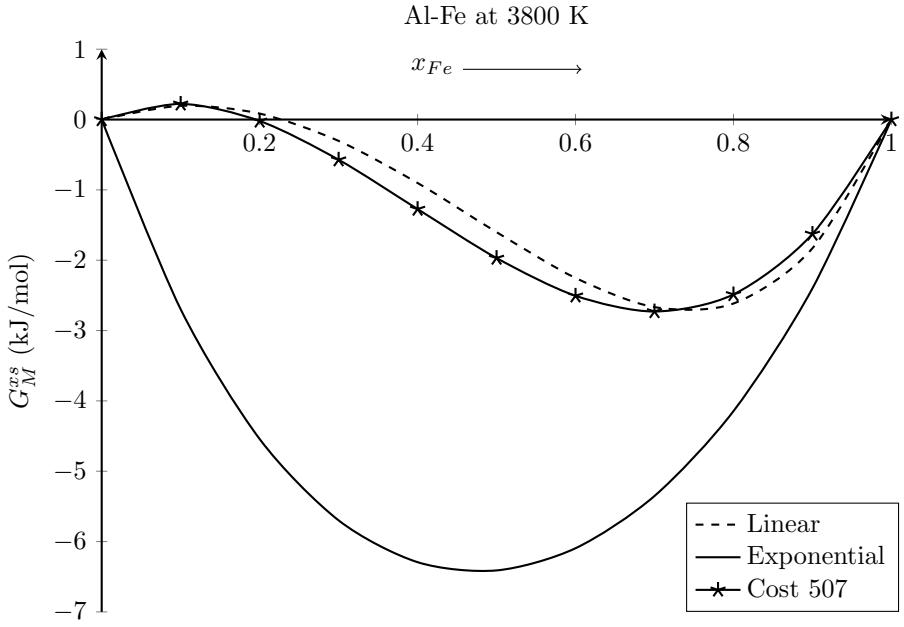

Figure 8: G_M^{xs} of liquid Al–Fe alloy at 3800 K.

system using different experimental methods and theoretical models. Du et al. (2007) detected the appearance of the inverted miscibility gap in the Al–Mn system at 4227 K while assuming the linear T-dependent interaction parameters. Shukla & Pelton (2009) assessed thermodynamic properties of Al–Mn and predicted Al–Mn-based ternary Al–Mn–Mg system using FactSage thermochemical software in the framework of modified quasi-chemical model.

Table 4: Optimised coefficients of R-K polynomial for G_M^{xs} of liquid Al–Mn alloy

	Interaction parameters (J/mol)		
	Exponential	Cost 507	Du et al. (2007)
L_0	$-80175.0\exp(-7.14\times10^{-4}T)$	$-66174 + 27.0988T$	$-70584.9 + 28.22693T$
L_1	$-47609.8\exp(-3.16\times10^{-3}T)$	$-7509 + 5.4836T$	$-13293.5 + 9.82551T$
L_2	-2639	-2639	-

To predict G_M^{xs} of Al–Mn liquid alloy at higher temperatures, we took the linear T-dependent interaction parameters of the R-K model from Cost 507 and Du et al. (2007). The values of parameter b_0 in Cost 507 and Du et al. (2007) were respectively 27.0988 J/(mol K) and 28.22693 J/(mol K) which are greater than 2R, leading to the artifact. According to Abe et al. (2012), there might be an inverted miscibility gap at higher temperatures when b_0 is greater than 2R. Therefore, exponential parameters were optimised by taking linear parameters from Cost 507 following a similar procedure as for the Al–Fe system. All these interaction parameters are displayed in Table 4.

We have computed the compositional dependence of G_M^{xs} of binary Al–Mn alloy at

Table 5: G_M^{xs} of liquid Al–Mn alloy at 1570 K and 1900 K

x_{Mn}	G_M^{xs} (kJ/mol)						
	T=1570 K				T=1900 K		
	Ref.1*	Exponential fit	Cost 507	Ref.2**	Ref.1*	Exponential fit	Cost 507
0.1	-2.211	-2.511	-2.199	-3.382	-1.139	-2.002	-1.264
0.2	-3.998	-4.335	-3.827	-5.857	-2.197	-3.437	-2.222
0.3	-5.337	-5.564	-4.958	-7.485	-3.109	-4.396	-2.928
0.4	-6.202	-6.267	-5.643	-8.322	-3.811	-4.942	-3.410
0.5	-6.567	-6.485	-5.907	-8.426	-4.238	-5.116	-3.672
0.6	-6.407	-6.235	-5.749	-7.857	-4.327	-4.931	-3.690
0.7	-5.696	-5.508	-5.143	-6.671	-4.012	-4.376	-3.417
0.8	-4.408	-4.270	-4.038	-4.928	-3.229	-3.415	-2.781
0.9	-2.518	-2.463	-2.358	-2.685	-1.913	-1.985	-1.683

*Du et al. (2007), **Bergman et al. (1994)

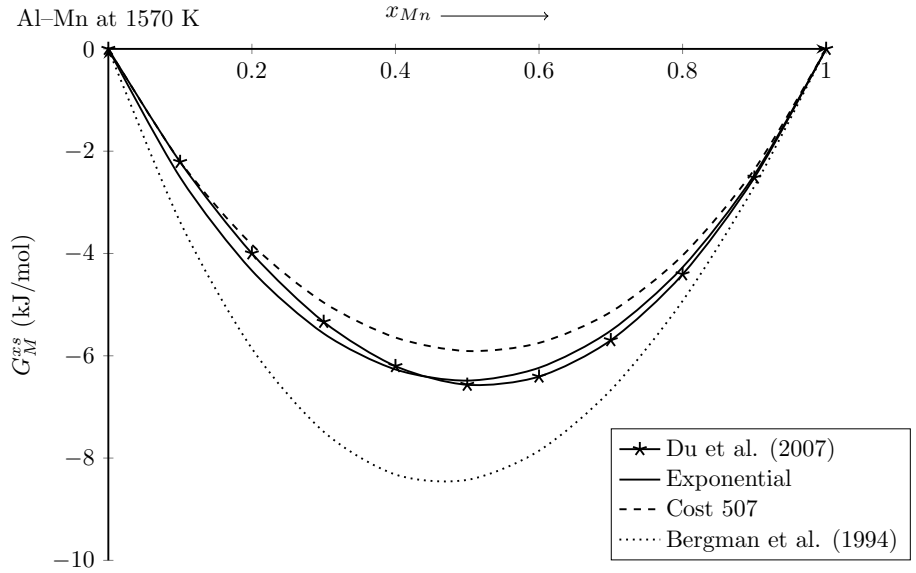

Figure 9: G_M^{xs} of liquid Al–Mn alloy at 1570 K.

temperatures 1570 K, 1900 K, 2200 K and 2500 K using the parameters of Table 4 in Equation (3.4). Bergman et al. (1994) optimised and used T-independent interaction parameters of Al–Mn alloy at melting temperature (1570 K) to calculate G_M^{xs}. The calculated values of G_M^{xs} are displayed in Table 5and plotted in Figures 9-12 as a function of the concentration of Mn (x_{Mn}). At temperature 1570 K, the calculated values of G_M^{xs} using exponential parameters are found in excellent agreement with the values computed using linear parameters of Du et al. (2007). But they differ slightly with the values calculated using linear parameters of Cost 507 and greatly with the values of Bergman et al. (1994). When the temperature of the system is increased to 1900 K, there is distinguishable variation among the computed values of G_M^{xs} using above mentioned parameters (Figure 10). The plot of G_M^{xs} at 2200 K and 2500 K, using linear parameters shows unsymmetrical behaviour. The values of G_M^{xs} at 2500 K using linear parameters shift

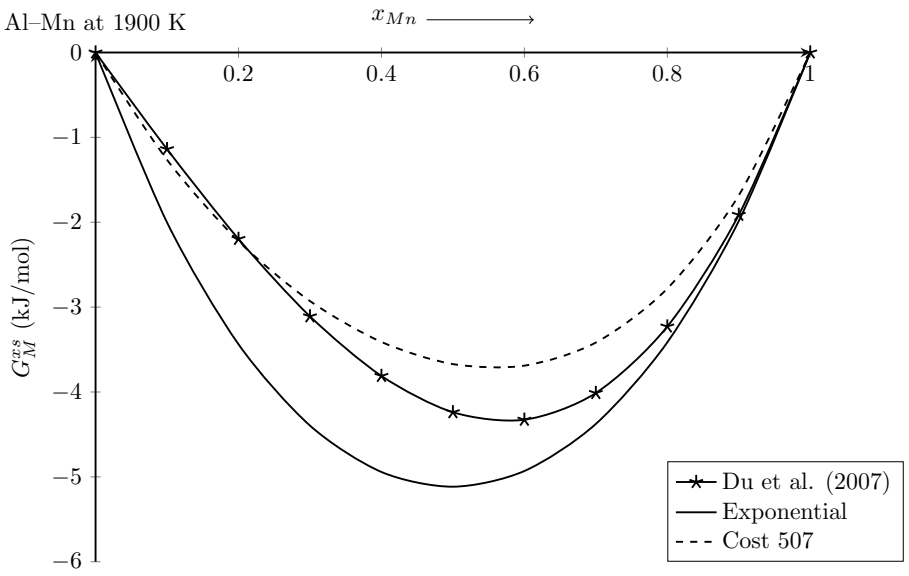

Figure 10: G_M^{xs} of liquid Al–Mn alloy at 1900 K.

Table 6: G_M^{xs} of liquid Al–Mn alloy at 2200 K and 2500 K

x_{Mn}	G_M^{xs} (kJ/mol)					
	T=2200 K			T=2500 K		
	Ref.*	Exponential fit	Cost 507	Ref.*	Exponential fit	Cost 507
0.1	-0.164	-1.640	-0.414	0.810	-1.350	0.436
0.2	-0.559	-2.796	-0.764	1.079	-2.281	0.695
0.3	-1.083	-3.556	-1.083	0.943	-2.882	0.762
0.4	-1.637	-3.986	-1.380	0.537	-3.217	0.650
0.5	-2.121	-4.124	-1.639	-0.004	-3.324	0.393
0.6	-2.436	-3.982	-1.818	-0.545	-3.215	0.055
0.7	-2.481	-3.549	-1.848	-0.950	-2.879	-0.279
0.8	-2.157	-2.787	-1.638	-1.085	-2.278	-0.496
0.9	-1.363	-1.633	-1.070	-0.813	-1.347	-0.457

*Du et al. (2007)

from negative to positive in the region $x_{Mn} < 0.6$ indicating the phase transformation from ordering to segregating. However, the computed values using exponential parameters at all above mentioned temperatures are symmetrical about the equiatomic composition which corresponds that there no such unusual phase transformation (Figure 12). Present investigation suggests that at higher temperatures exponential parameters well explain G_M^{xs} of the system as compared to the linear parameters.

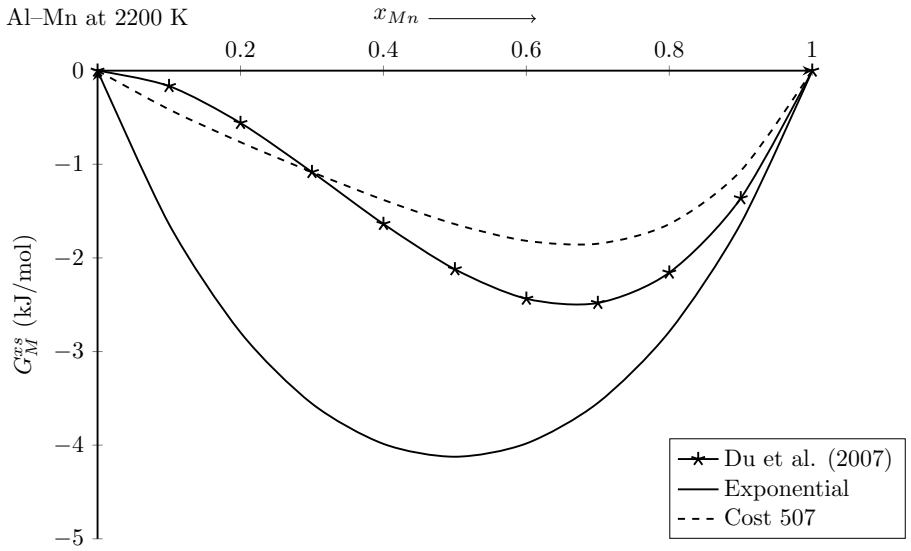

Figure 11: G_M^{xs} of liquid Al–Mn alloy at 2200 K.

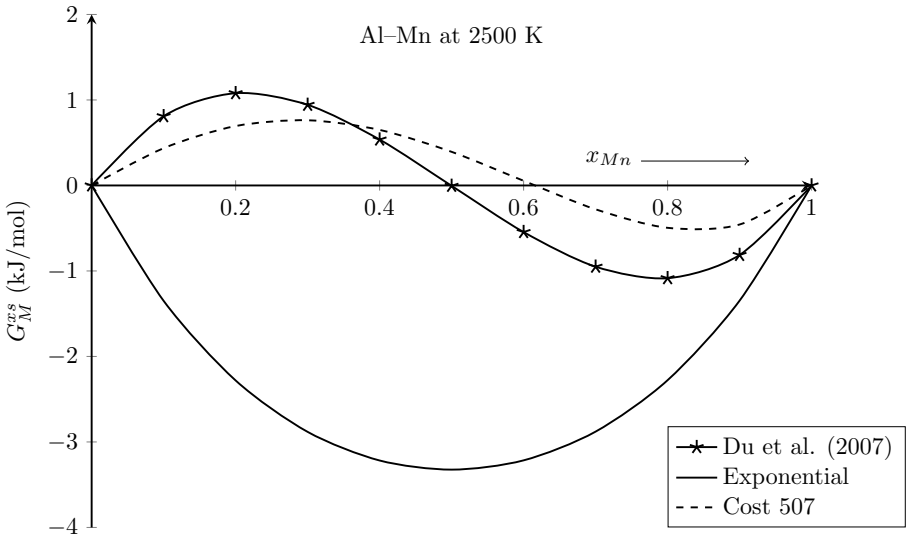

Figure 12: G_M^{xs} of liquid Al–Mn alloy at 2500 K.

4.3.3 G_M^{xs} for liquid Al–Ti alloy

The fabrication of materials for their various applications at high temperatures is one of the major tasks for researchers working in this field. Such high-temperature materials have been used as exhaust valves and turbine blades in aerospace and automotive vehicles. Al–Ti and Ti–based alloys have high melting temperatures, lightweight as well as high strength and hence they are often preferred as high-temperature materials. Therefore, knowledge of mixing properties of Al–Ti alloys is mandatory and hence many researchers have so far studied the phase diagram of this system. Witusiewicz et al. (2008) optimised the thermodynamic parameters of the Al–Ti system taking account of G_M^{xs} of different

phases using computer-based software PARROT optimizer of Thermo-Calc.

Table 7: Optimised coefficients of R-K polynomial for G_M^{xs} of liquid Al–Ti alloy

Interaction parameters (J/mol)		
	Exponential	Cost 507
L_0	$-134188.7\exp(-5.68\times10^{-4}T)$	$-108250+38T$
L_1	$-4343504.6\exp(-7.01\times10^{-3}T)$	$-6000+5T$
L_2	$41482.8\exp(-6.85\times10^{-4})$	15000
	F. Zhang et al. (1997)	Witusiewicz et al. (2008)
L_0	$-111811.4+34.199T$	$-118048+41.972T$
L_1	$9746.9+7.69T$	$-23613+19.704T$
L_2	-	$34757-13.844T$

Table 8: G_M^{xs} of liquid Al–Ti alloy at 1500 K and 2000 K

x_{Ti}	G_M^{xs} (kJ/mol)							
	T=1500 K				T=2000 K			
	Cost 507	Exponential fit	Ref.1*	Ref.2**	Cost 507	Exponential fit	Ref.1*	Ref.2**
0.1	-3.641	-4.308	-3.913	-3.724	-1.751	-3.275	-2.097	-1.525
0.2	-7.192	-8.321	-7.638	-7.438	-3.912	-6.294	-4.533	-3.533
0.3	-10.133	-11.540	-10.919	-10.600	-5.933	-8.703	-7.005	-5.598
0.4	-12.084	-13.611	-13.501	-12.802	-7.404	-10.250	-9.212	-7.359
0.5	-12.813	-14.320	-15.128	-13.773	-8.063	-10.782	-10.853	-8.526
0.6	-12.228	-13.599	-15.545	-13.373	-7.788	-10.250	-11.625	-8.875
0.7	-10.385	-11.520	-14.496	-11.598	-6.605	-8.703	-11.228	-8.251
0.8	-7.480	-8.298	-11.726	-8.579	-4.680	-6.293	-9.359	-6.566
0.9	-3.857	-4.292	-6.979	-4.580	-2.327	-3.274	-5.717	-3.799

*F. Zhang et al. (1997),**Witusiewicz et al. (2008)

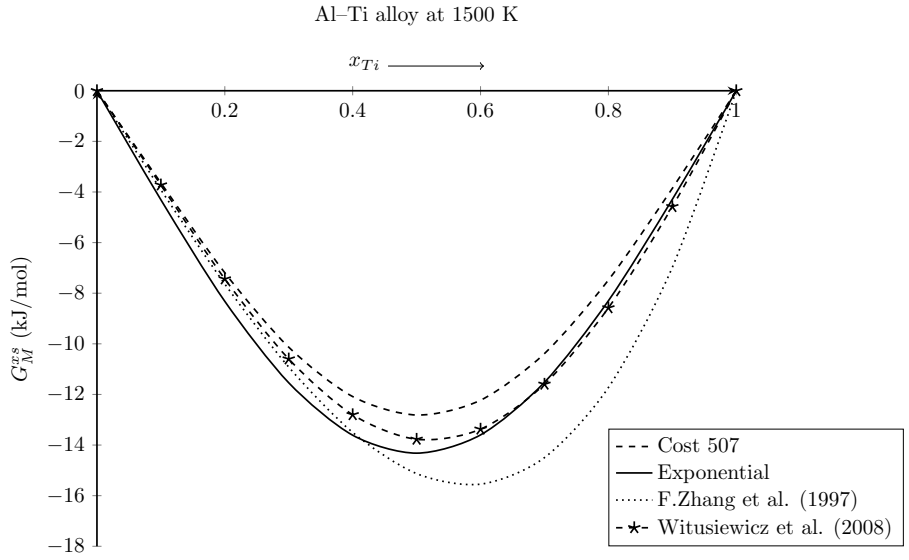

Figure 13: G_M^{xs} of liquid Al–Ti alloy at 1500 K.

The linear parameters from Cost 507, F. Zhang et al. (1997) and Witusiewicz et al. (2008) were used to compute G_M^{xs} of Al–Ti system at temperatures 1500 K, 2000 K, 2500 K and

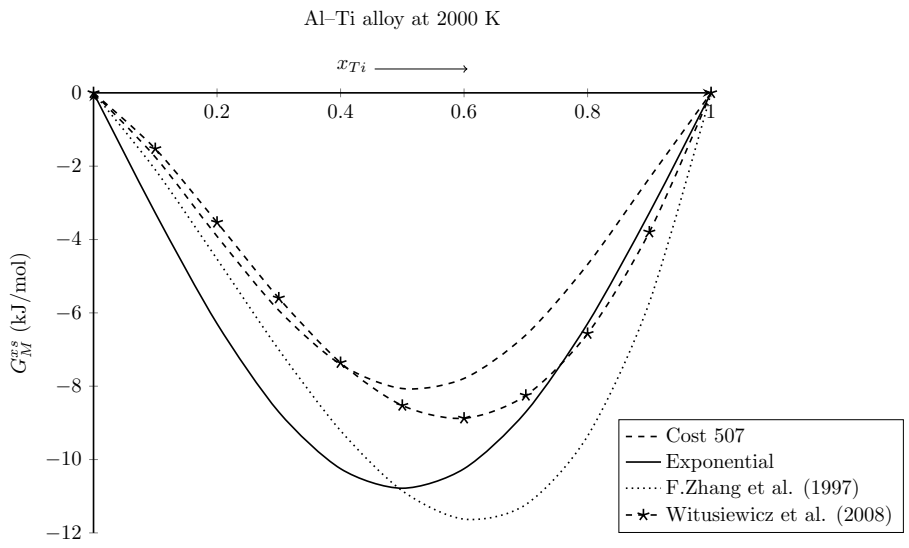

Figure 14: G_M^{xs} of liquid Al–Ti alloy at 2000 K.

Table 9: G_M^{xs} of liquid Al–Ti alloy at 2500 K and 2700 K

x_{Ti}	G_M^{xs} (kJ/mol)							
	T=2500 K				T=2700 K			
	Cost 507	Exponential fit	Ref.1*	Ref.2**	Cost 507	Exponential fit	Ref.1*	Ref.2**
0.1	0.140	-2.492	-0.281	0.674	0.896	-2.233	0.445	1.554
0.2	-0.632	-4.765	-1.428	0.372	0.680	-4.262	-0.186	1.934
0.3	-1.733	-6.568	-3.091	-0.595	-0.053	-5.869	-1.525	1.405
0.4	-2.724	-7.722	-4.924	-1.916	-0.852	-6.895	-3.208	0.261
0.5	-3.313	-8.119	-6.578	-3.280	-1.413	-7.248	-4.868	-1.181
0.6	-3.348	-7.722	-7.706	-4.378	-1.572	-6.895	-6.138	-2.579
0.7	-2.825	-6.568	-7.960	-4.904	-1.313	-5.869	-6.653	-3.565
0.8	-1.880	-4.765	-6.992	-4.553	-0.760	-4.262	-6.046	-3.747
0.9	-0.797	-2.492	-4.455	-3.019	-0.185	-2.233	-3.950	-2.706

*F. Zhang et al. (1997), **Witusiewicz et al. (2008)

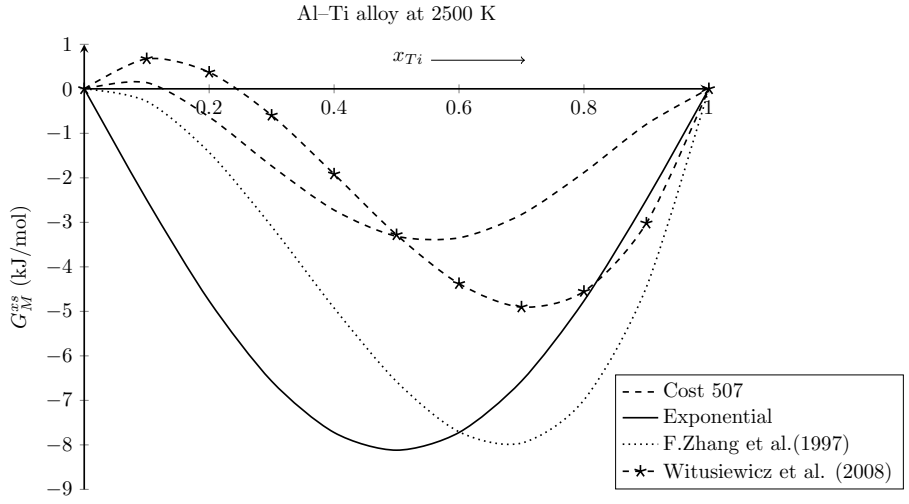

Figure 15: G_M^{xs} of liquid Al–Ti alloy at 2500 K.

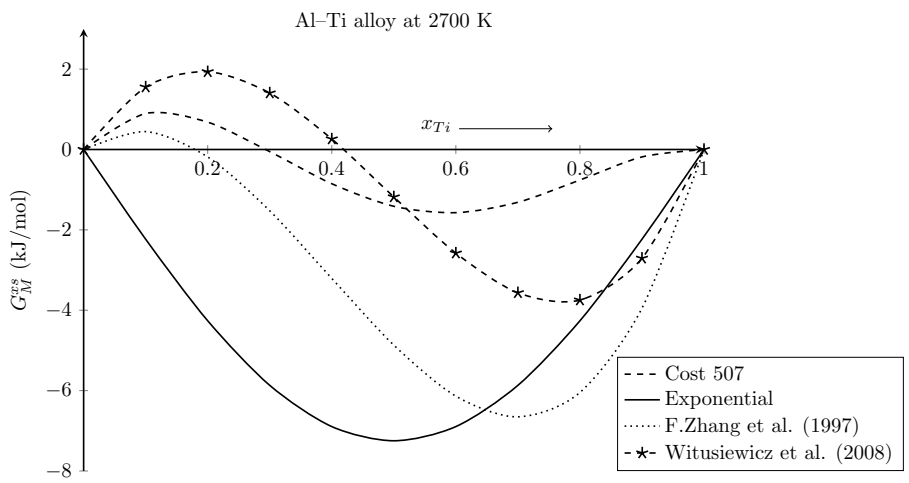

Figure 16: G_M^{xs} of liquid Al–Ti alloy at 2700 K.

2700 K using Equation (3.4). An artificial miscibility gap was observed at 2000 K and above. The presence of an artificial miscibility gap was due to b_0>2R. Therefore, the interaction parameters were re-optimised assuming them to be exponential T-dependent. For this purpose, we took interaction parameters of Witusiewicz et al. (2008) as reference. These linear and exponential interaction parameters are presented in Table 7.

We took exponential interaction parameters of Table 7 and employed Equation (3.4) to compute G_M^{xs} at above mentioned temperatures as a function of concentration. The computed values of G_M^{xs} using linear and exponential parameters are tabulated in Table 8 and plotted in Figures 13-15. It can be observed that as the temperature of system is gradually raised above 1500 K, the plots of G_M^{xs} using linear parameters show unusual variations, termed as the artificial miscibility gap. However, the plots of G_M^{xs} using exponential parameters did not show such behaviours. Hence, the present theoretical investigations revealed that exponential T-dependent interaction parameters were found to be more appropriate in predicting G_M^{xs} at elevated temperatures. Additionally, the plots of G_M^{xs} gradually shallow up with an increase in the temperature indicating a decrease in the complex forming tendency of the system.

4.3.4 G_M^{xs} for liquid Li–Mg alloy

Lithium-magnesium-based alloys are low-density metallic compounds and hence are mostly preferred in portable electronics, aerospace, and the automotive industries (Wu et al., 2015). Li–Mg alloys, in particular, are incredibly light, mechanically strong and stiff. Wang, Du, & Liu (2011) calculated the phase equilibria of the system using the interaction parameters of Gasior et al. (1996) and Braga et al. (2000). They noticed the appearance of an inverted miscibility gap above 973 K. In order to remove the gap at its melting

temperature, they re-evaluated the parameters taking account of new experimental data.

Table 10: Optimised coefficients of R-K polynomial for G_M^{xs} of liquid Li–Mg alloy

	Interaction parameters (J/mol)	
	Linear	Exponential
L_0	$-21318 + 2.9T$	$-31362.0\exp(-1.46\times10^{-4}T)$
L_1	$7930 - 15.1T$	$1154251.0\exp(-1.60\times10^{-2}T)$
L_2	$10668 - 8.9T$	$12138.0\exp(-1.34\times10^{-3}T)$
L_3	$-7765 + 7.4T$	$-9382.0\exp(-1.67\times10^{-3}T)$
	Wang, Du, & Liu (2011)	Cost 507 (Ansara et al., 1998)
L_0	$-13172 - 4.3009T$	$-14935 + 10.371T$
L_1	$912 + 2.7115T$	$-1789 + 1.143T$
L_2	2531	$6533 - 6.6915T$

Table 11: G_M^{xs} of liquid Li–Mg alloy at 1000 K and 1300 K

x_{Mg}	G_M^{xs} (kJ/mol)							
	T=1000 K					T=1300 K		
	Linear fit	Exponential fit	Experimental*	Ref.**	Cost 507	Linear fit	Exponential fit	Ref.**
0.1	-2.095	-1.558	-2.086	-1.369	-0.466	-2.336	-1.515	-1.427
0.2	-3.563	-2.829	-3.54	-2.573	-0.801	-3.798	-2.739	-2.701
0.3	-4.434	-3.791	-4.406	-3.517	-1.018	-4.533	-3.650	-3.720
0.4	-4.757	-4.400	-4.740	-4.131	-1.128	-4.682	-4.218	-4.401
0.5	-4.596	-4.612	-4.598	-4.368	-1.141	-4.376	-4.413	-4.691
0.6	-4.034	-4.393	-4.050	-4.208	-1.066	-3.737	-4.214	-4.556
0.7	-3.169	-3.743	-3.194	-3.651	-0.91	-2.880	-3.621	-3.991
0.8	-2.117	-2.707	-2.136	-2.727	-0.677	-1.908	-2.665	-3.011
0.9	-1.011	-1.396	-1.020	-1.484	-0.373	-0.919	-1.417	-1.659

*Hultgren et al. (1973), **Wang, Du, & Liu (2011)

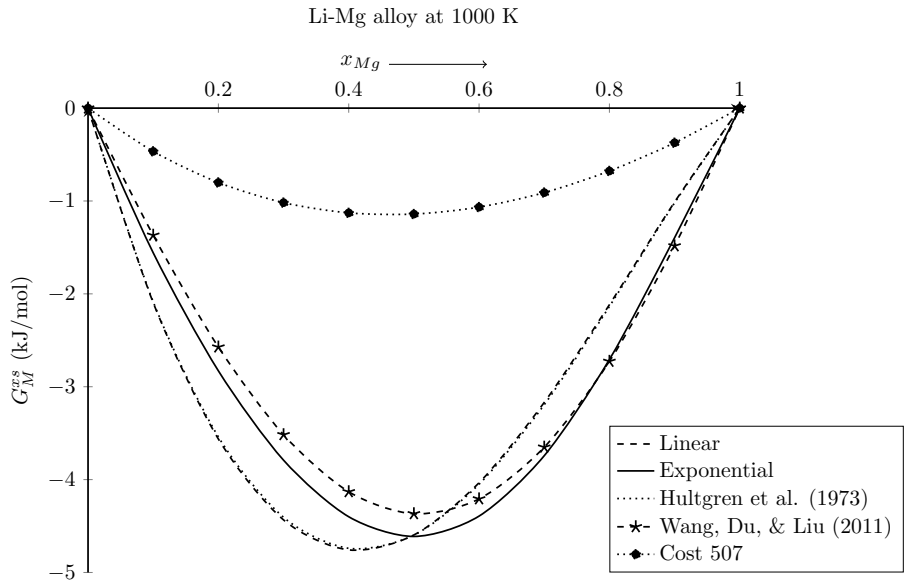

Figure 17: G_M^{xs} of liquid Li–Mg alloy at 1000 K.

We took the experimental data of H_M and S_M^{xs} for liquid Li–Mg alloy from Hultgren et al. (1973). These data were used to optimise the linear T-dependent interaction parameters

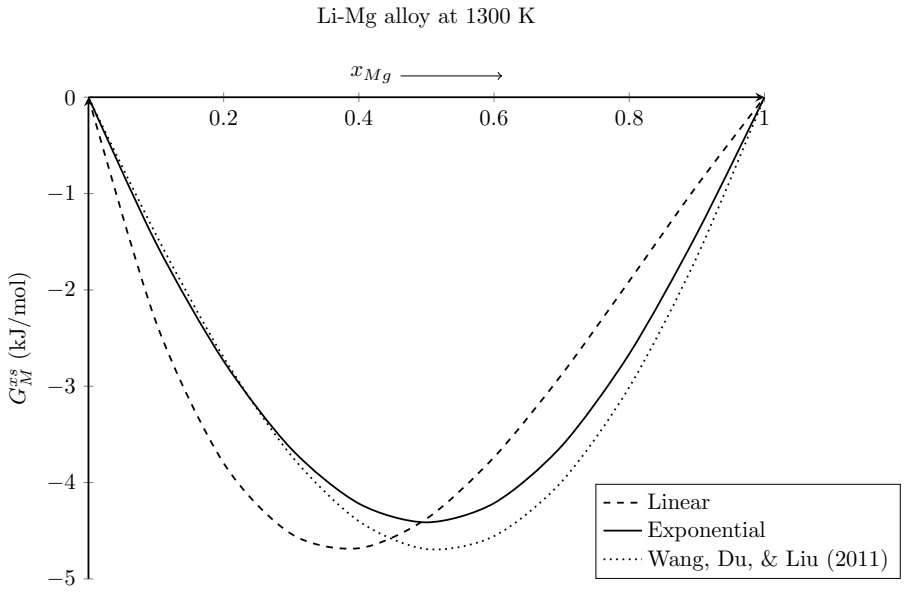

Figure 18: G_M^{xs} of liquid Li–Mg alloy at 1300 K.

Table 12: G_M^{xs} of liquid Li–Mg alloy at 1900 K and 2200 K

x_{Mg}	G_M^{xs} (kJ/mol)					
	T=1900 K			T=2200 K		
	Linear fit	Exponential fit	Ref.*	Linear fit	Exponential fit	Ref.*
0.1	-2.818	-1.418	-1.542	-3.059	-1.366	-1.599
0.2	-4.267	-2.545	-2.958	-4.502	-2.446	-3.087
0.3	-4.731	-3.368	-4.125	-4.830	-3.230	-4.328
0.4	-4.533	-3.871	-4.943	-4.458	-3.707	-5.213
0.5	-3.936	-4.041	-5.336	-3.716	-3.867	-5.658
0.6	-3.144	-3.870	-5.254	-2.848	-3.706	-5.602
0.7	-2.301	-3.357	-4.669	-2.012	-3.224	-5.009
0.8	-1.491	-2.518	-3.580	-1.282	-2.430	-3.865
0.9	-0.736	-1.382	-2.008	-0.644	-1.345	-2.183

*Wang, Du, & Liu (2011)

of R-K polynomials for (G_M^{xs}) using Equations (3.68 and 3.75). These parameters were then used to obtain exponential T-dependent interaction parameters using Equations (3.76-3.81). Table 10 displays the interaction parameters of this work, Cost 507 and Wang, Du, & Liu (2011). The values of G_M^{xs} for the system were computed using Equation (3.4) and parameters from Table 10 at 1000 K, 1300 K, 1900 K, and 2200 K. All the computed values and experimental data of G_M^{xs} are presented in Tables 11 & 12 and plotted in Figures 17-20.

The experimental and computed values of G_M^{xs} at 1000 K and $x_{Mg} = 0.5$ are found to be 4.598 ± 0.8360 kJ/mol (Hultgren et al., 1973) and −4.596 kJ/mol (using linear parameters) and −4.612 kJ/mol (using exponential parameters). Both the experimental

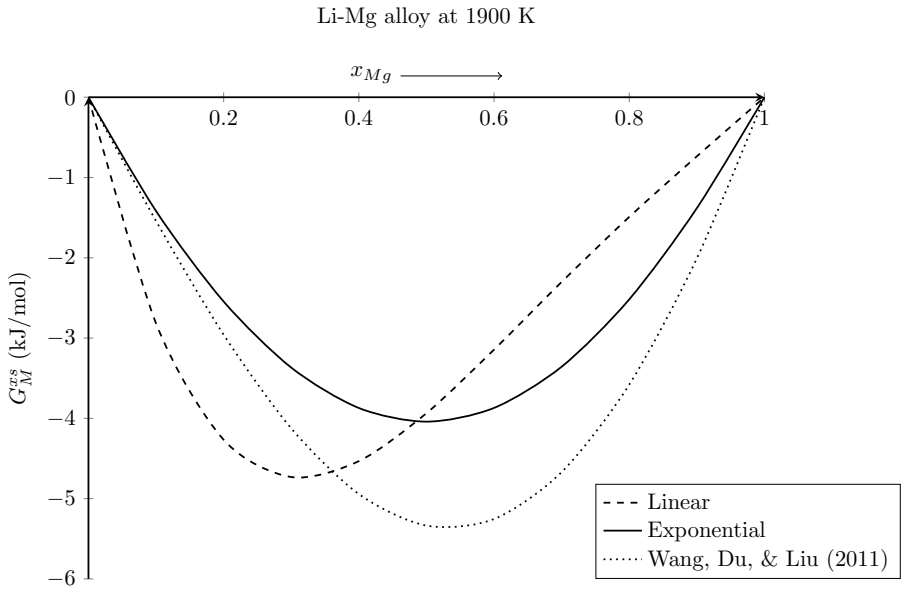

Figure 19: G_M^{xs} of liquid Li–Mg alloy at 1900 K.

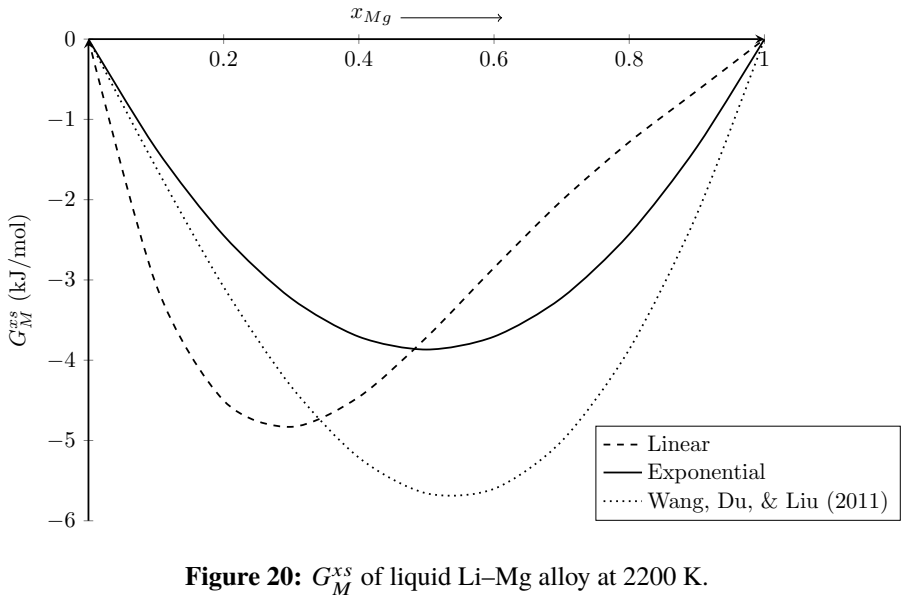

Figure 20: G_M^{xs} of liquid Li–Mg alloy at 2200 K.

and computed values of G_M^{xs} are found to be consistent with each other (Figures 17). Therefore, these optimised parameters have been considered for further computations of thermodynamic and structural properties of the system. When temperature of the system is gradually increased in the range of 1000 K–2200 K, the negative values of G_M^{xs} gradually decrease while using the exponential parameters. However, the values increase while using the linear interaction parameters of Wang, Du, & Liu (2011). It is obvious that the values of G_M^{xs} should decrease with an increase in the temperature of the liquid alloys Kaptay (2012). In this regard, it can be stated that the exponential parameters are

found to be more appropriate in order to predict the mixing tendency of Li–Mg system at higher temperatures (R. K. Gohivar, Yadav, et al., 2021b).

4.4 Enthalpy of mixing (H_M) of binary liquid alloys

It has already been mentioned that H_M is an important thermodynamic function for understanding the nature and extent of bonding among the constituent atoms of liquid alloys. Thus, understanding H_M is essential in materials processing, design, and characterization. We have derived the working expressions for H_M of binary liquid alloys within the framework of R-K polynomial in the Sections 3.1.3, 3.3, and 3.3.2 of the Chapter 3. In the Chapter 2, we highlighted a few efforts made by various researchers to investigate H_M of binary liquid alloys. The results, along with the discussion related to Al–Fe, Al–Mn, Al–Ti and Li–Mg binary and Al–Li–Zn ternary systems, of the present findings are presented in the following sub-sections. Furthermore, we have computed compositional contributions to H_M at various temperatures of the corresponding liquid alloys using exponential T-dependent interaction energy parameters.

4.4.1 H_M for liquid Al–Fe alloy

The linear and exponential parameters of Table 1 were used to calculate H_M of Al–Fe alloy at 1873 K with the help of Equations (3.25 and 3.26). The values so obtained were compared with observed values (Desai, 1987). At $x_{Fe} = 0.5$ and 1873 K, the experimental and computed values of H_M are (-19.742 ± 1.700) kJ/mol (Desai, 1987) and -19.730 kJ/mol (using exponential parameters)respectively. Both of these values are consistent with each other at all concentrations (Figure 21). This validates the present optimisation process. Hence, the values of H_M were computed higher temperatures 2500 K, 3500 K and 3800 K using the optimised exponential parameters. All these values are presented in Table 13 and plotted as a function of concentration in Figure 21. The computed negative values of H_M gradually decrease with the increase in temperature of the system, corresponding the decrease in its mixing tendency. Similar results were predicted as for other thermodynamic functions computed above.

4.4.2 H_M for liquid Al–Mn alloy

The values of H_M were calculated using exponential parameters of Table 4 in Equation (3.26) at 1600 K, 1900 K, 2200 K, and 2500 K. The computed as well as observed values (Desai, 1987) are presented in Table 14 and plotted in Figure 22. The values of H_M computed in this work have large deviation from those of Desai (1987) at 1600 K. The

Table 13: H_M of liquid Al–Fe alloy at different temperatures

x_{Fe}	H_M (kJ/mol)				
	Desai (1987)	Exponential fit			
	T= 1873 K	T= 1873 K	T= 2500 K	T= 3500 K	T= 3800 K
0.1	-8.380	-8.779	-7.870	-6.480	-6.100
0.2	-14.291	-14.780	-13.310	-11.030	-10.390
0.3	-14.997	-18.390	-16.640	-13.886	-13.100
0.4	-19.743	-19.942	-18.160	-15.290	-14.460
0.5	-19.742	-19.730	-18.120	-15.410	-14.610
0.6	-18.175	-18.041	-16.710	-14.380	-13.680
0. 7	-15.265	-15.060	-14.090	-12.300	-11.740
0.8	-11.165	10.988	-10.390	-9.210	-8.830
0.9	6.029	5.937	-5.680	-5.121	-4.931

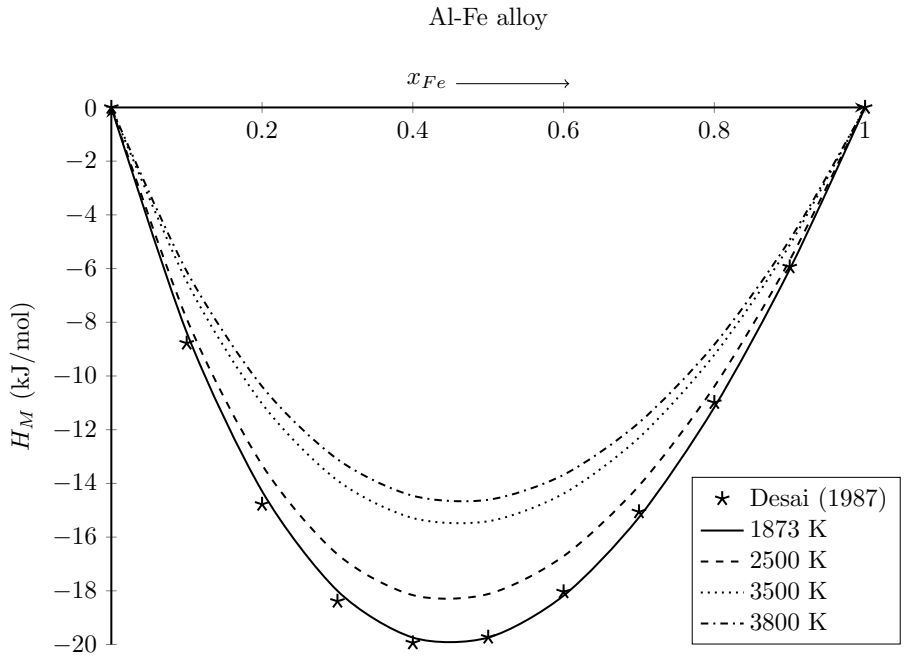

Figure 21: H_M of liquid Al–Fe alloy at various temperatures.

value of H_M at $x_{Mn} = 0.5$ was observed to be -16.848 ± 4.000 kJ/mol by (Desai, 1987). In this appreciable range, it is found to be in agreement with the results of present work ($H_M = -13.65$ kJ/mol) at the same concentration. Moreover, observed values of (Desai, 1987) show an asymmetric nature, whereas those of the present work show a symmetric nature. The computed negative values of H_M gradually decrease with an increase in the temperatures of the system, revealing the decrease in the bonding strength among the atoms of the complex.

Table 14: H_M of liquid Al–Mn alloy at different temperatures

x_{Mn}	H_M (kJ/mol)				
	Desai (1987)	Exponential fit			
	T=1600 K	T= 1600 K	T=1900 K	T=2200 K	T=2500 K
0.1	-6.392	-5.200	-4.570	-4.012	-3.214
0.2	-11.901	-9.064	-7.981	-7.000	-5.581
0.3	-15.414	-11.713	-10.323	-9.061	-7.207
0.4	-16.908	-13.210	-11.681	-10.260	-8.159
0.5	-16.848	-13.650	-12.102	-10.640	-8.472
0.6	-15.470	-13.04	-11.601	-10.230	-8.151
0.7	-13.171	-11.400	-10.180	-9.000	-7.192
0.8	-10.048	-8.710	-7.820	-6.931	-5.561
0.9	-5.687	-4.930	-4.450	-3.962	-3.190

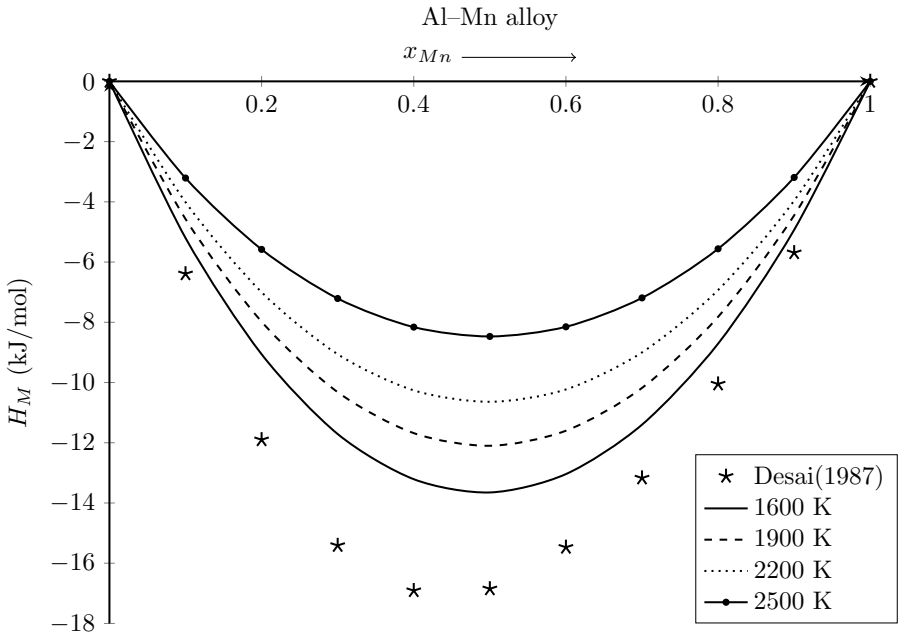

Figure 22: H_M of liquid Al–Mn alloy at various temperatures.

4.4.3 H_M for liquid Al–Ti alloy

The values of H_M were calculated using exponential parameters of Table 7 in Equation (3.26) at 1500 K, 2000 K, 2500 K and 2700 K. The computed and observed (Desai, 1987) values of H_M at 2000 K are presented in Table 15 and are plotted in Figure 23. The experimental and computed values of H_M are found to be (-27.710 ± 2.000) kJ/mol (Desai, 1987) and -23.022 kJ/mol respectively at 2000 K and $x_{Mn} = 0.5$. As the exponential parameters of the work were optimised using the linear parameters of Witusiewicz et al. (2008), the computed values of H_M deviated with those of Desai (1987). The computed values show symmetric variations at higher temperatures and their

curves gradually shallow up, indicating the decrease in mixing tendency of the system.

Table 15: H_M of liquid Al–Ti alloy at different temperatures

x_{Ti}	H_M (kJ/mol)				
	Desai (1987)	Exponential fit			
	T=2000 K	T=1500 K	T= 2000 K	T=2500 K	T=2700 K
0.1	-11.161	-7.912	-6.850	-5.901	-5.542
0.2	-19.949	-15.361	-13.301	-11.402	-10.668
0.3	-25.274	-21.370	-18.502	-15.810	-14.787
0.4	-27.669	-25.232	-21.861	-18.656	-17.440
0.5	-27.710	-26.511	-23.022	-19.634	-18.350
0.6	-25.752	-25.103	-21.861	-18.659	-17.441
0.7	-21.908	-21.140	-18.493	-15.806	-14.787
0.8	-16.275	-15.101	-13.292	-11.402	-10.664
0.9	-8.978	-7.713	-6.842	-5.900	-5.541

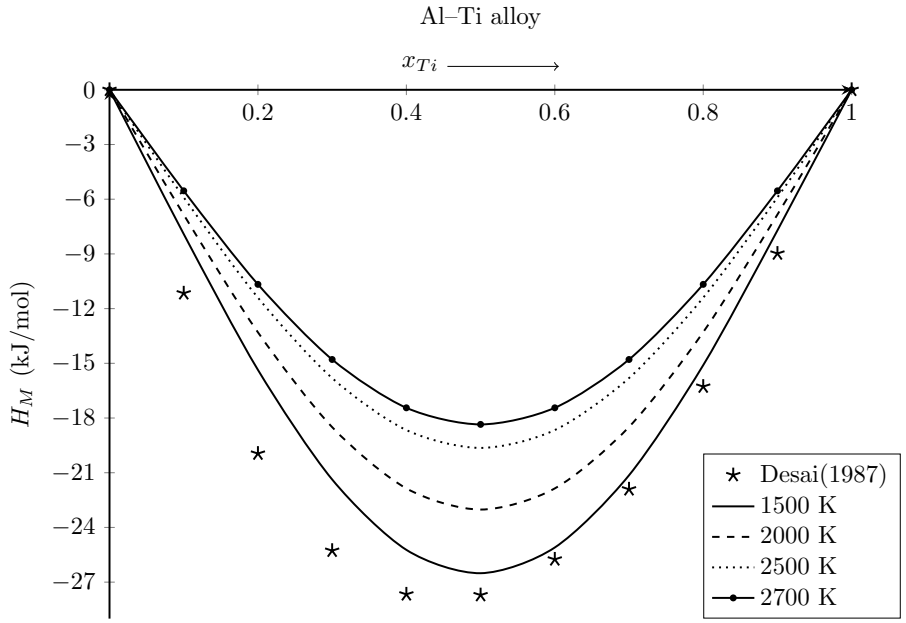

Figure 23: H_M of liquid Al–Ti alloy at various temperatures.

4.4.4 H_M for liquid Li–Mg alloy

Using the exponential T-dependent energy interaction parameters from Table 10, we calculated H_M of liquid Li-Mg alloy at 1000 K, 1300 K, 1900 K and 2200 K using Equation (3.26). Table 16 consists of the calculated values of H_M along with the literature values from Wang, Du, & Liu (2011) and experimental data from Hultgren et al. (1973). Since the values of H_M for Li–Mg system are very small, these values have expressed in terms of H_M/RT in this case. Figures 24 and 25 depict plots of the compositional

dependence of H_M at different temperatures. The computed and experimental values of H_M/RT at 1000 K and $x_{Li} = 0.5$ are found to be -0.636 and -0.645 ± 0.251 (Hultgren et al., 1973) respectively. There is appreciable agreement between the calculated and experimental values thereby validating the optimisation procedures. However, they differ greatly with the values of Wang, Du, & Liu (2011) at higher concentration of Mg (Figure 24). The computed negative values of H_M gradually decrease as the system's temperature rises above 1000 K (Figure 25). This variation is in accordance with expected trend. According to the current theoretical investigations, the compound forming tendency of the considered system gradually decreases as its temperature rises. These results support the results predicted by the excess free energy of mixing in the previous sections of the work and are also in accordance with the findings of other researchers (Kaptay (2017), Yadav, Jha, Jha, et al. (2016), R. K. Gohivar, Yadav, et al. (2021b)). This finding strengthens the applicability of exponential T-dependent parameters to calculate the H_M at various temperatures.

Table 16: H_M of liquid Li–Mg alloy at 1000 K, 1300 K, 1900 K and 2200 K

x_{Mg}	H_M/RT					
	T=1000 K			Exponential fit		
	Exponential fit	Experimental*	Wang, Du, & Liu (2011)	1300 K	1900 K	2200 K
0.1	-0.204	-0.131	-0.151	-0.158	-0.110	-0.095
0.2	-0.375	-0.282	-0.274	-0.291	-0.201	-0.173
0.3	-0.512	-0.431	-0.364	-0.394	-0.269	-0.231
0.4	-0.603	-0.559	-0.413	-0.462	-0.312	-0.267
0.5	-0.636	-0.645	-0.421	-0.486	-0.327	-0.280
0.6	-0.601	-0.647	-0.390	-0.461	-0.312	-0.267
0.7	-0.497	-0.554	-0.323	-0.386	-0.266	-0.223
0.8	-0.336	-0.385	-0.228	-0.269	-0.194	-0.169
0.9	-0.151	-0.183	-0.115	-0.130	-0.101	-0.090

*Hultgren et al. (1973)

4.5 Activity

The activity is a thermodynamic function that can be measured directly from experiments. It measures tendency of a component to leave the complex. In the absence of experimental data, it can be determined by using different modelling equations. It also gives information regarding the extent of bonding between the constituent atoms of complex.In Section 3.1.4, we have presented necessary theoretical basis and derived analytical expressions for activity. The optimised model parameters used for the computations of G_M^{xs} should also reproduce the activity of respective systems. For the assessment of the activity, the partial excess free energy of mixing (G_k^{xs}, k=A, B) of the components of liquid alloys were first calculated using the T-dependent interaction energy parameters. The activities of components were then computed at various temperatures and compositions using the

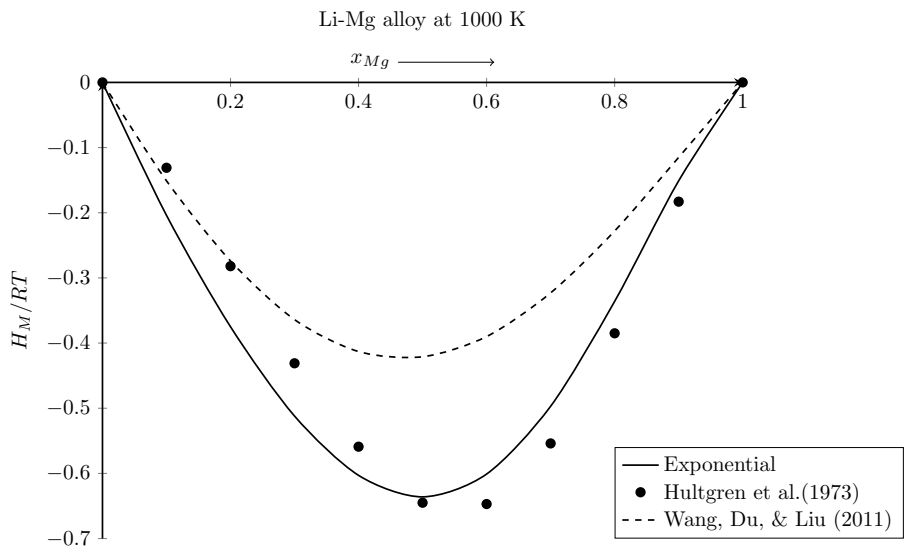

Figure 24: H_M of liquid Li–Mg alloy at 1000 K.

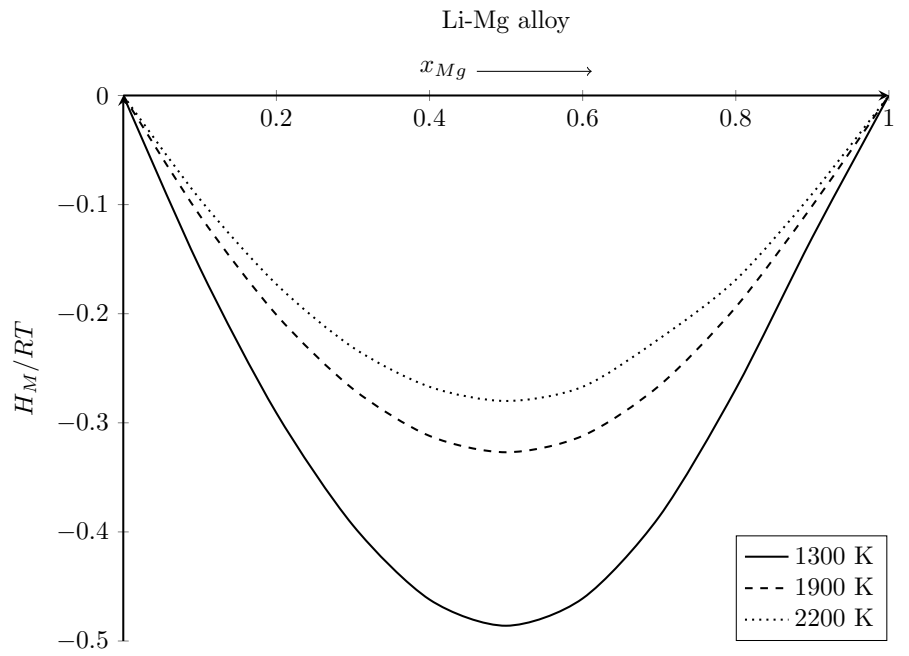

Figure 25: H_M of liquid Li–Mg alloy at 1300 K, 1900, 2200 K.

values of G_k^{xs}. The results of this work are presented in the following sub-sections. We have also compared the results with the available experimental and literature data in order to see the validity of optimised parameters.

4.5.1 Activity of liquid Al–Fe alloy

We first computed G_k^{xs} (k=Al, Fe) of components of liquid Al–Fe alloy at temperatures of 1873 K, 2500 K, 2500 K and 3800 K using Equations (3.33) and (3.34) with the aid of parameters from Table 1. The activities of components were then calculated from Equation (3.35) using these computed values. The results so obtained are presented in Tables 18–19 and plotted as a function of concentration in Figures 26–29 along with the experimental data (Hultgren et al., 1973) and literature values (Adhikari et al., 2014) in Figure 26.

Table 17: Activity of liquid Al–Fe alloy at 1873 K

x_{Fe}	Activity									
	This work				Experimental*		Cost 507		Ref.**	
	Linear fit		Exponential fit		a_{Al}	a_{Fe}	a_{Al}	a_{Fe}	a_{Al}	a_{Fe}
	a_{Al}	a_{Fe}	a_{Al}	a_{Fe}						
0.1	0.856	0.007	0.852	0.006	0.859	0.007	0.876	0.008	0.868	0.005
0.2	0.667	0.028	0.657	0.026	0.672	0.027	0.715	0.026	0.697	0.025
0.3	0.484	0.075	0.469	0.071	0.486	0.073	0.539	0.060	0.508	0.069
0.4	0.330	0.152	0.315	0.150	0.329	0.152	0.372	0.118	0.340	0.146
0.5	0.213	0.262	0.200	0.262	0.211	0.263	0.231	0.210	0.211	0.259
0.6	0.127	0.398	0.119	0.401	0.126	0.400	0.127	0.340	0.122	0.400
0.7	0.069	0.553	0.064	0.558	0.069	0.553	0.060	0.505	0.064	0.559
0.8	0.031	0.717	0.030	0.722	0.031	0.717	0.0230	0.690	0.027	0.729
0.9	0.010	0.874	0.010	0.876	0.010	0.875	0.006	0.866	0.009	0.879

*Hultgren et al. (1973), ** Adhikari et al. (2014)

The experimental values of $a_{Al} = 0.126 \pm 0.016$ and $a_{Fe} = 0.400 \pm 0.02$ (Hultgren et al., 1973) and computed values of $a_{Al} = 0.127$ and $a_{Fe} = 0.398$ (using linear parameters), and $a_{Al} = 0.119$ and $a_{Fe} = 0.401$ (using exponential parameters) at $x_{Fe} = 0.5$ and 1873 K. It is observed that the results obtained using both linear and exponential parameters are in good agreement with the experimental (Hultgren et al., 1973) and literature data of Adhikari et al. (2014) at 1873 K at all concentrations. These investigations validate the present optimisation processes. The computed values of the activities of both components are less than ideal values (large negative deviation from Raoult's law). These results indicate that the alloy is strongly interacting in nature at its melting temperature (1873 K). When the temperature of the system is raised in the range of 1873 K to 3800 K, the activity computed using exponential parameters shifts towards ideal values (Figures 26–29). These results correspond that the complex forming tendency of the alloy decreases with an increase in its temperature. However, the activity of Al component computed using linear parameters of this work as well as that of Cost 507 exceeds the ideal values above 3500 K (Figures 28–29). These behaviours do not support the usual trend that the thermodynamic functions should shift towards ideal values at higher temperatures. These unusual tendencies are termed as artificial miscibility gaps. Thus, the artificial

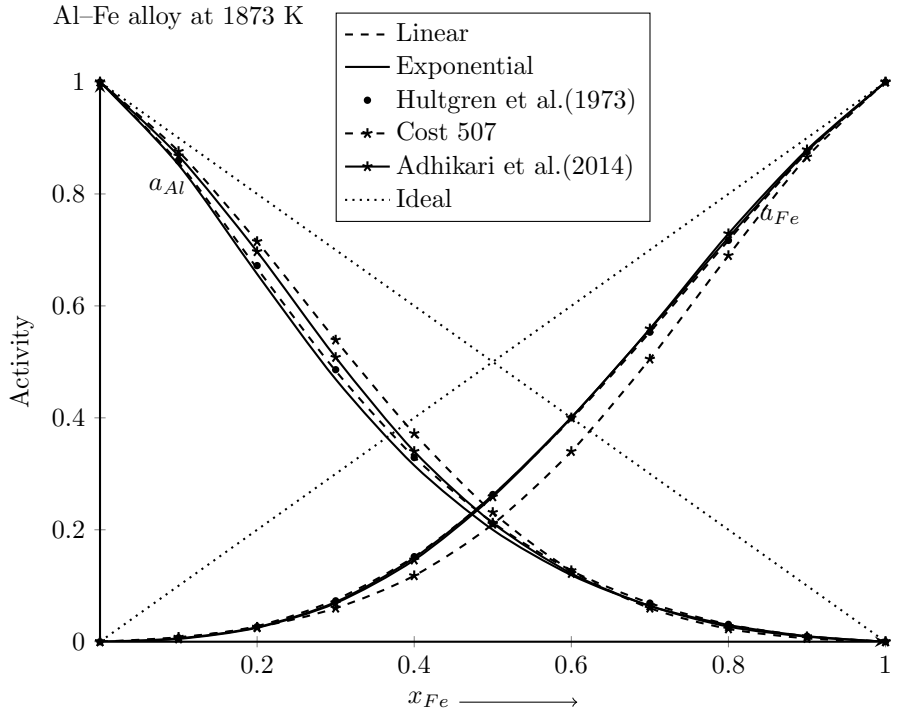

Figure 26: Activity of liquid Al–Fe alloy at 1873 K.

miscibility gaps that appeared in the activity of Al atom at higher temperatures using linear parameters have been removed by the use of exponential parameters. These findings are in accordance with the results obtained for G_M^{xs} in section 4.3 along with literature (Yadav et al., 2018; R. K. Gohivar, Yadav, et al., 2021a).

Table 18: Activity of liquid Al–Fe alloy at 2500 K and 3500 K

x_{Fe}	Activity											
	T=2500 K						T=3500 K					
	This work				Cost 507		This work				Cost 507	
	Linear fit		Exponential fit		a_{Al}	a_{Fe}	Linear fit		Exponential fit		a_{Al}	a_{Fe}
	a_{Al}	a_{Fe}	a_{Al}	a_{Fe}			a_{Al}	a_{Fe}	a_{Al}	a_{Fe}		
0.1	0.879	0.026	0.871	0.018	0.892	0.028	0.900	0.081	0.885	0.042	0.905	0.081
0.2	0.737	0.072	0.711	0.058	0.766	0.067	0.802	0.160	0.753	0.107	0.812	0.153
0.3	0.592	0.140	0.553	0.125	0.627	0.123	0.703	0.239	0.622	0.192	0.714	0.226
0.4	0.456	0.227	0.411	0.218	0.483	0.198	0.601	0.320	0.497	0.291	0.605	0.307
0.5	0.334	0.333	0.292	0.331	0.345	0.298	0.492	0.408	0.383	0.401	0.486	0.400
0.6	0.228	0.454	0.195	0.461	0.224	0.422	0.376	0.508	0.280	0.517	0.363	0.508
0.7	0.140	0.590	0.119	0.600	0.128	0.568	0.257	0.623	0.189	0.640	0.243	0.628
0.8	0.072	0.735	0.062	0.744	0.061	0.726	0.146	0.751	0.110	0.765	0.137	0.758
0.9	0.025	0.879	0.023	0.883	0.020	0.877	0.056	0.883	0.046	0.889	0.055	0.887

4.5.2 Activity of liquid Al–Mn alloy

We calculated G_k^{xs}, (k = Al, Mn) of components of liquid Al–Mn alloy using Equations (3.33) and (3.34) with the help of linear (Cost 507) and exponential parameters from

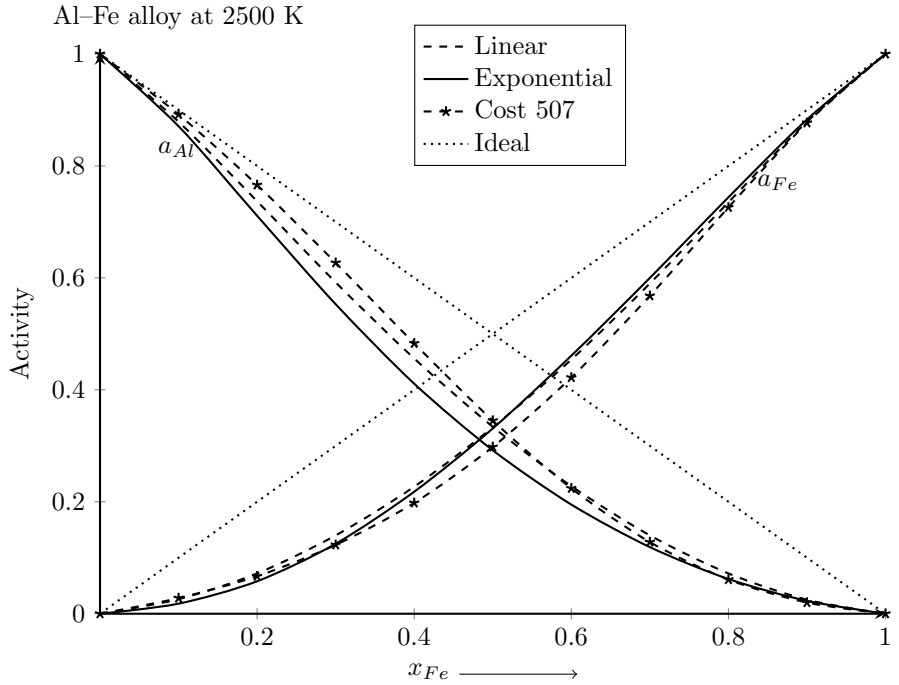

Figure 27: Activity of liquid Al–Fe alloy at 2500 K.

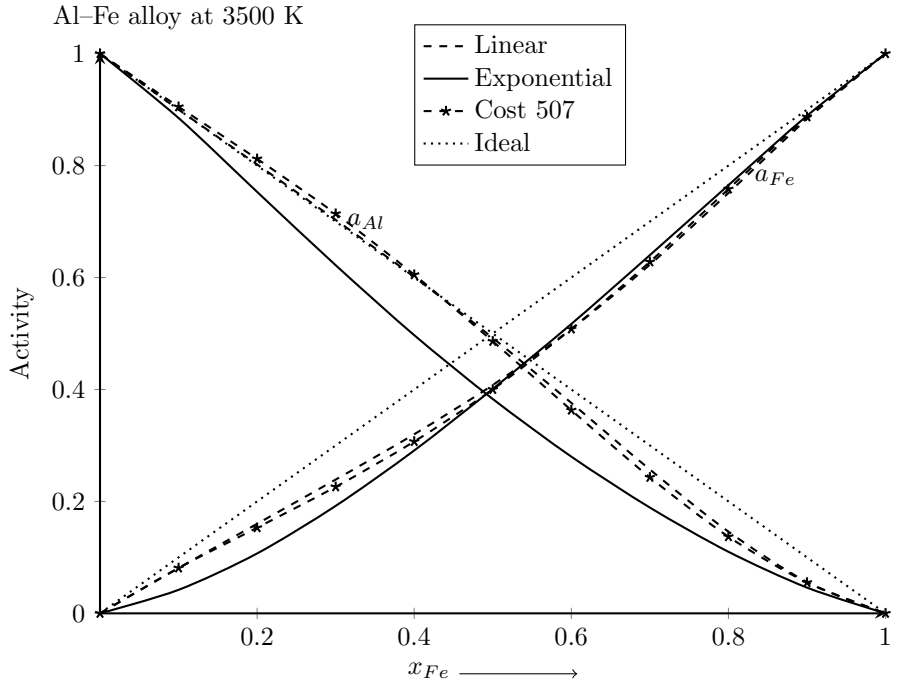

Figure 28: Activity of liquid Al–Fe alloy at 3500 K.

Table 4 at temperatures of 1600 K, 1900 K, and 2200 K. The values so obtained were then used in Equation (3.35) to compute the activities of Al and Mn. The results are presented in the Tables 20 & 21 and plotted as a function of concentration in Figures 30–33.

Table 19: Activity of liquid Al–Fe alloy at 3800 K

x_{Fe}	Activity					
	Linear fit		Exponential fit		Cost 507	
	a_{Al}	a_{Fe}	a_{Al}	a_{Fe}	a_{Al}	a_{Fe}
0.1	0.904	0.102	0.887	0.049	0.908	0.100
0.2	0.815	0.188	0.761	0.119	0.822	0.180
0.3	0.728	0.265	0.634	0.207	0.732	0.255
0.4	0.635	0.342	0.514	0.307	0.632	0.335
0.5	0.531	0.425	0.402	0.415	0.520	0.424
0.6	0.415	0.520	0.298	0.529	0.399	0.527
0.7	0.290	0.630	0.204	0.648	0.276	0.641
0.8	0.168	0.754	0.121	0.770	0.161	0.764
0.9	0.066	0.884	0.052	0.890	0.067	0.888

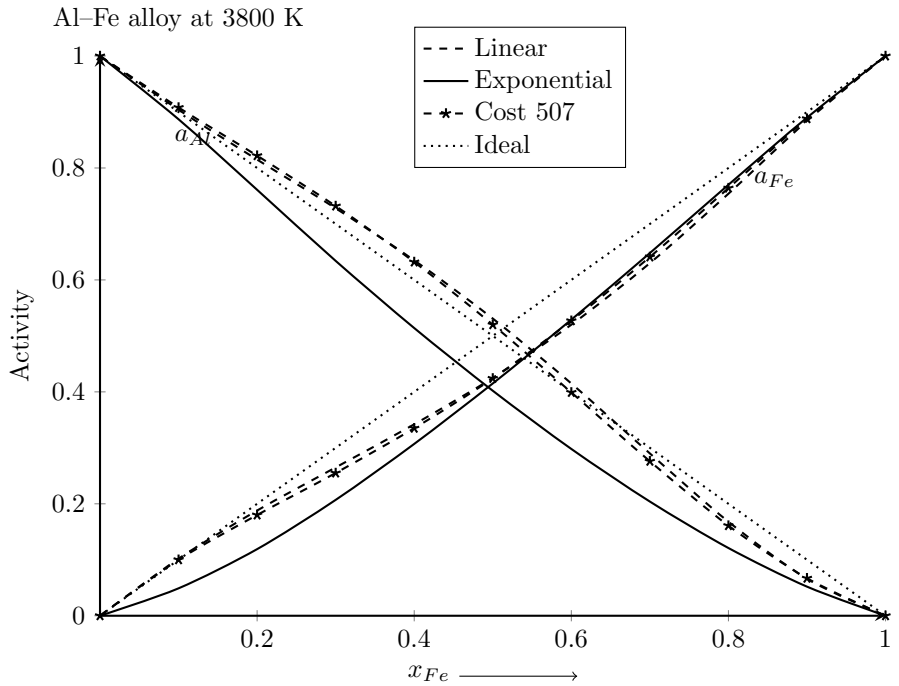

Figure 29: Activity of liquid Al–Fe alloy at 3800 K.

Figure 30 shows an excellent agreement between the values of activity calculated using linear and exponential interaction parameters at 1600 K. However, there is high negative deviation from ideal values throughout the entire concentration range indicating the system to be strongly interacting in nature. The activities of both the components were found to increase with increase in temperature. These results reveal that the compound forming tendency of the system decreases at higher temperatures. But the activity of Al calculated using linear interaction parameters was found to be greater than its ideal values at 2500 K while the results using exponential interaction parameters showed negative deviation from Raoult's law at 2500 K . These results are similar to those predicted

Table 20: Activity of liquid Al–Mn alloy at 1600 K and 1900 K

x_{Mn}	Activity							
	T=1600 K				T=1900 K			
	Cost 507		Exponential fit		Cost 507		Exponential fit	
	a_{Al}	a_{Mn}	a_{Al}	a_{Mn}	a_{Al}	a_{Mn}	a_{Al}	a_{Mn}
0.1	0.881	0.025	0.876	0.020	0.891	0.049	0.883	0.033
0.2	0.740	0.068	0.726	0.060	0.772	0.114	0.748	0.088
0.3	0.595	0.132	0.574	0.122	0.651	0.192	0.61	0.163
0.4	0.458	0.216	0.433	0.206	0.531	0.28	0.480	0.256
0.5	0.333	0.318	0.309	0.312	0.415	0.378	0.361	0.362
0.6	0.225	0.439	0.204	0.437	0.303	0.489	0.255	0.482
0.7	0.135	0.577	0.121	0.578	0.199	0.613	0.163	0.612
0.8	0.067	0.724	0.060	0.729	0.109	0.747	0.089	0.749
0.9	0.023	0.876	0.020	0.877	0.041	0.882	0.034	0.883

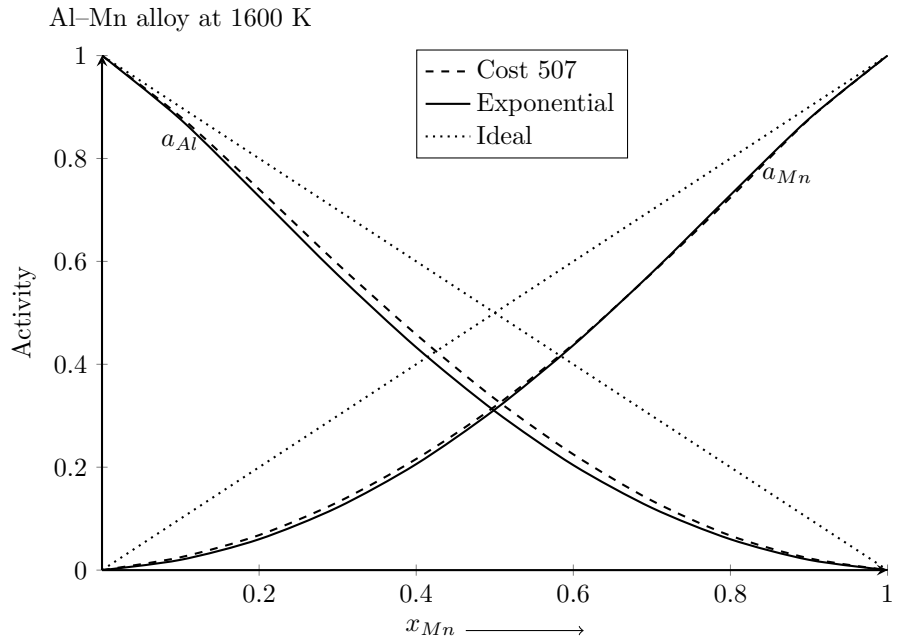

Figure 30: Activity of liquid Al–Mn alloy at 1600 K.

above for other systems. Further, this suggests that exponential interaction parameters are preferred over the linear parameters for study of the thermodynamic properties of liquid alloys at higher temperatures.

4.5.3 Activity of liquid Al–Ti alloy

The activities of the components Al (a_{Al}) and Ti (a_{Ti}) of Al–Ti liquid alloy were computed at temperatures 1500 K, 2000 K, 2500 K and 2700 K using Equations (3.33) and (3.34). For this purpose, both linear (Cost 507) and exponential (this work) parameters were used

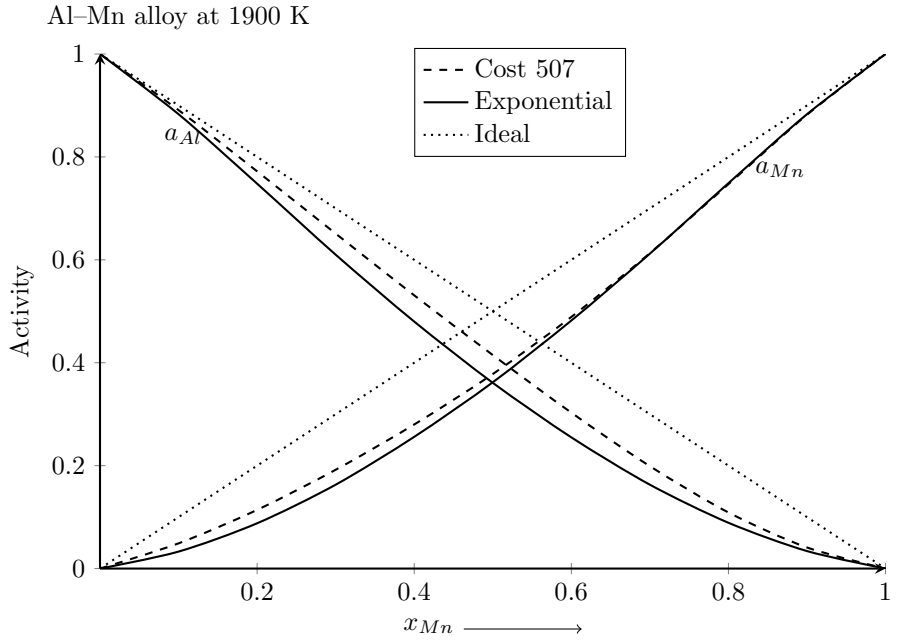

Figure 31: Activity of liquid Al–Mn alloy at 1900 K.

Table 21: Activity of liquid Al–Mn alloy at 2200 K and 2500 K

x_{Mn}	Activity							
	T=2200 K				T=2500 K			
	Cost 507		Exponential fit		Cost 507		Exponential fit	
	a_{Al}	a_{Mn}	a_{Al}	a_{Mn}	a_{Al}	a_{Mn}	a_{Al}	a_{Mn}
0.1	0.898	0.081	0.887	0.046	0.904	0.119	0.89	0.058
0.2	0.796	0.166	0.761	0.114	0.814	0.220	0.771	0.134
0.3	0.694	0.251	0.635	0.197	0.729	0.308	0.651	0.224
0.4	0.592	0.338	0.513	0.294	0.642	0.39	0.536	0.322
0.5	0.487	0.430	0.399	0.399	0.549	0.473	0.426	0.426
0.6	0.376	0.529	0.293	0.513	0.444	0.562	0.322	0.536
0.7	0.264	0.64	0.197	0.635	0.327	0.662	0.224	0.651
0.8	0.156	0.761	0.114	0.762	0.204	0.773	0.134	0.771
0.9	0.064	0.886	0.046	0.887	0.089	0.890	0.058	0.890

(Table 7). These values were computed following the similar procedure as mentioned above in the Section 4.4. The obtained values are presented in Tables 22 & 23 and plotted as a function of composition in Figures 34–37.

The estimated values of a_{Al} and a_{Ti} using both the linear and exponential parameters at 1500 K were found to be in good agreement. Moreover, their curves show large negative deviation from ideal values throughout the entire concentration range indicating the strong association between them in the complexes of initial melt. At the equiatomic composition, $a_{Al} = a_{Tl}$ which indicates both components have equal tendency to leave the compound at this temperature. At higher temperatures ($T > 1500K$), the computed

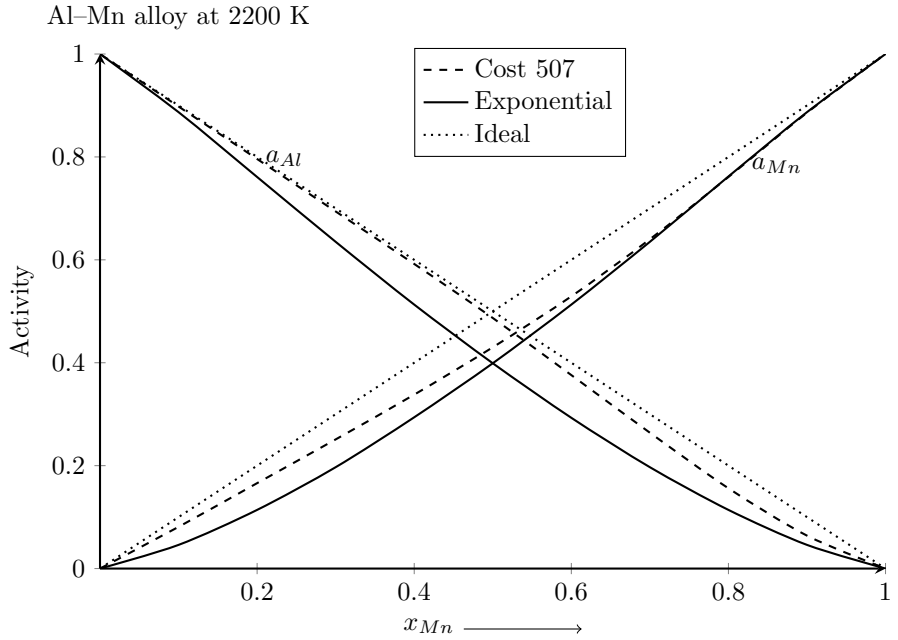

Figure 32: Activity of liquid Al–Mn alloy at 2200 K.

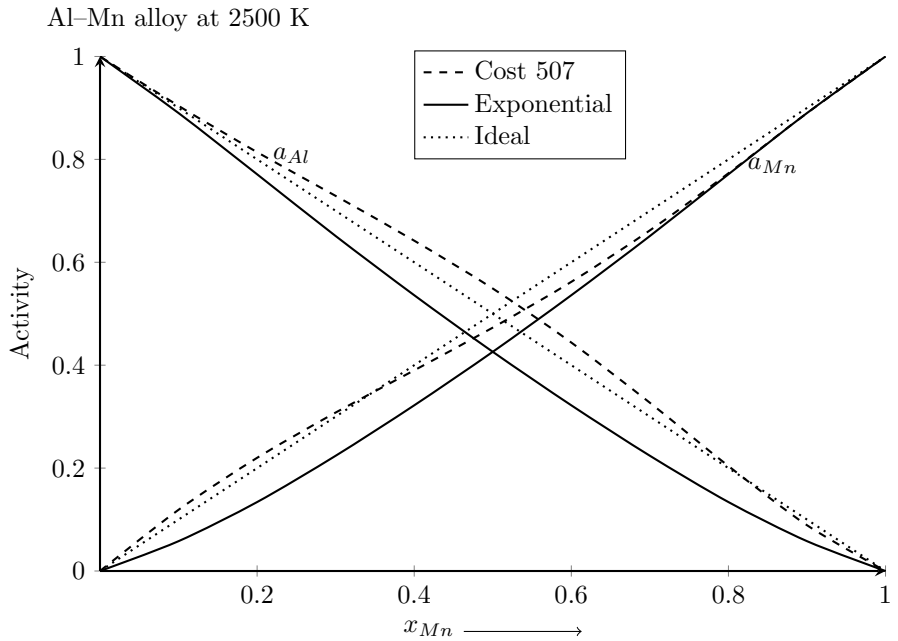

Figure 33: Activity of liquid Al–Mn alloy at 2500 K.

values of a_{Al} and a_{Ti} gradually increase and approach their respective ideal values indicating the decrease in mixing tendency of the system. Therefore, it may be concluded in this work that the system is the most interacting at its melting temperature. The computed value of a_{Al} at 2700 K calculated using linear parameters was found to be 0.510 at $x_{Ti} = 0.5$, greater than its respective ideal value. The results obtained using

linear parameters showed that the alloy changes its nature from ordering to segregating at higher temperatures. The values calculated using exponential parameters are found to be less than the ideal values at all compositions and the mentioned temperatures indicating no such phase transitions. Hence, the results for a_k and G_M^{xs} of this system also suggest that the exponential interaction parameters should be used in predicting the mixing properties in a wide temperature range.

Table 22: Activity of liquid Al–Ti alloy at 1500 K and 2000 K

x_{Ti}	Activity							
	T=1500 K				T=2000 K			
	Cost 507		Exponential fit		Cost 507		Exponential fit	
	a_{Al}	a_{Ti}	a_{Al}	a_{Ti}	a_{Al}	a_{Ti}	a_{Al}	a_{Ti}
0.1	0.904	0.005	0.896	0.003	0.920	0.047	0.897	0.021
0.2	0.765	0.013	0.741	0.010	0.837	0.082	0.770	0.050
0.3	0.566	0.033	0.530	0.026	0.712	0.133	0.614	0.099
0.4	0.353	0.079	0.317	0.068	0.550	0.214	0.447	0.178
0.5	0.184	0.174	0.158	0.159	0.382	0.333	0.295	0.295
0.6	0.083	0.334	0.068	0.318	0.240	0.487	0.178	0.447
0.7	0.034	0.545	0.026	0.532	0.140	0.652	0.099	0.614
0.8	0.013	0.749	0.010	0.743	0.077	0.797	0.050	0.770
0.9	0.005	0.898	0.003	0.897	0.036	0.907	0.021	0.897

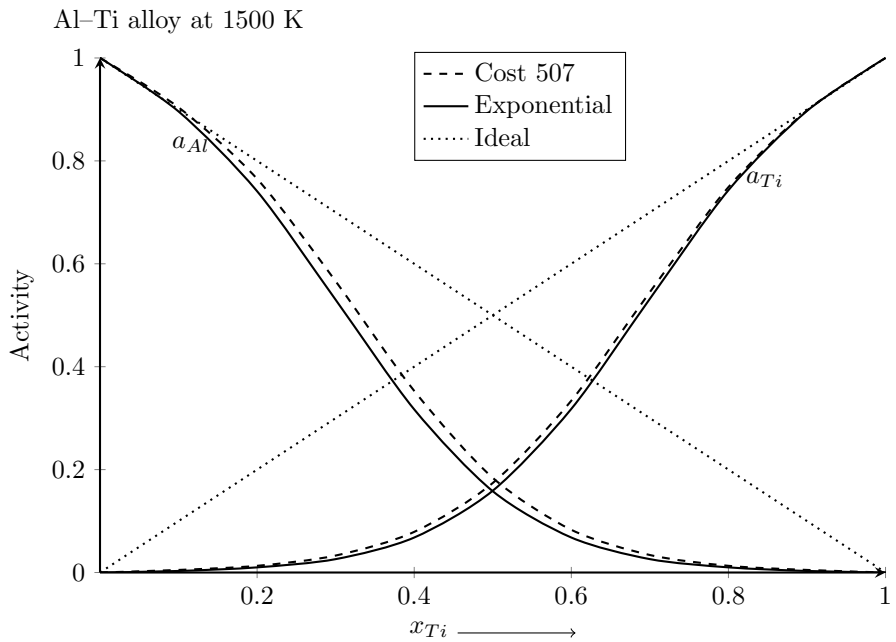

Figure 34: Activity of liquid Al–Ti alloy at 1500 K.

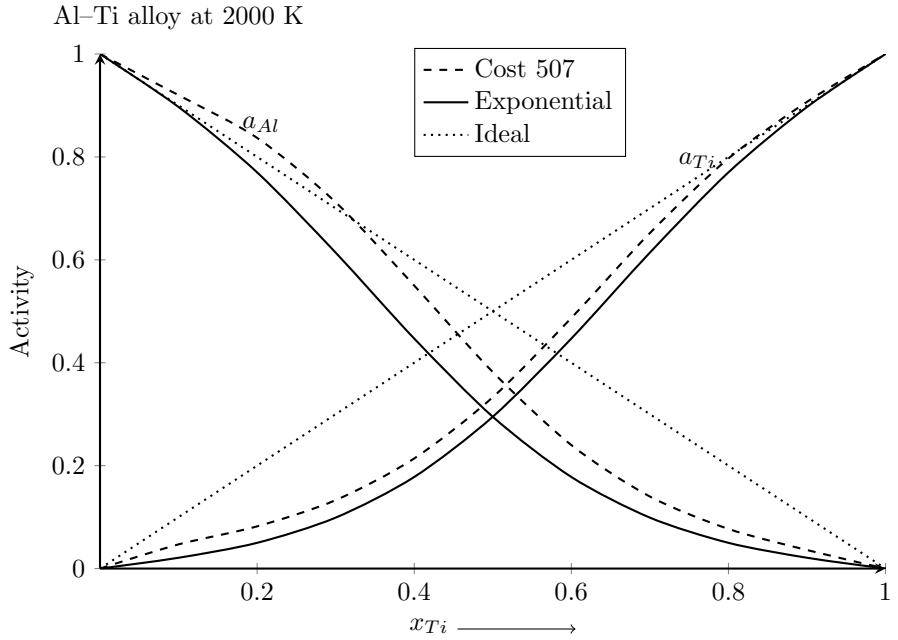

Figure 35: Activity of liquid Al–Ti alloy at 2000 K.

Table 23: Activity of liquid Al–Ti alloy at 2500 K and 2700 K

x_{Ti}	Activity							
	T=2500 K				T=2700 K			
	Linear fit		Exponential fit		Linear fit		Exponential fit	
	a_{Al}	a_{Ti}	a_{Al}	a_{Ti}	a_{Al}	a_{Ti}	a_{Al}	a_{Ti}
0.1	0.925	0.084	0.897	0.031	0.927	0.114	0.898	0.038
0.2	0.856	0.131	0.777	0.072	0.867	0.169	0.780	0.086
0.3	0.756	0.190	0.634	0.132	0.780	0.231	0.644	0.152
0.4	0.617	0.276	0.482	0.220	0.657	0.318	0.500	0.244
0.5	0.461	0.394	0.338	0.338	0.510	0.432	0.362	0.362
0.6	0.316	0.536	0.220	0.482	0.367	0.565	0.244	0.500
0.7	0.202	0.683	0.132	0.634	0.247	0.700	0.152	0.644
0.8	0.121	0.810	0.072	0.777	0.155	0.817	0.086	0.780
0.9	0.062	0.910	0.031	0.897	0.082	0.911	0.038	0.898

4.5.4 Activity of liquid Li–Mg alloy

The values of (G^{xs}_{Li}, G^{xs}_{Mg}) were calculated at 1000 K, 1300 K, 1900 K, and 2200 K using Equations (3.33) and (3.34) with the help of parameters in the Table 10. The obtained values of G^{xs}_{Li} and G^{xs}_{Mg}) were then used in Equation (3.35) to compute the values of activities of Li and Mg (a_{Li} and a_{Mg}) of the system at above-mentioned temperatures. The obtained values of a_{Li} and a_{Mg} are listed in Tables (24 & 25) and are plotted in Figures 38-41.

The calculated values of a_{Li} and a_{Mg} at 1000 K were compared with the experimental

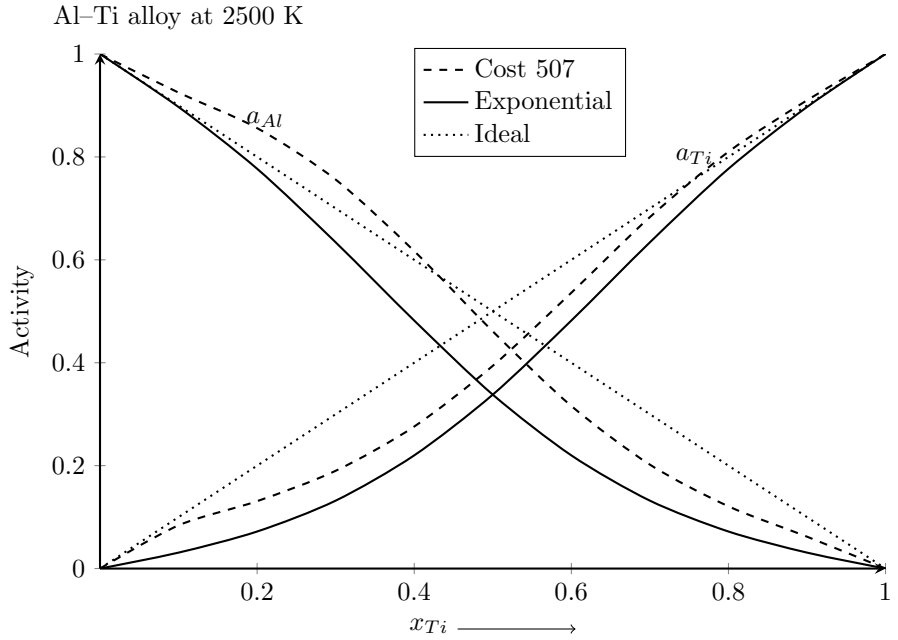

Figure 36: Activity of liquid Al–Ti alloy at 2500 K.

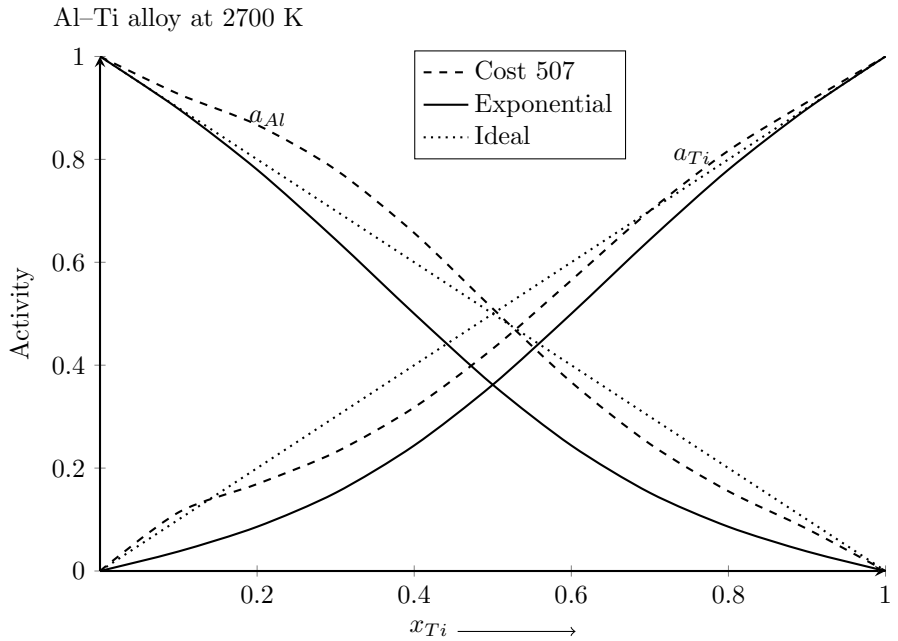

Figure 37: Activity of liquid Al–Ti alloy at 2700 K.

values (Hultgren et al., 1973) in Figure 38. It was found that the values computed using linear parameters in this work agreed well with the experimental data. The experimental values of $a_{Li} = 0.232 \pm 0.025$ and $a_{Mg} = 0.356 \pm 0.04$ and the computed values of $a_{Li} = 0.232$ and $a_{Mg} = 0.357$ (using linear parameters) and $a_{Li} = 0.287$ and $a_{Mg} = 0.287$ (using exponential parameters). But the values obtained using exponential parameters

Table 24: Activity of liquid Li–Mg alloy at 1000 K

x_{Mg}	Activity at 1000 K							
	Linear fit		Exponential fit		Experimental*		Wang, Du, & Liu (2011)	
	a_{Li}	a_{Mg}	a_{Li}	a_{Mg}	a_{Li}	a_{Mg}	a_{Li}	a_{Mg}
0.1	0.866	0.012	0.885	0.018	0.865	0.012	0.893	0.021
0.2	0.690	0.043	0.746	0.048	0.689	0.043	0.763	0.052
0.3	0.510	0.107	0.591	0.097	0.509	0.107	0.609	0.101
0.4	0.353	0.213	0.432	0.174	0.353	0.213	0.449	0.178
0.5	0.232	0.357	0.287	0.287	0.232	0.356	0.303	0.289
0.6	0.146	0.521	0.172	0.437	0.146	0.521	0.186	0.430
0.7	0.090	0.678	0.093	0.608	0.090	0.679	0.103	0.591
0.8	0.053	0.808	0.046	0.771	0.053	0.808	0.050	0.750
0.9	0.027	0.909	0.019	0.900	0.027	0.908	0.019	0.889

*Hultgren et al. (1973)

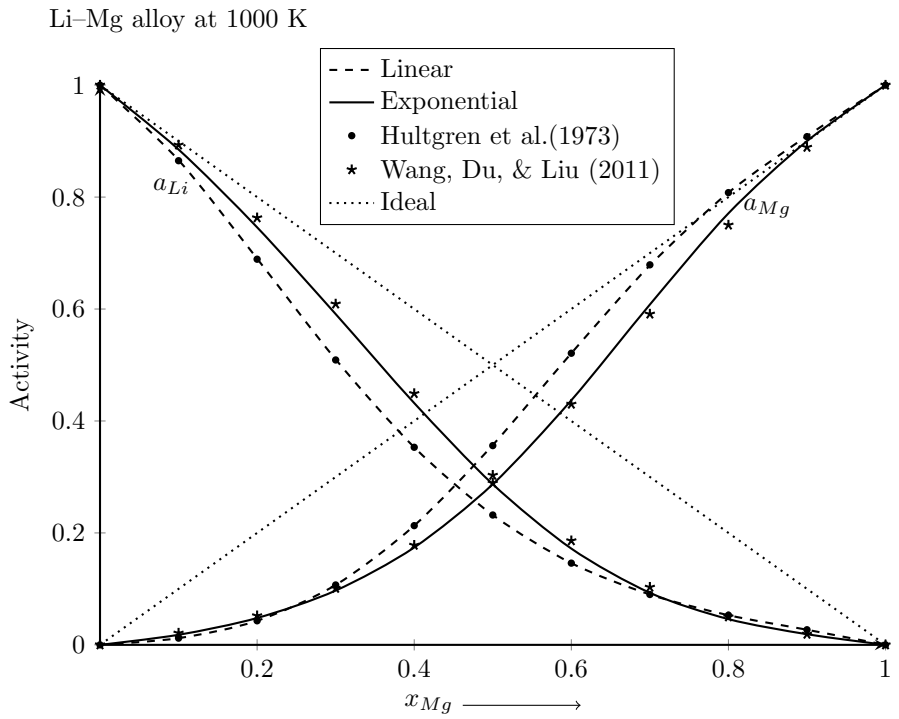

Figure 38: Activity of liquid Li–Mg alloy at 1000 K.

and linear parameters of Wang, Du, & Liu (2011) were in good agreement with each other at all concentrations. The experimental values of a_{Li} and a_{Mg} are very close to ideal values at their respective lower concentrations. However, they have large negative deviations from the ideality at and around equiatomic concentration (Figure 38). This indicates that these atoms have very little tendency to leave the complex at the equiatomic composition. In other words, the system has a large tendency of compound formation.

Due to scanty of experimental data at higher temperatures (1300 K,1900 K and 2200 K), the computed values of a_{Li} and a_{Mg} are compared with the values calculated using

Table 25: Activity of liquid Li–Mg alloy at 1300 K.

x_{Mg}	Activity					
	Linear fit		Exponential fit		Wang, Du, & Liu (2011)	
	a_{Li}	a_{Mg}	a_{Li}	a_{Mg}	a_{Li}	a_{Mg}
0.1	0.864	0.016	0.888	0.028	0.895	0.028
0.2	0.686	0.061	0.757	0.070	0.773	0.066
0.3	0.509	0.150	0.614	0.132	0.630	0.122
0.4	0.362	0.283	0.469	0.218	0.479	0.202
0.5	0.254	0.437	0.332	0.332	0.336	0.312
0.6	0.179	0.584	0.217	0.471	0.216	0.448
0.7	0.126	0.706	0.129	0.622	0.125	0.600
0.8	0.084	0.808	0.068	0.769	0.063	0.752
0.9	0.044	0.902	0.028	0.895	0.024	0.888

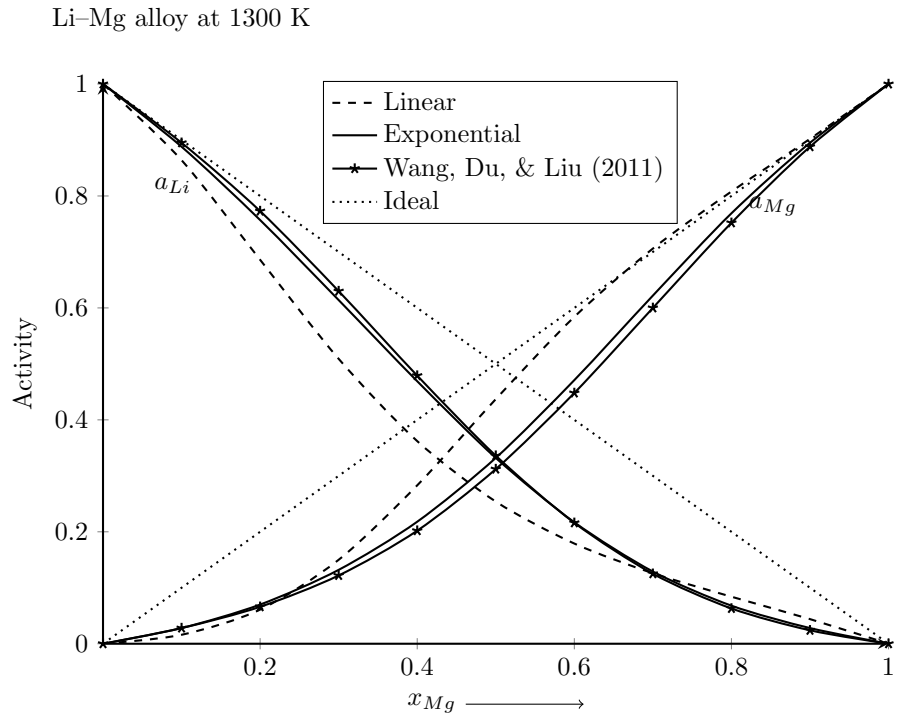

Figure 39: Activity of liquid Li–Mg alloy at 1300 K.

parameters of Wang, Du, & Liu (2011). The computed values of both components were found to increase gradually with increase in the temperature of the system, indicating decrease in the mixing tendency. It was found that the values of a_{Li} and a_{Mg} computed using exponential parameters agreed very well with those computed using parameters of Wang, Du, & Liu (2011). Moreover, they were found to be less than the ideal values throughout all compositions. But the values of a_{Mg} computed using linear parameters of this work R. K. Gohivar, Yadav, et al. (2021b) were found to have positive deviation from ideal value at x_{Mg} rich region with an increase in the temperature of system. It can be concluded that the exponential parameters of this work better explains a_k (k = Li, Mg)

Table 26: Activity of liquid Li–Mg alloy at 1900 K and 2200 K

x_{Mg}	Activity											
	T=1900 K						T =2200 K					
	This work				Ref.*		This work				Ref.*	
	Linear fit		Exponential fit		a_{Li}	a_{Mg}	Linear fit		Exponential fit		a_{Li}	a_{Mg}
	a_{Li}	a_{Mg}	a_{Li}	a_{Mg}			a_{Li}	a_{Mg}	a_{Li}	a_{Mg}		
0.1	0.863	0.022	0.892	0.044	0.898	0.039	0.862	0.024	0.893	0.051	0.898	0.042
0.2	0.681	0.087	0.771	0.104	0.783	0.085	0.680	0.097	0.775	0.116	0.786	0.092
0.3	0.507	0.213	0.642	0.180	0.653	0.148	0.507	0.237	0.651	0.197	0.660	0.157
0.4	0.372	0.381	0.512	0.275	0.513	0.232	0.375	0.417	0.525	0.294	0.523	0.241
0.5	0.281	0.541	0.387	0.387	0.375	0.339	0.289	0.577	0.405	0.405	0.388	0.347
0.6	0.222	0.658	0.275	0.512	0.253	0.468	0.236	0.682	0.294	0.526	0.265	0.474
0.7	0.180	0.737	0.179	0.644	0.154	0.611	0.200	0.746	0.197	0.652	0.164	0.614
0.8	0.136	0.807	0.103	0.774	0.081	0.755	0.157	0.807	0.116	0.777	0.087	0.756
0.9	0.073	0.895	0.044	0.894	0.032	0.888	0.085	0.893	0.051	0.894	0.034	0.888

*Wang, Du, & Liu (2011)

and G_M^{xs} than those of Wang, Du, & Liu (2011).

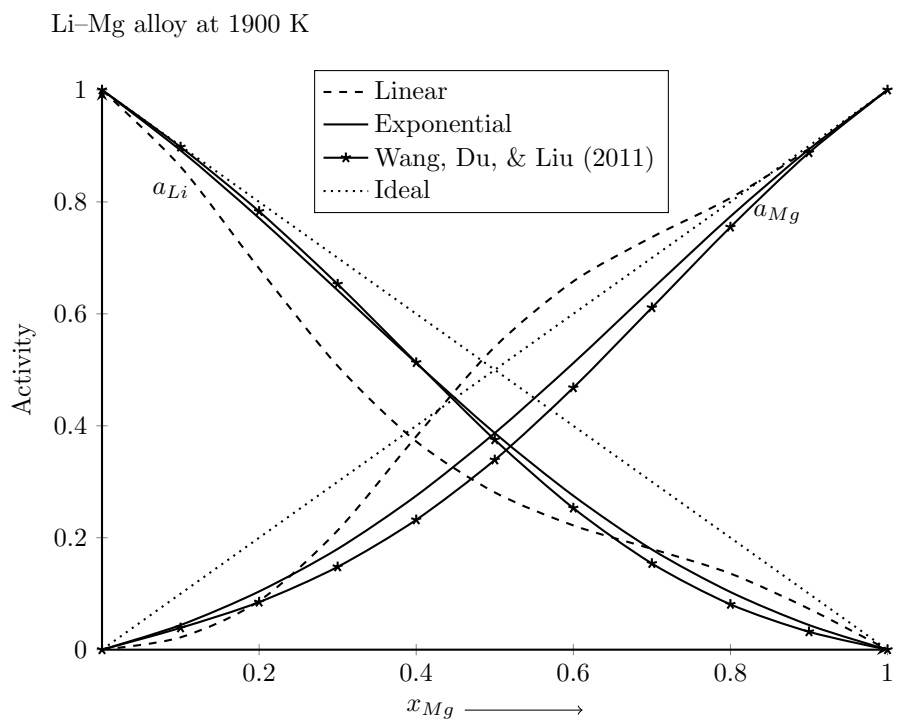

Figure 40: Activity of liquid Li–Mg alloy at 1900 K.

4.6 Structural properties

The thermodynamic functions basically G_M^{xs} and activity have direct effect on the structural properties of liquid alloys. Structural properties give information related to the atomic arrangements at the local level in the liquid mixtures. The phase transformations as a function of temperature and concentration can be analysed in a more appropriate

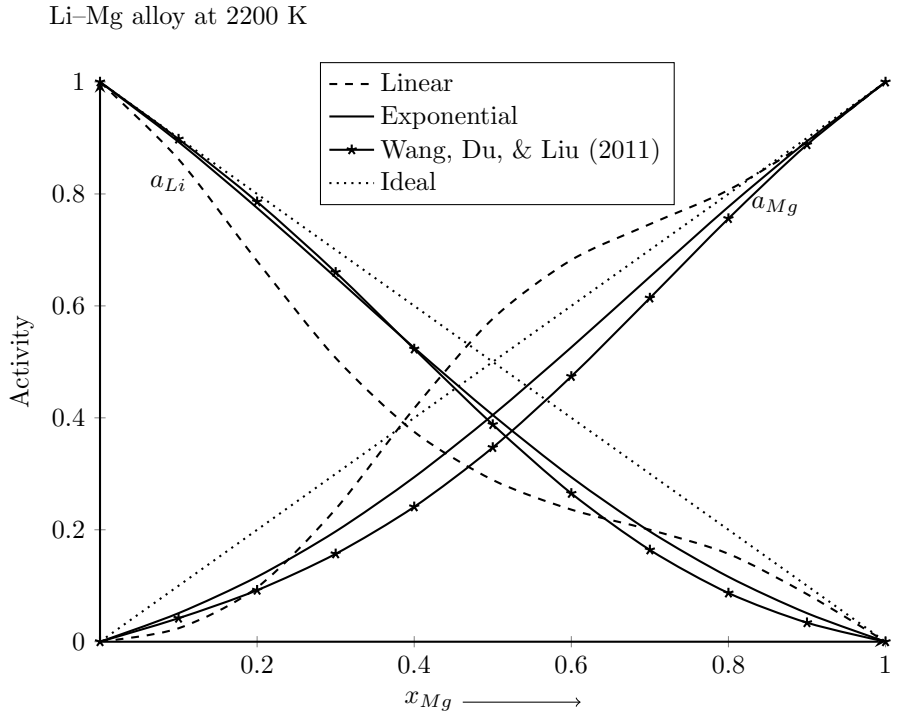

Figure 41: Activity of liquid Li–Mg alloy at 2200 K.

way in terms of the structural properties. In structural properties, we have computed concentration fluctuation in long wavelength limit ($S_{CC}(0)$) to strengthen previous findings related to the phase transformations predicted by the computations of thermodynamic properties at higher temperatures.

4.6.1 Concentration fluctuation in long wavelength limit ($S_{CC}(0)$)

It provides information about the ordering and segregating nature of liquid alloys. The expression required for the computation of $S_{CC}(0)$ in terms of interaction parameters of G_M^{xs} are presented in the formulation section of the Chapter 3. The values of $S_{CC}(0)$ were calculated using Equation (3.49) with the interaction parameters of G_M^{xs}. The computed values of $S_{CC}(0)$ were compared with the ideal values $S_{CC}^{id}(0)$ to determine whether the arrangement of alloy species is ordering (hetero-coordinating) or segregating (homo-coordinating). At a given concentration and temperature, if $S_{CC}(0) < S_{CC}^{id}(0)$, the alloy is expected to be ordering in nature; and if $S_{CC}(0) > S_{CC}^{id}(0)$, then it is expected to be segregating in nature and if $S_{CC}(0) = S_{CC}^{id}(0)$, then it is expected to be ideal in nature. In case of ideal alloy, there is no bonding or interaction between the constituent atoms of the alloy and hence $H_M = 0$.

In the following sub-sections, the results and discussion for $S_{CC}(0)$ of Al–Fe, Al–Mn, Al–Ti and Li–Mg liquid alloys are presented.

4.6.2 $S_{CC}(0)$ of liquid Al–Fe alloy

Adhikari et al. (2014) studied the structural properties of liquid Al–Fe alloy at 1873 K in the framework of a regular associated solution model. They stated that the system showed a strong ordering nature at its melting temperature. In this work, we have studied the structural properties of the system at different temperatures with the interaction parameters of the R-K polynomial. The values of $S_{CC}(0)$ for Al–Fe system at 1873 K were calculated from Equation (3.49) employing both the linear and exponential parameters of Table 1. The experimental values of $S_{CC}(0)$ were calculated with the aid of experimental data of activity (Hultgren et al., 1973) using the following expression (Bhatia & Thornton, 1970)

$$S_{CC}(0) = x_A a_B \left[(\frac{\partial a_B}{\partial x_B})_{T,P,N} \right]^{-1} = x_B a_A \left[(\frac{\partial a_A}{\partial x_A})_{T,P,N} \right]^{-1} \tag{4.1}$$

where x_A and x_B are concentrations of components A and B, and a_A and a_B are their corresponding activities.

Table 27: $S_{CC}(0)$ of liquid Al–Fe alloy at 1873 K and 2500 K

x_{Fe}	$S_{CC}(0)$							
	T=1873 K					T=2500 K		
	This work		Experimental*	Cost 507	Ref.**	This work		Cost 507
	Linear fit	Exponential fit				Linear fit	Exponential fit	
0.1	0.048	0.047	0.050	0.061	0.053	0.065	0.058	0.076
0.2	0.069	0.066	0.070	0.084	0.071	0.101	0.087	0.116
0.3	0.085	0.081	0.084	0.093	0.078	0.126	0.109	0.133
0.4	0.098	0.094	0.097	0.096	0.088	0.141	0.126	0.137
0.5	0.106	0.103	0.105	0.095	0.099	0.147	0.135	0.133
0.6	0.108	0.107	0.110	0.091	0.108	0.141	0.136	0.124
0.7	0.103	0.103	0.102	0.085	0.107	0.125	0.126	0.111
0.8	0.088	0.089	0.086	0.074	0.099	0.100	0.104	0.092
0.9	0.060	0.061	0.064	0.054	0.067	0.064	0.067	0.062

*Hultgren et al. (1973), **Adhikari et al. (2014)

The calculated, experimental and ideal values of $S_{CC}(0)$ for the system at 1873 K along with the literature data are presented in Table 27 and plotted in Figure 42 as a function of concentration. It can be observed that the computed values of $S_{CC}(0)$ using both linear and exponential parameters are in good agreement with each other. They are also in good agreement with experimental values and literature results of Adhikari et al. (2014). The values computed using the linear parameters of Cost 507 (Ansara et al., 1998) show reasonable agreement with the above mentioned results. The plots of all these values show negative deviation with respect to the ideal value curve (Figure 42) indicating the system to be ordering in nature at 1873 K. Further, the theoretical values of ($S_{CC}(0)$) were also computed at higher temperatures 2500 K, 3500 K and 3800 K following the similar procedure as mentioned above. The value so obtained are tabulated in the Table 27 & 28 and plotted in Figures 43-45. When temperature of the system was gradually

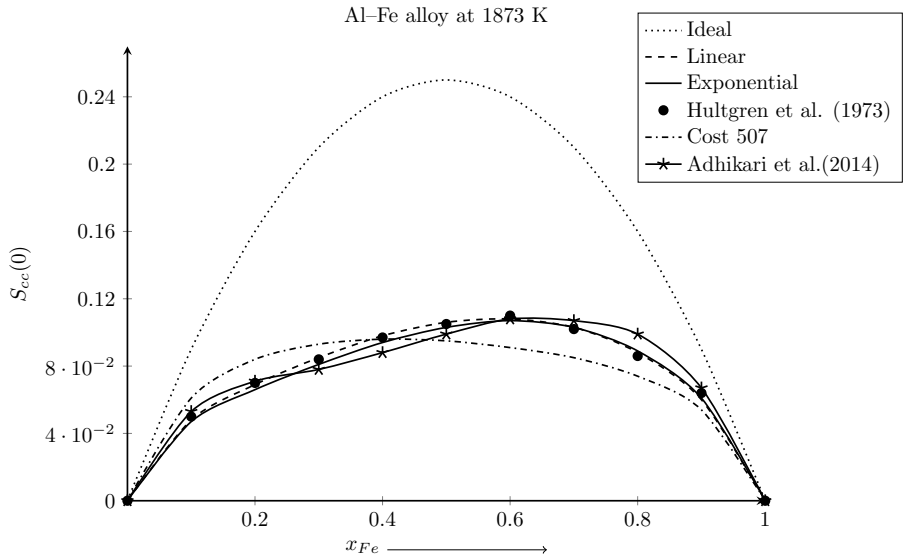

Figure 42: $S_{CC}(0)$ of liquid Al–Fe alloy at 1873 K.

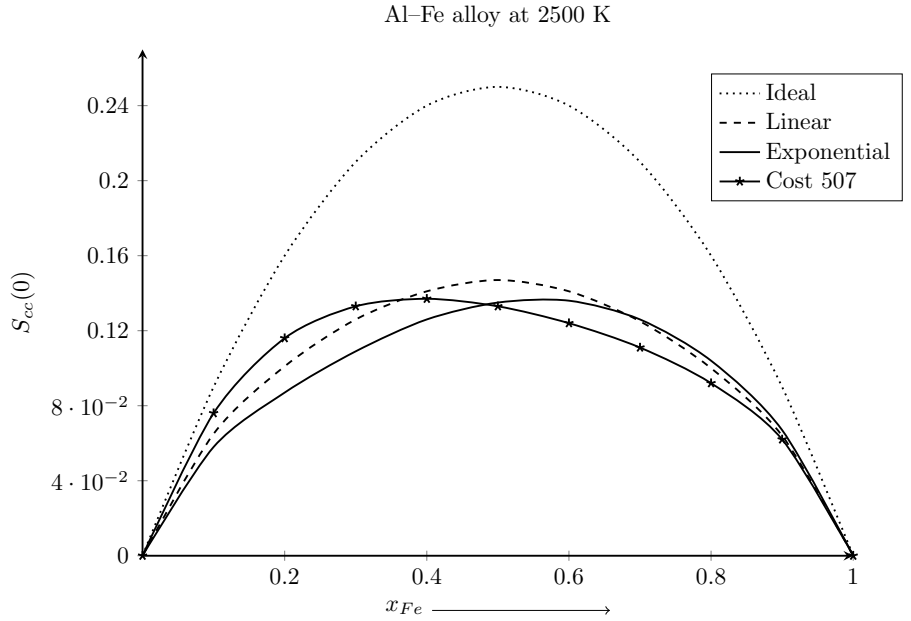

Figure 43: $S_{CC}(0)$ of liquid Al–Fe alloy at 2500 K.

increased beyond 1873 K, the value of $S_{CC}(0)$ obtained using linear parameters increased more rapidly than those of exponential parameters. At temperatures 3500 K and 3800 K, the computed values are found to be $S_{CC}(0) > S^{id}_{CC}(0)$ on using the linear interaction parameters in region of lower concentration of Fe. These results reveal the transformation of phase of the alloy from ordering to segregating which is termed as an artificial inverted miscibility gap. But when these values were computed using the exponential parameters, no such unusual tendencies were observed. Therefore, it can be stated that the exponential parameters well explain the structural as well as the thermodynamic properties of Al–Fe

Table 28: $S_{CC}(0)$ of liquid Al–Fe alloy at 3500 K and 3800 K

x_{Fe}	$S_{CC}(0)$					
	T=3500 K			T=3800 K		
	This work		Cost 507	This work		Cost 507
	Linear fit	Exponential fit		Linear fit	Exponential fit	
0.1	0.091	0.070	0.098	0.099	0.073	0.104
0.2	0.164	0.113	0.172	0.187	0.119	0.190
0.3	0.212	0.145	0.207	0.245	0.153	0.233
0.4	0.229	0.167	0.213	0.261	0.177	0.239
0.5	0.218	0.177	0.200	0.242	0.187	0.222
0.6	0.190	0.173	0.177	0.204	0.182	0.194
0.7	0.153	0.154	0.149	0.161	0.161	0.160
0.8	0.114	0.122	0.116	0.117	0.126	0.122
0.9	0.069	0.074	0.072	0.069	0.076	0.074

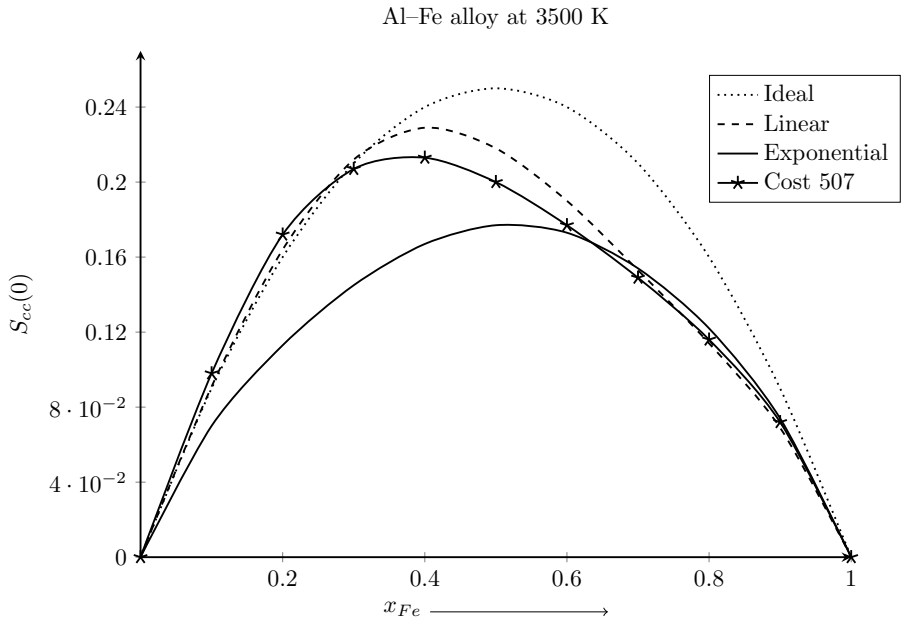

Figure 44: $S_{CC}(0)$ of liquid Al–Fe alloy at 3500 K.

system at higher temperatures. Moreover, the deviation between computed and ideal values of ($S_{CC}(0)$) gradually decreases at higher temperatures, indicating the decrease in ordering nature of the system.

4.6.3 $S_{CC}(0)$ of liquid Al–Mn alloy

The values of $S_{CC}(0)$ for Al–Mn system at 1600 K were calculated using Equation (3.49) with the help of parameters from the Table 4. The observed values of $S_{CC}(0)$ were computed using Equation (4.6.2) and experimental data of activity (Desai, 1987). The compositional dependence of all the computed values are depicted in Table 29

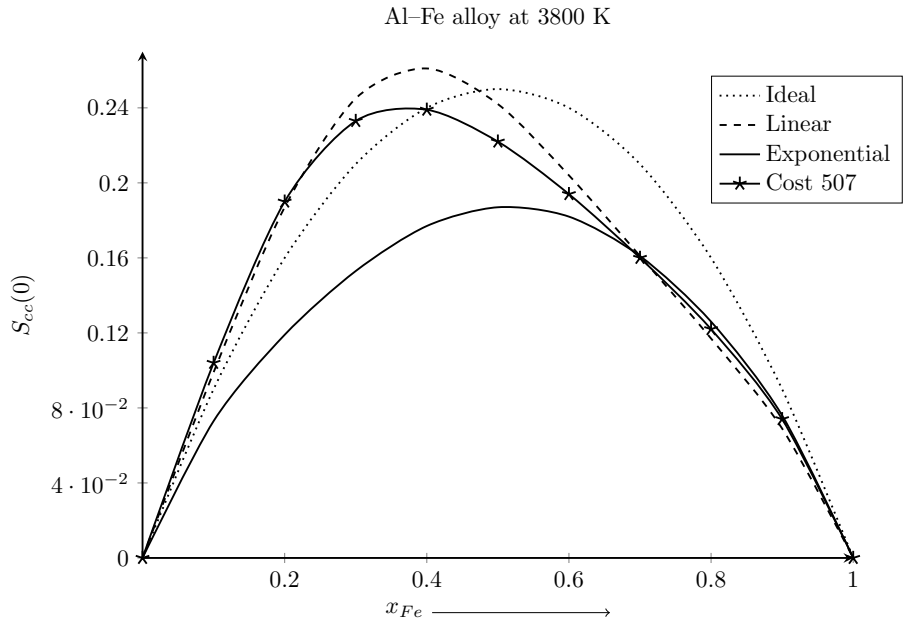

Figure 45: $S_{CC}(0)$ of liquid Al–Fe alloy at 3800 K.

and plotted in Figure 46. It can be observed that values computed using linear and exponential parameters were found to be in good agreement at 1600 K. However, the observed values of $S_{CC}(0)$ exceeded the ideal values at/around equiatomic composition (R. K. Gohivar, Yadav, et al., 2020). The minor difference between these values in the $S_{CC}(0)$ at $x_{Mn} = 0.5$ could be due to errors in the observed activity of Al (0.365 ± 0.11) and Mn (0.161 ± 0.44) at the equi-composition of Al and Mn (Desai, 1987). The values of $S_{CC}(0)$ computed using the linear and exponential parameters showed negative deviation from the ideal value at all concentrations revealing the system to be ordering in nature (Figure 46).

Table 29: $S_{CC}(0)$ of liquid Al–Mn alloy at 1600 K, 1900 K, 2200 K and 2500 K

x_{Mn}	$S_{CC}(0)$								
	T=1600 K			T=1900 K		T=2200 K		T=2500 K	
	Linear fit	Exponential fit	Ref.*	Linear fit	Exponential fit	Linear fit	Exponential fit	Linear fit	Exponential fit
0.1	0.066	0.062	0.062	0.077	0.068	0.087	0.073	0.098	0.076
0.2	0.102	0.094	0.090	0.128	0.108	0.156	0.119	0.188	0.128
0.3	0.126	0.116	0.115	0.162	0.136	0.205	0.152	0.258	0.166
0.4	0.139	0.130	0.196	0.180	0.154	0.229	0.174	0.289	0.190
0.5	0.142	0.135	0.254	0.181	0.160	0.226	0.181	0.278	0.199
0.6	0.135	0.131	0.129	0.167	0.154	0.202	0.174	0.239	0.190
0.7	0.119	0.118	0.079	0.142	0.137	0.165	0.153	0.182	0.166
0.8	0.095	0.096	0.049	0.109	0.109	0.122	0.119	0.134	0.128
0.9	0.062	0.063	0.031	0.068	0.068	0.072	0.073	0.076	0.076

*Desai (1987)

Theoretical values of $S_{CC}(0)$ for the system were also computed at higher temperatures 1900 K, 2200 K and 2500 K following the procedure as mentioned above. These values

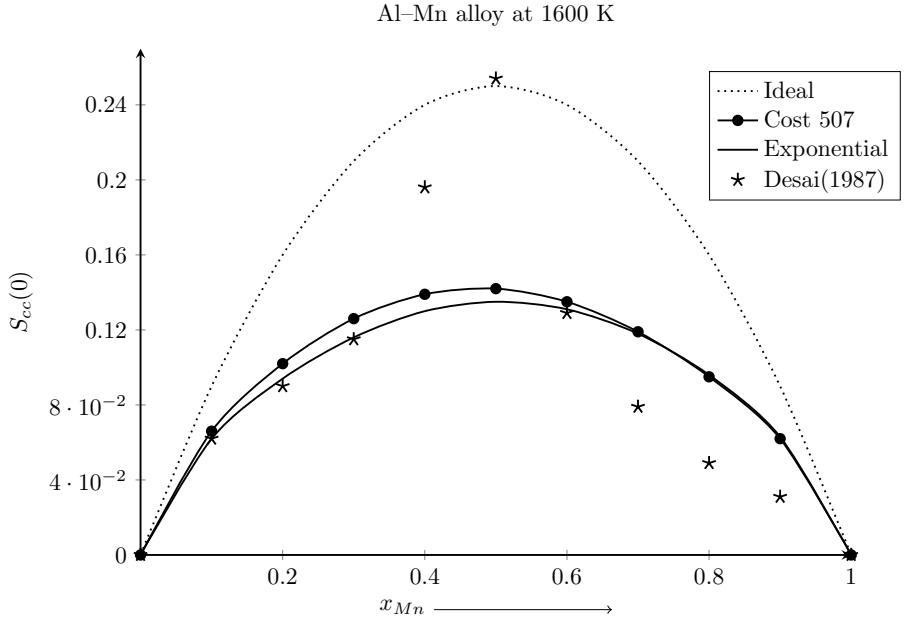

Figure 46: $S_{CC}(0)$ of liquid Al–Mn alloy at 1600 K.

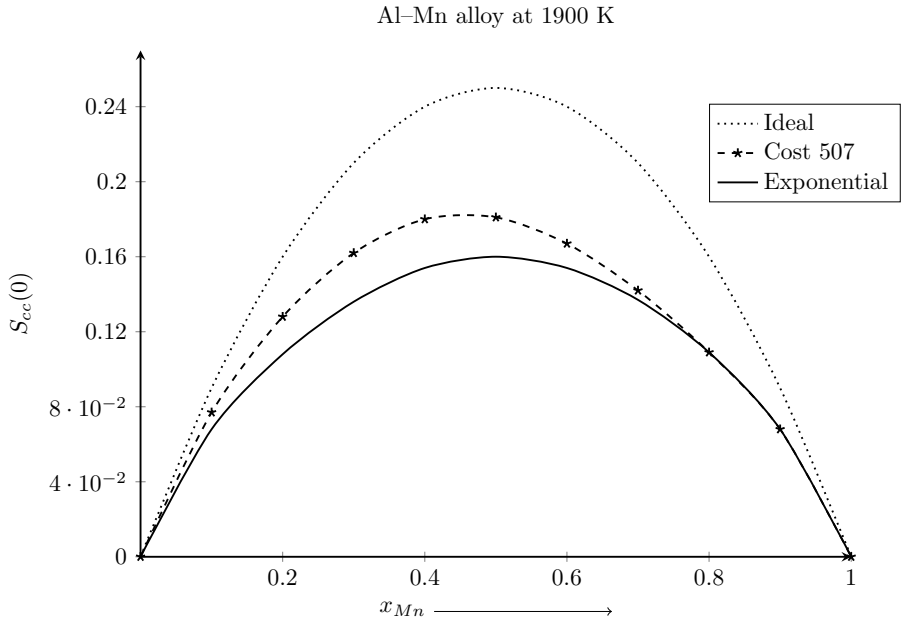

Figure 47: $S_{CC}(0)$ of liquid Al–Mn alloy at 1900 K.

are portrayed in Table 29 and plotted as a function of concentration in Figures 47-49. It can be observed that with the increase in temperature, the computed values of $S_{CC}(0)$ gradually increased and approached ideal values using both optimised parameters. At and above 2500 K, the computed values of $S_{CC}(0)$ using linear parameters exceeded ideal values at higher concentrations of Mn indicating the phase transformation from ordering to segregating nature (Figure 49). This discrepancy shown by linear parameters

indicated the presence of an artificial miscibility gap. But the values computed using exponential parameters still showed ordering nature. These results are in accordance with those predicted by the computations of thermodynamic properties of the system at higher temperatures in the previous sections.

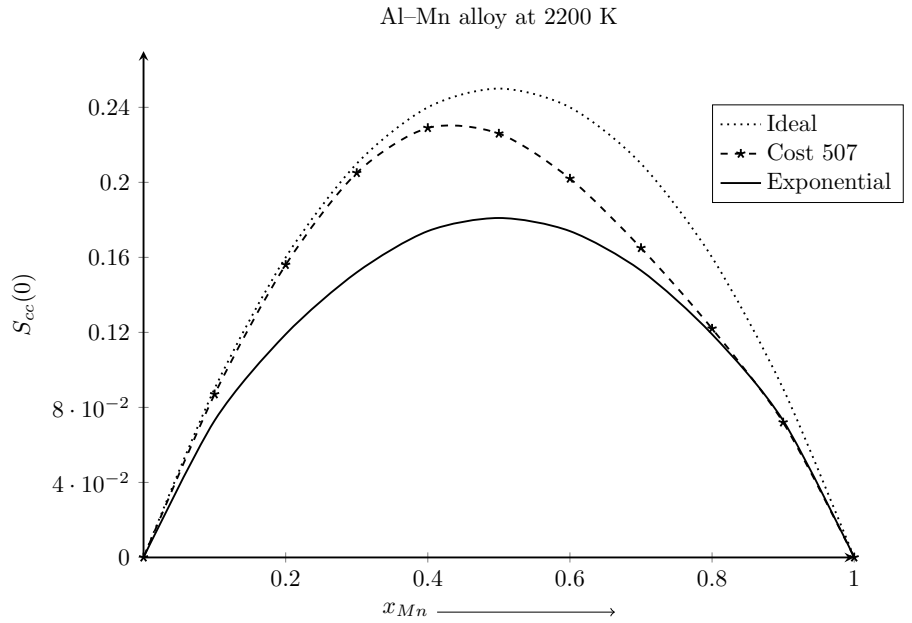

Figure 48: $S_{CC}(0)$ of liquid Al–Mn alloy at 2200 K.

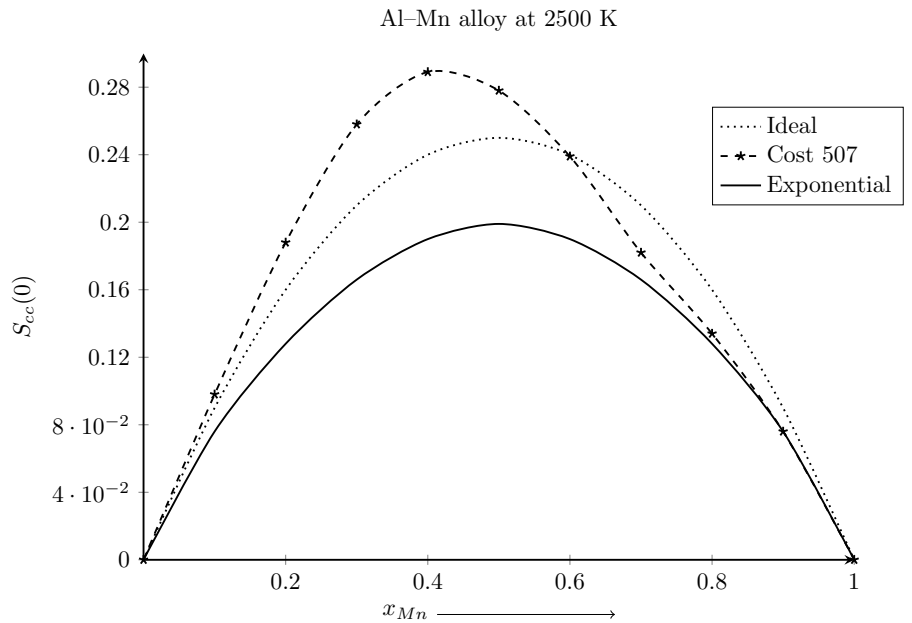

Figure 49: $S_{CC}(0)$ of liquid Al–Mn alloy at 2500 K.

4.6.4 $S_{CC}(0)$ of liquid Al–Ti alloy

We used the optimised parameters from Table 7 in Equation (3.49) to compute $S_{CC}(0)$ for this system at 1500 K, 2000 K, 2500 K and 2700 K. The computed values are presented in the Table 30 and plotted as a function of concentration in Figures 50–53.

Table 30: $S_{CC}(0)$ of liquid Al–Ti alloy at 1500 K, 2000 K, 2500 K and 2700 K

x_{Ti}	$S_{CC}(0)$							
	T=1500 K		T=2000 K		T=2500 K		T=2700 K	
	Cost 507	Exponential fit	Cost 507	Exponential fit	Cost 507	Exponential fit	Cost 507	Exponential fit
0.1	0.084	0.074	0.115	0.079	0.147	0.082	0.161	0.083
0.2	0.089	0.079	0.140	0.100	0.212	0.117	0.250	0.123
0.3	0.078	0.071	0.123	0.100	0.187	0.126	0.221	0.136
0.4	0.071	0.066	0.110	0.097	0.162	0.128	0.189	0.139
0.5	0.068	0.064	0.103	0.096	0.149	0.127	0.171	0.140
0.6	0.070	0.066	0.103	0.097	0.145	0.128	0.164	0.139
0.7	0.075	0.071	0.108	0.100	0.146	0.126	0.163	0.136
0.8	0.083	0.079	0.112	0.100	0.143	0.117	0.156	0.123
0.9	0.077	0.074	0.091	0.079	0.102	0.082	0.106	0.083

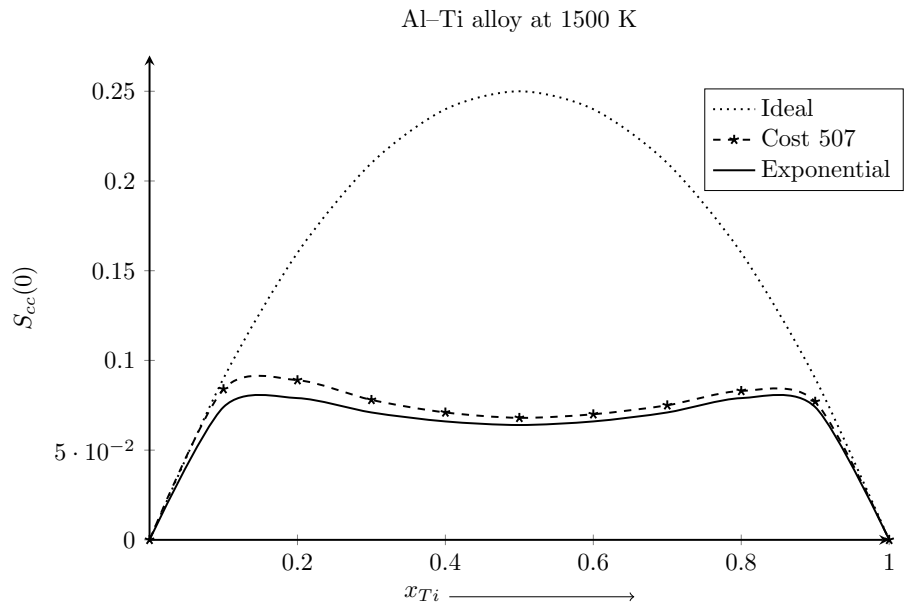

Figure 50: $S_{CC}(0)$ of liquid Al–Ti alloy at 1500 K.

At 1500 K, it can be observed that the computed values of $S_{CC}(0)$ using both the linear and exponential parameters were found to be in good agreement. These values were found to be less than the ideal values at all concentrations (Figure 50) indicating the ordering nature of the system. These computed values increased gradually with increase in temperature of the system in the temperature range of 1500-2700 K. The rate of increment of values computed using linear parameters was found to be more rapid in compared to those using exponential parameters. At lower concentration of Ti, the

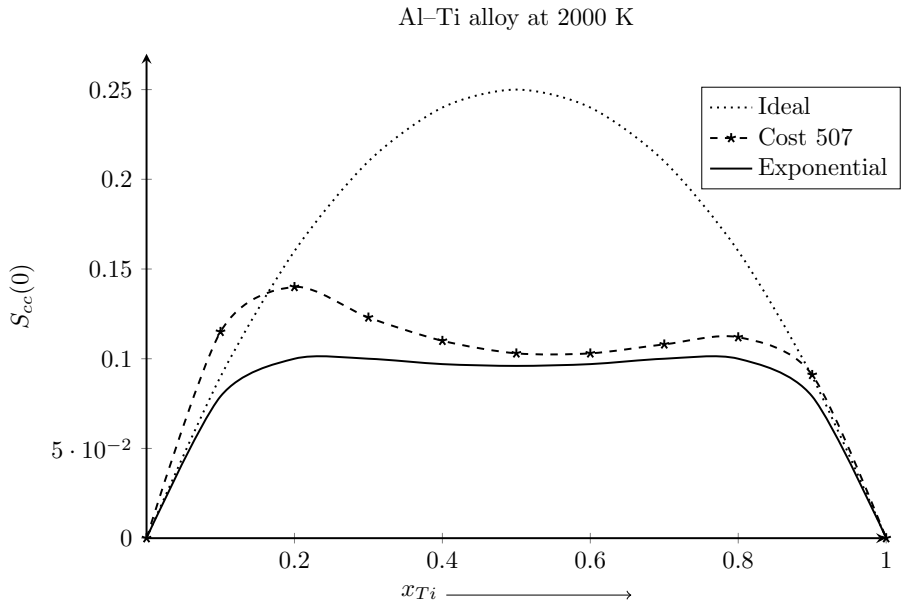

Figure 51: $S_{CC}(0)$ of liquid Al–Ti alloy at 2000 K.

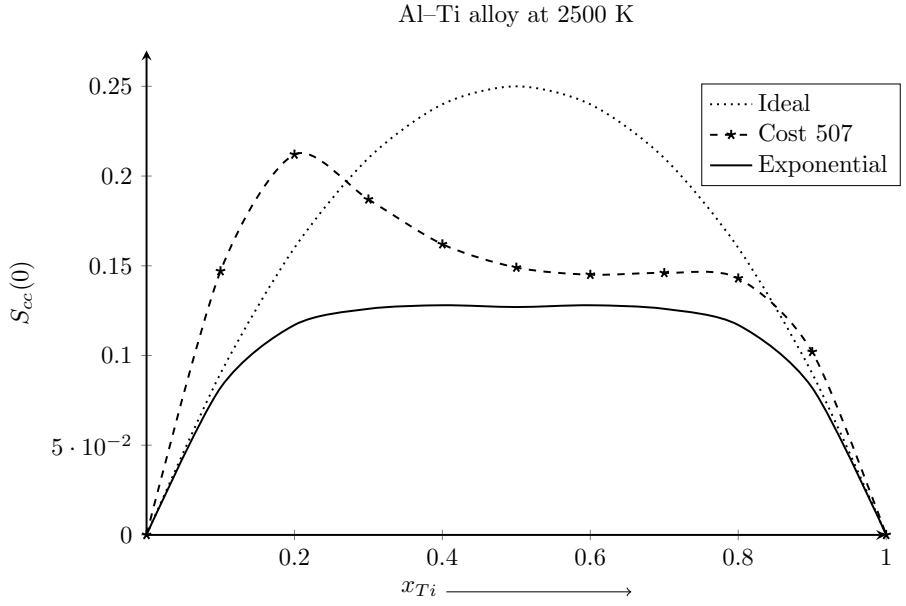

Figure 52: $S_{CC}(0)$ of liquid Al–Ti alloy at 2500 K.

computed values of $S_{CC}(0)$ using linear parameters were found to be greater than ideal values ($S_{CC}(0)$>$S^{id}_{CC}(0)$) indicating the phase transition from ordering to segregating nature of the system. This tendency (extent or region of phase transformation) was found to enhance with increase in temperature of the system (Figures 51–53). But the values of $S_{CC}(0)$ computed using exponential parameters were found to be less than the ideal values ($S_{CC}(0)$<$S^{id}_{CC}(0)$) in the entire concentration range and at all the preferred temperatures indicating the system to be ordering in nature. Thus, the artificial miscibility gap seen in

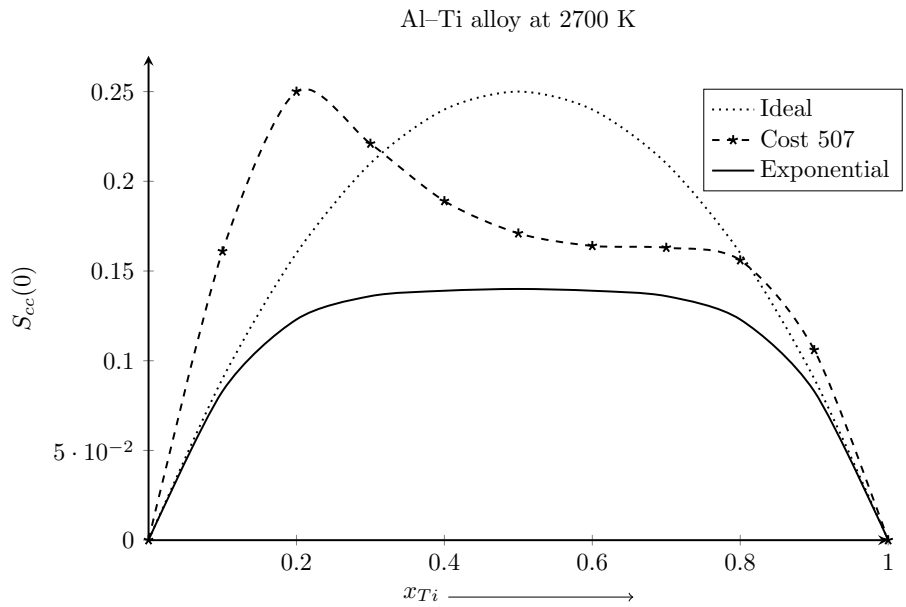

Figure 53: $S_{CC}(0)$ of liquid Al–Ti alloy at 2700 K.

the structural property of the system was eliminated using exponential parameters.

4.6.5 $S_{CC}(0)$ of liquid Li–Mg alloy

Singh et al. (1987) had investigated the $S_{CC}(0)$ of liquid Li–Mg alloy at 695 K, 830 K and 887 K using quasi-chemical approximation. They found that $S_{CC}(0)<S^{id}_{CC}(0)$ and the computed values shifted towards ideal with an increase in temperature. Further, they had computed the $S_{CC}(0)$ with the observed activity data using a standard thermodynamic relation and noticed that in the lower Li contents $S_{CC}(0)>S^{id}_{CC}(0)$. In this work, we computed the values of $S_{CC}(0)$ at 1000 K, 1300 K, 1900 K and 2200 K using the parameters from Table 10 in Equation (3.49). The experimental values of $S_{CC}(0)$ were computed using the activity data of Hultgren et al. (1973) in Equation (4.6.2). The computed values of $S_{CC}(0)$ using both the linear and exponential parameters are tabulated in Tables 31 & 32 and plotted in Figures 54–57.

From Figure 54, it can be observed that the computed values of $S_{CC}(0)$ at 1000 K using optimised linear interaction parameters were in excellent agreement with the calculated experimental values Hultgren et al. (1973). They showed positive deviation from ideal values at and above $x_{Mg} = 0.9$ and negative deviation at rest of concentrations ($x_{Mg} < 0.9$) indicting the transformation of phase in the system. But the values of $S_{CC}(0)$ computed using exponential parameters of this work and linear parameters of Wang, Du, & Liu (2011) were in good agreement and less than the ideal values at all compositions, indicating the complete ordering nature of the system. The values of $S_{CC}(0)$ calculated

Table 31: $S_{CC}(0)$ of liquid Li–Mg alloy at 1000 K and 1300 K

x_{Mg}	$S_{CC}(0)$						
	T=1000 K				T=1300 K		
	Linear fit	Exponential fit	Experimental*	Ref.**	Linear fit	Exponential fit	Ref.**
0.1	0.053	0.069	0.053	0.076	0.052	0.072	0.080
0.2	0.075	0.100	0.075	0.106	0.074	0.110	0.116
0.3	0.089	0.111	0.089	0.114	0.093	0.126	0.127
0.4	0.101	0.112	0.102	0.115	0.114	0.131	0.128
0.5	0.113	0.109	0.112	0.113	0.141	0.131	0.126
0.6	0.126	0.106	0.127	0.112	0.172	0.128	0.122
0.7	0.139	0.106	0.138	0.108	0.192	0.123	0.116
0.8	0.142	0.104	0.142	0.099	0.169	0.111	0.103
0.9	0.100	0.082	0.101	0.071	0.095	0.079	0.072

*Hultgren et al. (1973), **Wang, Du, & Liu (2011)

Table 32: $S_{CC}(0)$ of liquid Li–Mg alloy at 1900 K and 2200 K

x_{Mg}	$S_{CC}(0)$					
	T=1900 K			T=2200 K		
	Linear fit	Exponential fit	Ref.*	Linear fit	Exponential fit	Ref.*
0.1	0.051	0.077	0.084	0.051	0.079	0.085
0.2	0.074	0.122	0.128	0.073	0.127	0.131
0.3	0.097	0.147	0.143	0.098	0.155	0.149
0.4	0.132	0.159	0.146	0.139	0.170	0.152
0.5	0.192	0.162	0.142	0.215	0.174	0.148
0.6	0.280	0.158	0.136	0.344	0.169	0.140
0.7	0.320	0.146	0.125	0.399	0.155	0.129
0.8	0.212	0.123	0.107	0.229	0.127	0.109
0.9	0.089	0.079	0.072	0.088	0.079	0.072

*Wang, Du, & Liu (2011)

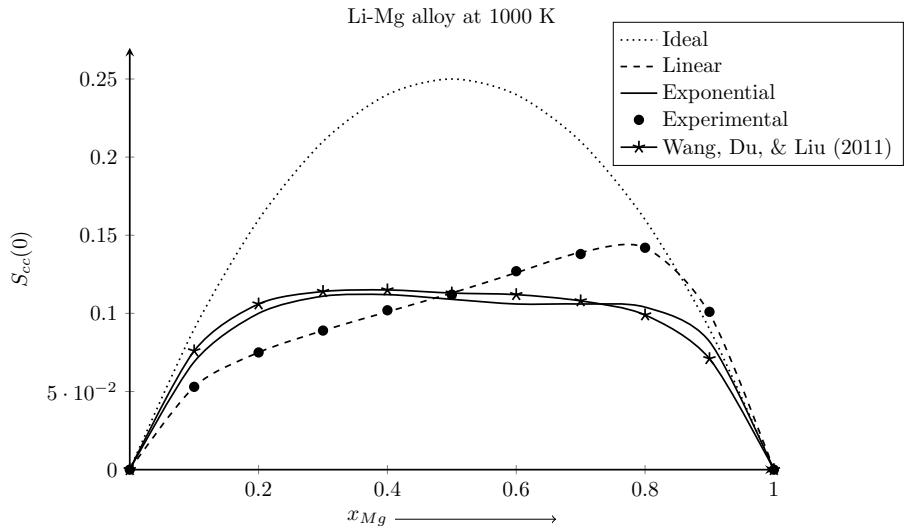

Figure 54: $S_{CC}(0)$ of liquid Li–Mg alloy at 1000 K.

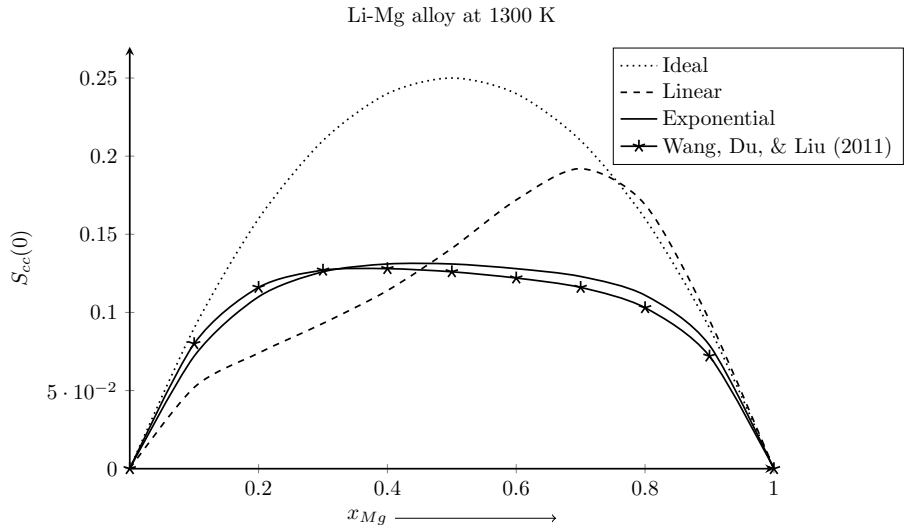

Figure 55: $S_{CC}(0)$ of liquid Li–Mg alloy at 1300 K.

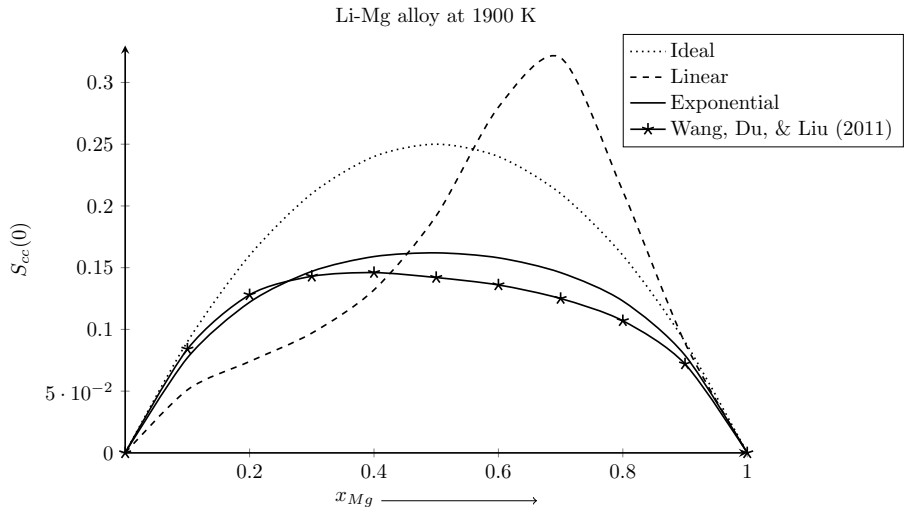

Figure 56: $S_{CC}(0)$ of liquid Li–Mg alloy at 1900 K.

using all the preferred parameters were in excellent agreement at $x_{Mg} = 0.5$ at this temperature (Figure 54). At higher temperatures (above 1000 K), the computed values of $S_{CC}(0)$ using linear parameters gradually decreased at higher $x_{Mg} \geq 0.9$ and lower $x_{Mg} < 0.3$ concentrations of Mg. Moreover, these values exceeded ideal at higher concentrations of Mg, indicating the transformation from ordering to segregating nature. These unusual behaviours are known as artificial inverted miscibility gaps. However, the values computed using exponential parameters and the parameters of Wang, Du, & Liu (2011) gradually increased and got closer to ideal values at higher temperatures (Figures 55–57). They were found to be less than ideal values in the entire concentration range and considered temperature range, indicating the preservation of ordering tendencies.

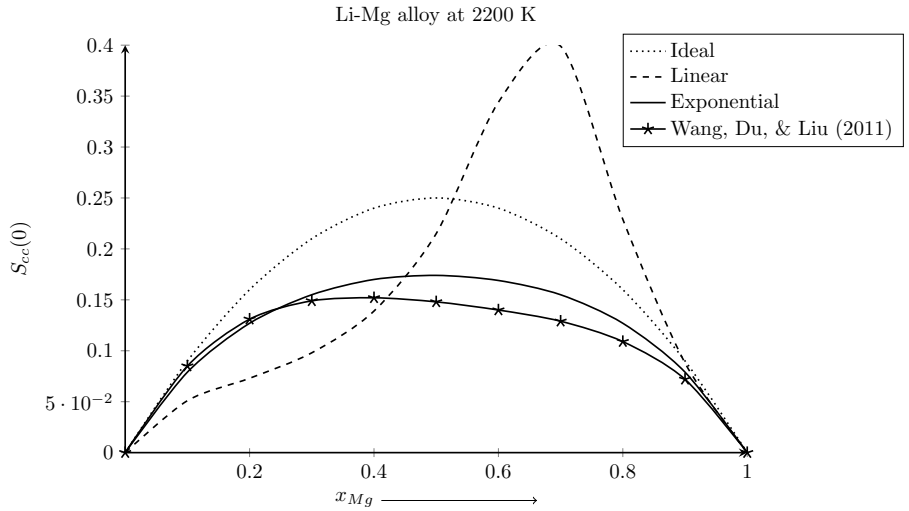

Figure 57: $S_{CC}(0)$ of liquid Li–Mg alloy at 2200 K.

4.7 Thermodynamic properties of ternary liquid Al–Li–Zn alloy

The thermodynamic properties and phase diagram of ternary systems can be predicted with the help of different theoretical models (geometrical models and empirical model) (Chou & Chang, 1989). These models for ternary system are actually derived in terms of their constituent sub-binary systems. Therefore, we have also calculated thermodynamic and structural functions of liquid Al–Li, Li–Zn and Al–Zn sub-binary systems before predicting the mixing properties of ternary liquid Al–Li–Zn alloy.

Because of low density and high specific strength of Al–Li alloys, they are promising materials for the use in aerospace, military, and automobile industries. Furthermore, they have the potential to be used as new sustainable energy storage materials, such as for safe hydrogen storage in hydrogen power systems and as negative electrodes in high temperature batteries (Debski & Terlicka, 2016). The mechanical properties of this binary system are improved by the addition of zinc, expanding its range of potential applications. These materials might be employed in a number of sectors, including the automotive, military, or aerospace industries as well.

4.8 G_M^{xs} ternary liquid Al–Li–Zn alloy

In theoretical modelling, the mixing properties of ternary liquid alloys are studied by considering the interaction of their constituent sub-binary pairs. To predict the mixing properties of ternary alloys, several theoretical models (Chou & Chang, 1989; Muggianu et al., 1975) have been developed. Chou & Chang (1989) summarized the different geometrical models (Kohler, Colinet, Muggianu, Toop, and Hillert) and suggested new

model called General Solution Model (GSM) or Chou model to explain the mixing properties of ternary systems. In these geometrical models, the interaction parameters for G_M^{xs} of sub-binary systems are used to compute G_M^{xs} of ternary systems.

In the present work, we computed the mixing properties of the ternary Al–Li–Zn system using the thermodynamic database of its sub-binary systems. We used Redlich-Kister-Muggianu model (Muggianu et al., 1975) to study the thermodynamic properties of the ternary Al–Li–Zn alloy at temperatures of 973 K and 1573 K by using the linear and exponential interaction parameters of sub-binary Al–Li, Li–Zn and Zn-Al systems. We have first calculated values of S_M^{xs} using the parameters for G_M^{xs} of Hallstedt & Kim (2007) and values H_M from parameters of Debski & Terlicka (2016). These values were then used to optimise the linear parameters for G_M^{xs}. Finally, they were used to optimise the exponential interaction parameters of liquid Al–Li alloy. The exponential interaction parameters of sub-binary Li–Zn and Zn-Al systems were optimised using equations of the Section (3.4) with the help of linear parameters from Y. Liang et al. (2008); Mathon et al. (2000); Trybula et al. (2014). Following a similar procedure, the ternary interaction parameters were also optimised. These optimised parameters for sub-binary and ternary systems are presented in the Table 33.

Table 33: Optimised coefficients of R-K polynomial for G_M^{xs} sub-binary liquid Al–Li, Li–Zn and Al–Zn alloys and ternary liquid Al–Li–Zn alloy

Interaction parameters (J/mol)			
Systems		Hallstedt & Kim (2007)	Exponential
Al–Li	L_0	$-44200 + 20.6T$	$-61954.0\exp(-9.85\times10^{-4}T)$
	L_1	$13600 - 5.3T$	$22608.0\exp(-7.97\times10^{-4}T)$
	L_2	14200	$44253.2\exp(-1.57\times10^{-3}T)$
	L_3	−12100	$-20589.4\exp(-3.13\times10^{-4}T)$
	L_4	−7100	-
		Y. Liang et al. (2008)	Exponential
Li–Zn	L_0	$-45258.6 + 26.3677T$	$-56462.0\exp(-1.06\times10^{-3}T)$
	L_1	$22887.2 - 4.1921T$	$23168.8\exp(-2.14\times10^{-4}T)$
	L_2	$-4552.6 + 4.0715T$	$-13536.9\exp(-2.96\times10^{-3}T)$
		Mathon et al. (2000)	Exponential
Al–Zn	L_0	$10466.6 - 3.39259T$	$11564.5\exp(-5.55\times10^{-4}T)$
		Trybula et al. (2014)	Exponential
Al–Li–Zn	L^0	$7700 - 52T$	$-11624.7\exp(13.78\times10^{-4}T)$
	L^1	$-112500 - 4T$	$-112554.6\exp(3.44\times10^{-5}T)$
	L^2	$29000 - 14T$	$35296.4\exp(-8.56\times10^{-4}T)$

4.8.1 G_M^{xs} of sub-binary systems (Al–Li, Li–Zn and Al–Zn)

Using Equation (3.4), we calculated G_M^{xs} of the sub-binary Al–Li, Li–Zn and Al–Zn liquid alloys at 973 K and 1573 K using the parameters of Table 33. The values so

calculated are presented in Tables 34-36 and are plotted as a function of concentration in Figures 58 -60. Among the three sub-binary alloys, Al–Li and Li–Zn was found to be ordering whereas Al-Zn was found to be segregating in nature. We also found that the computed values of G_M^{xs} of the systems using both the parameters (linear and exponential) at 973 K were in good agreement. At 1573 K, the graph of G_M^{xs} calculated using linear interaction parameters has more pronounced S-shaped in Al–Li and Li–Zn systems in the region of higher x_{Li}. These results indicates that the system changes its behaviour from ordering to segregating in that concentration range in Li–Zn alloy. The exponential interaction parameters of this work suppressed such behaviours.

Table 34: G_M^{xs} of liquid Al–Li alloy at 973 K and 1573 K

x_{Li}	G_M^{xs} (kJ/mol)			
	T = 973 K		T = 1573 K	
	Hallstedt & Kim (2007)	Exponential fit	Hallstedt & Kim (2007)	Exponential fit
0.1	-1.568	-1.537	-0.684	-1.085
0.2	-2.802	-2.775	-1.13	-1.705
0.3	-4.087	-3.997	-1.759	-2.264
0.4	-5.282	-5.136	-2.468	-2.835
0.5	-6.039	-5.939	-2.949	-3.288
0.6	-6.046	-6.080	-2.927	-3.407
0.7	-5.180	-5.338	-2.318	-3.011
0.8	-3.587	-3.725	-1.304	-2.075
0.9	-1.668	-1.637	-0.327	-0.855

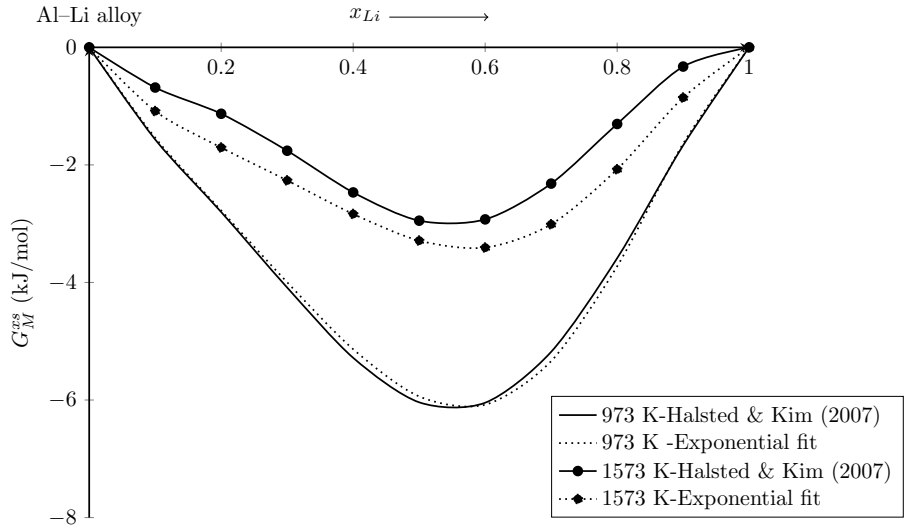

Figure 58: G_M^{xs} of liquid Al–Li alloy.

Table 35: G_M^{xs} of liquid Li–Zn alloy at 973 K and 1573 K

x_{Li}	G_M^{xs} (kJ/mol)			
	T = 973 K		T = 1573 K	
	Y. Liang et al. (2008)	Exponential fit	Y. Liang et al. (2008)	Exponential fit
0.1	-0.444	-0.492	0.939	0.233
0.2	-1.365	-1.443	1.066	-0.111
0.3	-2.557	-2.653	0.637	-0.835
0.4	-3.808	-3.914	-0.108	-1.746
0.5	-4.901	-5.010	-0.946	-2.645
0.6	-5.613	-5.721	-1.672	-3.336
0.7	-5.716	-5.815	-2.101	-3.617
0.8	-4.976	-5.057	-2.063	-3.290
0.9	-3.153	-3.203	-1.407	-2.152

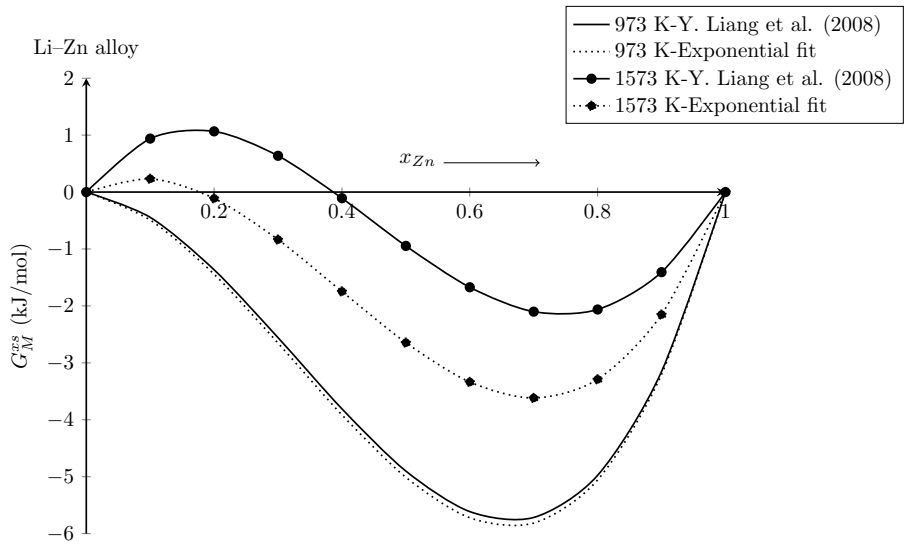

Figure 59: G_M^{xs} of liquid Li–Zn alloy.

Table 36: G_M^{xs} of liquid Al–Zn alloy at 973 K and 1573 K

x_{Zn}	G_M^{xs} (kJ/mol)			
	T = 973 K		T = 1573 K	
	Mathon et al. (2000)	Exponential fit	Mathon et al. (2000)	Exponential fit
0.1	0.645	0.607	0.462	0.435
0.2	1.147	1.079	0.821	0.774
0.3	1.505	1.416	1.077	1.015
0.4	1.720	1.618	1.231	1.160
0.5	1.791	1.686	1.283	1.209
0.6	1.720	1.618	1.231	1.160
0.7	1.505	1.416	1.077	1.015
0.8	1.147	1.079	0.821	0.774
0.9	0.645	0.607	0.462	0.435

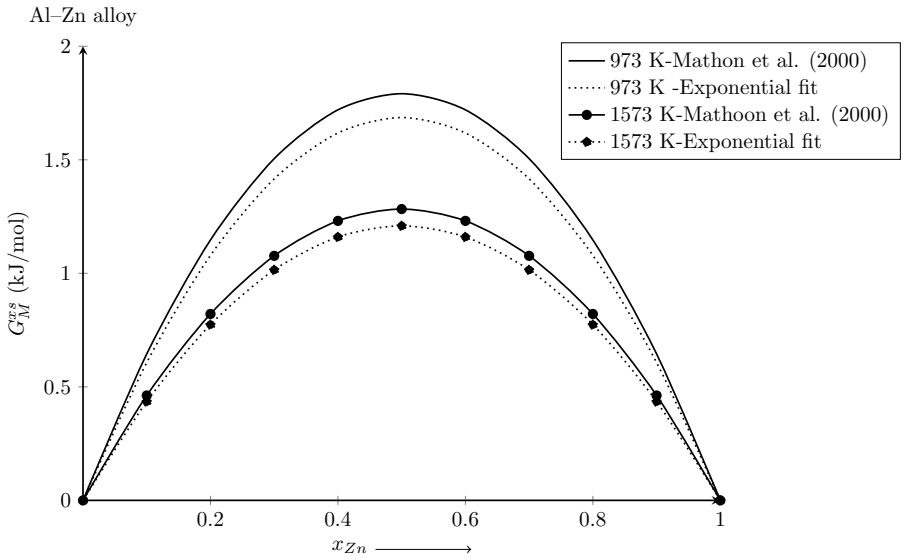

Figure 60: G_M^{xs} of liquid Al–Zn alloy.

4.8.2 G_M^{xs} of ternary liquid Al–Li–Zn alloy

The interaction parameters of sub-binary Al–Li, Li–Zn and Al–Zn and ternary systems of Table (33) were used to calculated G_M^{xs} of ternary liquid Al–Li–Zn alloy. In the present work, G_M^{xs} of the ternary alloy were computed at cross-sections $x_{Al} : x_{Zn}$ = 3 : 1, 1 : 1 and 0.136 : 1 and temperatures 973 K, 1273 K and 1573 K using the frame work of Redlich-Kister-Muggianu (R-K-M) model (using Equation (3.1.2)). The calculated values are presented in Tables (37-39) and plotted from Li-corner in Figures 61 -63. The variation in the values of G_M^{xs} with linear parameters are more rapid with increase of temperature when concentration of Zn increases than those with exponential parameters. The graph of G_M^{xs} at 1573 K calculated with linear interaction parameters was S-shaped in nature indicating the phase transition in the region of higher concentration of Li at two cross-sections, $x_{Al} : x_{Zn}$ = 1 and 0.136 (Figures 62& 63). The use of exponential T-dependent interaction parameters suppressed the unusual trend in the calculated thermodynamic function, G_M^{xs} of both sub-binary and ternary liquid alloys. These results suggest that the exponential parameters can better explain G_M^{xs} of this system at high temperature rather than linear parameters.

4.9 Enthalpy of mixing of ternary liquid Al–Li–Zn alloy

In this work, H_M for ternary system were computed using exponential interaction parameters of G_M^{xs} employing the similar process as mentioned above. The values of H_M for this system were computed using R-K-M and Toop models. In R-K-M model, the

Table 37: G_M^{xs} of ternary liquid Al–Li–Zn alloy at $x_{Al} : x_{Zn} = 3 : 1$

x_{Li}	G_M^{xs} (kJ/mol)					
	T= 973 K		T= 1273 K		T =1573 K	
	Linear fit	Exponential fit	Linear fit	Exponential fit	Linear fit	Exponential fit
0	1.344	1.264	1.153	1.070	0.962	0.906
0.1	-1.164	-1.241	-0.957	-1.256	-0.750	-1.457
0.2	-3.362	-3.401	-2.753	-3.092	-2.144	-3.126
0.3	-5.174	-5.165	-4.198	-4.482	-3.222	-4.247
0.4	-6.395	-6.381	-5.124	-5.369	-3.854	-4.849
0.5	-6.831	-6.876	-5.371	-5.649	-3.910	-4.908
0.6	-6.392	-6.526	-4.874	-5.250	-3.356	-4.405
0.7	-5.150	-5.328	-3.731	-4.188	-2.312	-3.388
0.8	-3.363	-3.475	-2.220	-2.642	-1.077	-2.031
0.9	-1.461	-1.431	-0.787	-1.014	-0.113	-0.698

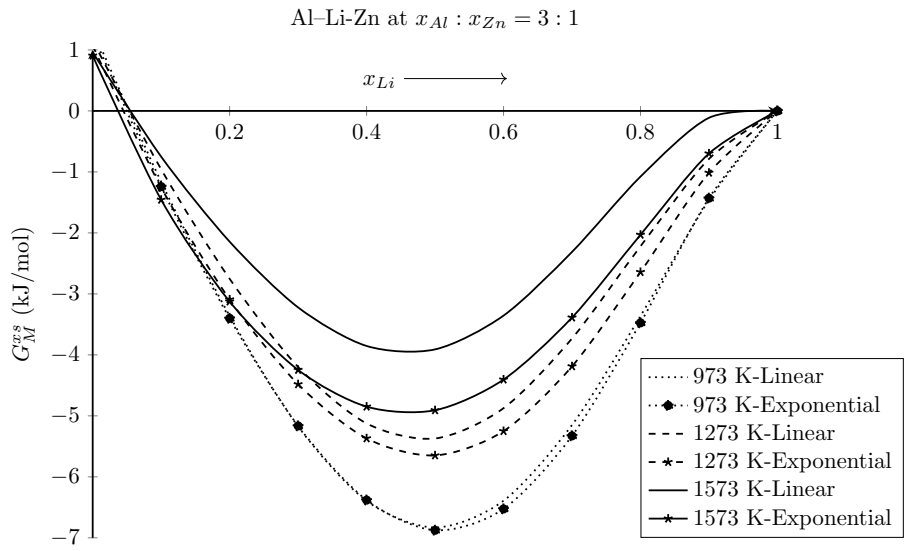

Figure 61: G_M^{xs} of ternary liquid Al–Li–Zn alloy in $x_{Al} : x_{Zn} = 3 : 1$.

Table 38: G_M^{xs} of ternary liquid Al–Li–Zn alloy at $x_{Al} : x_{Zn} = 1 : 1$

x_{Li}	G_M^{xs} (kJ/mol)					
	T= 973 K		T= 1273 K		T =1573 K	
	Linear fit	Exponential fit	Linear fit	Exponential fit	Linear fit	Exponential fit
0	1.791	1.686	1.537	1.427	1.283	1.209
0.1	-1.121	-1.219	-0.874	-1.181	-0.628	-1.335
0.2	-3.582	-3.658	-2.881	-3.268	-2.179	-3.227
0.3	-5.405	-5.472	-4.320	-4.742	-3.234	-4.451
0.4	-6.437	-6.526	-5.064	-5.524	-3.690	-4.995
0.5	-6.605	-6.738	-5.061	-5.576	-3.517	-4.875
0.6	-5.943	-6.112	-4.365	-4.931	-2.788	-4.159
0.7	-4.608	-4.768	-3.153	-3.717	-1.699	-2.994
0.8	-2.886	-2.972	-1.726	-2.189	-0.566	-1.633
0.9	-1.184	-1.166	-0.504	-0.754	0.175	-0.456

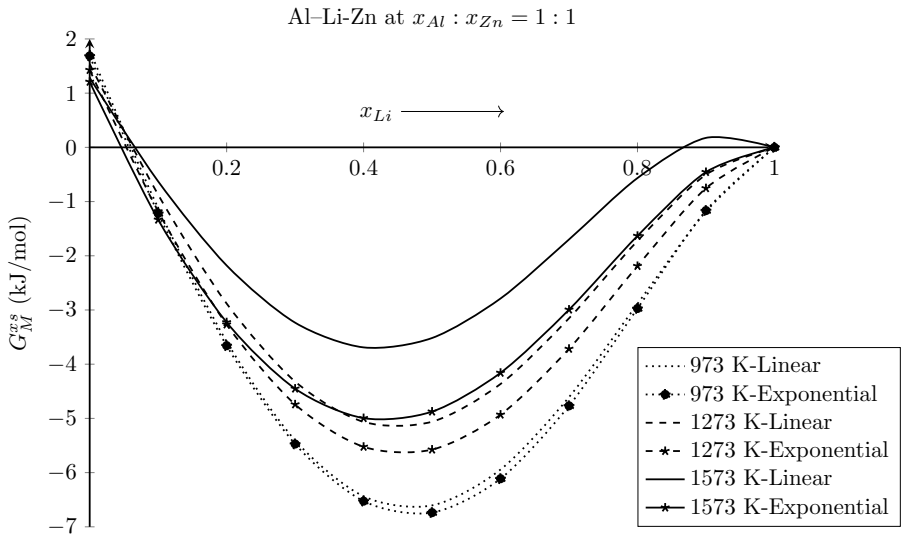

Figure 62: G_M^{xs} of ternary liquid Al–Li–Zn alloy in $x_{Al} : x_{Zn} = 1 : 1$.

Table 39: G_M^{xs} of ternary liquid Al–Li–Zn alloy at $x_{Al} : x_{Zn} = 0.136 : 1$

x_{Li}	G_M^{xs} (kJ/mol)					
	T= 973 K		T= 1273 K		T =1573 K	
	Linear fit	Exponential fit	Linear fit	Exponential fit	Linear fit	Exponential fit
0	0.757	0.712	0.649	0.603	0.542	0.511
0.1	-2.288	-2.363	-1.611	-1.917	-0.933	-1.612
0.2	-4.333	-4.430	-3.097	-3.575	-1.861	-2.973
0.3	-5.447	-5.561	-3.844	-4.434	-2.24	-3.632
0.4	-5.731	-5.859	-3.926	-4.585	-2.121	-3.675
0.5	-5.319	-5.453	-3.460	-4.149	-1.600	-3.219
0.6	-4.381	-4.510	-2.604	-3.284	-0.828	-2.415
0.7	-3.123	-3.230	-1.564	-2.183	-0.004	-1.447
0.8	-1.785	-1.855	-0.584	-1.077	0.618	-0.539
0.9	-0.642	-0.668	0.047	-0.243	0.735	0.046

interaction parameters of sub-binary and ternary systems were used to compute H_M. In case of Toop model, only the interaction parameters of sub-binary systems were used for this process. In the upcoming sub-sections, results for H_M of sub-binary systems and the ternary system are presented.

4.9.1 H_M of sub-binary systems (Al–Li, Li–Zn and Al–Zn)

In order to compute the temperature dependent values of H_M for sub-binary pairs Al–Li, Li–Zn and Al–Zn, the exponential interaction parameters of G_M^{xs} from Table 33 were used in Equation (3.26). The values of H_M were calculated at 973 K and 1573 K and are presented in Table 40 and plotted in Figure 64.

The computed values H_M of Al–Li at 973 K were found to be in good agreement with

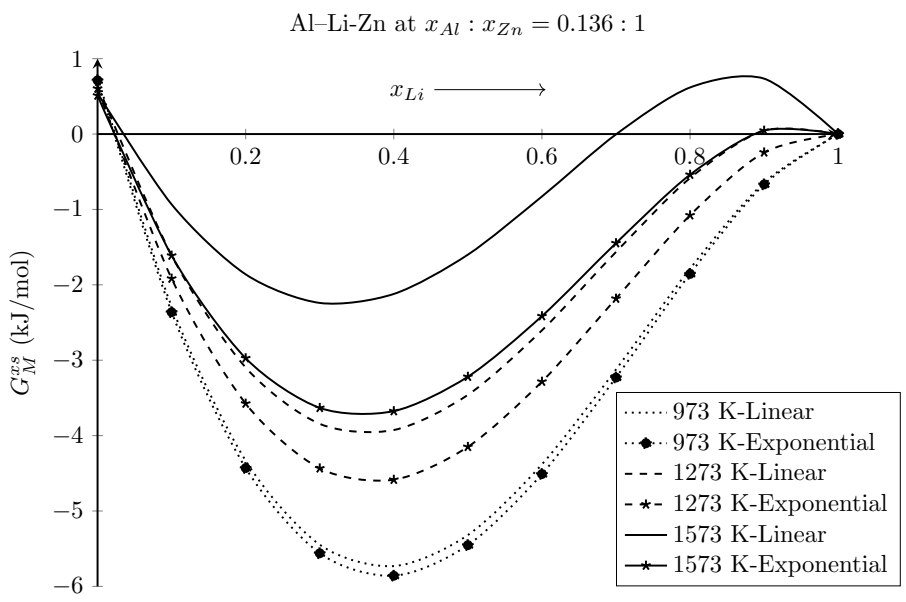

Figure 63: G_M^{xs} of ternary liquid Al–Li–Zn alloy in $x_{Al} : x_{Zn}$ = 0.136 : 1.

the experimental data at 1023 K (Debski & Terlicka, 2016) (Figure 64). The sub-binary systems Al–Li and Li–Zn have negative values of H_M whereas those of Al–Zn are positive at all compositions. At equi-atomic composition, $H_M = -11.632$ and -10.200 kJ/mol for Al–Li and Li–Zn respectively at 973 K. alloys. The plots of H_M for Al–Li and Al–Zn sub-binary systems are symmetric about equi-atomic composition whereas that of Li–Zn is asymmetric (Figure 64). The calculated values of H_M of the sub-binary systems showed ideal behaviours with increase in temperature.

Table 40: H_M of liquid (Al–Li, Li–Zn and Al–Zn) alloys

x_{Li} / x_{Zn}	H_M (kJ/mol)						
	Al–Li			Li–Zn		Al–Zn	
	973 K	Ref.*(1023 K)	1573 K	973 K	1573 K	973 K	1573 K
0.1	-2.375	-2.381	-2.092	-5.478	-4.181	0.934	0.815
0.2	-4.960	-5.001	-3.874	-8.880	-6.693	1.661	1.448
0.3	-7.671	-7.755	-5.639	-10.576	-7.826	2.180	1.901
0.4	-10.085	-10.205	-7.263	-10.911	-7.861	2.491	2.172
0.5	-11.632	-11.770	-8.384	-10.200	-7.075	2.595	2.263
0.6	-11.783	-11.918	-8.587	-8.729	-5.737	2.491	2.172
0.7	-10.244	-10.353	-7.578	-6.757	-4.109	2.180	1.901
0.8	-7.140	-7.209	-5.369	-4.515	-2.446	1.661	1.448
0.9	-3.211	-3.237	-2.456	-2.205	-0.996	0.934	0.815

* Debski & Terlicka (2016)

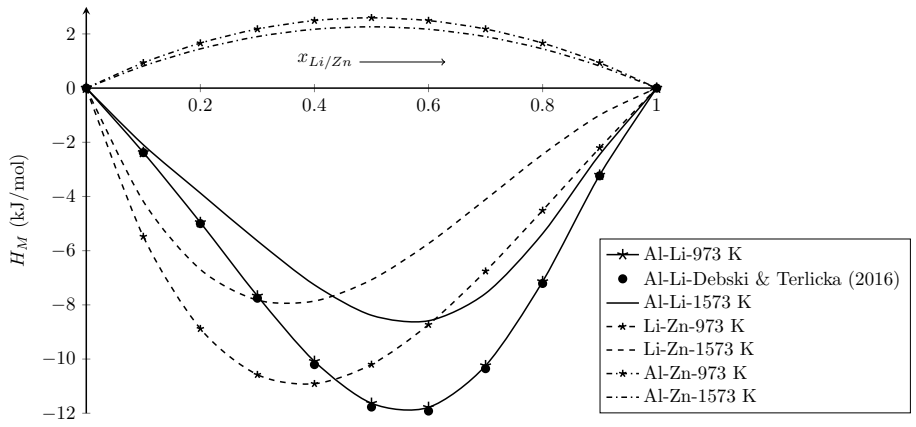

Figure 64: H_M of liquid Al–Li, Li–Zn and Al–Zn alloys.

4.9.2 H_M of ternary liquid Al–Li–Zn liquid alloy

The values of H_M for ternary alloy at various compositions were calculated at different temperatures using two different models, namely the R–K–M and Toop model. The values of H_M were calculated using Equations (3.1.5) and (3.1.5) with the help of exponential interaction parameters of Table 33. These values were calculated at three

Table 41: H_M of ternary liquid Al–Li–Zn alloy at 995 K, $x_{Al} : x_{Li} = 3 : 1$

	H_M (kJ/mol)				
x_{Zn}	R-K-M polynomial	Toop model	x_{Zn}	Experimental*	Ref.2**
0	-6.26	-6.26	0	-6.15	-6.23
0.1	-5.60	-5.38	0.021	-6.00	-6.14
0.2	-4.87	-4.65	0.058	-5.80	-5.70
0.3	-4.16	-4.04	0.092	-5.60	-5.49
0.4	-3.49	-3.51	0.126	-5.40	-5.23
0.5	-2.88	-3.02	0.170	-5.10	-4.99
0.6	-2.34	-2.55	0.212	-4.90	-4.67
0.7	-1.84	-2.04	0.262	-4.60	-4.40
0.8	-1.33	-1.47	0.305	-4.40	-4.14
0.9	-0.75	-0.80	-	-	-

* Kim & Sommer (1997), **Morachevskii et al. (2012)

different cross-sections, such as $x_{Al} : x_{Li} = 3$, $x_{Al} : x_{Zn} = 1$ and $x_{Al} : x_{Zn} = 7 : 3$ in the temperature range of 883 K–995 K. The calculated and experimental values of the system are presented in Tables (41-43) and plotted in Figures 65-67.

At 995 K and cross-section $x_{Al} : x_{Li} = 3$, the calculated values from both the models were in excellent agreement and also very close to the available experimental (Kim & Sommer, 1997) and theoretical values (Morachevskii et al., 2012) (Figure 65). Therefore,

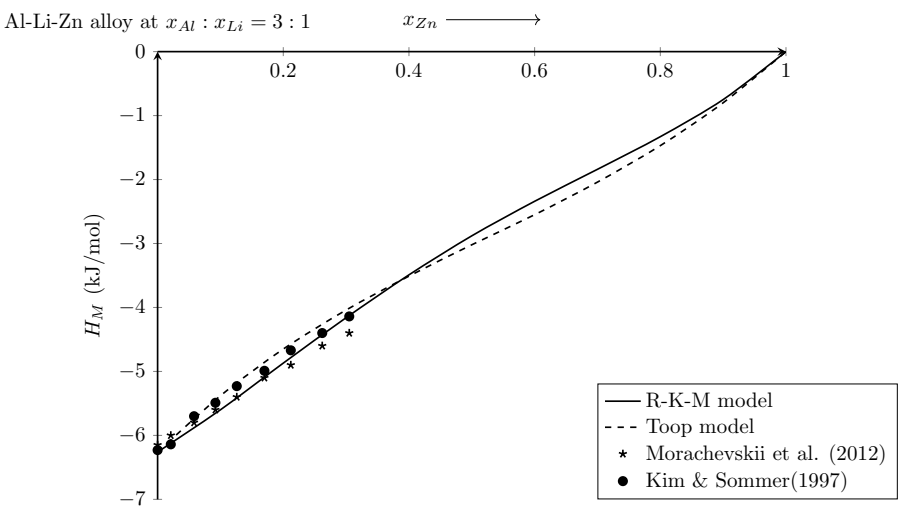

Figure 65: H_M of ternary liquid Al–Li–Zn alloy in $x_{Al} : x_{Li} = 3 : 1$ at 995 K.

it can be stated that the exponential parameters well explain the enthalpy of mixing of the ternary system.

Table 42: H_M of ternary liquid Al–Li–Zn alloy at $x_{Al} : x_{Zn} = 1 : 1$

x_{Li}	H_M (kJ/mol)				
	R-K-M polynomial (951 K)	Toop model (951 K)	Ref.* (973 K)	x_{Li}	Experimental** (951 K)
0	2.61	2.61	-	0	-6.40
0.1	-1.69	-1.85	-2.06	0.218	-7.20
0.2	-5.59	-5.31	-6.06	0.259	-8.90
0.3	-8.71	-7.94	-9.12	0.297	-10.50
0.4	-10.75	-9.67	-11.06	0.327	-11.50
0.5	-11.48	-10.39	-11.73	0.356	-12.50
0.6	-10.83	-9.96	-11.13	0.385	-13.40
0.7	-8.91	-8.37	-9.36	0.413	-14.10
0.8	-6.02	-5.80	-6.66	0.438	-14.60
0.9	-2.76	-2.72	-3.39	-	-

*Trybula et al. (2014), **Kim & Sommer (1997)

The calculated values of H_M at 951 K and $x_{Al} : x_{Zn} = 1 : 1$ are compared with available experimental results of Kim & Sommer (1997) at 951 K and theoretical values of Morachevskii et al. (2012) (Figure 66). The results obtained using the R–K–M polynomial framework were in perfect agreement with the values obtained by Trybula et al. (2014).

In addition, we compared the values of H_M computed using both the models at cross-section $x_{Al} : x_{Zn} = 7 : 3$ and 883 K with experimental values (Kim & Sommer, 1997) at 883 K and available literature values (Trybula et al., 2014) at 973 K and $x_{Al} : x_{Zn} = 3 : 1$ (Figure 67). The results of this work are found to be in very good agreement with

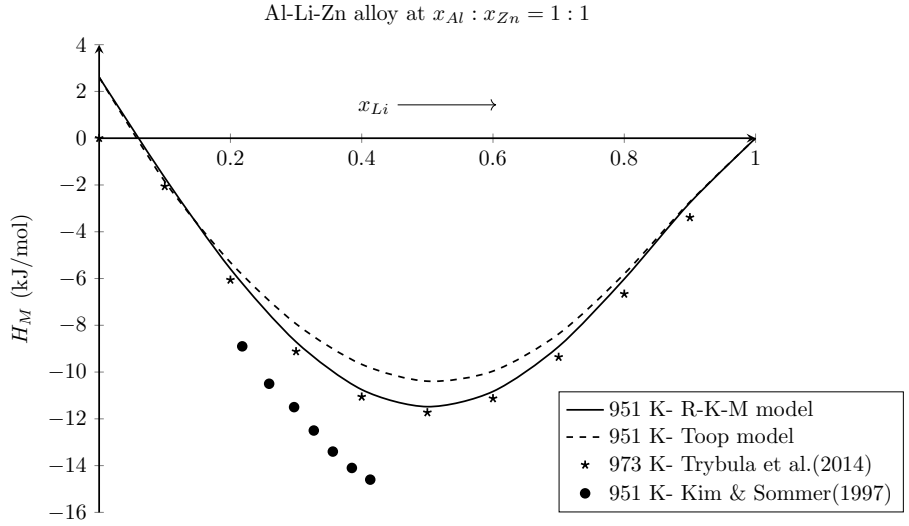

Figure 66: H_M of ternary liquid Al–Li–Zn alloy at $x_{Al} : x_{Zn} = 1 : 1$.

Table 43: H_M of ternary liquid Al–Li–Zn alloy at $x_{Al} : x_{Zn} = 7 : 3$

x_{Li}	H_M (kJ/mol)				
	R-K-M polynomial (883 K)	Toop model (883 K)	Ref.* (973 K)	x_{Li}	Experimental** (883 K)
0	2.22	2.22	-	0.014	1.20
0.1	-1.58	-1.59	-1.68	0.099	-2.40
0.2	-5.36	-4.93	-5.37	0.131	-3.60
0.3	-8.69	-7.80	-8.52	0.192	-5.10
0.4	-11.12	-9.99	-10.70	0.219	-6.80
0.5	-12.25	-11.15	-11.71	0.248	-7.00
0.6	-11.86	-11.00	-11.52	0.275	-7.90
0.7	-9.92	-9.41	-10.20	0.297	-8.70
0.8	-6.75	-6.54	-7.88	-	-
0.9	-3.05	-3.02	-4.57	-	-

*Trybula et al. (2014), **Kim & Sommer (1997)

available experimental values but slightly different from the literature values due to some differences in temperature and preferred cross-sections.

The potentiality of exponential T-dependent interaction parameters is to determine H_M of an alloy system at different temperatures. In other words, the values of H_M cannot be calculated at different temperatures using linear T-dependent interaction energy parameters.

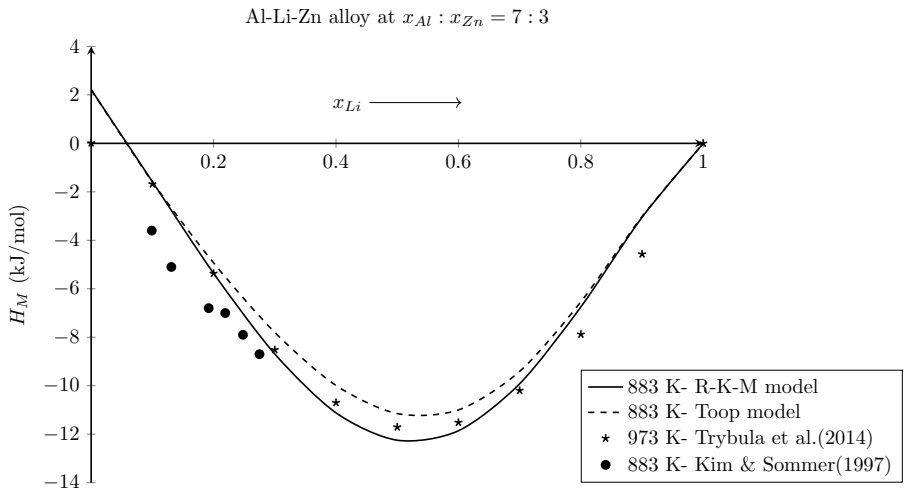

Figure 67: H_M of ternary liquid Al–Li–Zn alloy at $x_{Al} : x_{Zn} = 7 : 3$.

4.10 Activity of ternary liquid Al–Li–Zn alloy

Activities of sub-binary systems of ternary alloy were calculated following the similar steps as mentioned for above binary systems. For the ternary system, the expressions of partial excess free energy of mixing were formulated to obtain the values of activities of its components. The results of activities of sub-binary and ternary systems are presented in following sub-sections.

4.10.1 Activities of sub-binary systems (Al–Li, Li–Zn and Al–Zn)

The activities of sub-binary Al–Li, Li–Zn and Al–Zn liquid alloys were calculated at 973 K and 1573 K with the help of parameters in Table 33 and following the similar procedure adopted for above binary systems. The obtained values are presented in the Tables (44-46) and plotted in Figures 68-70.

Present theoretical investigations revealed that the activity of Li (a_{Li}) showed positive deviation from its ideal value in both of the sub-binary systems, Al–Li and Li–Zn (Figures 68 & 69). These behaviours were observed in high concentration region of Li at 973 K and 1573 K indicating homo-coordinating tendency of the systems at these conditions. At rest of the compositions, values of a_{Li} showed negative deviations from ideal values in both of the systems indicating them to be hetero-coordinating in nature. In Al–Zn liquid alloy, the activities of both components showed positive deviations throughout entire compositions (Figure 70) which indicate the system to be segregating in nature (R. K. Gohivar, Yadav, et al., 2021c). These results are in accordance with the results shown by the computations of other thermodynamic functions for the systems mentioned

in above sub-sections.

Table 44: Activity of liquid Al–Li alloy at 973 K and 1573 K

x_{Li}	Activity							
	T=973 K				T =1573 K			
	Ref.*		Exponential fit		Ref.*		Exponential fit	
	a_{Al}	a_{Li}	a_{Al}	a_{Li}	a_{Al}	a_{Li}	a_{Al}	a_{Li}
0.1	0.868	0.020	0.874	0.019	0.880	0.037	0.877	0.055
0.2	0.771	0.041	0.767	0.043	0.782	0.075	0.764	0.125
0.3	0.681	0.059	0.670	0.064	0.688	0.110	0.672	0.186
0.4	0.522	0.096	0.527	0.099	0.550	0.166	0.571	0.251
0.5	0.308	0.183	0.331	0.174	0.370	0.268	0.440	0.344
0.6	0.138	0.351	0.154	0.325	0.207	0.431	0.292	0.479
0.7	0.052	0.592	0.055	0.566	0.102	0.631	0.166	0.650
0.8	0.021	0.810	0.018	0.819	0.049	0.806	0.084	0.814
0.9	0.010	0.926	0.008	0.949	0.024	0.916	0.041	0.923

*Hallstedt & Kim (2007)

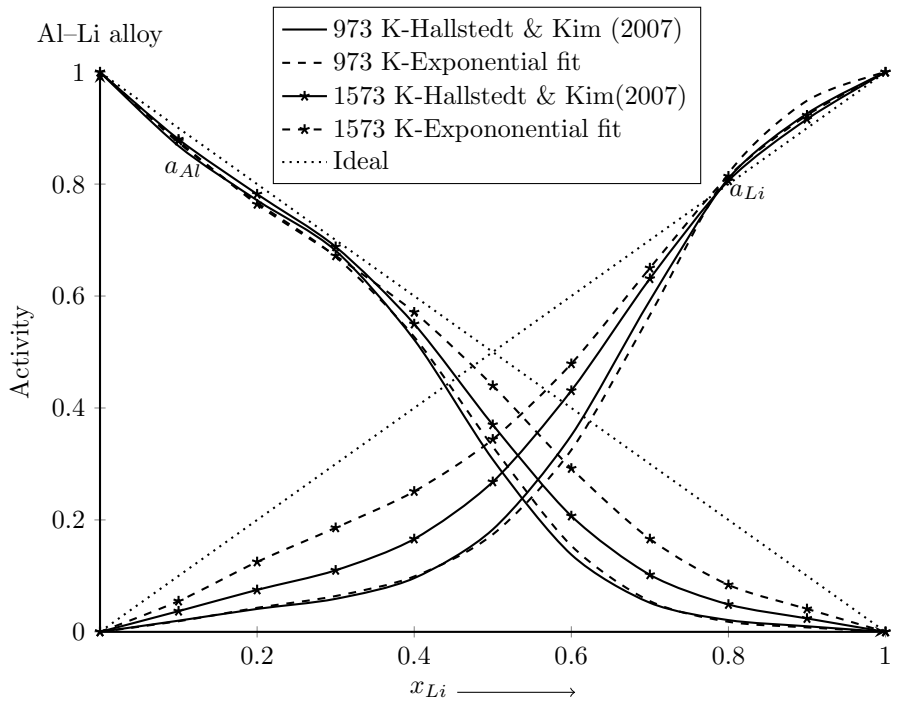

Figure 68: Activity of liquid Al–Li alloy.

4.10.2 Activity of ternary Al–Li–Zn liquid alloy

The activities of components Al, Li and Zn of the ternary liquid Al–Li–Zn alloy were calculated at three different cross-sections $x_{Al} : x_{Zn}$ = 3 : 1, 1 : 1 and 0.136 : 1; and at 973 K and 1573 K. In due process, the values of interaction parameters were taken

Table 45: Activity of liquid Li–Zn alloy at 973 K and 1573 K

x_{Zn}	Activity							
	T=973 K				T =1573 K			
	Ref.*		Exponential fit		Ref.*		Exponential fit	
	a_{Li}	a_{Zn}	a_{Li}	a_{Zn}	a_{Li}	a_{Zn}	a_{Li}	a_{Zn}
0.1	0.931	0.043	0.930	0.041	0.932	0.150	0.922	0.096
0.2	0.885	0.057	0.882	0.056	0.894	0.193	0.865	0.140
0.3	0.813	0.074	0.808	0.072	0.848	0.225	0.798	0.179
0.4	0.681	0.102	0.674	0.100	0.766	0.272	0.699	0.228
0.5	0.488	0.153	0.482	0.150	0.635	0.341	0.561	0.298
0.6	0.278	0.240	0.274	0.238	0.465	0.439	0.393	0.397
0.7	0.116	0.383	0.114	0.380	0.288	0.567	0.229	0.530
0.8	0.032	0.588	0.031	0.585	0.140	0.718	0.101	0.692
0.9	0.004	0.825	0.004	0.824	0.045	0.873	0.028	0.864

*Y. Liang et al. (2008)

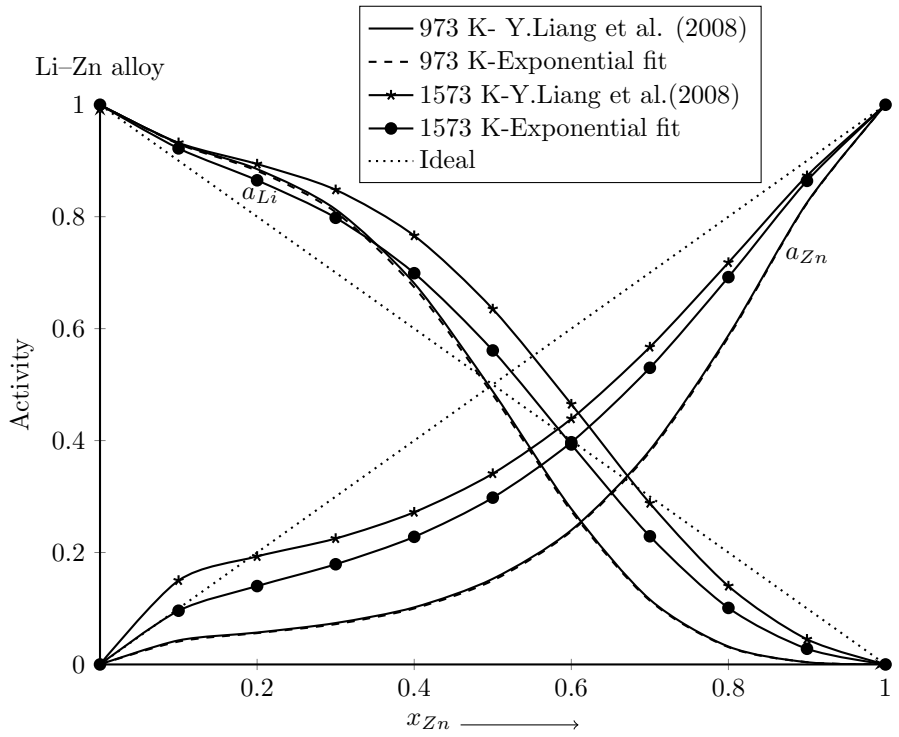

Figure 69: Activity of liquid Li–Zn alloy.

from Table 33 and used in Equation (3.43). The calculated values are presented in Table (47-52) and plotted in Figures 71-73.

It can be observed that the values of activities of the components computed at 973 K using linear and exponential parameters were found to be in well agreement at all cross-sections from Li corner (Figures 71-73). Further, the computed values of activities of Li at 973 K were found to be in good agreement with the results of Trybula et al. (2014) at lower concentration of Li at all cross-sections. The activity of Li was found

Table 46: Activity of liquid Al–Zn alloy at 973 K and 1573 K

x_{Zn}	Activity							
	T=973 K				T =1573 K			
	Ref.*		Exponential fit		Ref.*		Exponential fit	
	a_{Al}	a_{Zn}	a_{Al}	a_{Zn}	a_{Al}	a_{Zn}	a_{Al}	a_{Zn}
0.1	0.908	0.205	0.908	0.205	0.904	0.137	0.904	0.137
0.2	0.829	0.353	0.829	0.353	0.813	0.257	0.813	0.257
0.3	0.758	0.463	0.758	0.463	0.725	0.364	0.725	0.364
0.4	0.691	0.550	0.691	0.550	0.639	0.461	0.639	0.461
0.5	0.624	0.624	0.624	0.624	0.552	0.552	0.552	0.552
0.6	0.550	0.691	0.550	0.691	0.461	0.639	0.461	0.639
0.7	0.463	0.758	0.463	0.758	0.364	0.725	0.364	0.725
0.8	0.353	0.829	0.353	0.829	0.257	0.813	0.257	0.813
0.9	0.205	0.908	0.205	0.908	0.137	0.904	0.137	0.904

*Mathon et al. (2000)

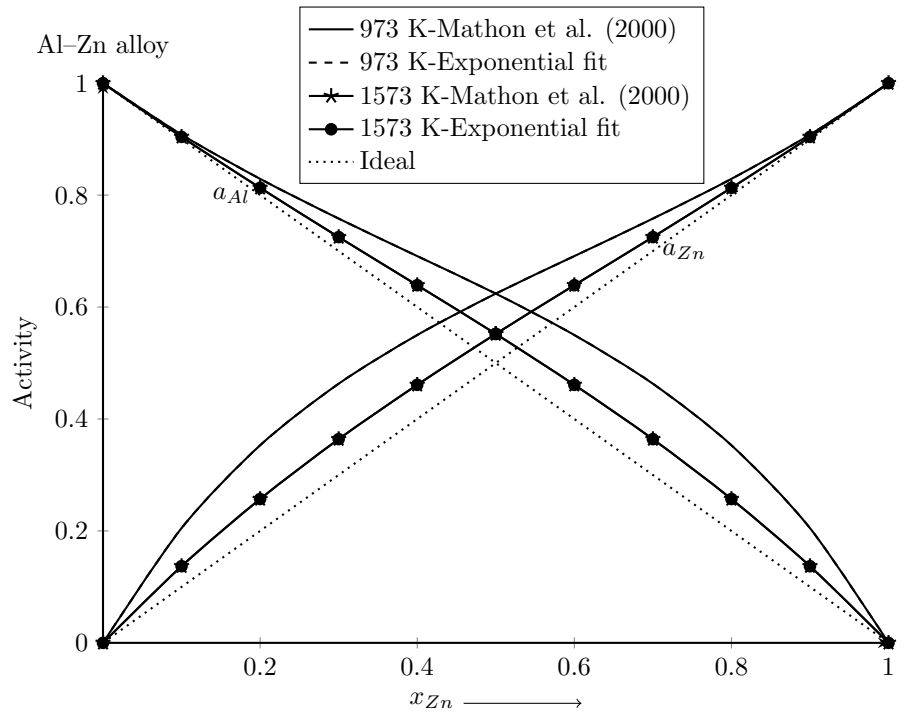

Figure 70: Activity of liquid Al–Zn alloy.

to increase gradually and that of Al and Zn were found to decrease with increase in concentration of Li at all cross-sections. At equi-composition, the activities of Al and Zn were found to be comparable, however, that of Li was found to be very small (Figure 72). The activity of Li at $x_{Li} = 0.5$ increases when the content of Al decreases or that of Zn increases (Figures 71-73).

As the temperature of system is increased, the activity of Al calculated using both linear and exponential parameters decreases at its higher concentration region, however, it

increases at its lower concentration region. In the case of Zn, its activity increases with increasing its content as well as temperature. Further, the activities of all the components (Al, Li and Zn) calculated using linear parameters increase more than those calculated using exponential parameters with increase in temperature. When the temperature rises from 973 K to 1573 K, the difference in activities of components Li and Al at respective concentrations of $x_{Li} = 0.5$ and $x_{Al} = 0.375$ increases from 23% to 53% (Figure 71). This result indicates that the activity of Li increases more rapidly than that of Al as the temperature of the system is gradually increased.

Table 47: Activity of ternary liquid Al–Li–Zn alloy at 973 K, $x_{Al} : x_{Zn} = 3 : 1$

x_{Li}	Activity						
	Linear fit			Exponential fit			*Experimental
	a_{Al}	a_{Li}	a_{Zn}	a_{Al}	a_{Li}	a_{Zn}	a_{Li}
0	0.793	0.000	0.412	0.790	0.000	0.400	0.000
0.1	0.756	0.006	0.288	0.752	0.006	0.279	0.004
0.2	0.689	0.018	0.187	0.682	0.019	0.180	0.013
0.3	0.545	0.041	0.121	0.547	0.043	0.115	0.023
0.4	0.345	0.096	0.077	0.359	0.094	0.072	0.051
0.5	0.170	0.215	0.046	0.183	0.203	0.044	0.117
0.6	0.069	0.418	0.026	0.074	0.396	0.026	0.251
0.7	0.027	0.664	0.015	0.026	0.651	0.015	0.459
0.8	0.012	0.851	0.010	0.010	0.865	0.009	0.693
0.9	0.006	0.936	0.007	0.006	0.954	0.006	0.879

*Trybula et al. (2014)

Table 48: Activity of ternary liquid Al–Li–Zn alloy at 1573 K, $x_{Al} : x_{Zn} = 3 : 1$

x_{Li}	Activity					
	Linear fit			Exponential fit		
	a_{Al}	a_{Li}	a_{Zn}	a_{Al}	a_{Li}	a_{Zn}
0	0.769	0.000	0.312	0.768	0.000	0.308
0.1	0.712	0.033	0.243	0.704	0.023	0.232
0.2	0.643	0.079	0.182	0.619	0.068	0.163
0.3	0.537	0.146	0.137	0.512	0.137	0.114
0.4	0.399	0.253	0.103	0.388	0.237	0.080
0.5	0.260	0.409	0.077	0.263	0.374	0.058
0.6	0.155	0.599	0.057	0.159	0.543	0.042
0.7	0.091	0.773	0.043	0.089	0.717	0.031
0.8	0.058	0.884	0.034	0.049	0.852	0.023
0.9	0.039	0.937	0.028	0.028	0.931	0.017

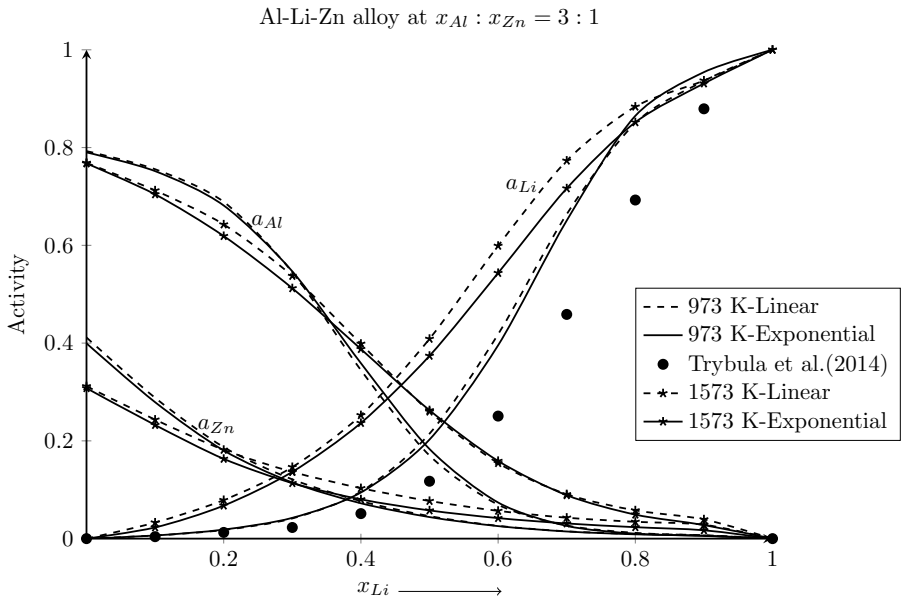

Figure 71: Activity of ternary liquid Al–Li–Zn alloy at $x_{Al} : x_{Zn} = 3 : 1$.

Table 49: Activity of ternary liquid Al–Li–Zn alloy at 973 K, $x_{Al} : x_{Zn} = 1 : 1$

x_{Li}	Activity						
	Linear fit			Exponential fit			*Experimental
	a_{Al}	a_{Li}	a_{Zn}	a_{Al}	a_{Li}	a_{Zn}	a_{Li}
0	0.624	0.000	0.624	0.616	0.000	0.616	0.000
0.1	0.579	0.004	0.519	0.571	0.004	0.511	0.007
0.2	0.466	0.015	0.415	0.464	0.015	0.405	0.018
0.3	0.305	0.044	0.309	0.311	0.043	0.299	0.022
0.4	0.161	0.115	0.207	0.167	0.111	0.202	0.042
0.5	0.070	0.260	0.126	0.073	0.249	0.124	0.094
0.6	0.028	0.480	0.071	0.028	0.466	0.070	0.270
0.7	0.012	0.713	0.040	0.011	0.710	0.039	0.488
0.8	0.006	0.871	0.025	0.005	0.885	0.023	0.758
0.9	0.004	0.940	0.017	0.004	0.951	0.015	0.930

*Trybula et al. (2014)

4.11 Concentration fluctuation in long wave length limit of ternary liquid Al–Li–Zn alloy

The mathematical formulations of $S_{CC}(0)$ for the ternary system are presented in the Section 3.2.2. These expressions are obtained in terms of energy interaction parameters of the R-K-M model. The results of sub-binary systems and ternary system are presented in the following sub-sections.

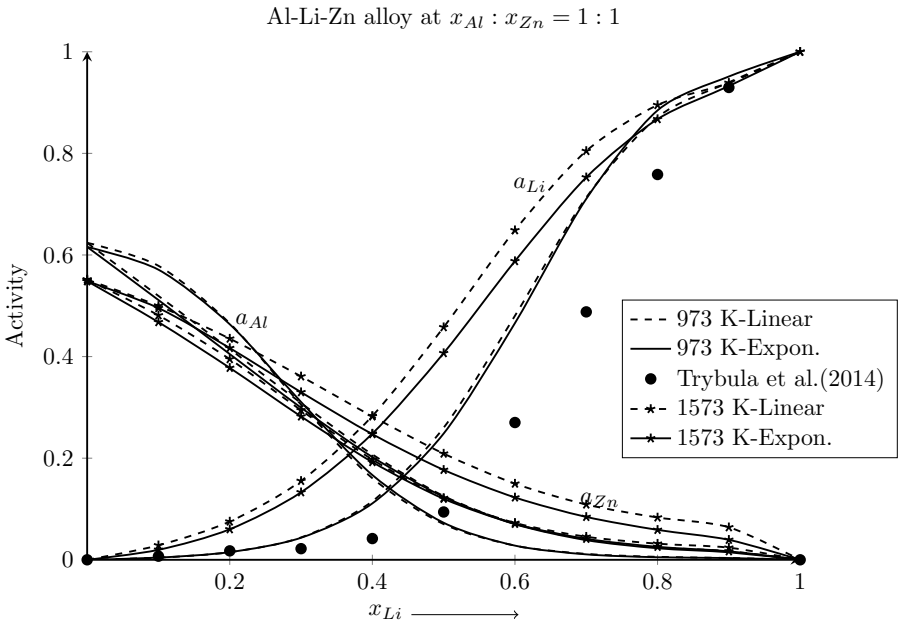

Figure 72: Activity of ternary liquid Al–Li–Zn alloy at $x_{Al} : x_{Zn} = 1 : 1$.

Table 50: Activity of ternary liquid Al–Li–Zn alloy at 1573 K, $x_{Al} : x_{Zn} = 1 : 1$

x_{Li}	Activity					
	Linear fit			Exponential fit		
	a_{Al}	a_{Li}	a_{Zn}	a_{Al}	a_{Li}	a_{Zn}
0	0.552	0.000	0.552	0.548	0.000	0.548
0.1	0.481	0.029	0.500	0.468	0.020	0.496
0.2	0.395	0.075	0.435	0.378	0.060	0.417
0.3	0.294	0.155	0.361	0.282	0.133	0.330
0.4	0.197	0.283	0.282	0.192	0.248	0.247
0.5	0.122	0.458	0.209	0.120	0.407	0.177
0.6	0.073	0.649	0.150	0.071	0.588	0.123
0.7	0.045	0.805	0.109	0.041	0.753	0.084
0.8	0.032	0.895	0.083	0.026	0.867	0.059
0.9	0.024	0.939	0.064	0.017	0.933	0.039

4.11.1 $S_{CC}(0)$ of sub-binary systems (Al–Li, Li–Zn and Al–Zn)

Like thermodynamic functions, the structural properties of ternary liquid alloys can also be explained in terms of its sub-binary systems. In this regard, the value of $S_{CC}(0)$ of the sub-binary systems (Al–Li, Li–Zn and Al–Zn) of the ternary liquid Al–Li–Zn alloy were calculated at 973 K and 1573 K. The same interaction parameters that were used to compute thermodynamic functions were used for this purpose. The values of $S_CC(0)$ for these sub-binary systems were calculated in a manner similar to that of binary systems. The values so calculated are presented in Tables 53 & 54 and plotted as a function of concentration in Figures 74-76.

Table 51: Activity of ternary liquid Al–Li–Zn alloy at 973 K, $x_{Al} : x_{Zn} = 0.136 : 1$

x_{Li}	Activity						
	Linear fit			Exponential fit			*Experimental
	a_{Al}	a_{Li}	a_{Zn}	a_{Al}	a_{Li}	a_{Zn}	a_{Li}
0	0.238	0.000	0.891	0.229	0.000	0.891	0.000
0.1	0.230	0.005	0.740	0.224	0.004	0.737	0.005
0.2	0.147	0.025	0.561	0.144	0.024	0.558	2.959
0.3	0.068	0.085	0.393	0.067	0.083	0.390	0.092
0.4	0.026	0.211	0.258	0.025	0.206	0.256	0.198
0.5	0.009	0.401	0.164	0.009	0.394	0.163	0.396
0.6	0.003	0.612	0.105	0.003	0.606	0.103	0.491
0.7	0.002	0.782	0.071	0.001	0.781	0.068	0.679
0.8	0.001	0.882	0.051	0.001	0.884	0.048	0.778
0.9	0.001	0.934	0.036	0.001	0.936	0.033	0.918

*Trybula et al. (2014)

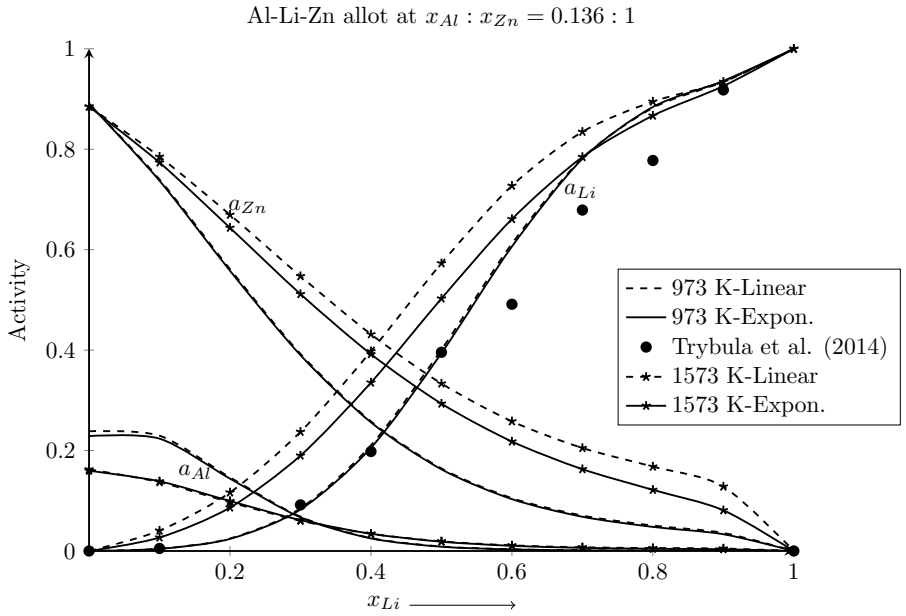

Figure 73: Activity of ternary liquid Al–Li–Zn alloy at $x_{Al} : x_{Zn} = 0.136 : 1$.

The values of $S_{CC}(0)$ calculated from both linear (Hallstedt & Kim, 2007) and exponential parameters (this work) for sub-binary Al-Li liquid alloy showed negative deviation from ideal value in the concentration range $x_{Li} < 0.2$ and $0.2 < x_{Li} < 0.9$ at 973 K. This indicates the system to be ordering in nature. However, it showed positive deviation in rest of the concentrations indicating the system to be segregating in nature (Figure 74). Therefore, it can be stated that there are transformations of phases from ordering to segregating and segregating to ordering at above mentioned conditions. When the temperature of the system is increased from 973 K to 1573 K, the values computed from linear parameters increased in the region $x_{Li} < 0.2$ and then gradually decreased in rest

Table 52: Activity of ternary liquid Al–Li–Zn alloy at 1573 K, $x_{Al} : x_{Zn} = 0.136 : 1$

x_{Li}	Activity					
	Linear fit			Exponential fit		
	a_{Al}	a_{Li}	a_{Zn}	a_{Al}	a_{Li}	a_{Zn}
0	0.163	0.000	0.885	0.160	0.000	0.885
0.1	0.137	0.041	0.785	0.139	0.027	0.774
0.2	0.097	0.117	0.670	0.100	0.087	0.644
0.3	0.060	0.237	0.547	0.061	0.190	0.512
0.4	0.034	0.398	0.432	0.034	0.335	0.392
0.5	0.019	0.573	0.334	0.019	0.503	0.293
0.6	0.011	0.727	0.258	0.010	0.661	0.218
0.7	0.007	0.835	0.205	0.006	0.785	0.163
0.8	0.006	0.895	0.168	0.005	0.867	0.122
0.9	0.005	0.934	0.128	0.004	0.926	0.081

of the concentrations. It is obvious that the liquid system should show ideal tendency at elevated temperatures (Kaptay, 2012; Yadav, Jha, Jha, et al., 2016). But the computed values of $S_{CC}(0)$ from exponential parameters got closure to ideal values with increase in temperature. Moreover, there is shift in the phase transformation concentration from $x_{Li} = 0.2$ at 973 K to $x_{Li} = 0.3$ at 1573 K (Figure 74).

In case of sub-binary Li–Zn liquid alloy, calculated values of $S_{CC}(0)$ from both linear and exponential parameters are the same at 973 K. Further, $S_{CC}(0) > S^{id}_{CC}(0)$ in the concentration range $x_{Zn} < 0.4$ indicating it to be segregating in nature. The values of $S_{CC}(0) < S^{id}_{CC}(0)$ at rest of concentrations indicating it to be ordering in nature. The values computed using linear parameters gradually shifted away from the ideal vales when the temperature was increased to 1573 K. But those computed using exponential parameters gradually shifted towards ideal values in this temperature range. However, these values shifted away from ideal values only at $x_{Zn} = 0.3$ (Figure 75). From Figure 76, it can be observed that the computed values of $S_{CC}(0) > S^{id}_{CC}(0)$ for sub-binary Al–Zn liquid alloy throughout the entire concentration range at 973 K indicting it to be complete segregating in nature. When the temperature of the system is increased from 973 K to 1573 K, the values computed using both linear and exponential parameters gradually moved towards ideal values.

4.11.2 $S_{CC}(0)$ for ternary liquid Al–Li–Zn alloy

Like binary liquid alloys, the knowledge regarding the local arrangement of atoms in the nearest vicinity of ternary liquid alloys can be studied by computing $S_{CC}(0)$. In theoretical approaches, the values of $S_{CC}(0)$ for ternary systems are obtained using the thermodynamic database of their respective sub-binary systems. In this regard, the

Table 53: $S_{CC}(0)$ of liquid Al–Li alloy at 973 K and 1573 K

x_{Li}	$S_{CC}(0)$			
	T=973 K		T=1573 K	
	Exponential fit	Ref.*	Exponential fit	Ref.*
0.1	0.070	0.067	0.070	0.137
0.2	0.164	0.207	0.153	0.129
0.3	0.181	0.170	0.221	0.096
0.4	0.120	0.093	0.199	0.078
0.5	0.082	0.064	0.152	0.070
0.6	0.065	0.057	0.122	0.067
0.7	0.063	0.062	0.110	0.068
0.8	0.079	0.088	0.115	0.072
0.9	0.160	0.136	0.116	0.067

Hallstedt & Kim (2007)

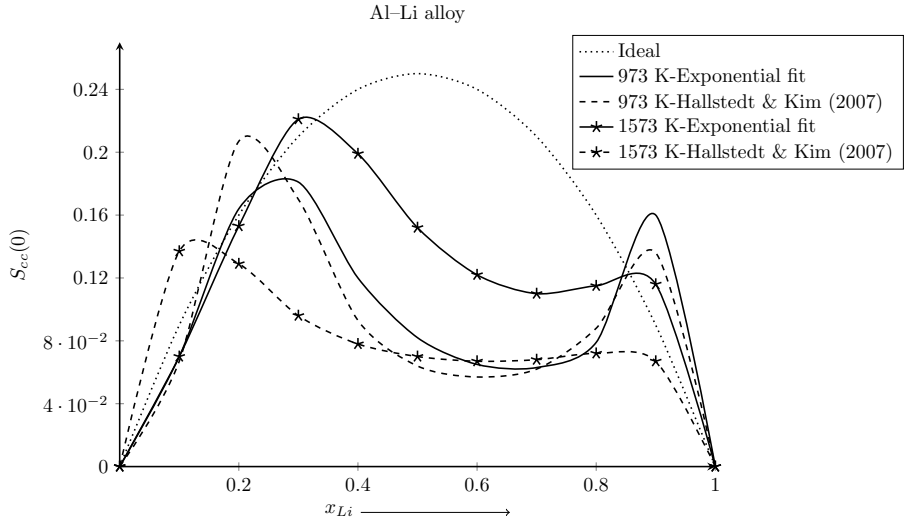

Figure 74: $S_{CC}(0)$ of liquid Al–Li alloy.

Table 54: $S_{CC}(0)$ of liquid Al–Zn and Li-Zn alloys at 973 K and 1573 K

x_{Zn}	$S_{CC}(0)$							
	Li–Zn alloy				Al–Zn alloy			
	973 K		1573 K		973 K		1573 K	
	Ref.*	Exponential fit	Ref.*	Exponential fit	Ref.**	Exponential fit	Ref.**	Exponential fit
0.1	0.192	0.184	0.204	0.149	0.106	0.106	0.096	0.099
0.2	0.345	0.328	0.496	0.300	0.218	0.218	0.180	0.192
0.3	0.249	0.242	0.423	0.299	0.323	0.323	0.245	0.268
0.4	0.164	0.162	0.289	0.235	0.400	0.400	0.287	0.319
0.5	0.115	0.114	0.206	0.179	0.429	0.429	0.302	0.337
0.6	0.086	0.085	0.155	0.137	0.400	0.400	0.287	0.319
0.7	0.066	0.065	0.120	0.106	0.323	0.323	0.245	0.268
0.8	0.051	0.051	0.091	0.080	0.218	0.218	0.180	0.192
0.9	0.036	0.036	0.059	0.053	0.106	0.106	0.096	0.099

*Y. Liang et al. (2008), **Mathon et al. (2000)

structural properties of ternary liquid alloys can be interpreted by computing different

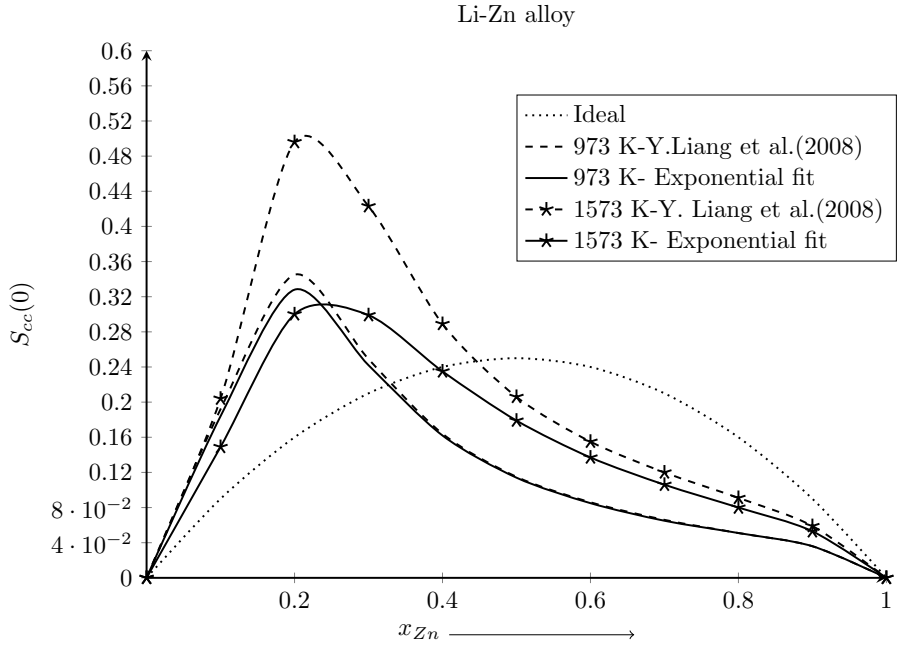

Figure 75: $S_{CC}(0)$ of liquid Li–Zn alloy.

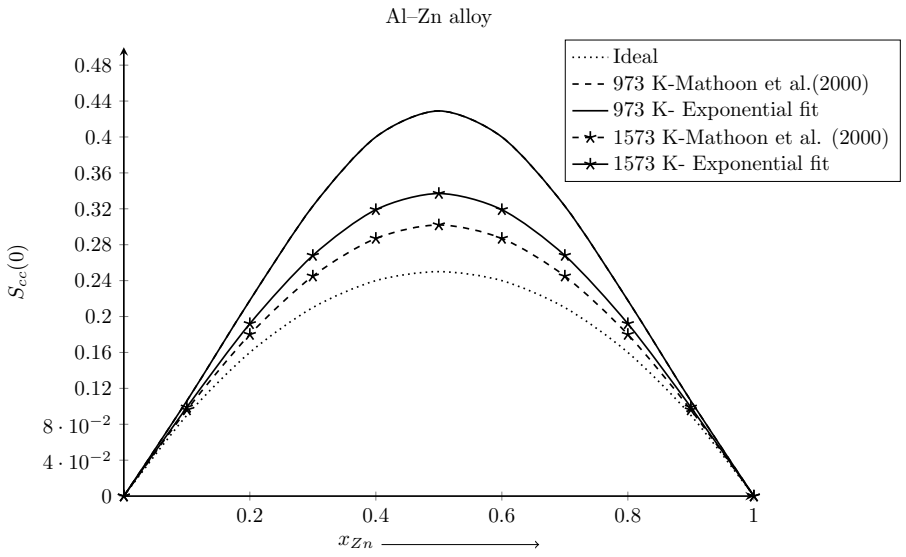

Figure 76: $S_{CC}(0)$ of liquid Al–Zn alloy.

values of $S_{C_iC_j}(0)$ which are $S_{C_1C_1}(0)$, $S_{C_2C_2}(0)$ and $S_{C_1C_2}(0)$.

In this work, the values of $S_{C_iC_j}(0)$ were computed at three different cross-sections $x_{Al} : x_{Zn} = 3 : 1$, $1 : 1$, and $0.136 : 1$ and at temperatures 973 K and 1573 K. In order to know the extent of interactions, the values of $S_{C_iC_j}(0)$ were compared with their respective ideal values ($S^{id}_{C_iC_j}(0)$). The values of $S_{C_1C_1}(0)$, $S_{C_2C_2}(0)$ and $S_{C_1C_2}(0)$ were computed using interaction parameters from Table 33 in Equations (3.51-3.53) and (3.60). The values so obtained are presented in Tables (55-63) and plotted as a function

of concentration in Figures 77-85.

The computed values of $S_{C_1C_1}(0)$ at 973 K and $x_{Al} : x_{Zn} = 3 : 1$ from both linear and exponential parameters were found to be greater than ideal values in the region $x_{Li} > 0.8$ and less at rest of the concentrations (Figure 77). These results indicate that Al atoms segregates in the ternary liquid Al–Li–Zn alloy in the region $x_{Li} > 0.8$. When the temperature of system was increased from 973 K to 1573 K, the values of $S_{C_1C_1}(0)$ computed using exponential parameters got closure to ideal values. However, the values computed using linear parameters showed this tendency in the region $x_{Li} < 0.8$ only. The computed values of $S_{C_2C_2}(0) > S^{id}_{C_2C_2}(0)$ at 973 K and this cross-section at lower and higher concentrations of Li (Figure 78). At 1573 K, the values computed using both the parameters showed unusual tendency at/around $x_{Li} = 0.3$. At rest of the concentrations usual temperature dependence behaviour is obtained. As the same cross-section and temperatures, the computed values of $S_{C_1C_2}(0) > S^{id}_{C_1C_2}(0)$ in the composition range $x_{Li} > 0.8$ whereas in the remaining compositions, $S_{C_1C_2}(0) < S^{id}_{C_1C_2}(0)$ (Figure 79). The results of temperature dependence of $S_{C_1C_2}(0)$ are similar as those obtained for $S_{C_1C_1}(0)$.

Table 55: $S_{C_1C_1}(0)$ of liquid Al–Li–Zn alloy at $x_{Al} : x_{Zn} = 3 : 1$

x_{Li}	$S_{C_1C_1}(0)$				
		973 K		1573 K	
	Ideal	Linear fit	Exponential fit	Linear fit	Exponential fit
0	0.188	0.188	0.188	0.188	0.188
0.1	0.219	0.184	0.182	0.196	0.189
0.2	0.240	0.156	0.159	0.187	0.183
0.3	0.249	0.124	0.129	0.160	0.168
0.4	0.248	0.104	0.105	0.136	0.147
0.5	0.234	0.090	0.089	0.123	0.127
0.6	0.210	0.084	0.079	0.119	0.114
0.7	0.174	0.085	0.077	0.125	0.107
0.8	0.128	0.095	0.089	0.140	0.106
0.9	0.069	0.090	0.127	0.108	0.089

At cross-section $x_{Al} : x_{Zn} = 1 : 1$, the computed values of $S_{C_1C_1}(0)$, $S_{C_2C_2}(0)$ and $S_{C_1C_2}(0)$ using both linear and exponential parameters show peculiar properties at 973 K and $x_{Li} = 0.3$ (Figures 80 -82). These values were found to be $S_{C_1C_1}(0) = (9.831, 214.950)$, $S_{C_2C_2}(0) = (15.751, 367.898)$ and $S_{C_1C_2}(0) = (12.331, 281.094)$ using linear and exponential parameters respectively (Tables 58-60). These results demonstrate that at 973 K, this ternary liquid alloy has critical composition at $x_{Li} = 0.3$ and hence there appears liquid-liquid phase separation at this concentration. It may be stated that this system segregates into two liquid phases. The liquid-liquid phase separation at critical concentration and temperature in above mentioned similar conditions have been discussed by Singh & Sommer (1997); Karlhuber et al. (1999) for binary and (X. Sun et

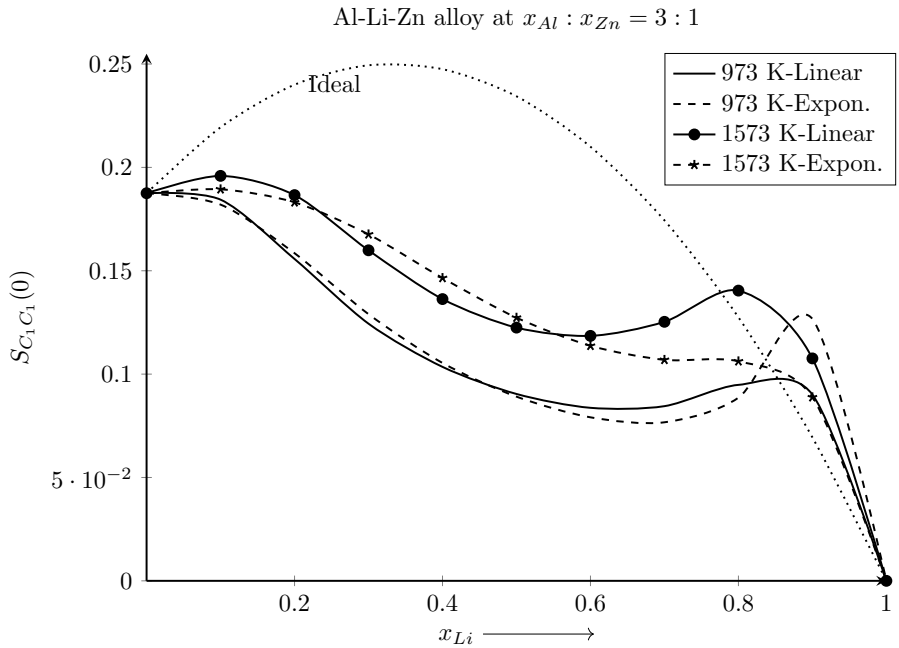

Figure 77: $S_{C_1C_1}(0)$ of liquid Al–Li–Zn alloy at $x_{Al} : x_{Li} = 3 : 1$.

Table 56: $S_{C_2C_2}(0)$ of liquid Al–Li–Zn alloy at $x_{Al} : x_{Zn} = 3 : 1$

x_{Li}	$S_{C_2C_2}(0)$				
		973 K		1573 K	
	Ideal	Linear fit	Exponential fit	Linear fit	Exponential fit
0.1	0.09	0.108	0.105	0.094	0.083
0.2	0.16	0.194	0.188	0.162	0.141
0.3	0.21	0.181	0.188	0.170	0.164
0.4	0.24	0.139	0.149	0.149	0.157
0.5	0.25	0.108	0.113	0.131	0.140
0.6	0.24	0.091	0.090	0.124	0.125
0.7	0.21	0.087	0.080	0.131	0.118
0.8	0.16	0.099	0.089	0.153	0.120
0.9	0.09	0.104	0.136	0.128	0.106

al., 2016) ternary liquid systems in terms of different physical parameters. Moreover, present findings for the ternary system are also comprehended by the results of $S_{CC}(0)$ of its constituent sub-binary systems. However, the ternary system did not show above mentioned behaviours at elevated temperature (1573 K). This further strengthen the criticality tendency of ternary liquid Al–Li–Zn alloy at $x_{Li} = 0.3$ and 973 K.

In the entire concentration and temperature range, computed values of $S_{C_1C_1}(0)$ at $x_{Al} : x_{Li} = 0.316 : 1$ using both linear and exponential parameters were found to be higher than ideal values at both of the temperatures (Figure 83). When the temperature of system was increased from 973 K to 1573 K, the computed values of $S_{C_1C_1}(0)$ gradually shifted towards ideal values as expected. The computed values of $S_{C_2C_2}(0) > S^{id}_{C_2C_2}(0)$ in

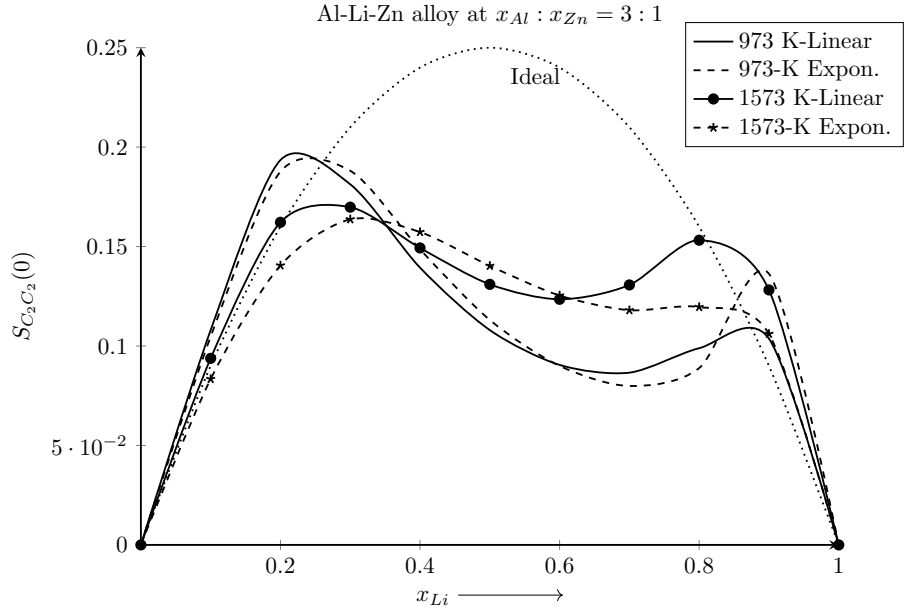

Figure 78: $S_{C_2C_2}(0)$ of liquid Al–Li–Zn alloy at $x_{Al} : x_{Li} = 3 : 1$.

Table 57: $S_{C_1C_2}(0)$ of liquid Al–Li–Zn alloy at $x_{Al} : x_{Zn} = 3 : 1$

x_{Li}	$S_{C_1C_2}(0)$				
		973 K		1573 K	
	Ideal	Linear fit	Exponential fit	Linear fit	Exponential fit
0.1	-0.068	-0.019	-0.015	-0.037	-0.016
0.2	-0.120	-0.031	-0.030	-0.069	-0.046
0.3	-0.158	-0.018	-0.024	-0.068	-0.063
0.4	-0.180	-0.012	-0.017	-0.061	-0.066
0.5	-0.188	-0.017	-0.018	-0.061	-0.065
0.6	-0.180	-0.027	-0.024	-0.070	-0.067
0.7	-0.158	-0.045	-0.037	-0.091	-0.075
0.8	-0.120	-0.072	-0.064	-0.123	-0.089
0.9	-0.068	-0.085	-0.120	-0.106	-0.085

the concentration range $x_{Li} > 0.7$ and $S_{C_2C_2}(0) < S^{id}_{C_2C_2}(0)$ at remaining concentrations. At 973 K, the computed values of $S_{C_2C_2}(0)$ show critical behaviour at $x_{Li} = 0.5$ (Figure 84). The values of $S_{C_1C_2}(0) > S^{id}_{C_1C_2}(0)$ at almost all concentrations and show ideal nature at elevated temperature (Figure 85 and Table 63).

4.12 Discussion

As stated earlier, we have studied the thermodynamic and structural properties of a few binary (Al–Fe, Al–Mn, Al–Ti and Li–Mg) and a ternary Al–Li–Zn liquid alloys at different temperatures in the framework of R-K polynomial. At first, these properties of the

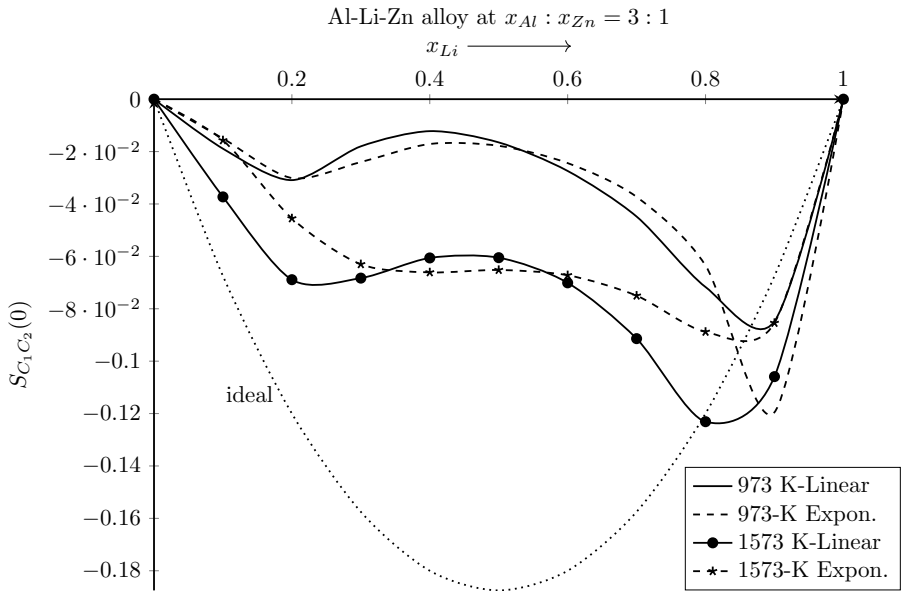

Figure 79: $S_{C_1C_2}(0)$ of liquid Al–Li–Zn alloy at $x_{Al} : x_{Li} = 3 : 1$.

Table 58: $S_{C_1C_1}(0)$ of liquid Al–Li–Zn alloy at $x_{Al} : x_{Zn} = 1 : 1$

x_{Li}	$S_{C_1C_1}(0)$				
		973 K		1573 K	
	Ideal	Linear fit	Exponential fit	Linear fit	Exponential fit
0	0.250	0.250	0.250	0.250	0.250
0.1	0.248	0.317	0.326	0.257	0.313
0.2	0.240	1.211	1.211	0.247	0.328
0.3	0.228	9.831	214.951	0.218	0.275
0.4	0.210	0.548	0.581	0.181	0.206
0.5	0.188	0.216	0.214	0.149	0.156
0.6	0.160	0.130	0.126	0.128	0.123
0.7	0.128	0.097	0.094	0.115	0.102
0.8	0.090	0.081	0.085	0.103	0.087
0.9	0.048	0.057	0.078	0.063	0.058

systems were computed using optimised linear T-dependent parameters which depicted the presence of unusual trends, called artificial inverted miscibility gaps or artifacts. In order to remove such artifacts, coefficients of R-K polynomial were reoptimised assuming them to be exponential T-dependent.

4.12.1 Mixing properties of liquid alloys

The knowledge of phase transformation from ordering to segregating or vice-versa of liquid alloys is critical in many metallurgical processes, including characterization, fabrication, and design. The determination of reliable or self-consistent optimised

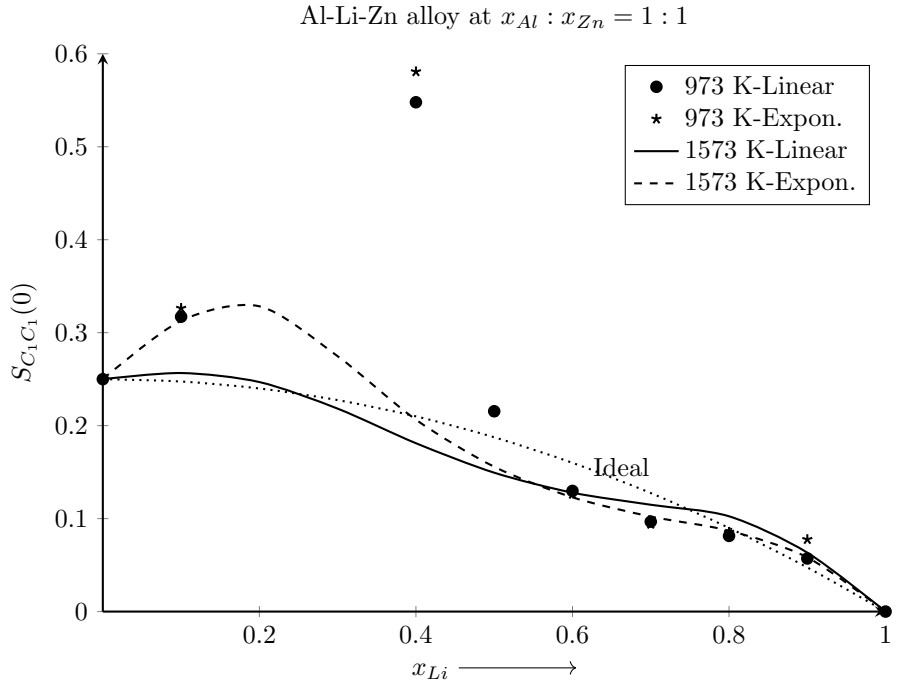

Figure 80: $S_{C_1C_1}(0)$ of liquid Al–Li–Zn alloy at $x_{Al} : x_{Li} = 1 : 1$.

Table 59: $S_{C_2C_2}(0)$ of liquid Al–Li–Zn alloy at $x_{Al} : x_{Zn} = 1 : 1$

x_{Li}	$S_{C_2C_2}(0)$				
		973 K		1573 K	
	Ideal	Linear fit	Exponential fit	Linear fit	Exponential fit
0.1	0.09	0.197	0.196	0.118	0.128
0.2	0.16	1.733	1.733	0.222	0.255
0.3	0.21	15.751	367.898	0.240	0.277
0.4	0.24	0.782	0.908	0.205	0.230
0.5	0.25	0.271	0.293	0.168	0.183
0.6	0.24	0.151	0.154	0.146	0.150
0.7	0.21	0.113	0.108	0.141	0.133
0.8	0.16	0.106	0.101	0.144	0.125
0.9	0.09	0.091	0.111	0.106	0.097

parameters for thermodynamic functions, specially G_M^{xs} of binary liquid alloys is outmost essential in this field to predict their phase behaviours at elevated temperatures. In mixing properties, we have computed and studied excess free energy of mixing (G_M^{xs}), enthalpy of mixing (H_M), activity (a) and ($S_{CC}(0)$) of above mentioned liquid alloys. The discussion related to the results of each system is outlined in the following sub-sections.

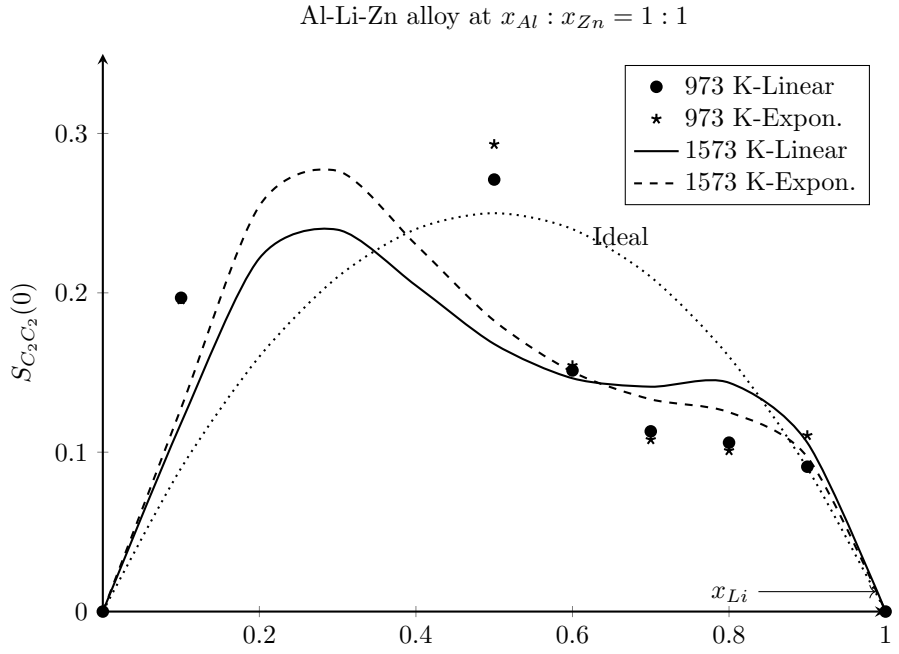

Figure 81: $S_{C_2C_2}(0)$ of liquid Al–Li–Zn alloy at $x_{Al} : x_{Li} = 1 : 1$.

Table 60: $S_{C_1C_2}(0)$ of liquid Al–Li–Zn alloy at $x_{Al} : x_{Zn} = 1 : 1$

x_{Li}	$S_{C_1C_2}(0)$				
		973 K		1573 K	
	Ideal	Linear fit	Exponential fit	Linear fit	Exponential fit
0.1	-0.05	0.127	0.130	0.034	0.077
0.2	-0.08	1.320	1.317	0.069	0.136
0.3	-0.11	12.331	281.095	0.068	0.116
0.4	-0.12	0.554	0.624	0.039	0.062
0.5	-0.13	0.145	0.156	0.005	0.017
0.6	-0.12	0.039	0.045	-0.026	-0.016
0.7	-0.11	-0.010	-0.005	-0.055	-0.041
0.8	-0.08	-0.043	-0.043	-0.078	-0.059
0.9	-0.05	-0.050	-0.071	-0.061	-0.054

4.12.2 Al–Fe system

According to Kaptay (2012), the entropy contribution term b_i in linear T-dependent energy interaction parameters ($L_i = a_i + b_i.T$, i = 0, 1, 2, ...) should be less than 2R to avoid any miscibility gap. The b_0 of this work and Cost 507 for liquid Al–Fe alloy are 20.96 J/(mol K) and 22.1314 J/(mol K) respectively which are greater than 2R. In this regard, the value of term containing b_i increases rapidly with the rise of temperature which has changed the values of thermodynamic and structural functions of the system resulting in unusual trends. These unusual trends are known as "artificial inverted miscibility gaps". In order to remove the artificial gaps, the exponential T-dependent

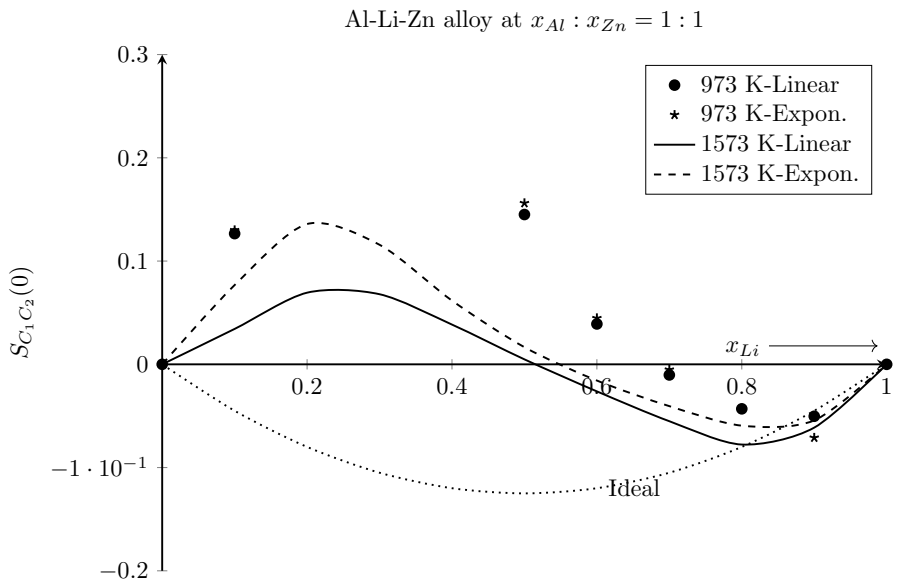

Figure 82: $S_{C_1C_2}(0)$ of liquid Al–Li–Zn alloy at $x_{Al} : x_{Li} = 1 : 1$.

Table 61: $S_{C_1C_1}(0)$ of liquid Al–Li–Zn alloy at $x_{Al} : x_{Zn} = 0.136 : 1$

x_{Li}	$S_{C_1C_1}(0)$				
		973 K		1573 K	
	Ideal	Linear fit	Exponential fit	Linear fit	Exponential fit
0.0	0.11	0.106	0.106	0.106	0.106
0.1	0.10	0.114	0.114	0.106	0.111
0.2	0.09	0.157	0.157	0.108	0.117
0.3	0.08	0.241	0.254	0.104	0.116
0.4	0.07	0.244	0.271	0.089	0.100
0.5	0.06	0.134	0.143	0.069	0.075
0.6	0.05	0.069	0.070	0.051	0.053
0.7	0.03	0.040	0.040	0.037	0.037
0.8	0.02	0.024	0.026	0.025	0.025
0.9	0.01	0.012	0.014	0.013	0.013

interaction parameters were presented in this work to study of the mixing properties of the systems at high temperatures. These interaction parameters have been used to calculate thermodynamic (G_M^{xs}, a_{Al}, a_{Fe}, H_M) and structural properties ($S_{CC}(0)$) of the systems at different temperatures. Kostov & Živković (2008) had used FactSage Thermo-chemical Software and calculated activity of Al and Fe in Al–Fe alloys in the range 1873 K–2073 K. Their results showed negative deviation from Raoult's law throughout the entire concentration range indicating the system to be ordering in nature.

In present work, the unusual trends were observed in above mentioned properties when they were computed using linear parameters at higher temperatures. The plots of computed values of $S_{CC}(0)$ using linear parameters (Figures 42-45) depicted the

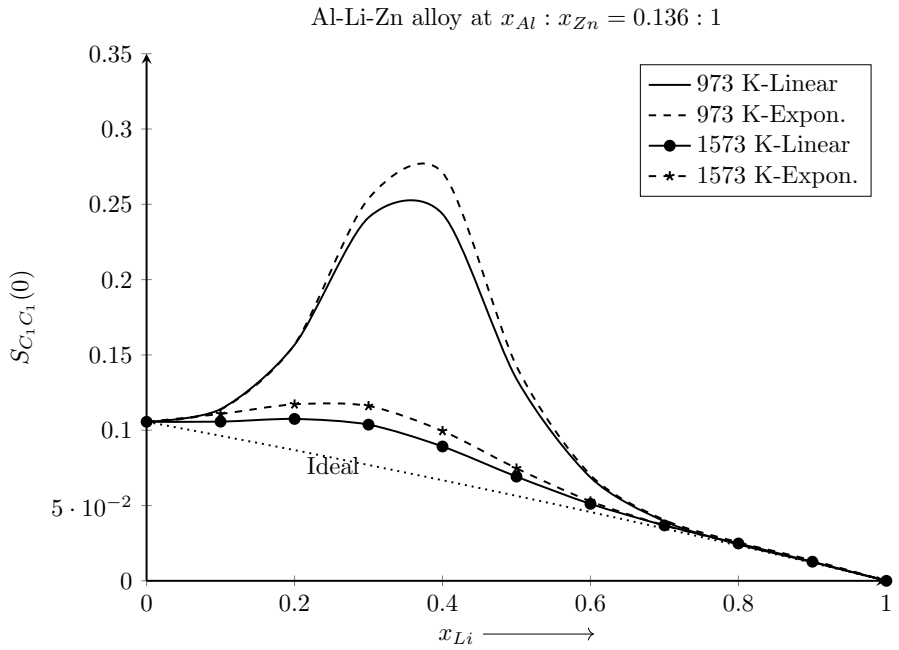

Figure 83: $S_{C_1C_1}(0)$ of liquid Al–Li–Zn alloy at $x_{Al} : x_{Zn} = 0.136 : 1$.

Table 62: $S_{C_2C_2}(0)$ of liquid Al–Li–Zn alloy at $x_{Al} : x_{Zn} = 0.136 : 1$

x_{Li}	$S_{C_2C_2}(0)$				
		973 K		1573 K	
	Ideal	Linear fit	Exponential fit	Linear fit	Exponential fit
0.1	0.09	0.0943	0.0943	0.0923	0.0913
0.2	0.16	0.2270	0.2308	0.1683	0.1719
0.3	0.21	0.4687	0.5054	0.2193	0.2347
0.4	0.24	0.5846	0.6660	0.2329	0.2560
0.5	0.25	0.3896	0.4179	0.2186	0.2377
0.6	0.24	0.2442	0.2450	0.1961	0.2062
0.7	0.21	0.1753	0.1701	0.1741	0.1761
0.8	0.16	0.1360	0.1341	0.1456	0.1437
0.9	0.09	0.0874	0.0906	0.0908	0.0898

transition of phase at 3500 K and 3800 K since $S_{CC}(0)$> $S^{id}_{CC}(0)$. But when exponential T-dependent interaction parameters were used, no such transformations were observed as both S^{xs}_M and H_M varied correspondingly with temperature. Therefore, exponential T-dependent parameters should be preferred in order to investigate the mixing properties of this system at higher temperatures. Moreover, the computed negative values of G^{xs}_M and the deviation between $S_{CC}(0)$ from $S^{id}_{CC}(0)$ gradually decreased at higher temperatures, revealing decrease in compound forming tendency of the system.

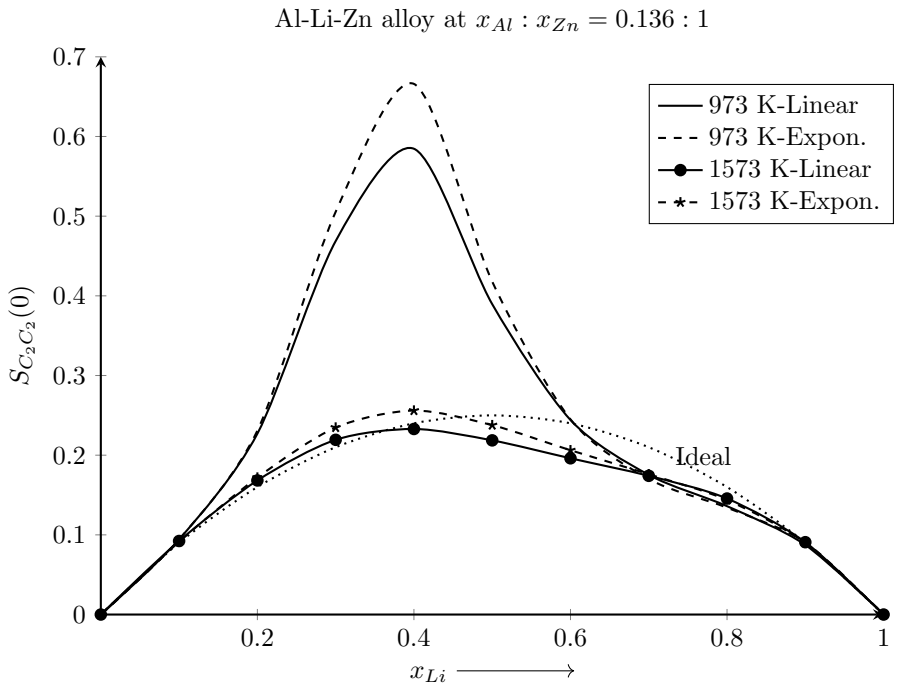

Figure 84: $S_{C_2C_2}(0)$ of liquid Al–Li–Zn alloy at $x_{Al} : x_{Li} = 0.136 : 1$.

Table 63: $S_{C_1C_2}(0)$ of liquid Al–Li–Zn alloy at $x_{Al} : x_{Zn} = 0.136 : 1$

x_{Li}	$S_{C_1C_2}(0)$				
		973 K		1573 K	
	Ideal	Linear fit	Exponential fit	Linear fit	Exponential fit
0.1	-0.01	0.036	0.035	0.016	0.020
0.2	-0.02	0.120	0.122	0.043	0.052
0.3	-0.03	0.271	0.293	0.059	0.075
0.4	-0.03	0.314	0.363	0.054	0.072
0.5	-0.03	0.166	0.183	0.034	0.047
0.6	-0.03	0.066	0.068	0.012	0.020
0.7	-0.03	0.018	0.017	-0.005	0.000
0.8	-0.02	-0.004	-0.007	-0.014	-0.012
0.9	-0.01	-0.010	-0.013	-0.012	-0.011

4.12.3 Al–Mn system

The optimised values of b_0 for linear parameter L_0 for liquid Al–Mn system were 27.0988 J/(mol K) (Cost 507) and 28.22693 J/(mol K) (Du et al., 2007). Since both of these values were greater than 2R, unusual trends appeared in the thermodynamic and structural functions of the system when calculated using linear parameters at higher temperatures. In this work, the plot of computed values of $S_{CC}(0)$ using linear parameters versus concentration (Figures 46-49) showed that $S_{CC}(0) > S^{id}_{CC}(0)$ at 2500 K. Due to $b_0 > 2R$, the values of $S_{CC}(0)$ increased more rapidly and exceeded the ideal values with increase in

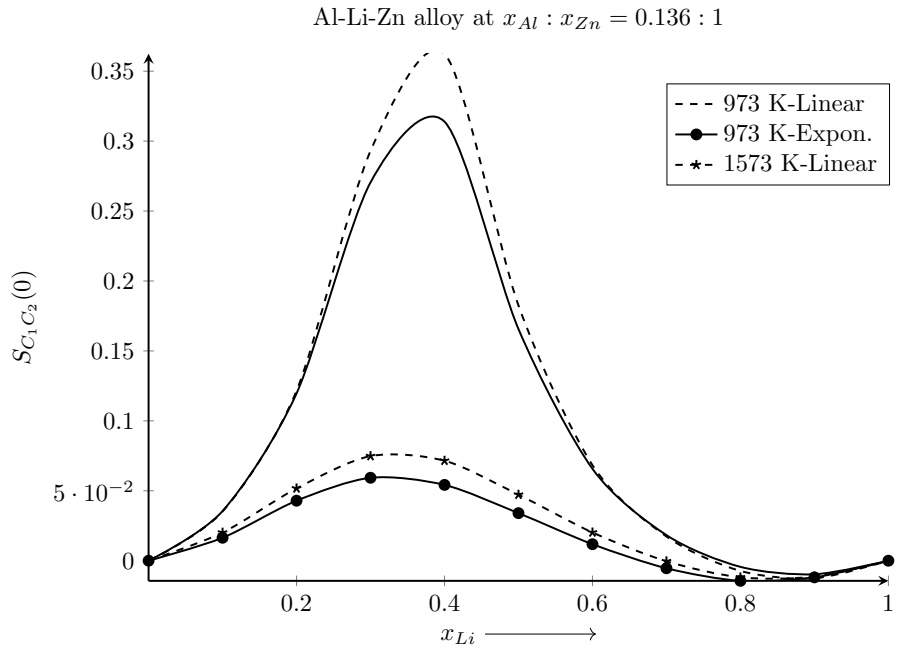

Figure 85: $S_{C_1C_2}(0)$ of liquid Al–Li–Zn alloy at $x_{Al} : x_{Li} = 0.136 : 1$.

temperature. This tendency might have appeared as the variation of H_M with temperature is not considered during the optimisation of linear interaction parameters.

Moreover, the values of $S_{CC}(0)$ calculated using exponential parameters shifted toward ideal values with rise of temperatures up to 2500 K. However, the system still showed ordering tendency in the preferred temperature range. The unusual behaviours seen in the thermodynamic and structural properties while using linear parameters have been removed using exponential parameters in this work. Additionally, the present theoretical investigations predict that the mixing tendency of the system was found to decrease with the rise in temperature of the system beyond its melting temperature.

4.12.4 Al–Ti system

The optimised value of b_0 of L_0 for liquid Al-Ti system from Cost 507 and Witusiewicz et al. (2008) are 38 J/(mol K) and 41.972 J/(mol K) respectively and hence are greater than 2R. Due to which, unusual trends were observed in the thermodynamic and structural functions of the system when calculated using the linear parameters of Cost 507. The activities of components of Al–Ti alloy using linear parameters agreed well with the results of Kostov & Živković (2008). The activity of Al has positive deviation from Raoult's law. This positive deviation further increases with increase of temperature. For comprehensive analysis, we plotted the compositional dependence of the computed values of $S_{CC}(0)$ using linear parameters (Cost 507) and exponential parameters (this

work) at different temperatures in Figures 50-53.

It can be observed that the plots of $S_{CC}(0)$ at 1500 K using linear parameters showed negative deviation with respect to ideal values while showed positive deviation above 2000 K at both lower and higher concentrations of Ti. Novakovic et al. (2012) analysed $S_{CC}(0)$ of Al–Ti alloys and noticed pronounced segregation in the region of lower concentration of Ti at 1973 K. These results indicate the transformation of phase from ordering to segregating. When exponential parameters were used, the plots showed negative deviations with respect to ideal values at all preferred temperatures, indicating the predominance of ordering tendency in the entire composition range. As these values gradually got closer to ideal, it can be stated that the compound forming or mixing tendency of the system gradually decreased with increase in its temperature.

4.12.5 Li–Mg system

The linear parameters of Wang, Du, & Liu (2011) for the system are $L_0 = -13172 - 4.3009T$, $L_1 = 912 + 2.7115T$ and $L_2 = 2531$. Though the values of b_i are less than 2R, both a_0 and b_0 are negative due to which the values of thermodynamic and structural functions computed using these parameters do not shift towards ideal values at higher temperatures as expected. The linear interaction parameters optimized in this work for the system are $L_0 = -21318 + 2.9T$, $L_1 = 7930 - 15.1T$, $L_2 = 10668 - 8.9T$ and $L_3 = -7765 + 7.4T$. Comparing these parameters with $L_i = a_i + b_iT$, the values of b_i are found to be less than 2R. Therefore, unusual trends are not observed in the thermodynamic properties (basically in G_M^{xs}) when computed at different temperatures using these parameters.

However, when the values of $S_{CC}(0)$ are computed using these parameters, they showed unusual trends above 1000 K (melting temperature) both at lower and higher concentrations of Mg. Therefore, exponential parameters were optimised for the system in this work. The unusual trends, also called artificial inverted miscibility gaps, observed in the thermodynamic and structural functions have been removed with the aid of exponential parameters.

4.12.6 Al–Li–Zn system

The optimised values of b_0 for Al–Li and Li–Zn sub-binary systems of ternary liquid Al–Li–Zn alloy are 20.6 J /(mol K) (Hallstedt & Kim, 2007) and 26.36 J/(mol K) (Y. Liang et al., 2008) respectively. These values of b_0 are greater than 2R. Therefore, the computed values of G_M^{xs} of these sub-binary systems at higher temperatures showed artificial inverted miscibility gaps in the region of higher concentration of Li. The strength of

interaction among the sub-binary pairs affects the energetic of ternary system. The value of b_0 of ternary interaction parameter for the ternary system was found to be 52 J/(mol K) (Trybula et al., 2014) resulting in calculated artifacts. The results of $S_{CC}(0)$ obtained at higher temperatures for Li-based sub-binary systems (Al–Li and Li–Zn) also depicted the presence of artifacts with linear interaction parameters. While using the exponential interaction parameters, no such unusual trends were observed. This discussion justifies the necessity of exponential parameters for these sub-binary pairs. Therefore, the exponential T-dependent parameters were optimised for the above-mentioned systems in order to explain their mixing behaviours at higher temperatures.

The structural properties of ternary system have been studied by computing $S_{C_iC_j}(0)$, namely $S_{C_1C_1}(0)$, $S_{C_2C_2}(0)$ and $S_{C_1C_2}(0)$ as a function of concentration and temperature. From the study of $S_{C_iC_j}(0)$ for this ternary system, it may be stated that the extent of interactions among the sub-binary pairs have great influence on its mixing tendency, including the information regarding phase transitions as well as critical composition and temperature. Furthermore, when the compositions of constituent atoms in the ternary system and temperature are changed, the critical mixing (unusual behaviour at particular concentration and temperature) is observed only at $x_{Li} = 0.3$, 973 K, and $x_{Al} : x_{Zn} = 1 : 1$.

CHAPTER 5

5. CONCLUSION AND RECOMMENDATIONS

Thermodynamic properties, such as excess free energy of mixing, enthalpy of mixing and activity and microscopic structural properties, such as concentration fluctuation in long wavelength limit of a few binaries and ternary liquid alloys were studied and explained in this work. The binary liquid alloys namely Al–Fe, Al–Mn, Al–Ti and Li–Mg and a ternary Al–Li–Zn liquid alloy were selected for the purpose. The important conclusions related to the study and recommendation fo the work are presented in this chapter.

5.1 Conclusion

As stated earlier, we have studied the thermodynamic and structural properties of a few binary (Al–Fe, Al–Mn, Al–Ti and Li–Mg) and a ternary Al–Li–Zn liquid alloys at different temperatures in the framework of R-K polynomial. At first, these properties of the systems were computed using optimised linear T-dependent parameters which depicted as follows:

i. The thermodynamic functions computed using linear and exponential T-dependent interaction energy parameters were in good agreement with each other and also with the experimental and literature results for the selected systems near their melting temperatures.

ii. Present theoretical investigations predict that the thermodynamic and structural functions of the preferred liquid alloys above their melting points shift towards ideal values.

iii. The thermodynamic and structural functions of these systems showed unusual behaviours at higher temperatures when computed using linear T-dependent parameters called "artificial inverted miscibility gap". These behiours were clearly observed as the transformation of ordering to segregation nature or vice-versa at higher temperatures.

iv. When linear parameters were replaced by exponential parameters, these unexpected results were not observed.

v. Therefore, the current work recommends that the thermodynamic properties of binary Al–Fe, Al–Mn, Al–Ti, Li–Mg and ternary Al–Li–Zn liquid alloys should be computed using the exponential T-dependent parameters at higher temperatures.

vi. Similar results were also forecasted from the study of the structural properties of these systems at higher temperatures.

vii. Since in linear parameters, the terms contributing to enthalpy of mixing is not considered to be T-dependent, these values can be determined using exponential T-dependent parameters only.

viii. The ternary Al–Li–Zn liquid alloys showed the critical behaviour only at $x_{Li} = 0.3$, 973 K and $x_{Al} : x_{Zn} = 1 : 1$.

5.2 Recommendations for further work

The present work is a purely statistical study and based on theoretical modelling of the mixing properties of the above mentioned liquid alloys at higher temperatures. The recommendations from the work are listed below.

i. Due to the inaccessibility of computational software, the results of the present work could not be used to predict the phase diagrams of the systems. Therefore, one can use the exponential temperature-dependent interaction energy parameters in computer-based software in order to study the phase diagrams of these systems.

ii. One may design and perform experiment undertaking the results of the present work as reference data in order to fabricate, design and characterize new materials.

iii. One can use exponential T-dependent interaction parameters of the present work in order to compute the mixing properties of higher order alloys constituting these sub-binary systems. Moreover, the formulations developed in this work can be used for the optimization of T-dependent self-consistent parameters for thermodynamic functions of other binary and ternary systems. These expressions can be extended to study the mixing behaviours of multi-component systems.

CHAPTER 6

6. SUMMARY

At higher temperatures, unusual trends are observed in the mixing behaviours of some liquid alloys when computed using available linear T-dependent parameters of published works. As these unusual tendencies are rarely observed in the experimental results, they are often referred to as artificial inverted miscibility gaps or artifacts. Among the various factors resulting in these gaps, one of them may be due to the inaccuracy of optimised T-dependent thermodynamic parameters. Therefore, the mixing behaviours of a few liquid alloys (Al–Fe, Al–Mn, Al–Ti, Li–Mg and Al–Li–Zn) have been analysed at different temperatures in terms of linear and exponential T-dependent optimised parameters in this work.

A brief summary of the present work are as follows:

I. Thermodynamic properties

   a. Excess free energy of mixing (G_M^{xs})

      i. The calculated values of G_M^{xs} for Al–Fe system at 1873 K were in good agreement with the available experimental and literature results. The negative values of G_M^{xs} were found to decrease rapidly while using linear parameters and their compositional dependence plots showed S-shape characteristics at higher temperatures, usually termed as artificial inverted miscibility gaps. When these values were computed using exponential parameters of this work, their plots showed symmetric nature in the temperature range 1873 K–3800 K.

      ii. For Al–Mn system, the values calculated using exponential parameters at 1570 K agreed well with those calculated using linear parameters. The plots of calculated values of G_M^{xs} using linear parameters showed unsymmetric nature at higher teperatures (1900 K–2500 K) depicting the presence of artificial inverted miscibility gaps. Moreover, the value of G_M^{xs} was found to be positive at 2500 K below equiatomic composition. But the compositional dependence plots of G_M^{xs} using exponential parameters showed symmetric nature indicating the removal of such gaps.

      iii. For Al–Ti system, the values calculated using linear parameter and exponential parameters at 1500 K were in close agreement. The computed values of G_M^{xs} using linear parameters at 2500 K indicated the phase transition from

ordering to segregating in lower concentration region of Ti. This unusual tendency was removed when exponential parameters of this work were used for the purpose. The later results predicted that the ordering nature of the system prevails in the preferred temperature range.

iv. In Li–Mg system, the values calculated at 1000 K using linear parameters of this work were in excellent agreement with experimental values. The values calculated using exponential parameters were in agreement with the results of Wang, Du, & Liu (2011). As the temperature of system was increased, the negative values of G_M^{xs} using linear parameters gradually increased representing the unusual tendency. However, the computed values of G_M^{xs} using exponential parameters of this work were found to gradually decrease at higher temperatures as expected.

v. In case of ternary Al–Li–Zn system, the plots of G_M^{xs} of sub-binary Al–Li and Li–Zn alloys using linear parameters showed unusual trends at 1573 K in higher concentration region of Li. The same trend was also observed in the ternary system at the same temperature and composition range using linear parameters. These unusual trends were not observed in sub-binary as well as and ternary system when exponential parameters were used.

b. Enthalpy of mixing (H_M)

i. The variation of H_M with temperature is not considered in the linear parameters. Therefore, the theoretical values of H_M for the preferred systems were computed using exponential parameters only.

ii. For Al–Fe system, the values of H_M calculated using exponential parameters at 1873 K was found to be in excellent agreement with the observed values of Desai (1987). The negative values calculated using exponential parameters were found to decrease at higher temperatures.

iii. The negative values of H_M of Al–Mn system calculated using exponential parameters of this work was found to gradually decrease with increase in its temperature. Moreover, their plots showed symmetric variations at higher temperatures.

iv. In case of Al–Ti system, the calculated values of H_M using exponential parameters were found to decrease and their plots showed symmetric variations in the temperature range 1500 K–2700 K.

v. The computed values of H_M using exponential parameters of this work for Li–Mg system at 1000 K were in good agreement with the experimental values (Hultgren et al., 1973). Moreover, their compositional dependence

curves showed symmetric variations at higher temperatures.

vi. The values of H_M of the Al–Li–Zn ternary system calculated using R-K-M model at different cross-sections and temperatures were found to be in good agreement with experimental values Trybula et al. (2014).

c. Activity (a)

i. The activities of components of the selected systems were calculated using both linear and exponential parameters at different temperatures.

ii. For Al–Fe system, the computed values using both linear and exponential parameters were in good agreement with the experimental (Hultgren et al., 1973) and literature (Adhikari et al., 2014) data at 1873 K. When the temperature of the system was raised in the range 1873 K to 3800 K, the activity computed using exponential parameters shifts towards ideal values.

iii. In case of Al–Mn system, activities of the monomers calculated using linear and exponential interaction parameters at 1600 K were in excellent agreement. The activity of Al calculated using linear interaction parameters showed positive deviation and that computed using exponential parameters showed negative deviation with respect to ideal value at 2500 K.

iv. In case of Al–Ti binary system, the estimated values of a_{Al} and a_{Ti} using both the linear and exponential parameters at 1500 K were found to be in good agreement. At higher temperatures (T > 1500 K), the computed values of a_{Al} and a_{Ti} gradually increased and approached their respective ideal values. The results obtained using linear parameters showed that the alloy changes its nature from ordering to segregating at higher temperatures. This unusual tendency was not observed when exponential parameters were used.

v. For Li–Mg system, the calculated values of a_{Li} and a_{Mg} using linear parameters at 1000 K were found to be in excellent agreement with the experimental values (Hultgren et al., 1973). They have large negative deviations from ideal values at and around equiatomic composition.

vi. The activity of the ternary Al–Li–Zn system has been computed using the thermodynamic database of its sub-binary Al–Li, Li–Zn and Al–Zn system. In case of Al–Li sub-binary system, the computed values of a_{Al} and a_{Li} using exponential parameters at 973 K were found to be consistent with the data of Hallstedt & Kim (2007). The computed values of a_{Li} and a_{Zn} of Li–Zn system at 973 K were found to be in excellent agreement with the results of Y. Liang et al. (2008). Further, the computed values of a_{Al} and a_{Zn}

using exponential parameters at 973 K were in excellent agreement with the results of Mathon et al. (2000). The computed values of activities of all the components using both linear and exponential parameters of ternary system at 973 K were found to be consistent with each other at all cross-sections.

vii. The computed values of activities of all the preferred systems in this work were found to increase at higher temperatures. These results predicted that the interacting nature of these systems gradually decreases at higher temperatures.

II. Structural property (Concentration fluctuation in long wavelength limit $S_{CC}(0)$)

i. The thermodynamic parameters, such as G_M^{xs} and a of the binary and ternary systems have direct influence on $S_{CC}(0)$. The mixing and demixing behaviours of the liquid alloys can be interpreted more clearly in terms of $S_{CC}(0)$.

ii. For Al–Fe system, the computed values of $S_{CC}(0)$ using both linear and exponential parameters were in well agreement with each other. They were also in well agreement with the calculated experimental values and results of Adhikari et al. (2014). The comparison of computed values of with ideal value shows that the system was found to be ordering in nature near melting temperature. The system showed segregating nature with respect to $S_{CC}(0)$ when linear parameters were used at higher temperatures. But it still showed ordering tendency at higher temperatures when exponential parameters were used.

iii. In case of Al–Mn system, the values computed using the linear and exponential parameters were found to be less than the ideal values at all concentrations of Mn which reveals the system to be ordering in nature. At 2500 K and above it, the computed values of $S_{CC}(0)$ using linear parameters exceeded ideal values at higher concentrations of Mn indicating the phase transformation from ordering to segregating nature. But the values computed using exponential parameters still showed ordering nature.

iv. In case of Al–Ti system at 1500 K, it can be observed that the computed values using both the linear and exponential parameters were found to be in good agreement. At lower concentration of Ti, the values computed using linear parameters were found to be greater than ideal values indicating the phase transformation from ordering to segregating nature of the system. The values computed using exponential parameters were found to be less than the ideal values in the entire concentration range and at all the preferred temperatures indicating the ordering nature.

v. In case of Li–Mg system, it can be observed that the computed values at 1000 K using optimised linear interaction parameters were in excellent agreement with

the calculated experimental values. These values exceeded ideal values at higher concentrations of Mg indicating the transformation from ordering to segregating nature of the system. The values computed using exponential parameters gradually increased and got closer to ideal values at higher temperatures.

vi. The structural properties of ternary Al–Li–Zn liquid alloy have been studied by computing $S_{CC}(0)$ of its sub-binary systems as well as ternary system at different temperatures. The sub-binary systems Al–Li and Li–Zn showed phase transitions whereas Al–Zn showed complete segregating tendency. The values of $S_{CC}(0)$ computed using exponential parameters showed ideal behaviour with temperature variation. However, those computed using linear parameters do not show such variations. In case of ternary system, $S_{C_1C_1}(0)$, $S_{C_2C_2}(0)$ and $S_{C_1C_2}(0)$ were computed at cross-sections $x_{Al} : x_{Zn} = 3 : 1, 1 : 1$ and $0.136 : 1$ and at temperatures 973 K and 1573 K. Again, the values computed using exponential parameters showed ideal tendency at elevated temperatures.

REFERENCES

Abe, T., Ogawa, K., & Hashimoto, K. (2012). Analysis of miscibility gaps based on the Redlich-Kister polynomial for binary solutions. *Calphad*, *38*, 161–167. doi: 10.1016/j.calphad.2012.06.006

Adhikari, D. (2011). Inhomogeneity in structure of MgPb liquid alloy. *Physica B: Condensed Matter*, *406*(3), 445–448. doi: 10.1016/j.physb.2010.11.009

Adhikari, D., Jha, I. S., & Singh, B. P. (2010). Thermodynamic and microscopic structure of liquid Cu–Sn alloys. *Physica B: Condensed Matter*, *405*(7), 1861–1865. doi: 10.1016/j.physb.2010.01.064

Adhikari, D., Singh, B. P., Jha, I. S., & Singh, B. K. (2010). Thermodynamic properties and microscopic structure of liquid Cd–Na alloys by estimating complex concentration in a regular associated solution. *Journal of Molecular Liquids*, *156*(2-3), 115–119. doi: 10.1016/j.molliq.2010.05.020

Adhikari, D., Yadav, S. K., & Jha, L. N. (2014). Thermo-physical properties of Al–Fe melt. *Journal of the Chinese Advanced Materials Society*, *2*(3), 149-158. doi: 10.1080/22243682.2014.928603

Alblas, B. P., Van der Lugt, W., Dijkstra, J., Geertsma, W., & Van Dijk, C. (1983). Structure of liquid Na–Sn alloys. *Journal of Physics F: Metal Physics*, *13*(12), 2465–2477. doi: 10.1088/0305-4608/13/12/007

Alcock, C. B., Jacob, K. T., & Palamutcu, T. (1973). Thermodynamics of α-solid solutions of silver with indium and tin. *Acta Metallurgica*, *21*(7), 1003–1009. doi: 10.1016/0001-6160(73)90156-9

Ansara, I., Dinsdale, A. T., & Rand, M. H. (1998). *Thermochemical database for light metal alloys (COST 507)*.

Anusionwu, B. C. (2000). Concentration fluctuations and chemical complexes in the Zn-Au liquid alloy. *Physics and Chemistry of Liquids*, *38*(6), 671–682. doi: 10.1080/00319100008030314

Anusionwu, B. C. (2006). Thermodynamic and surface properties of Sb-Sn and In-Sn liquid alloys. *Pramana*, *67*, 319–330. doi: 10.1007/s12043-006-0076-z

Arroyave, R., & Liu, Z. K. (2006). Thermodynamic modelling of the Zn–Zr system. *Calphad*, *30*(1), 1–13. doi: 10.1016/j.calphad.2005.12.006

Arslan, H., & Dogan, A. (2022). Investigation of surface tension and viscosity properties of liquid Al–Au binary alloys. *Canadian Metallurgical Quarterly*, *61*(1), 108–119. doi: 10.1080/00084433.2021.2021498

Ashcroft, N. W., & Mermin, N. D. (1976). *Solid state physics*. Saunders College Publishing, Philadelphia.

Awe, O. E. (2019). Thermodynamic investigation of thermophysical properties of thallium–based liquid alloys. *Physics and Chemistry of Liquids*, *57*(3), 296–310. doi: 10.1080/00319104.2018.1443453

Balakumar, T., & Medraj, M. (2005). Thermodynamic modeling of the Mg–Al–Sb system. *Calphad*, *29*(1), 24–36. doi: 10.1016/j.calphad.2005.03.001

Basuki, E. A., Prajitno, D. H., & Muhammad, F. (2017). Alloys developed for high temperature applications. In *AIP Conference Proceedings* (Vol. 1805, pp. 020003–0200015). doi: 10.1063/1.4974409

Beeby, J. L. (1964). Electronic structure of alloys. *Physical Review.*, *135*, A130–A143. doi: 10.1103/PhysRev.135.A130

Bencze, L., & Popovic, A. (2013). Determination of the Mixing Thermodynamic Properties of Liquid Ternary Alloys by Fitting the Knudsen Effusion Mass Spectrometric Data to the Redlich-Kister-Muggianu Sub-Regular Solution Model. *The Open Thermodynamics Journal*, *7*(1), 21-34. doi: 10.2174/1874396X01307010021

Bergman, C., Saito, M., & Chastel, R. (1994). Thermodynamic properties of quasi-crystal-forming AlMn alloys from Knudsen cell mass spectrometric measurements. *Materials Science and Engineering: A*, *178*(1-2), 89–92. doi: 10.1016/0921-5093(94)90524-X

Bhatia, A. B., & Hargrove, W. H. (1974). Concentration fluctuations and thermodynamic properties of some compound forming binary molten systems. *Physical Review B*, *10*(8), 3186–3196. doi: 10.1103/PhysRevB.10.3186

Bhatia, A. B., Hargrove, W. H., & March, N. H. (1973). Concentration fluctuations in conformal solutions and partial structure factor in alloys. *Journal of Physics C: Solid State Physics*, *6*(4), 621–630. doi: 10.1088/0022-3719/6/4/008

Bhatia, A. B., & Ratti, V. K. (1977). Number-concentration structure factors and their long wavelength limit in multicomponent fluid mixtures. *Physics and Chemistry of Liquids*, *6*(3), 201–213. doi: 10.1080/00319107708084140

Bhatia, A. B., & Singh, R. N. (1982). Short range order and concentration fluctuations in regular and compound forming molten alloys. *Physics and Chemistry of Liquids an International Journal*, *11*(4), 285–313. doi: 10.1080/00319108208080752

Bhatia, A. B., & Singh, R. N. (1984). A quasi-lattice theory for compound forming molten alloys. *Physics and Chemistry of Liquids an International Journal*, *13*(3), 177–190. doi: 10.1080/00319108408080778

Bhatia, A. B., & Thornton, D. E. (1970). Structural aspects of the electrical resistivity of binary alloys. *Physical Review B*, *2*(8), 3004–3012. doi: 10.1103/PhysRevB.2.3004

Bo, L., Li, S., Wang, L., Wu, D., Zuo, M., & Zhao, D. (2018). Liquid-liquid phase separation and solidification behaviour of Al55Bi36Cu9 monotectic alloy with different cooling rates. *Results in Physics*, *8*, 1086–1091. doi: 10.1016/j.rinp.2018.01.056

Braga, M. H., Malheiros, L. F., & Hämäläinen, M. (2000). The Cu-Li-Mg system at room temperature. *Thermochimica Acta*, *344*(1-2), 47–54. doi: 10.1016/S0040-6031(99)00325-1

Butler, J. A. V. (1932). The thermodynamics of the surfaces of solutions. *Proceedings of the Royal Society of London. Series A, Containing Papers of a Mathematical and Physical Character*, *135*(827), 348–375. doi: 10.1098/rspa.1932.0040

Carnahan, N. F., & Starling, K. E. (1969). Equation of state for nonattracting rigid spheres. *The Journal of chemical physics*, *51*(2), 635–636. doi: 10.1063/1.1672048

Chang, Y. A., Chen, S., Zhang, F., Yan, X., Xie, F., Schmid-Fetzer, R., & Oates, W. A. (2004). Phase diagram calculation: past, present and future. *Progress in Materials Science*, *49*(3-4), 313–345. doi: 10.1016/S0079-6425(03)00025-2

Chen, S. L., Daniel, S., Zhang, F., Chang, Y. A., Oates, W. A., & Schmid-Fetzer, R. (2001). On the calculation of multicomponent stable phase diagrams. *Journal of Phase Equilibria*, *22*(4), 373–378. doi: 10.1361/105497101770332910

Chevalier, P. Y. (1989). A thermodynamic evaluation of the Cu–Tl system. *Thermochimica Acta*, *156*(2), 383–392. doi: 10.1016/0040-6031(89)87205-3

Chou, K. C., & Chang, A. Y. (1989). A study of ternary geometrical models. *Berichte der Bunsengesellschaft für physikalische Chemie*, *93*(6), 735–741. doi: 10.1002/bbpc.19890930615

Cobos, J. C. (1997). An exact quasi-chemical equation for excess heat capacity with W-shaped concentration dependence. *Fluid Phase Equilibria*, *133*(1-2), 105–127. doi: 10.1016/S0378-3812(97)00012-5

Darken, L. S. (1950). Application of the Gibbs-Duhem equation to ternary and multicomponent systems. *Journal of the American Chemical Society*, *72*(7), 2909–2914. doi: 10.1021/ja01163a030

Debski, A., & Terlicka, S. (2016). Calorimetric measurements of liquid (Al+ Li+ Zn) alloys. *The Journal of Chemical Thermodynamics*, *92*, 91–96. doi: 10.1016/j.jct.2015.09.008

Derimow, N., & Abbaschian, R. (2018). Liquid phase separation in high-entropy alloys-a review. *Entropy*, *20*(11), 890–909. doi: 10.3390/e20110890

Desai, P. D. (1987). Thermodynamic properties of selected binary aluminum alloy systems. *Journal of Physical and Chemical Reference Data*, *16*(1), 109–124. doi: 10.1063/1.555788

Dinsdale, A. T. (1984). *The generation and application of metallurgical thermodynamic data* (Unpublished doctoral dissertation).

Du, Y., Schuster, J. C., Liu, Z. K., Hu, R., Nash, P., Sun, W., ... others (2008). A thermodynamic description of the Al–Fe–Si system over the whole composition and temperature ranges via a hybrid approach of CALPHAD and key experiments. *Intermetallics*, *16*(4), 554–570. doi: 10.1016/j.intermet.2008.01.003

Du, Y., Wang, J., Zhao, J., Schuster, J. C., Weitzer, F., Schmid-Fetzer, R., ... others (2007). Reassessment of the Al–Mn system and a thermodynamic description of the Al–Mg–Mn system. *International Journal of Materials Research*, *98*(9), 855–871. doi: 10.3139/146.101547

Faber, T. E. (2010). *Introduction to the theory of liquid metals*. Cambridge University Press.

Feufel, H., Gödecke, T., Lukas, H. L., & Sommer, F. (1997). Investigation of the Al–Mg–Si system by experiments and thermodynamic calculations. *Journal of Alloys and Compounds*, *247*(1-2), 31–42. doi: 10.1016/S0925-8388(96)02655-2

Flory, P. J. (1942). Thermodynamics of high polymer solutions. *The Journal of Chemical Physics*, *10*(1), 51–61. doi: 10.1063/1.1723621

Gancarz, T., Gąsior, W., & Henein, H. (2013). Physicochemical properties of Sb, Sn, Zn, and Sb–Sn system. *International Journal of Thermophysics*, *34*(2), 250–266. doi: 10.1007/s10765-013-1407-1

Gancarz, T., Moser, Z., Gąsior, W., Pstruś, J., & Henein, H. (2011). A comparison of surface tension, viscosity, and density of Sn and Sn–Ag alloys using different measurement techniques. *International Journal of Thermophysics*, *32*(6), 1210–1233. doi: 10.1007/s10765-011-1011-1

Gasior, W., Debski, A., & Terlicka, S. (2016). Calorimetric and Electromotive Force Measurements of Al–Li–Zn Liquid Solutions. *Journal of Phase Equilibria and Diffusion*, *37*(4), 481–490. doi: 10.1007/s11669-016-0474-y

Gasior, W., Moser, Z., Zakulski, W., & Schwitzgebel, G. (1996). Thermodynamic studies and the phase diagram of the Li–Mg system. *Metallurgical and Materials Transactions A*, *27*(9), 2419–2428. doi: 10.1007/BF02652335

Ghasemi, M., Stutz, E., Steinvall, S. E., Zamani, M., & i Morral, A. F. (2019). Thermodynamic re-assessment of the Zn–P binary system. *Materialia*, *6*, 100301-100307. doi: 10.1016/j.mtla.2019.100301

Gohivar, R. K., Koirala, R. P., Yadav, S. K., & Adhikari, D. (2020). Temperature dependence of interaction parameters of Cu–Si liquid alloy. *AIP Advances*, *10*(8), 085121–085126. doi: 10.1063/5.0012834

Gohivar, R. K., Yadav, S. K., Koirala, R. P., & Adhikari, D. (2020). Artifacts in Al–Mn liquid alloy. *Physica B: Condensed Matter*, *595*, 412348-412354. doi: 10.1016/j.physb.2020.412348

Gohivar, R. K., Yadav, S. K., Koirala, R. P., & Adhikari, D. (2021a). Assessment of thermo-structural properties of Al-Fe and Fe-Si alloys at high temperatures. *Physics and Chemistry of Liquids*, *59*(5), 679–689. doi: 10.1080/00319104.2020.1793985

Gohivar, R. K., Yadav, S. K., Koirala, R. P., & Adhikari, D. (2021b). Study of artifacts in thermodynamic and structural properties of Li–Mg alloy in liquid state using linear and exponential models. *Heliyon*, *7*(3), e06613–e06621. doi: 10.1016/j.heliyon.2021.e06613

Gohivar, R. K., Yadav, S. K., Koirala, R. P., & Adhikari, D. (2021c). Study of excess free energy of mixing and heat of mixing of liquid ternary Al–Li–Zn alloy by assessing the thermodynamic properties of sub-binary alloys. *Physica B: Condensed Matter*, *610*, 412941–412945. doi: 10.1016/j.physb.2021.412941

Gohivar, R. K., Yadav, S. K., Koirala, R. P., Shrestha, G. K., & Adhikari, D. (2021). Temperature dependence of interaction parameters for Al–Li liquid alloy. *Philosophical Magazine*, *101*(2), 179–192. doi: 10.1080/14786435.2020.1825858

Guthrie, F. (1884). On eutexia. *Proc. Phys. Soc. London*, *6*, 462–482. doi: 10.1088/1478-7814/6/1/312

Hallstedt, B., & Kim, O. (2007). Thermodynamic assessment of the Al–Li system. *International Journal of Materials Research*, *98*(10), 961–969. doi: 10.3139/146.101553

Harada, S., Takahashi, S., Takeda, S., Tamaki, S., Gray, P., & Cusack, N. E. (1988). Thermodynamic properties of liquid Na-Cd and Na-In. *Journal of Physics F: Metal Physics*, *18*(12), 2559-2567. doi: 10.1088/0305-4608/18/12/007

Harrison, W. A. (1966). Pseudopotentials in the Theory of Metals. *1966, 336 P. W. A. Benjamin, Inc., New York*.

Heine, V. (1970). The pseudopotential concept. *Solid State Physics*, *24*, 1–36. doi: 10.1016/S0081-1947(08)60069-7

Hildebrand, J. H., & Scott, R. L. (1950). Solutions of nonelectrolytes. *Annual Review of Physical Chemistry*, *1*(1), 75–92. doi: 10.1146/annurev.pc.01.100150.000451

Hillert, M., & Staffansson, L. I. (1970). Regular-solution model for stoichiometric phases and ionic melts. *Acta chem. scand.*, *24*(10), 3618–3626. doi: 10.3891/acta.chem.scand.24-3618

Hultgren, R., Desai, P. D., Hawkins, D. T., Gleiser, M., & Kelley, K. K. (1973). *Selected values of the thermodynamic properties of binary alloys* (Tech. Rep.). National Standard Reference Data System.

Iida, T., Tripathi, N., Isac, M., & Guthrie, R. I. L. (2007). Models and equations for atomic transport coefficients of liquid metals: Viscosity and self-diffusivity. In *Materials Science Forum* (Vol. 539, pp. 2509–2517). doi: 10.4028/www.scientific.net/MSF.539-543.2509

Ishiguro, T., Takeda, S., & Tamaki, S. (1982). EMF measurements on liquid Na-Hg alloys and their thermodynamic properties. *Journal of Physics F: Metal Physics*, *12*(5), 845–856. doi: 10.1088/0305-4608/12/5/005

Jansson, Å. (1992). A thermodynamic evaluation of the Al-Mn system. *Metallurgical Transactions A*, *23*(11), 2953–2962. doi: 10.1007/BF02646113

Kanibolotsky, D. S., Bieloborodova, O. A., Kotova, N. V., & Lisnyak, V. V. (2002). Thermodynamic properties of liquid Al-Si and Al-Cu alloys. *Journal of Thermal Analysis and Calorimetry*, *70*(3), 975–983. doi: 10.1023/A:1022285010138

Kaptay, G. (2004). A new equation for the temperature dependence of the excess Gibbs energy of solution phases. *Calphad*, *28*(2), 115–124. doi: 10.1016/j.calphad.2004.08.005

Kaptay, G. (2005). A method to calculate equilibrium surface phase transition lines in monotectic systems. *Calphad*, *29*(1), 56–67. doi: 10.1016/j.calphad.2005.04.004

Kaptay, G. (2012). On the tendency of solutions to tend toward ideal solutions at high temperatures. *Metallurgical and Materials Transactions A*, *43*(2), 531–543. doi: 10.1007/s11661-011-0902-x

Kaptay, G. (2014). On the abilities and limitations of the linear, exponential and combined models to describe the temperature dependence of the excess Gibbs energy of solutions. *Calphad*, *44*, 81–94. doi: 10.1016/j.calphad.2013.08.007

Kaptay, G. (2015). Partial surface tension of components of a solution. *Langmuir*, *31*(21), 5796–5804. doi: 10.1021/acs.langmuir.5b00217

Kaptay, G. (2017). The exponential excess Gibbs energy model revisited. *Calphad*, *56*, 169–184. doi: 10.1016/j.calphad.2017.01.002

Karlhuber, S., Mikula, A., Singh, R. N., & Sommer, F. (1999). Direct measurement of the concentration fluctuations in liquid Bi–Zn alloys. *Journal of Alloys and Compounds*, *283*(1-2), 198–202. doi: 10.1016/S0925-8388(98)00887-1

Kattner, U. R. (1997). The thermodynamic modeling of multicomponent phase equilibria. *JOM*, *49*(12), 14–19. doi: 10.1007/s11837-997-0024-5

Kehr, M., Schick, M., Hoyer, W., & Egry, I. (2008). Viscosity of the binary system Al-Ni. *High Temperatures–High Pressures*, *37*(4), 361–369.

Kelley, J. D., Martin, B. G., Szofran, F. R., & Lehoczky, S. L. (1982). Application of the Regular Associated Solution Model to the Cd–Te and Hg–Te Binary Systems. *Journal of The Electrochemical Society*, *129*(10), 2360-2365. doi: 10.1149/1.2123527

Kevorkov, D., Schmid-Fetzer, R., & Zhang, F. (2004). Phase equilibria and thermodynamics of the Mg–Si–Li system and remodeling of the Mg–Si system. *Journal of Phase Equilibria and Diffusion*, *25*(2), 140–151. doi: 10.1007/s11669-004-0007-y

Kim, Y. B., & Sommer, F. (1997). Calorimetric measurement of liquid aluminium–lithium–zinc alloys. *Thermochimica Acta*, *291*(1-2), 27–34. doi: 10.1016/S0040-6031(96)03087-0

Kittel, C., & McEuen, P. (2018). *Introduction to solid state physics*. John Wiley & Sons.

Kobayashi, M., & Tanaka, H. (2016). The reversibility and first-order nature of liquid-liquid transition in a molecular liquid. *Nature communications*, *7*(1), 1–8. doi: 10.1038/ncomms13438

Kohler, F. (1960). Estimation of the thermodynamic data for a ternary system from the corresponding binary systems. *Monatsh. Chem*, *91*(4), 738–740. doi: 10.1007/BF00899814

Koirala, R. P., Singh, B. P., Jha, I. S., & Adhikari, D. (2013). Thermodynamic, structural and surface properties of liquid Cd–Zn alloys. *Journal of Molecular Liquids*, *179*, 60–66. doi: 10.1016/j.molliq.2012.12.008

Kostov, A., & Živković, D. (2008). Thermodynamic analysis of alloys Ti–Al, Ti–V, Al–V and Ti–Al–V. *Journal of Alloys and Compounds*, *460*(1-2), 164–171. doi: 10.1016/j.jallcom.2007.05.059

Kumar, A., Rafique, S. M., Jha, N., & Mishra, A. K. (2005). Structure, thermodynamic, electrical and surface properties of Cu–Mg binary alloy: complex formation model. *Physica B: Condensed Matter*, *357*(3-4), 445–451. doi: 10.1016/j.physb.2004.12.031

Lebowitz, J. L. (1964). Exact solution of generalized Percus-Yevick equation for a mixture of hard spheres. *Physical Review*, *133*(4A), A895-A899. doi: 10.1103/PhysRev.133.A895

Lele, S., & Ramachandrarao, P. (1981). Estimation of complex concentration in a regular associated solution. *Metallurgical Transactions B*, *12*(4), 659–666.

Liang, S. M., Wang, P., & Schmid-Fetzer, R. (2016). Inherently consistent temperature function for interaction parameters demonstrated for the Mg–Si assessment. *Calphad*, *54*, 82–96. doi: 10.1016/j.calphad.2016.06.003

Liang, Y., Du, Z., Guo, C., & Li, C. (2008). Thermodynamic modeling of the Li–Zn system. *Journal of Alloys and Compounds*, *455*(1-2), 236–242. doi: 10.1016/j.jallcom.2007.01.154

Liu, Y., Zhou, B., Lv, W., Wu, C., Su, X., & Wang, J. (2016). Experimental investigation and thermodynamic assessment of the Zn–Si–P system. *Surface and Coatings Technology*, *306*, 370–377. doi: 10.1016/j.surfcoat.2016.01.016

Longuet-Higgins, H. C. (1951). The statistical thermodynamics of multicomponent systems. *Proceedings of the Royal Society of London. Series A. Mathematical and Physical Sciences*, *205*(1081), 247–269. doi: 10.1098/rspa.1951.0028

Lüdecke, D. (1987). A thermodynamic assessment of the Cu–Si system. *Calphad*, *11*(2), 135–142. doi: 10.1016/0364-5916(87)90005-8

Malakhov, D. V., & Balakumar, T. (2007). Post-optimization elimination of inverted miscibility gaps. *International Journal of Materials Research*, *98*(9), 786–796. doi: 10.3139/146.101540

Mallinson, J. C. (2001). *Magneto-resistive and spin valve heads: fundamentals and applications*. Elsevier. doi: 10.1016/B978-012466627-6/50013-8

Manzoor, A., Pandey, S., Chakraborty, D., Phillpot, S. R., & Aidhy, D. S. (2018). Entropy contributions to phase stability in binary random solid solutions. *NPJ Computational Materials*, *4*(1), 1–10. doi: 10.1038/s41524-018-0102-y

Mathon, M., Jardet, K., Aragon, E., Satre, P., & Sebaoun, A. (2000). Al-Ga-Zn system: reassessments of the three binary systems and discussion on possible estimations and on optimisation of the ternary system. *Calphad*, *24*(3), 253–284. doi: 10.1016/S0364-5916(01)00004-9

Mehta, U., Yadav, S. K., Koirala, I., & Adhikari, D. (2020). Thermo-physical properties of ternary Al–Cu–Fe alloy in liquid state. *Philosophical Magazine*, *100*(19), 2417–2435. doi: 10.1080/14786435.2020.1775907

Mishra, A. K., Singh, R. N., & Sahay, B. B. (1993). Electrical resistivity and thermodynamic properties of alkali-alkali liquid binary alloys. *Physics and Chemistry of Liquids*, *25*(3), 153–168. doi: 10.1080/00319109308030357

Mishra, R. K., Lalnuntluanga, C., & Mishra, S. K. (2023). Theoretical Investigation of Structure, Dynamics and Entropy Correlation in Liquid Fe–Al Alloys. *Metallurgical and Materials Transactions B*, *54*(1), 331–341. doi: 10.1007/s11663-022-02693-1

Morachevskii, A. G., Butukhanova, T. V., & Val'Kovskaya, E. N. (2012). Thermodynamic analysis of liquid alloys of the system aluminum–lithium–zinc. *Russian Journal of Applied Chemistry*, *85*(12), 1955–1958. doi: 10.1134/S1070427212120269

Muggianu, Y. M., Gambino, M., & Bros, J. P. (1975). Enthalpies of formation of liquid alloys bismuth–gallium–tin at 723 K-choice of an analytical representation of integral and partial thermodynamic functions of mixing for this ternary-system. *Journal de Chimie Physique et de Physico-Chimie Biologique*, *72*(1), 83–88.

Nic, M., Hovorka, L., Jirat, J., Kosata, B., & Znamenacek, J. (2005). *Iupac compendium of chemical terminology-the gold book*. International Union of Pure and Applied Chemistry.

Novakovic, R. (2010). Thermodynamics, surface properties and microscopic functions of liquid Al–Nb and Nb–Ti alloys. *Journal of Non-Crystalline Solids*, *356*(31-32), 1593–1598. doi: 10.1016/j.jnoncrysol.2010.05.055

Novakovic, R., Giuranno, D., Ricci, E., Tuissi, A., Wunderlich, R., Fecht, H. J., & Egry, I. (2012). Surface, dynamic and structural properties of liquid Al–Ti alloys. *Applied Surface Science*, *258*(7), 3269–3275. doi: 10.1016/j.apsusc.2011.11.080

Novakovic, R., Ricci, E., Giuranno, D., & Gnecco, F. (2002). Surface properties of Bi–Pb liquid alloys. *Surface Science*, *515*(2-3), 377–389. doi: 10.1016/S0039-6028(02)01923-4

Pelton, A. D., Chartrand, P., & Eriksson, G. (2001). The modified quasi-chemical model: Part IV. Two-sublattice quadruplet approximation. *Metallurgical and Materials Transactions A*, *32*(6), 1409–1416. doi: 10.1007/s11661-001-0230-7

Pelton, A. D., Degterov, S., Eriksson, G., Robelin, C., & Dessureault, Y. (2000). The modified quasichemical model I-Binary solutions. *Metallurgical and Materials Transactions B*, *31*(4), 651–659. doi: 10.1007/s11663-000-0103-2

Pettit, F. S., Meier, G. H., Gell, M., Kartovich, C. S., Bricknel, R. H., Kent, W. B., & Radovich, J. F. (1984). Oxidation and hot corrosion of superalloys. *Superalloys*, *85*(1), 651–687. doi: 10.7449/1984/Superalloys_1984_651_687

Plevachuk, Y., Sklyarchuk, V., Eckert, S., Gerbeth, G., & Novakovic, R. (2014). Thermophysical properties of the liquid Ga–In–Sn eutectic alloy. *Journal of Chemical & Engineering Data*, *59*(3), 757–763. doi: 10.1021/je400882q

Porter, D. A., & Easterling, K. E. (2009). *Phase transformations in metals and alloys (revised reprint)*. CRC press. doi: 10.1201/9781439883570

Prasad, L. C., & Jha, R. K. (2005). Surface tension and viscosity of sn-based binary liquid alloys. *Physica Status Solidi (A)*, *202*(14), 2709–2719. doi: 10.1002/pssa.200520080

Prasad, L. C., & Singh, R. N. (1990). A quasi-lattice model for the thermodynamic properties of Au-Zn liquid alloys. *Physics and Chemistry of Liquids*, *22*(1-2), 1–9. doi: 10.1080/00319109008036406

Prasad, L. C., & Singh, R. N. (1991). Surface segregation and concentration fluctuations at the liquid-vapor interface of molten Cu-Ni alloys. *Physical Review B*, *44*(24), 13768–13771. doi: 10.1103/PhysRevB.44.13768

Prigogine, I., & Defay, R. (1954). Chemical Thermodynamics: Longmans. *Green and Co., London*, 357.

Ramachandrarao, P., Singh, R., & Lele, S. (1984). Role of concentration fluctuations in metallic glass formation. *Journal of Non-crystalline Solids*, *64*(3), 387–398. doi: 10.1016/0022-3093(84)90191-1

Redlich, O., & Kister, A. T. (1948). Algebraic representation of thermodynamic properties and the classification of solutions. *Industrial & Engineering Chemistry*, *40*(2), 345–348. doi: 10.1021/ie50458a036

Sarmiento-Pérez, R., Cerqueira, T. F., Valencia-Jaime, I., Amsler, M., Goedecker, S., Romero, A. H., . . . Marques, M. A. L. (2015). Novel phases of lithium–aluminum binaries from first-principles structural search. *The Journal of Chemical Physics*, *142*(2), 024710. doi: 10.1063/1.4905141

Saunders, N., & Miodownik, A. P. (1998). *CALPHAD (calculation of phase diagrams): a comprehensive guide*. Elsevier.

Schmid-Fetzer, R., Andersson, D., Chevalier, P.-Y., Eleno, L., Fabrichnaya, O., Kattner, U., . . . others (2007). Assessment techniques, database design and software facilities for thermodynamics and diffusion. *Calphad*, *31*(1), 38–52. doi: 10.1016/j.calphad.2006.02.007

Shukla, A., & Pelton, A. D. (2009). Thermodynamic assessment of the Al–Mn and Mg-Al-Mn systems. *Journal of Phase Equilibria and Diffusion*, *30*(1), 28–39. doi: 10.1007/s11669-008-9426-5

Singh, R. N. (1987). Short-range order and concentration fluctuations in binary molten alloys. *Canadian Journal of Physics*, *65*(3), 309–325. doi: 10.1139/p87-038

Singh, R. N., & Choudhary, R. B. (1981). Entropies of molten alloys. *Journal of Physics F: Metal Physics*, *11*(8), 1577–1583. doi: 10.1088/0305-4608/11/8/012

Singh, R. N., Jha, I. S., & Sinha, S. K. (1991). The segregation-order transformation in CdNa liquid alloy. *Journal of Physics: Condensed Matter*, *3*(16), 2787–2793. doi: 10.1088/0953-8984/3/16/017

Singh, R. N., Pandey, D. K., Sinha, S., Mitra, N. R., & Srivastava, P. L. (1987). Thermodynamic properties of molten LiMg alloy. *Physica B+ C*, *145*(3), 358–364. doi: 10.1016/0378-4363(87)90105-7

Singh, R. N., & Sommer, F. (1992). A simple model for demixing binary liquid alloys. *International Journal of Materials Research*, *83*(7), 533–540. doi: 10.1515/ijmr-1992-830710

Singh, R. N., & Sommer, F. (1997). Segregation and immiscibility in liquid binary alloys. *Reports on Progress in Physics*, *60*(1), 57–150. doi: 10.1088/0034-4885/60/1/003

Soon-Don, C. (1992). Thermodynamic analysis of the Co-Si system. *Calphad*, *16*(2), 151–159. doi: 10.1016/0364-5916(92)90003-G

Stroud, D. (1973). Theory of Phase Separation in Liquid-Metal Alloys: Lix Na 1- x. *Physical Review B*, *7*(10), 4405–4408. doi: 10.1103/PhysRevB.7.4405

Su, Y. H., & Wang, W. L. (2013). Surface plasmon resonance of Au-Cu bimetallic nanoparticles predicted by a quasi-chemical model. *Nanoscale Research Letters*, *8*(1), 1–6. doi: 10.1186/1556-276X-8-408

Sun, K., Weber, H., Wang, G., Wu, Y. H., Andreoli, A. F., Tseng, J. C., . . . others (2023). Structural heterogeneity in levitated glassy alloys with different undercoolings. *Journal of Alloys and Compounds*, *947*, 169532. doi: 10.1016/j.jallcom.2023.169532

Sun, X., Li, M., Jia, P., & Geng, H. (2016). Liquid–liquid phase equilibrium in ternary immiscible Al–Bi–Sn melts. *Physics and Chemistry of Liquids*, *54*(6), 740–746. doi: 10.1080/00319104.2016.1149174

Sundman, B., Lukas, H. L., & Fries, S. G. (2007). *Computational thermodynamics: the Calphad method*. Cambridge University Press Cambridge.

Tang, Y., Du, Y., Zhang, L., Yuan, X., & Kaptay, G. (2012). Thermodynamic description of the Al–Mg–Si system using a new formulation for the temperature dependence of the excess Gibbs energy. *Thermochimica Acta*, *527*, 131–142. doi: 10.1016/j.tca.2011.10.017

Tang, Y., Yuan, X., Du, Y., & Xiong, W. (2011). Thermodynamic modeling of the Fe-Zn system using exponential temperature dependence for the excess Gibbs energy. *Journal of Mining and Metallurgy B: Metallurgy*, *47*(1), 1–10. doi: 10.2298/JMMB1101001T

Teichert, G. H., Gunda, N. S. H., Rudraraju, S., Natarajan, A. R., Puchala, B., Garikipati, K., & Van der Ven, A. (2017). A comparison of Redlich-Kister polynomial and cubic spline representations of the chemical potential in phase field computations. *Computational Materials Science*, *128*, 127–139. doi: 10.1016/j.commatsci.2016.11.024

Thakur, A., Negi, N. S., & Ahluwalia, P. K. (2005). Electrical resistivity of NaPb compound-forming liquid alloy using abinitio pseudopotentials. *Pramana*, *65*(2), 349–358. doi: 10.1007/BF02898622

Toop, G. W. (1965). Predicting ternary activities using binary data. *Trans. TMS-AIME*, *223*, 850–855.

Trybula, M. E., Fima, P., & Gasior, W. (2014). Thermodynamic properties of liquid Al–Li–Zn alloys determined from electromotive force measurement. *Thermochimica Acta*, *588*, 16–21. doi: 10.1016/j.tca.2014.04.022

Trybula, M. E., Szafrański, P. W., & Korzhavyi, P. A. (2018). Structure and chemistry of liquid Al–Cu alloys: molecular dynamics study versus thermodynamics-based modelling. *Journal of Materials Science*, *53*(11), 8285–8301. doi: 10.1007/s10853-018-2116-8

Tu, H., Yin, F., Su, X., Liu, Y., & Wang, X. (2009). Experimental investigation and thermodynamic modeling of the Al–P–Zn ternary system. *Calphad*, *33*(4), 755–760. doi: 10.1016/j.calphad.2009.10.003

Vahlas, C., Chevalier, P. Y., & Blanquet, E. (1989). A thermodynamic evaluation of four Si–M (M= Mo, Ta, Ti, W) binary systems. *Calphad*, *13*(3), 273–292. doi: 10.1016/0364-5916(89)90007-2

Vera, J. H., Sayegh, S. G., & Ratcliff, G. A. (1977). A quasi lattice-local composition model for the excess Gibbs free energy of liquid mixtures. *Fluid Phase Equilibria*, *1*(2), 113–135. doi: 10.1016/0378-3812(77)85002-4

Visser, E. G., Van der Lugt, W., & De Hosson, J. T. M. (1980). Thermodynamic calculations for liquid alloys with an application to sodium-caesium. *Journal of Physics F: Metal Physics*, *10*(8), 1681–1692. doi: 10.1088/0305-4608/10/8/008

Vora, A. M. (2010). Study of thermodynamic properties of liquid binary alloys by a pseudopotential method. *Journal of Engineering Physics and Thermophysics*, *83*(5), 1070–1079. doi: 10.1007/s10891-010-0432-1

Wang, P., Du, Y., & Liu, S. (2011). Thermodynamic optimization of the Li–Mg and Al–Li–Mg systems. *Calphad*, *35*(4), 523–532. doi: 10.1016/j.calphad.2011.09.003

Wang, P., Zhou, L., Du, Y., Xu, H., Liu, S., Chen, L., & Ouyang, Y. (2011). Thermodynamic optimization of the Cu–Nd system. *Journal of Alloys and Compounds*, *509*(6), 2679–2683. doi: 10.1016/j.jallcom.2010.11.160

Witusiewicz, V. T., Bondar, A. A., Hecht, U., Rex, S., & Velikanova, T. Y. (2008). The Al–B–Nb–Ti system: III. Thermodynamic re-evaluation of the constituent binary system Al–Ti. *Journal of Alloys and Compounds*, *465*(1-2), 64–77. doi: 10.1016/j.jallcom.2007.10.061

Wu, R., Yan, Y.-d., Wang, G.-x., Murr, L., Han, W., Zhang, Z.-w., & Zhang, M.-l. (2015). Recent progress in magnesium–lithium alloys. *International Materials Reviews*, *60*(2), 65–100. doi: 10.1179/1743280414Y.0000000044

Xu, W., Sandor, M. T., Yu, Y., Ke, H.-B., Zhang, H.-P., Li, M.-Z., ... Wu, Y. (2015). Evidence of liquid–liquid transition in glass-forming La 50 Al 35 Ni 15 melt above liquidus temperature. *Nature Communications*, *6*(1), 1–9. doi: 10.1038/ncomms8696

Yadav, S. K., Jha, L. N., & Adhikari, D. (2016). Thermodynamic, structural, transport and surface properties of Pb–Tl liquid alloy. *Bibechana*, *13*, 100–113. doi: 10.3126/bibechana.v13i0.13443

Yadav, S. K., Jha, L. N., & Adhikari, D. (2018). Modeling equations to predict the mixing behaviours of Al- Fe liquid alloy at different temperatures. *Bibechana*, *15*, 60–69. doi: 10.3126/bibechana.v15i0.18624

Yadav, S. K., Jha, L. N., Jha, I. S., Singh, B. P., Koirala, R. P., & Adhikari, D. (2016). Prediction of thermodynamic and surface properties of Pb–Hg liquid alloys at different temperatures. *Philosophical Magazine*, *96*(18), 1909–1925. doi: 10.1080/14786435.2016.1181281

Yakymovych, A., Plevachuk, Y., Mudry, S., Brillo, J., Kobatake, H., & Ipser, H. (2014). Viscosity of liquid Co–Sn alloys: thermodynamic evaluation and experiment. *Physics and Chemistry of Liquids*, *52*(4), 562–570. doi: 10.1080/00319104.2013.876639

Yan, X., & Chang, Y. A. (2000). A thermodynamic analysis of the Cu–Si system. *Journal of Alloys and Compounds*, *308*(1-2), 221–229. doi: 10.1016/S0925-8388(00)00983-X

Yuan, X., Sun, W., Du, Y., Zhao, D., & Yang, H. (2009). Thermodynamic modeling of the Mg–Si system with the Kaptay equation for the excess Gibbs energy of the liquid phase. *Calphad*, *33*(4), 673–678. doi: 10.1016/j.calphad.2009.08.004

Zhang, F., Chen, S. L., Chang, Y. A., & Kattner, U. R. (1997). A thermodynamic description of the Ti–Al system. *Intermetallics*, *5*(6), 471–482. doi: 10.1016/S0966-9795(97)00030-7

Zhang, L., Du, Y., Xu, H., & Pan, Z. (2006). Experimental investigation and thermodynamic description of the Co–Si system. *Calphad*, *30*(4), 470–481. doi: 10.1016/j.calphad.2006.06.001

Zhang, S. B., & Li, D. Z. (1986). *Phase Diagram–Principle, Calculation and Application in Metallurgy.* Metallurgical Industry Press Beijing.

Zhao, X., Wang, C., Zheng, H., Tian, Z., & Hu, L. (2017). The role of liquid–liquid transition in glass formation of CuZr alloys. *Physical Chemistry Chemical Physics*, *19*(24), 15962–15972. doi: 10.1039/C7CP02111A

APPENDIX

A. Papers published in international journals

Gohivar, R., Yadav, S., Koirala, R., Shrestha, G., & Adhikari, D. (2021). Temperature dependence of interaction parameters for Al–Li liquid alloy. *Philosophical Magazine*, *101*(2), 179–192. doi: 10.1080/14786435.2020.1825858

Gohivar, R. K., Koirala, R. P., Yadav, S. K., & Adhikari, D. (2020). Temperature dependence of interaction parameters of Cu–Si liquid alloy. *AIP Advances*, *10*(8), 085121-085126. doi: 10.1063/5.0012834

Gohivar, R. K., Mehta, U., Yadav, S. K., Koirala, R. P., Jha, I. S., & Adhikari, D. (2021). Thermodynamic, surface and transport properties of ternary Al–Sn–Zn liquid alloy and its sub binaries. *Philosophical Magazine*, *101*(11), 1380–1399. doi: 10.1080/14786435.2021.1912845

Gohivar, R. K., Yadav, S. K., Koirala, R. P., & Adhikari, D. (2020). Artifacts in Al–Mn liquid alloy. *Physica B: Condensed Matter*, *595*, 412348-412354. doi: 10.1016/j.physb.2020.412348

Gohivar, R. K., Yadav, S. K., Koirala, R. P., & Adhikari, D. (2021a). Assessment of thermo-structural properties of Al-Fe and Fe-Si alloys at high temperatures. *Physics and Chemistry of Liquids*, *59*(5), 679–689. doi: 10.1080/00319104.2020.1793985

Gohivar, R. K., Yadav, S. K., Koirala, R. P., & Adhikari, D. (2021b). Study of artifacts in thermodynamic and structural properties of Li–Mg alloy in liquid state using linear and exponential models. *Heliyon*, *7*(3), e06613-e06621. doi: 10.1016/j.heliyon.2021.e06613

Gohivar, R. K., Yadav, S. K., Koirala, R. P., & Adhikari, D. (2021c). Study of excess free energy of mixing and heat of mixing of liquid ternary Al–Li–Zn alloy by assessing the thermodynamic properties of sub-binary alloys. *Physica B: Condensed Matter*, *610*, 412941–412945. doi: 10.1016/j.physb.2021.412941

B. Papers published in national journal

Gohivar, R. K., Yadav, S. K., Koirala, R. P., & Adhikari, D. (2022). Exponential Temperature-Dependent Parameters for Thermodynamic and Structural Properties

of Al-Ti Melt. *BIBECHANA*, *19*(1-2), 75–82. doi: 10.3126/bibechana.v19i1-2.46392

Yadav, S. K., Mehta, U., Gohivar, R. K., Dhungana, A., Koirala, R. P., & Adhikari, D. (2020). Reassessments of thermo-physical properties of Si-Ti melt at different temperatures. *BIBECHANA*, *17*, 146–153. doi: 10.3126/bibechana.v17i0.26877

C. Participation in conferences and workshops

- 3rd International Conference on Condensed Matter & Applied Physics (ICC 2019) will be held at Govt. Engineering College, Bikaner, Rajasthan during October 14-15, 2019 entitled "Removal of Thermodynamic Miscibility Gap in Al-Fe-Si Liquid Alloy"
- International Conference on Material Science and Characterization Technology (ICMSCT) held on September 26-28, 2021 entitled "Exponential temperature dependent Parameters for thermodynamics and structural properties of AL-TI metal"

Physica B 595 (2020) 412348

Contents lists available at ScienceDirect

Physica B: Physics of Condensed Matter

journal homepage: http://www.elsevier.com/locate/physb

Artifacts in Al–Mn liquid alloy

R.K. Gohivar [a,b], S.K. Yadav [b], R.P. Koirala [b], D. Adhikari [b,*]

[a] Central Department of Physics, T.U., Kirtipur, Nepal
[b] Department of Physics, Mahendra Morang Adarsh Multiple Campus, T.U., Biratnagar, Nepal

ARTICLE INFO

Keywords:
Artifacts
Al–Mn alloy
Interaction parameters
Thermodynamic properties
Structural properties

ABSTRACT

The presence of artifacts in thermodynamic and structural properties of the Al–Mn liquid alloy at higher temperatures has been investigated assuming the interaction parameters present in the modeling equations to be linearly and exponentially temperature dependent. When the concept of linear temperature dependence of interaction parameters is employed to explain the thermo-structural properties of the Al–Mn liquid alloy some asymmetric artifacts appear in these properties at higher temperatures. However, these artifacts are successfully eliminated from the thermo-structural properties of the Al–Mn liquid alloy when the interaction parameters present in the modeling equations are considered to be exponentially temperature dependent.

1. Introduction

The assessment of the properties of the Al–Mn alloy has become a matter of interest to many researchers [1–10] for a long because of its wide applications, such as in manufacturing foil, roof sheets, cooking utensils, rigid containers, bearing assembly, step soldering and radiation shielding [11,12], etc. Bergman et al. [1] studied the thermodynamic properties of Al–Mn system at 1570 K using intensity ratio method from Knudsen cell mass spectrometric measurements. Jansson [2] and Du et al. [3] studied the Al–Mn system using PARROT software techniques employing different modeling equations. They reported the presence of high temperature inverted miscibility gap in the liquid phase at 4227 K when the interaction energy parameters were assumed to be linear temperature dependent. Shukla and Pelton [4] assessed the thermodynamic properties of the Al–Mn and Mg–Al–Mn systems using FactSage thermochemical software in the framework of modified quasi-chemical model (MQM). Khan and Medraj [13] presented the thermodynamic description of the Al–Mn alloy using the quasi-chemical model for the liquid phases. McAlister and Murray [14] provided their assessments on some experimental information of the Al–Mn alloys [14].

When the thermodynamic and structural properties of the Al–Mn alloys in liquid state are computed assuming linear temperature dependent interaction parameters in the framework of R–K polynomial [15–19], some asymmetric behaviours are observed in certain regions at high temperature. These asymmetric tendencies are termed as high temperature artifact [16]. Kaptay [16] has suggested that the high temperature artifacts that appear while considering the linear temperature dependent interaction parameters can be removed by assuming exponential temperature dependent interaction parameters. Later, Kaptay [20] and Ghasemi et al. [21] provided a method for the reassessment of thermodynamic data set on this basis. Schmid-Fetzer et al. [22] gave emphasis for the requirement of Calphad type analysis after making critical assessment of the methods used for the evaluation of artifacts in different alloys. In a thorough review of literature [1–4, 23–26], authors found that the assessments of high temperature artifacts have been addressed only in thermodynamic functions for different systems till date. Therefore, we attempt to study the presence of high temperature artifacts in the thermodynamic as well as structural properties of the Al–Mn liquid alloy assuming the interaction parameters to be linear and exponential temperature dependent in the framework of R–K polynomials.

The theoretical outline for this work is given in section 2, the results and discussion of investigation is presented in section 3 and conclusion of the work is outlined in section 4.

2. Theoretical basis

The enthalpy and entropy of an alloy, on solving power-series law, are obtained as [19].

$$H = A - CT - DT^2 + 2ET^{-1} - \ldots \quad (1)$$

$$S = -B - (C + lnT) - 2DT + ET^{-2} - \ldots \quad (2)$$

* Corresponding author.
E-mail address: devendra.adhikari@mmamc.tu.edu.np (D. Adhikari).

https://doi.org/10.1016/j.physb.2020.412348
Received 22 March 2020; Received in revised form 28 May 2020; Accepted 20 June 2020
Available online 14 July 2020

where T is the absolute temperature. The coefficients A, B, C, D, E…. are to be determined. These coefficients are determined by least squares method.

Now using the relation $G = H - TS$ we have

$$G = A + BT + CT\ \ lnT + DT^2 + ET^{-1}\ldots \tag{3}$$

$$S_{cc}(0) = \frac{RT}{\left[-2L_0 + (-12c_A + 6)L_1 + (-48c_A^2 + 48c_A - 10)L_2 + (-160c_A^3 + 240c_A^2 - 108c_A + 14)L_3 + \frac{RT}{c_A(1-c_A)}\right]} \tag{12}$$

For the binary A-B alloys in liquid state the compositional dependence of the excess Gibbs free energy of mixing (G_M^{xs}) in the framework of R–K polynomial method can be given as [15–19,27].

$$G_M^{xs} = c_A c_B \sum_{i=0}^{3} L_i (c_A - c_B)^i \tag{4}$$

where c_A and c_B are mole fractions of constituents A and B of binary A-B alloy. The coefficients Li is assumed to be the same linear temperature dependence as excess Gibbs free energy of mixing in Equation (3) and it can be expressed as

$$L_i = A_i + B_i T \tag{5}$$

Since the linear temperature dependent interaction parameters cannot explain the artifacts seen in the thermodynamic and structural properties of alloys at higher temperatures, Kaptay [16] proposed exponential interaction parameter as

$$L_i = h_{0i}\exp\left(\frac{-T}{\tau_{0i}}\right) \tag{6}$$

where the model parameter h_{0i} (J/mol) is the enthalpy part of L_i at T = 0 K, while parameters τ_{0i} (K) is the temperature at which L_i would change its sign on extrapolating linearly from T = 0 K. Parameter h_{0i} can have any sign, but parameter τ_{0i} must be always positive [16].

The excess Gibbs free energy of mixing in Eq. (4) can be expressed in the form of exponential interaction parameters as

$$G_M^{xs} = c_A c_B \left[h_{00}\exp\left(\frac{-T}{\tau_{00}}\right) + h_{10}\exp\left(\frac{-T}{\tau_{10}}\right)(c_A - c_B) + h_{20}\exp\left(\frac{-T}{\tau_{20}}\right)(c_A - c_B)^2 + h_{30}\exp\left(\frac{-T}{\tau_{30}}\right)(c_A - c_B)^3\right] \tag{7}$$

The partial excess Gibbs free energy of constituents of the system can be expressed as [19].

$$G_1^{xs} = x_B^2 \sum_{i=1}^{3} L_i[(1+2i)c_A - c_B](c_A - c_B)^{i-1} \tag{8}$$

and

$$G_2^{xs} = c_A^2 \sum_{i=1}^{3} L_i[c_A - c_B(1+2i)](c_A - c_B)^{i-1} \tag{9}$$

The activity of the constituents of the system are calculated from the standard expressions

$$a_1 = c_A\exp\left(\frac{G_1^{xs}}{RT}\right) \text{ and } a_2 = c_B\exp\left(\frac{G_2^{xs}}{RT}\right) \tag{10}$$

The concentration fluctuations in the long wavelength limit (S_{cc} (0)) of the binary system for liquid phase is important function that describes the nature of ordering or segregation of mixing behavior and is computed from the standard expression [19].

$$S_{cc}(0) = RT\left(\frac{\partial^2 G_M}{\partial c^2}\right)^{-1} \tag{11}$$

The analytical expression for concentration fluctuations in long-wavelength limit is obtained by using Eq. (4) in Eq. (11) in the following form:

The S_{cc} (0) can also be calculated using observed value of activity and it is referred as the observed activity in the literature. Ideal value of the $S_{cc}(0)$ is calculated as

$$S_{cc}^{id}(0) = c_A c_B \tag{13}$$

The mixing behavior of the alloys can also be studied at the microscopic level in terms of the coefficient of diffusion. Darken thermodynamic equation for diffusion provides the relation between the $S_{cc}(0)$ and diffusion coefficients as follows [28,29]:

$$\frac{D_M}{D_{id}} = \frac{c_A c_B}{S_{cc}(0)} \tag{14}$$

where D_M is the chemical or mutual diffusion coefficient and D_{id} is the intrinsic diffusion coefficient for an ideal mixture. These parameters are related [28,29] as

$$D_M = D_{id}\ \frac{\partial a_A}{\partial c_A} \tag{15}$$

with

$$D_{id} = c_A D_B + c_B D_A$$

where a_A is the activity of the component A in A-B alloy, D_A and D_B are the self-diffusion coefficients of pure components A and B respectively.

3. Results and discussion

The excess Gibbs free energy of mixing (G_M^{xs}) of the Al–Mn liquid alloy was computed at 1570 K [3,30], 1900 K, 2200 K and 2500 K [1,3, 30] assuming the interaction parameters of the modeling equation to be linearly temperature dependent (also called linear model) in the framework of R–K polynomial from Eq. (4). The computed values of the excess free energy of mixing of the Al–Mn liquid alloy at these temperatures were plotted in Fig. 1(a–d). It was clearly observed that there was no artifact in the excess free energy of mixing for the Al–Mn liquid alloy up to the temperature 2200 K (Fig. 1(a–c)). When the temperature was elevated to 2500 K an asymmetric artifact appeared in the excess free energy of mixing in the concentration range $c_{Mn} \leq 0.4$ (Fig. 1(d)). Kaptay [20] has explained the inability of the linear model to describe the thermodynamic properties of an alloy at high temperatures if $A_0 < 0$ and $B_0 > 2.R$ in Eq. (5). It was also observed from this study that if $A_0 < 0$ and $B_0 > 2.R$ in Eq. (5) the linear model could not explain the thermodynamic properties of the Al–Mn alloy at high temperature.

Since an asymmetric artifact appeared in the excess free energy of mixing of the Al–Mn alloy at 2500 K when it was computed using linear model it was endeavored to study the excess free energy of mixing of the alloy using exponential model. For this, the optimized exponential temperature dependent parameters were determined for the Al–Mn alloy in the framework of R–K polynomial using the linear parameters of

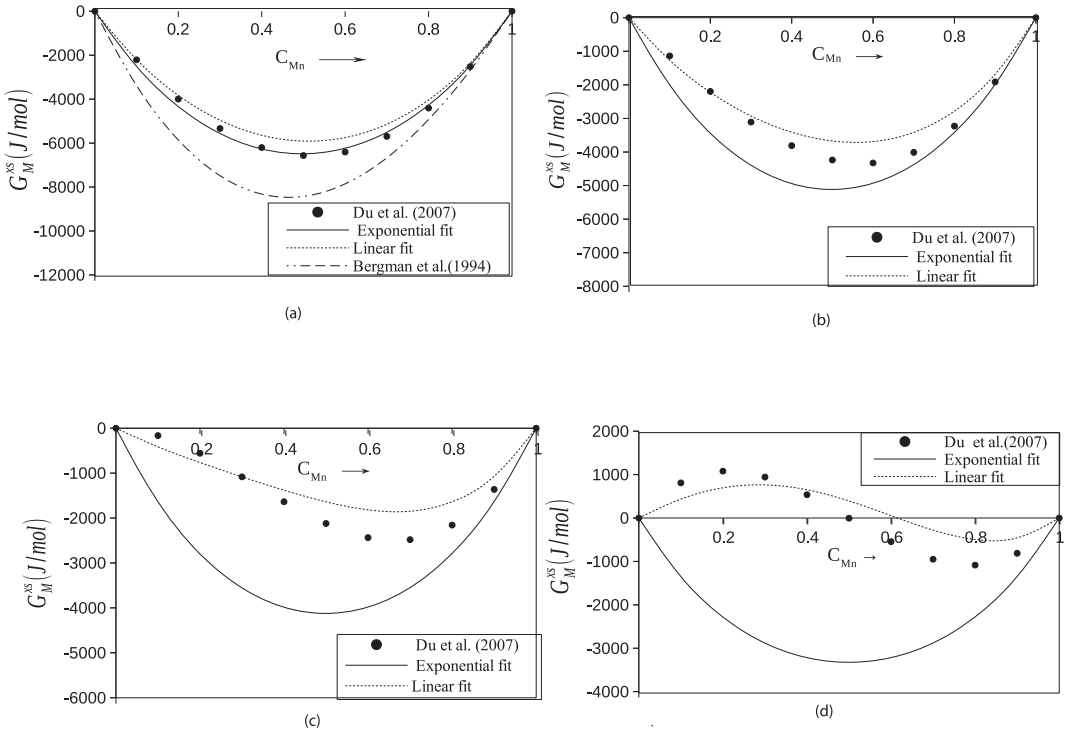

Fig. 1. Excess Gibbs free energy of mixing (G_M^{xs}) of the Al–Mn liquid alloy versus the concentration of Mn (C_{Mn}) at (a) 1570 K (b) 1900 K (c) 2200 K and (d) 2500 K.

Cost 507 [30] in Eqs. (4)–(6). The computed values of optimized exponential parameters are given below

$$L_0 = -80175.04\ exp\left(-7.14 \times 10^{-4}T\right),$$
$$L_1 = -47609.8\ exp\left(-3.16 \times 10^{-3}T\right),$$
$$L_2 = -2639.$$

The excess free energy of mixing for the Al–Mn alloy was computed at 1570 K, 1900 K, 2200 K and 2500 K using the optimized exponential parameters. The excess free energy of mixing for the Al–Mn liquid alloy computed at aforementioned temperatures by using exponential temperature dependent parameters (also called exponential model) were compared with the values computed by using linear parameters in Fig. 1 (a–d). It was clearly seen that no artifact was observed in the excess free energy of mixing of the Al–Mn alloy at all temperatures when it was computed by using exponential model. Additionally, the plots of the G_M^{xs}

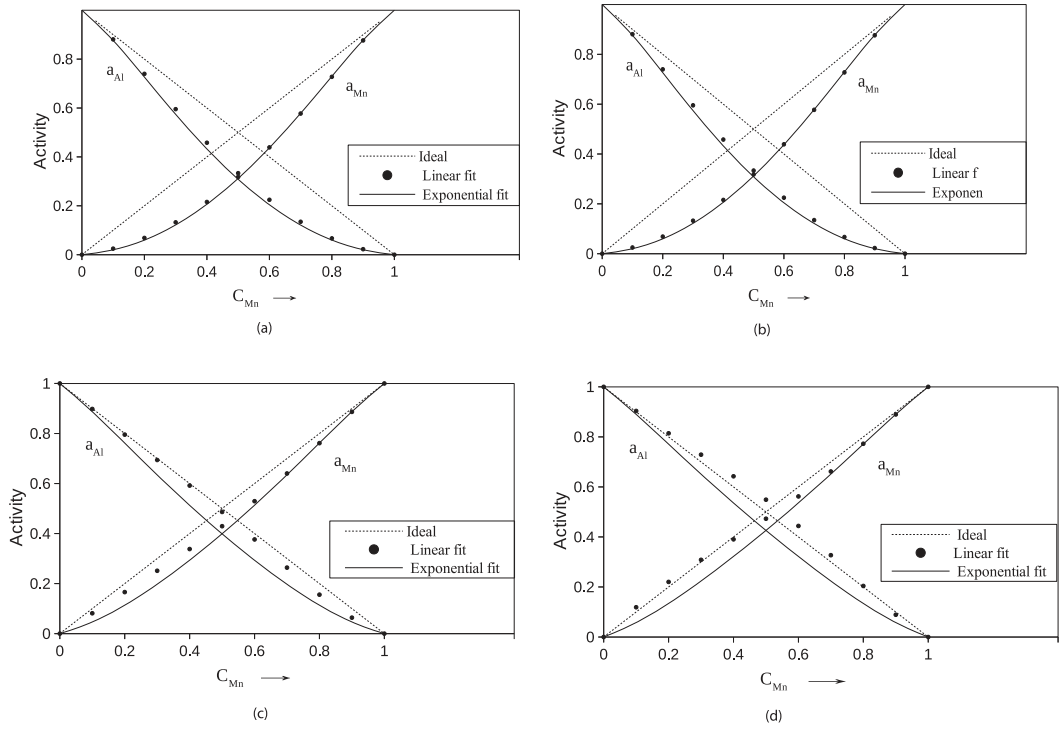

Fig. 2. Activity (a) of the components of the Al–Mn liquid alloy versus concentration of Mn (C_{Mn}) at (a) 1600 K (b) 1900 K (c) 2200 K and (d) 2500 K.

gradually shallow up with increase in temperature indicating a decrease of the compound forming tendency of the system [31].

Activity is a very important quantity which incorporates the deviation of alloys from ideality. It also measures the tendency of the atoms to leave the solution. The activities of the components of the Al–Mn liquid alloys were computed using linear model [30] and exponential model in Eq. (10) at 1600 K, 1900 K, 2200 K and 2500 K separately and plotted in Fig. 2(a–d). The activities of the monomers of the Al–Mn alloy were found to have negative deviation from Raoult's law (Fig. 2(a–c)) up to 2200 K in both of the cases; either the interaction parameters were assumed to be linearly temperature dependent or exponentially temperature dependent. However, at 2500 K Al-component showed positive deviation and Mn-component negative deviation above the equiatomic composition (Fig. 2(d)) when the interaction parameters were assumed to be linearly temperature dependent. This positive deviation of the activity from Raoult's law only on increasing the temperature is unusual behavior which is termed as artifact (Fig. 2(d)). The tendency of positive deviation of activity from Raoult's law was corrected when the interaction parameter were assumed to be exponentially temperature dependent (Fig. 2(d)). It can, therefore, be mentioned that the artifact for the Al–Mn liquid alloy at higher temperature can be eliminated when the interaction parameters are considered as exponentially temperature dependent.

The value of $S_{CC}(0)$ for liquid Al–Mn alloy was computed at 1600 K, 1900K, 2200 K and 2500 K from Eq. (13) assuming the interaction parameter to be linearly temperature dependent [30]. The $S_{CC}(0)$ can be used to understand the nature of atomic order in the binary liquid alloys. At a given composition, ordering in a binary alloy is expected if $S_{CC}(0) < S^{id}_{CC}(0)$ and there is tendency of segregation if $S_{CC}(0) > S^{id}_{CC}(0)$. The computed values of the $S_{CC}(0)$ for the Al–Mn liquid alloy was observed to be less than ideal values at 1600 K, 1900 K and 2200 K in the entire range of concentration indicating the ordering behavior of the alloy (Fig. 3(a–c)). At 1600 K, the observed values of the $S_{CC}(0)$ was found to be slightly greater that the ideal value at $c_{Mn} = 0.5$ and less than the ideal values at rest of the compositions (Fig. 3(a)). The minor discrepancy of the observed value with the computed value in the $S_{CC}(0)$ at $c_{Mn} = 0.5$ may be due to the error in observed values of activities of Al (0.365 ± 0.11) and Mn (0.161 ± 0.044) [32] at the composition Al-50at %Mn-50at%. When the temperature became 2500 K the $S_{CC}(0)$ computed by using linear model crossed the ideal value in the range $c_{Al} \geq 0.4$ (Fig. 3(d)). This indicates that there is the demixing tendency of the alloy in the range $c_{Al} \geq 0.4$. This is unusual trend as the alloying behavior cannot be changed from ordering to segregating only on increasing temperature. This unusual behavior is termed as artifact. We again computed the $S_{CC}(0)$ for the Al–Mn liquid alloy at the above mentioned temperatures using the optimized exponential parameters. In this case, the $S_{CC}(0)$ was found to be less than the ideal values at all above mentioned temperatures. This clearly indicates that the artifact in the $S_{CC}(0)$ for the Al–Mn liquid alloy can be removed when the interaction parameters are supposed to be exponentially temperature dependent.

The ordering or segregating tendency of an alloy can also be understood by calculating the ratio of chemical diffusion coefficient and intrinsic diffusion coefficient $\left(\frac{D_M}{D_{id}}\right)$ [28,29,33]. The $\frac{D_M}{D_{id}} > 1$ for the alloy indicates the tendency for compound formation and the $\frac{D_M}{D_{id}} < 1$ indicates phase separation. For ideal mixing, $\frac{D_M}{D_{id}}$ approaches 1. We compute the $\frac{D_M}{D_{id}}$ at the temperatures 1600 K, 1900K, 2200 K and 2500 K by using Eq. (14) assuming the interaction parameters in the modeling equations to be exponentially temperature dependent. The value of the $\frac{D_M}{D_{id}}$ is greater than

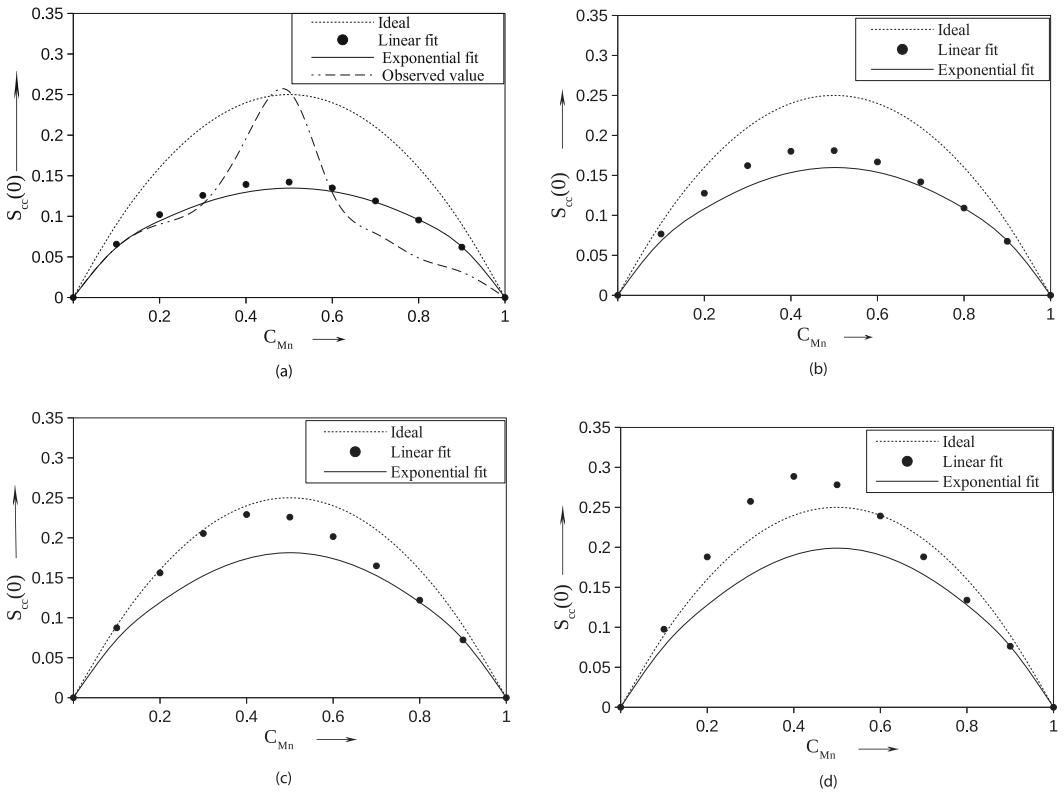

Fig. 3. Concentration fluctuations in the long-wavelength limit ($S_{cc}(0)$) of the Al–Mn liquid alloy versus concentration of Mn (C_{Mn}) at (a) 1600 K (b) 1900 K (c) 2200 K and (d) 2500 K.

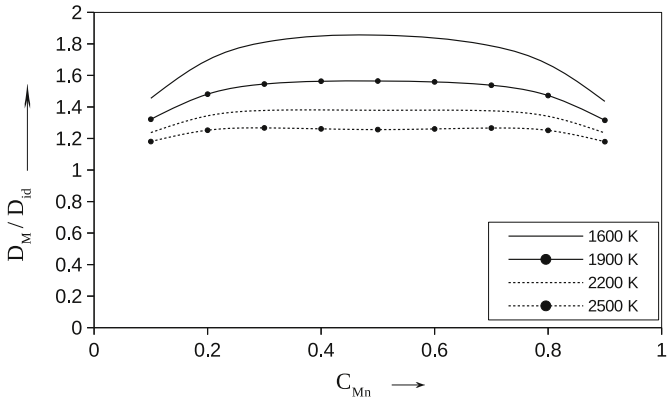

Fig. 4. The ratio of chemical diffusion coefficients and intrinsic diffusion coefficients $\left(\frac{D_M}{D_{id}}\right)$ of the AL-Mn liquid alloy versus concentration of Mn (C_{Mn}) at different temperatures.

unity in the entire range of concentration (Fig. 4) at all above mentioned temperatures, which is indicative for the presence of chemical order in the alloy at these temperatures. At intermediate concentration of Mn $(0.3 < c_{Mn} < 0.7)$, the $\frac{D_M}{D_{id}}$ has greater value than neighboring ones which suggests that the degree of order in this liquid alloy is stronger at intermediate concentration of Mn, as evidenced in the calculation of the $S_{CC}(0)$. The value of the $\frac{D_M}{D_{id}}$ went on decreasing on increasing the temperature. This result indicates that the ordering tendency of the alloy decreases as the temperature is increased.

Further, considerable efforts have been applied by the researchers in order to investigate the temperature or pressure dependence of liquid-liquid structure change in liquids, liquid metals and alloys [34–36]. We also computed the $S_{CC}(0)$ in temperature range 1550 K–3700 K in order to investigate the possibility of the temperature dependence of liquid-liquid structure change in the Al–Mn liquid alloy. The $S_{CC}(0)$ for this alloy shifts towards the ideal values at the elevated temperature but does not cross it and return to the ordering side. Thus the result of this theoretical study does not indicate the existence of liquid-liquid transition in the Al–Mn liquid alloy in the temperature range 1550 K–3700 K.

4. Conclusion

The artifacts appear in the thermodynamic and structural functions of liquid Al–Mn alloy at higher temperatures when the interaction parameters are assumed to be linearly temperature dependent. These artifacts are appeared in these properties of the alloys due to the application of inappropriate modeling parameters for the computation of these properties. When the correct modeling parameters are applied there should not be any artifact in the properties of the alloy. Our theoretical investigation revealed that no artifact appears in the thermo-structural properties of the Al–Mn liquid alloys at large range of temperature when the interaction parameters of the modeling equation are assumed to be exponentially temperature dependent. Thus it is concluded that the interaction parameters of the modeling equations are exponentially temperature dependent. Further, no evidence of liquid-liquid structure change is observed in the Al–Mn liquid alloy in the temperature range considered for the investigation.

Credit author statement

R.K. Gohivar: Investigation, Formal analysis, Writing - original draft. **S.K. Yadav:** Validation, Writing - review and editing. **R.P. Koirala:** Methodology, Writing - review and editing. **D. Adhikari:** Conceptualization, Supervision, Funding acquisition:

Declaration of competing interest

The authors declare that they have no known competing financial interests or personal relationships that could have appeared to influence the work reported in this paper.

Acknowledgement

Authors gratefully acknowledge the partial financial support of University Grants Commission (UGC) Nepal to conduct this work under Faculty Research Grant (FRG-S&T-73/74-14).

References

[1] C. Bergman, M. Saito, R. Chastel, Thermodynamic properties of quasi-crystal-forming Al-Mn alloys from Knudsen cell mass spectrometric measurements, Mater. Sci. Eng. A 178 (1994) 89–92.
[2] A. Jansson, A thermodynamic evaluation of the AI-Mn system, Metall. Trans. A 23 (1992) 2953–2962.
[3] Y. Du, J. Wang, J. Zhao, J.C. Schuster, F. Weitzer, R. Schmid-Fetzer, M. Ohno, H. Xu, Z. Liu, S. Shang, W. Zhang, Reassessment of the Al-Mn system and a thermodynamic description, Int. J. Mat. Res. 98 (2007) 855–871.
[4] A. Shukla, A.D. Pelton, Thermodynamic assessment of the Al-Mn and Mg-Al-Mn systems, J. Phase Equil. and Diff. 30 (2009) 28–39.
[5] Aruna Bahadur, Intermetallic phases in Al-Mn alloys, J. Mater. Sci. 23 (1988) 48–54.
[6] Soo Woo Nam, Duck Hee Lee, the effect of Mn on the mechanical behavior of Al alloys, Met. Mater. 6 (2000) 13.
[7] Kun Xia Wei, Wei Wei, Qing Bo Du, Jing Hu, Microstructure and tensile properties of Al–Mn alloy processed by accumulative roll bonding, Mater. Sci. Eng. A 525 (2009) 55–59.
[8] Ney José Luiggi Agreda, Isochronal study of Al-Mg, Al-Mn, and Al-Mn-Mg alloys using electrical resistivity and thermoelectric power, Res. 8 (2005).
[9] Julian H. Driver, Claire Maurice, Fabrice Barou, Arnaud Lens, Boundary mobilities in binary Al-Mn alloys, Mater. Sci. Forum 519–521 (2006) 1597–1604.
[10] D. Adhikari, I.S. Jha, B.P. Singh, Transport and surface properties of molten Al-Mn alloy, Adv. Mat. Lett. 3 (2012) 226–230.
[11] https://www.americanelements.com/aluminum-manganese-alloy.
[12] https://www.substech.com/dokuwiki/doku.php?id=wrought_aluminum-manganese_alloys_3xxx.
[13] Mohammad Asgar-Khan, Mamoun Medraj, Thermodynamic description of the Mg-Mn, Al-Mn and Mg-Al-Mn systems using the modified quasichemical model for the liquid phases, Mater. Trans. 50 (2009) 1113–1122.
[14] A.J. McAlister, J.L. Murray, Bull. Alloy Phase Diag. 8 (1987) 438–447.
[15] R. Arroyave, Z.K. Liu, Thermodynamic modelling of the Zn-Zr system, Calphad Comput. Coupling Phase Diagrams Thermochem. 30 (2006) 1–13.
[16] G. Kaptay, A new equation for the temperature dependence of the excess Gibbs energy of solution phases, Calphad. Comput. Coupling Phase Diagrams Thermochem. 28 (2004) 115–124.
[17] X. Yuan, W. Sun, Y. Du, D. Zhao, H. Yang, Thermodynamic modeling of the Mg–Si system with the Kaptay equation for the excess Gibbs energy of the liquid phase, Calphad Comput. Coupling Phase Diagrams Thermochem. 33 (2009) 673–678.
[18] X. Yan, F. Zhang, Y.A. Chang, A thermodynamic analysis of the Mg-Si system, Basic Appl. Res. 21 (2000) 379–384.
[19] R.N. Singh, F. Sommer, Segregation and immiscibility in liquid binary alloys, Rep. Prog. Phys. 60 (1997) 57–150.
[20] Kaptay George, The exponential excess Gibbs energy model revisited, Calphad 56 (2017) 169.
[21] Masoomeh Ghasemi, E. Stutz, S. Escobar Steinvall, M.A. Zamani, Fontcuberta Morral, Thermodynamic re-assessment of the Zn–P binary system, Materialia 6 (2019), 100301.
[22] R. Schmid-Fetzer, D. Andersson, P.Y. Chevalier, L. Eleno, O. Fabrichnaya, U. R. Kattner, B. Sundman, C. Wang, A. Watson, L. Zabdyr, M. Zinkevich, Assessment techniques, database design and software facilities for thermodynamics and diffusion, Calphad Comput. Coupling Phase Diagrams Thermochem. 31 (2007) 38–52.
[23] H. Azza, N. Selhaoui, S. Kardellass, A. Iddaoudi, L. Bouirden, Thermodynamic description of the Aluminum-Lithium phase diagram, J. Mater. Environ. Sci. 6 (2015) 3501–3510.
[24] Y. Kim, F. Sommer, Calorimetric measurement of liquid aluminium-lithium-zinc alloys, Thermochim. Acta 291 (1997) 27–34.
[25] B. Hallstedt, O. Kim, Thermodynamic assessment of the Al-Li system, Int. J. Mat. Res. 98 (2007) 961–969.
[26] M. Trybula, P. Fima, G. Władysław, Thermodynamic properties of liquid Al-Li-Zn alloys determined from electromotive force measurement, Thermochim. Acta 588 (2014) 16–21.
[27] O. Redlich, A. Kister, Indust. Eng. Chem. 40 (1948) 345.
[28] L.S. Darken, R.W. Gurry, Physical Chemistry of Metals, McGraw Hill, New York, 1953, p. 535.
[29] M. Trybuła, N. Jakse, W. Gąsior, A. Pasturel, Thermodynamics and concentration fluctuations of liquid Al-Cu and Al-Zn alloys, Arch. Metall. Mater. 60 (2015) 649–655.

[30] I. Ansara, A.T. Dinsdale, M.H. Rand, Thermochemical database for light metal alloys, Cost 507 (1998) 2.
[31] S.K. Yadav, L.N. Jha, I.S. Jha, B.P. Singh, R.P. Koirala, D. Adhikari, Prediction of thermodynamic and surface properties of Pb -Hg liquid alloys at different temperatures, Philos. Mag. 96 (2016) 1909–1925.
[32] P.D. Desai, Thermodynamic properties of selected binary aluminum alloy systems, J. Phys. Chern. Ref. Data. 16 (1987) 109–124.
[33] Marcela E. Trybula, Przemysław W. Szafrański, Pavel A. Korzhavyi, Structure and chemistry of liquid Al–Cu alloys: molecular dynamics study versus thermodynamics-based modeling, J. Mater. Sci. 53 (2018) 8285–8301.
[34] Q. Wang, K.Q. Lu, Y.X. Li, The relationship between electrical resistivity, thermopower and temperature for liquid In-Sb, Acta Phys. Sin. 50 (2001) 1355–1358.
[35] T. Gu, J. Qin, X. Bian, C. Xu, Y. Qi, Ab initio molecular dynamics simulations of liquid structure change with temperature for a GaSb alloy, Phys. Rev. B 70 (2004), 245214.
[36] Xianfen Li, Fangqiu Zu, Lanjun Liu, Jigang Li, Jie Chen, Chengming Hu, Effect of Sn on reversibility of liquid–liquid transition in Bi–Sb–Sn alloys, J. Alloys Compd. 453 (2008) 508–512.

Assessment of thermo-structural properties of Al-Fe and Fe-Si alloys at high temperatures

Article *in* Physics and Chemistry of Liquids · July 2020

DOI: 10.1080/00319104.2020.1793985

4 authors:

Ramesh Kumar Gohivar
Tribhuvan University
5 PUBLICATIONS **2** CITATIONS
SEE PROFILE

Shankardyal kumar Yadav
Indian Institute of Technology Patna
30 PUBLICATIONS **96** CITATIONS
SEE PROFILE

R.P. Koirala
Tribhuvan University, M.M.A.M. Campus, Biratnagar, Nepal
33 PUBLICATIONS **69** CITATIONS
SEE PROFILE

Devendra Adhikari
Mahendra Morang A. M. Campus, Biratnagar, Tribhuvan University
103 PUBLICATIONS **392** CITATIONS
SEE PROFILE

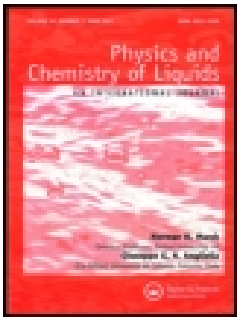

Taylor & Francis
Taylor & Francis Group

Physics and Chemistry of Liquids
An International Journal

ISSN: (Print) (Online) Journal homepage: https://www.tandfonline.com/loi/gpch20

Assessment of thermo-structural properties of Al-Fe and Fe-Si alloys at high temperatures

R.K. Gohivar , S.K. Yadav , R.P. Koirala & D. Adhikari

To cite this article: R.K. Gohivar , S.K. Yadav , R.P. Koirala & D. Adhikari (2020): Assessment of thermo-structural properties of Al-Fe and Fe-Si alloys at high temperatures, Physics and Chemistry of Liquids, DOI: 10.1080/00319104.2020.1793985

To link to this article: https://doi.org/10.1080/00319104.2020.1793985

PHYSICS AND CHEMISTRY OF LIQUIDS
https://doi.org/10.1080/00319104.2020.1793985

Taylor & Francis
Taylor & Francis Group

ARTICLE

Assessment of thermo-structural properties of Al-Fe and Fe-Si alloys at high temperatures

R.K. Gohivar[a,b], S.K. Yadav[b], R.P. Koirala[b] and D. Adhikari[b]

[a]Central Department of Physics, Tribhuvan University, Kathmandu, Nepal; [b]Department of Physics, Mahendra Morang Adarsh Multiple Campus, Tribhuvan University, Biratnagar, Nepal

ABSTRACT

The thermodynamic and structural properties of Fe – based (Al-Fe and Fe-Si) alloys in their liquid states at different higher temperatures have been studied assuming the interaction parameters of R-K polynomial are linearly and exponentially dependent on temperature. It has been observed that artificial miscibility gaps (also called artefacts) appear in the thermodynamic and structural properties of the aforementioned alloys at high temperature when the interaction parameters are assumed to be linearly dependent on temperature. The artificial miscibility gaps or artefacts observed in the former case are eliminated when the interaction parameters are supposed to be exponentially dependent on temperature. This implies that the interaction parameters of RK-
polynomial for liquid alloys vary exponentially at elevated temperatures.

ARTICLE HISTORY
Received 21 April 2020
Accepted 5 July 2020

KEYWORDS
Fe-based alloy; artefacts; thermo-structural properties; interaction parameters; R-K polynomial

1. Introduction

Understanding the thermo-structural properties of an alloy at high temperature is a vital to explore the nature of the alloy. The study of the thermo-structural properties of the alloy at high temperature can reveal the information about surface and transport properties of the alloy. These studies also help us to understand the stability of the material in solid state. In addition to the fundamental importance, knowing thermo-structural properties of material at high temperature is important for its various applications. However, alloy at high temperature in liquid state is of disorder nature and has complex structure. The complexity in the structure of the liquid alloys, therefore, demands extensive theoretical investigations and hence several theoretical models [1–13] have long been employed by the researchers to comprehend the properties of the liquid alloys.

In present work, we have employed linear [14] and exponential models [15,16] in the framework of R-K polynomial [17,18] to explain the thermodynamic and structural properties of Al-Fe and Fe-Si binary alloys in their liquid states and evaluated the applicability of these models to understand the thermo-structural properties of these alloys at high temperature. In both of these models the interaction parameters are assumed to be composition independent but temperature dependent. In former model these parameters are supposed to vary linearly with temperature whereas in later model these parameters are supposed to vary exponentially with temperature. The Al-Fe and Fe-Si alloys have also been studied by several researchers using various theoretical models [9–24] for the assessment of their different properties. The main focus of the present work is to analyse the artificial miscibility gaps or artefacts that appear in thermodynamic and structural properties of the Al-Fe and Fe-Si alloys at high temperatures (also called High – T artefact) [16]. Since the reliability of the models depends on its ability to explain every unusual behaviour in the properties of the alloy, the study of the artificial

CONTACT D. Adhikari adksbdev@yahoo.com

miscibility gaps at higher temperatures and their removal has been the subject of interest to authors. Moreover, the study of the Al-Fe and Fe-Si alloys at high temperature has attracted a considerable interest to the authors due to their high temperature applications [23–26]. The Fe-Si alloy has Fe_2Si, Fe_5Si_3, FeSi, $\alpha FeSi_2$ (orthorhombic) and $\beta Fesi_2$ (tetragonal) intermediate phases [27]. Similarly, in Al-Fe alloy the intermetallic phases Al_3Fe, Al_5Fe_2 (end-centred orthorhombic), Al-Fe, Al-Fe_3, Al_6Fe (orthorhombic) and Al_2Fe (complex rhombohedral) have been reported [27]. The formulation of the work is presented in the Section 2, the results and discussion presented in the Section 3 and the conclusions are listed in the Section 4.

2. Theoretical formulations

Thermodynamic properties like excess Gibbs free energy of mixing (ΔG^{xs}), heat of mixing (ΔH) and excess entropy of mixing (ΔS^{xs}) are computed in frame-work of Redlich-Kister (R-K) polynomials in terms of linear temperature dependent parameters and exponential temperature dependent parameters. The excess Gibbs free energy of mixing is related with heat of mixing and excess entropy of mixing by standard relation

$$\Delta G^{xs} = \Delta H - T\Delta S^{xs} \tag{1}$$

The excess entropy of mixing is calculated by taking partial derivative of excess Gibbs free energy of mixing as

$$\Delta S^{xs} = \frac{-\partial(\Delta G^{xs})}{\partial T} \tag{2}$$

Thermodynamic property (ΔZ) of liquid A-B alloy is calculated using R-K polynomials [2]

$$\Delta Z = x_1 x_2 \sum_{i=0}^{n} K_i (x_1 - x_2)^i \tag{3}$$

where x_1 and x_2 are concentration of components A (x_A) and B (x_B) of liquid A-B alloy and K_i is known as coefficient of R-K polynomials and its value is different for $\Delta Z = \Delta G^{xs}$, ΔH and ΔS^{xs}. For excess Gibbs free energy of mixing (ΔG^{xs}) and assuming K_i as linear temperature dependent parameter (L_i) also known as interaction parameters between components A and B of liquid A-B alloy

$$L_i = a_i - b_i T \tag{4}$$

where a_i and $b_i$are coefficients of R-K polynomials for heat of mixing and excess entropy of mixing respectively. Using Equation(4) in Equation (3), we get

$$\Delta G^{xs} = x_1 x_2 \sum_{i=0}^{n} (a_i - b_i T)(x_1 - x_2)^i \tag{5}$$

Using Equation (5) in Equation (3) then excess entropy of mixing is obtained as

$$\Delta S^{xs} = x_1 x_2 \sum_{i=0}^{n} b_i (x_1 - x_2)^i \tag{6}$$

Using Equations (5) and (6) in Equation (1) we obtain heat of mixing (ΔH) as

$$\Delta H = x_1 x_2 \sum_{i=0}^{n} a_i (x_1 - x_2)^i \tag{7}$$

Similarly, K_i or (L_i) exponential temperature dependent interaction parameter for excess Gibbs free energy of mixing is suggested by Kaptay [3] as

$$L_i = h_i \exp\left(\frac{-T}{\tau_i}\right) \tag{8}$$

where h_i and τ_i are exponential parameters.

Similarly, using Equation (8), Equations (6) and (7) are transformed to

$$\Delta S^{xs} = x_1 x_2 \sum_{i=0}^{n} \left(\frac{h_i}{\tau_i}\right) h_i \exp\left(\frac{-T}{\tau_i}\right) (x_1 - x_2)^i \tag{9}$$

and

$$\Delta H = x_1 x_2 \sum_{i=0}^{n} \left(1 + \frac{1}{\tau_i}\right) h_i \exp\left(\frac{-T}{\tau_i}\right) (x_1 - x_2)^i \tag{10}$$

The activity of components of liquid A-B alloy can be computed using relations

$$a_i = x_i \exp\left(\frac{G_i^{xs}}{RT}\right) \cdot i = 1, 2 \text{ for components A and B} \tag{11}$$

where G_i^{xs} are partial excess Gibbs free energy of components of liquid A-B alloy and is calculated from Equation (12) [4]

$$G_i^{xs} = \Delta G^{xs} + \sum_{j-1}^{2} \left(\delta_i^{\,j} - x_j\right) \frac{\partial(\Delta G^{xs})}{\partial x_j} \tag{12}$$

The structural property of binary liquid alloy is explained in terms of concentration fluctuations in long-wavelength limit ($S_{cc}(0)$) which gives information about arrangement components of the alloy. The standard relation for $S_{cc}(0)$ is

$$S_{cc}(0) = RT\left[\frac{\partial^2(\Delta G)}{\partial x_1^2}\right]^{-1} \tag{13}$$

Using Equation (3) in Equation (13), we get

$$\begin{aligned} S_{cc}(0) = RT\big[&-2L_0 + (-12x_1 + 6)L_1 + \left(-48x_1^2 + 48x_1 - 10\right)L_2 \\ &+ \left(-160x_1^3 + 240x_1^2 - 108x_1 + 14\right)L_3 + \frac{RT}{x_1(1 - x_1)}\Big]^{-1} \end{aligned} \tag{14}$$

and ideal value of concentration fluctuations in long-wavelength limit $S_{cc}^{id}(0) = x_1 x_2$

This observed values of $S_{cc}(0)$ can also be calculated using activity of components of binary liquid alloy.

$$S_{cc}(0) = (1 - x_i) a_i \left[\frac{\partial a_i}{\partial x_i}\right]^{-1} \tag{15}$$

Here liquid A-B alloy stands for liquid Al-Fe alloy and liquid Fe-Si alloy.

3. Results and discussion

The linear temperature dependent interaction parameters (a_i and b_i) for the Al-Fe and Fe-Si alloys in liquid state were optimised using their respective observed values of heat of mixing and excess entropy of mixing [27] in Equations (6) and (7). Further the exponential temperature dependent

parameters (h_i and τ_i) for these alloys were also estimated using optimised linear temperature dependent interaction parameters and Equations (4) and (8). The optimised parameters for these alloys are listed in Table 1. The excess Gibbs free energy of mixing (ΔG^{xs}) of the Al-Fe alloy computed using linear interaction parameters and exponential interaction parameters in the framework R-K polynomials were compared with observed value [27] at 1873 K (Figure 1(a)). All the values were in well agreement with one another. The computed values were also very close to the values obtained by Adhikari et al [21]. The peak value of the excess free energy of mixing was found to be in the same compositions in all cases. However, a small discrepancy was found with values derived from Cost 507 [14]. The excess free energy of mixing for the Al-Fe alloy in liquid state was also computed at higher temperatures 2500 K, 3500 K and 3800 K using linear temperature dependent parameters and exponential temperature dependent parameters. The computed values were then compared with the values derived from Cost 507 at the respective same temperatures (Figure 1(b-d)). Below 3800 K no artificial miscibility gap or artefact was observed in all cases. However, at temperature 3800 K a miscibility gap or artefact was detected in the values of the excess free energy of mixing for the Al-Fe alloys in the concentration range $x_{Fe} \leq 0.2$, where x_{Fe} is concentration of Fe, when it was computed using linear temperature dependent parameters and ref. [14]. This artificial miscibility gap was not noticed in the excess free energy of mixing for the Al-Fe alloy at all temperatures when it was computed using the exponential temperature dependent parameters. This clearly indicates that the interaction parameters for the Al-Fe alloy are dependent exponentially on temperature, and not linearly at high temperature. Here it important to have a notice that Kaptay [16] reassessed the thermodynamic data of different alloys and suggested that High-T artefact appears in the properties of the alloys if there occurs $a_0 < 0$ and $b_0 > 2R$ in the optimised linear parameters, where R is universal gas constant. It was observed in the present work that the linear parameters optimised from observed values [27] has $L_0 = -86088.09 + 20.96\text{T}$ and optimised linear parameter given in ref [14] has $L_0 = -91976.5 + 21.13\text{T}$. In both of the cases $a_0 < 0$ and $b_0 > 2R$ and hence High-T artefact appeared in the thermodynamic properties of the alloys when linear parameters were used for the calculation.

We also computed excess free energy of mixing for the Fe-Si alloy in liquid state at 1873 K using linear and exponential temperature-dependent parameters and compared with observed values [27] and the values obtained from ref. [14] (Figure 2(a)). The computed excess free energies of mixing for the Fe-Si alloy were found to be in excellent agreement with one another and also with the observed value. The computed values at 1873 K were also in good agreement with the value computed by Adhikari et al. [22] using regular associated solution model [28–30]. The computation of excess free energy of mixing for the Fe-Si alloy was further extended to temperatures 2500 K and 3500 K (Figure 2(b-c)). For the Fe-Si alloy no artifact was observed in the excess free energy of mixing in all cases. However, the discrepancy in the excess free energy of mixing computed with different assumptions was found to increase with an increase in temperature.

The heat of mixing (ΔH) for the liquid Al-Fe and Fe-Si alloys was computed at 1873 K using the exponential parameters of Table 1 from Equation (10). The computed value of heats of mixings were in well agreement with the respective observed values [27] and also with the respective value obtained by Adhikari et al. [21](Figure 3 and Figure 4). The heat of mixings for the Al-Fe alloy alloys was extrapolated to temperatures 2500 K, 3500 K and 3800 K. Similarly the heat of mixing for

Table 1. Optimised linear and exponential parameters of interaction of liquid Al-Fe and Fe-Si alloys.

System	L_0	L_1	L_2	L_3
Al-Fe	−86,088.09 + 20.96 T	−26,415.27 + 10.65 T	−4457.84 + 0.073 T	-
	−90,837.21exp	−32,581.59exp	−4458.56exp	-
	$(-3.33 \times 10^{-4}$ T)	$(-7.26 \times 10^{-4}$ T)	$(-1.66 \times 10^{-5}$ T)	
Fe-Si	150,430.24 + 29.2 T	−35,044.82–2.63 T	34,332.26 − 12.73 T	26,349.62–0.22 T
	−155,177.35 exp	−35,151.35 exp	40,435.10exp	26,350.76 exp
	$(-2.47 \times 10^{-4}$ T)	$(6.93 \times 10^{-5}$ T)	$(-6.27 \times 10^{-4}$ T)	$(-8.52 \times 10^{-6}$ T)

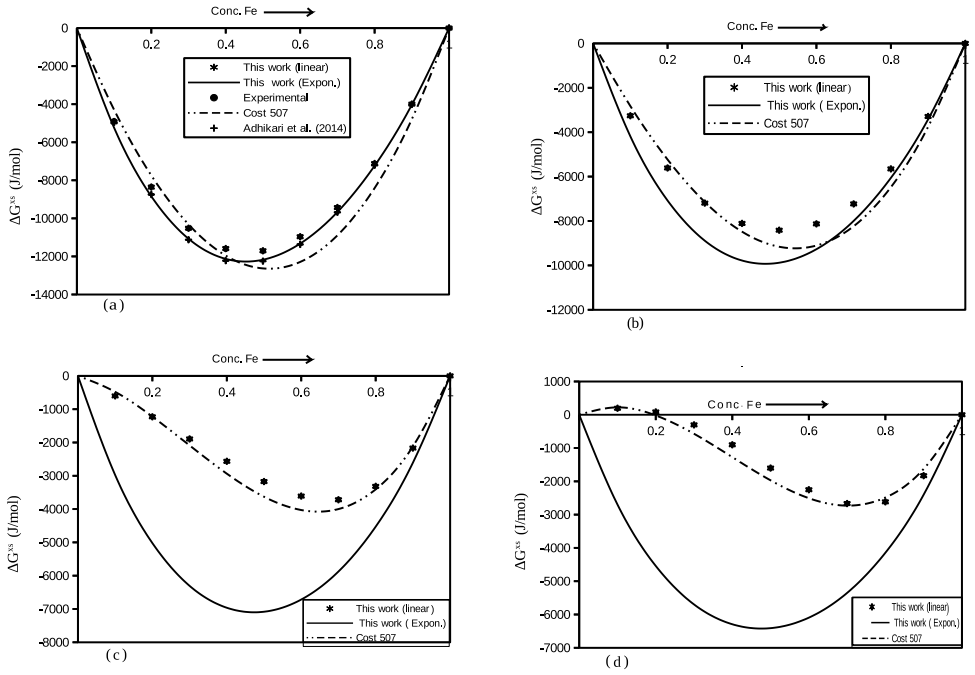

Figure 1. Excess Gibbs free energy of mixing (ΔG^{xs}) of liquid Al-Fe alloy with respect to concentration of Fe at temperatures (a) 1873 K, (b) 2500 K, (c) 3500 K and (d) 3800 K.

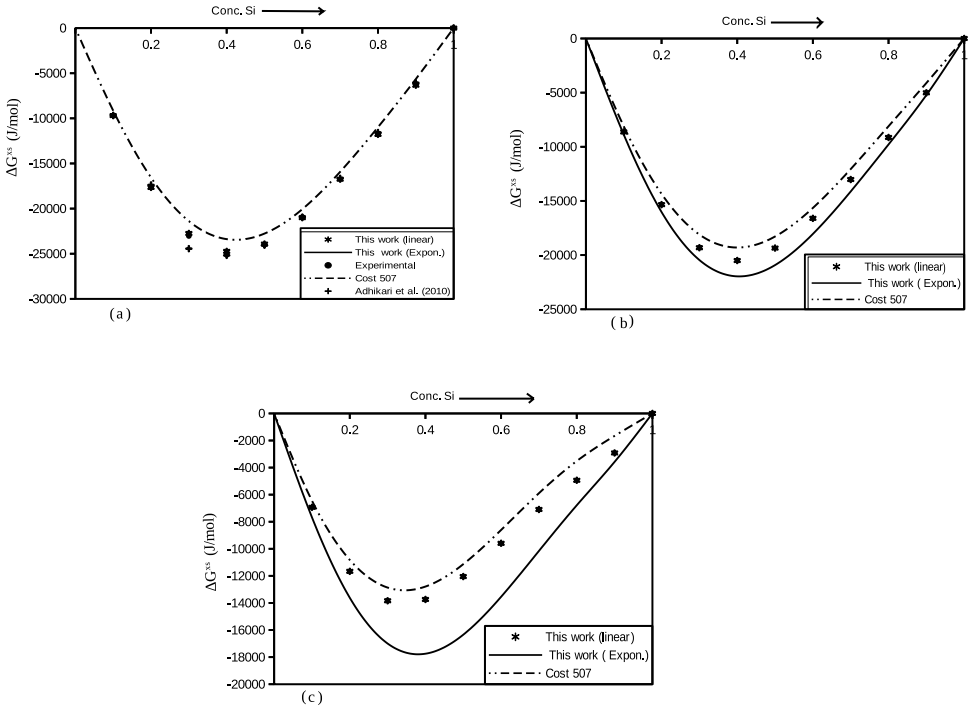

Figure 2. Excess Gibbs free energy of mixing (ΔG^{xs}) of liquid Fe-Si alloy with respect to concentration of Si at temperatures (a) 1873 K, (b) 2500 K and (c) 3500 K.

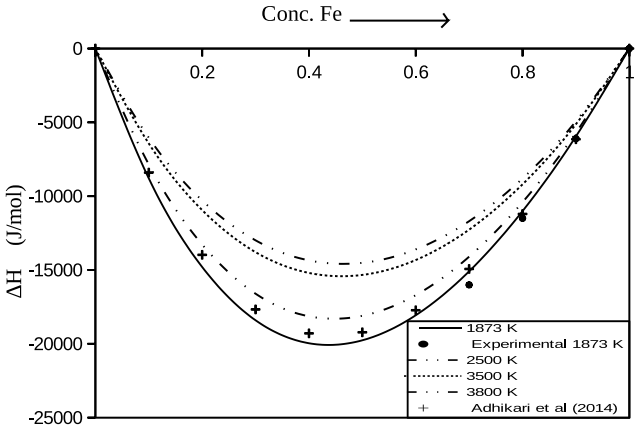

Figure 3. Heat of mixing of liquid Al-Fe alloy with respect to concentration of Fe at 1800 K, 2500 K, 3500 K and 3800 K.

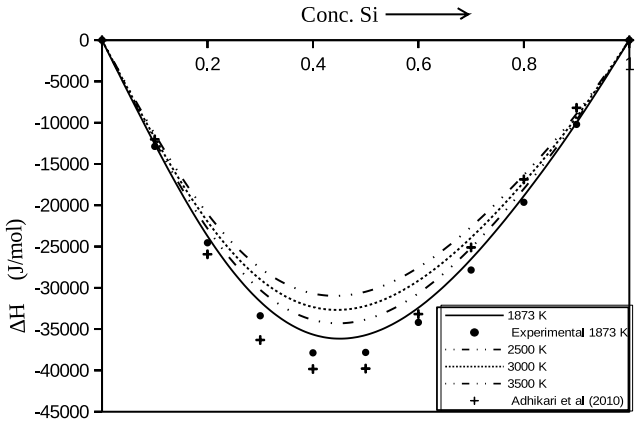

Figure 4. Heat of mixing of liquid Fe-Si alloy with respect to concentration of Si at 1873 K, 2500 K, 3000K and 3500 K.

the Fe-Si alloy was extrapolated to temperatures 2500 K, 3000 K and 3500 K. With increase of temperature the heat of mixing was found to be less negative for both of these alloys. This indicates that the nature of the alloys shift from ordering to ideal as the temperature increases which is usual behaviour.

The activity of the components of the liquid Al-Fe alloy was computed at 1873 K using linear and exponential parameters of Table 1 and Equations (11) and (12). The computed values of the activities were compared with the observed value [27] and also with the value derived from Cost 507 [14] (Figure 5(a)). The computed values of the activities of both of the components of Al-Fe alloys were found to be in good agreement with one another and also with the value obtained by Aahikari et. al [21]. The activities of both Al and Fe components were less than the ideal value at all compositions. The activities of the components of the Al-Fe alloy were then extrapolated to temperatures 2500 K, 3500 K and 3800 K (Figure 5(b-d)). The activities of the components of Al-Fe alloy showed negative to positive deviation on increasing the temperature when optimised linear parameters were used for the computation. The activity of any component cannot exceed the ideal value only on changing the temperature. Again High-T artefact appeared in the case of activities. Then the activities of the monomers of the Al-Fe alloys were computed at different temperatures using exponential parameters. It was found, in this case, that the activities of the components of the Al-Fe alloy did not shift from negative to positive side. This means the exponential interaction

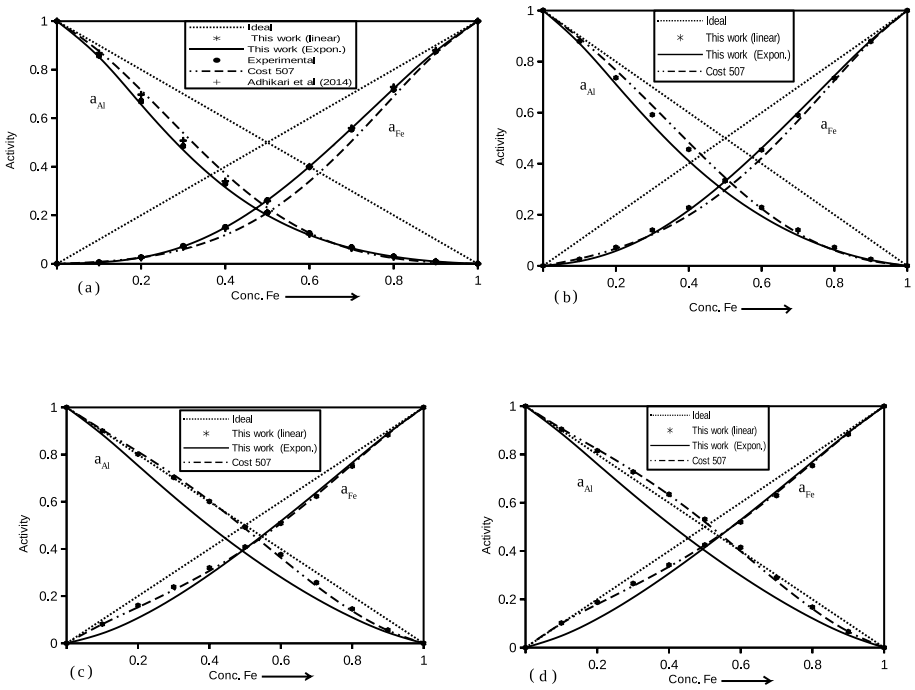

Figure 5. Activity of components Al (a_{Al}) and Fe (a_{Fe}) of liquid Al-Fe alloy with respect to concentration of Fe at temperatures (a) 1873 K, (b) 2500 K, (c) 3500 K and (d) 3800 K.

parameters correctly explains the activities of the monomers of the alloy at all temperatures, that is, the High-T artefact can be eliminated when exponential parameters are used for the computation of the activities.

The activities of Fe and Si components of the Fe-Si alloy in liquid state at 1873 K have also been computed using optimised linear and exponential interaction parameters. The computed values of the activities of Fe and Si were then compared with the observed values [27] and also with the values obtained from ref. [14]. The values of activities of Fe and Si components computed by assuming the interaction parameters to be dependent on temperature linearly and exponentially agreed well with one another and also with the observed value [27] (Figure 6(a)). This value also agreed well with the values obtained by Adhikari et al. [22]. However, discrepancy in activities of the components Fe and Si were observed with the values obtained from ref. [14]. The activities of Fe and Si components of the Fe-Si alloy were extrapolated to higher temperatures 2500 K and 3500 K. At elevated temperatures the activities of Fe and Si components exceeded the ideal values in some regions when these were computed using optimised linear parameters. This clearly indicated that even though no artefact was observed in the excess free energy of mixing of the Fe-Si alloys it was appeared in the activities of the monomers of the alloy. The high-T artefacts in the activities of the monomers were eliminated when exponential parameters were used for the computation of the activities of the monomers of the alloy. Thus the interaction parameters of the Fe-Si alloys are exponential dependent on temperature rather than linear dependent in view of the activities.

The concentration fluctuations in long-wavelength limit ($S_{cc}(0)$), an important parameter to understand the ordering and segregating nature of an alloy was computed for the Al-Fe and Fe-Si alloys in their liquid states at 1873 K assuming the interaction parameters to be linearly and exponentially dependent on temperature. The computed values of the $S_{cc}(0)$ were compared with the respective observed values (Figure 7(a) and 8(a)). For both of these alloys the computed values of the $S_{cc}(0)$ were in good agreement with one another and also with

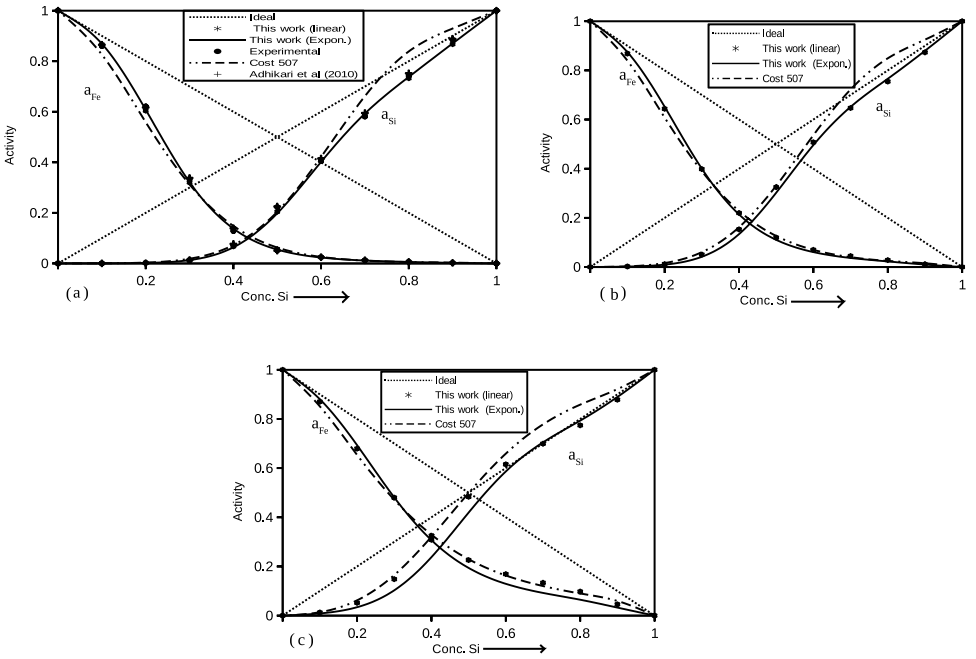

Figure 6. Activity of components Al (a_{Fe}) and Fe (a_{Si}) of liquid Fe-Si alloy with respect to concentration of Si at temperatures (a) 1873 K, (b) 2500 K and (c) 3500 K.

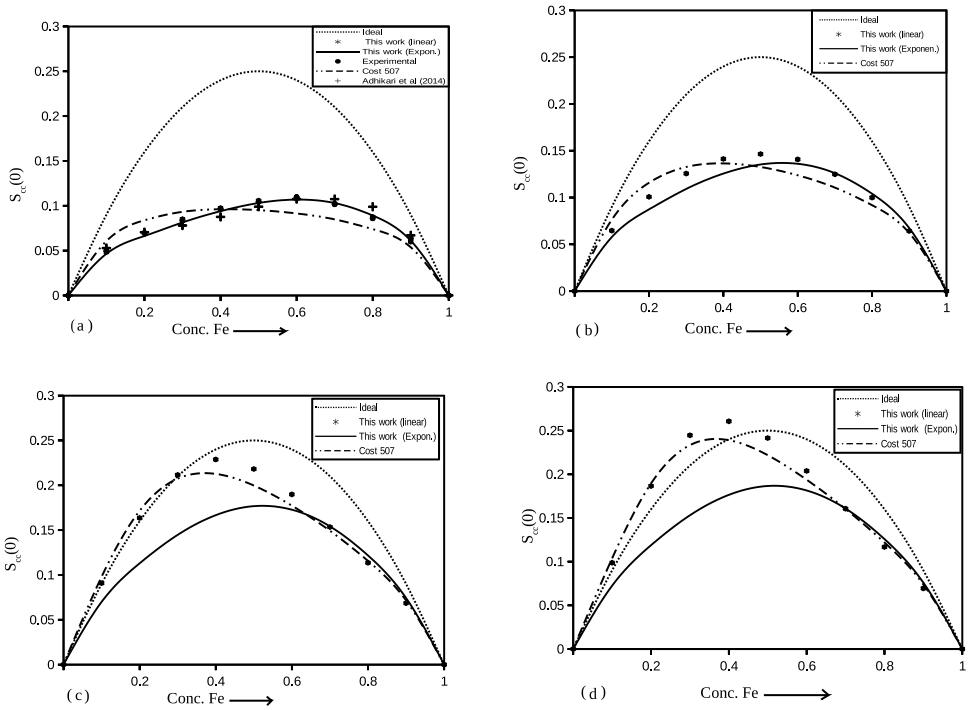

Figure 7. Concentration fluctuations in long-wavelength limit (S_{cc} (0)) of liquid Al-Fe alloy with respect to concentration of Fe at temperatures (a) 1873 K, (b) 2500 K, (c) 3500 K and (d) 3800 K.

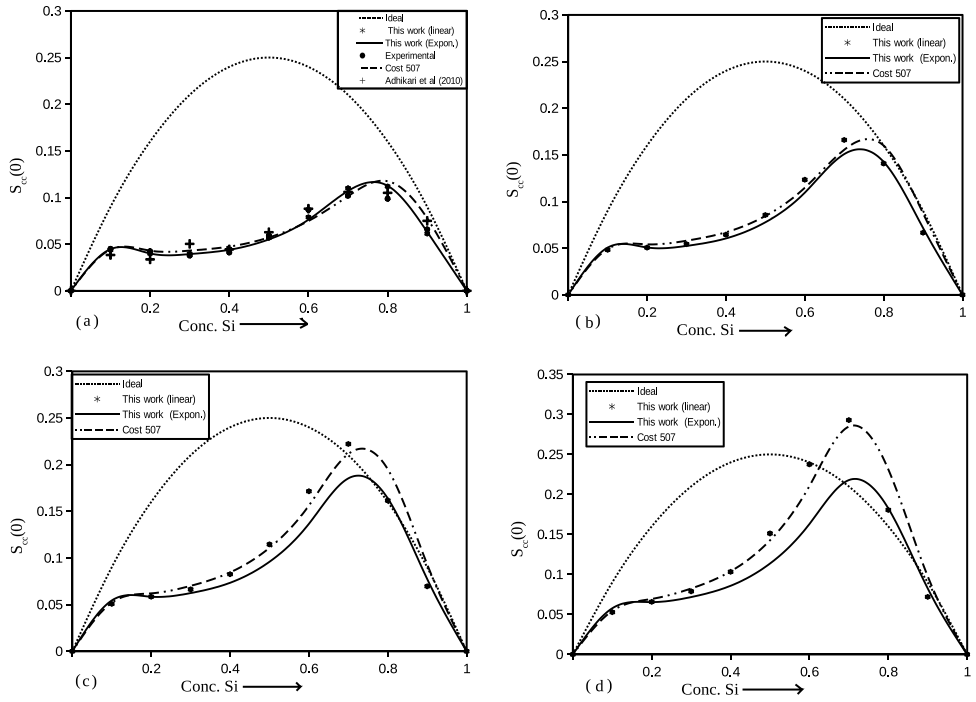

Figure 8. Concentration fluctuations in long-wavelength limit (S_{cc} (0)) of liquid Fe-Si alloy with respect to concentration of Si at temperatures (a) 1873 K, (b) 2500 K, (c) 3000 K and (d) 3500 K.

respective observed values [27]. The theoretical analysis revealed that both of these alloys are ordering in nature. The $S_{cc}(0)$ for the Al-Fe and Fe-Si alloys was also computed from the ref. [14] and compared with the observed values. The computed $S_{cc}(0)$ of the Al-Fe alloy was extrapolated to temperatures 2500 K, 3500 K and 3800 K (Figure 7 b-d) and that of the Fe-Si alloy was extrapolated to temperatures 2500 K, 3000 K and 3500 K(Figure 8(b-d)). It was found that the $S_{cc}(0)$ for the liquid Al-Fe alloy computed using linear parameter and value derived from cost 507 exceeded ideal value in concentration range 0–30% of Fe at temperature 3500 K and 0–40% of Fe at temperature 3800 K. In case of the liquid Fe-Si alloy the $S_{cc}(0)$ was found to shift towards ideal value with increase in temperature and exceeded ideal value in concentration range 0–30% of Fe at temperature 3000 K and around 0–38% of Fe at temperature 3500 K under the same assumption as above. However, the $S_{cc}(0)$ computed for both of the alloys using exponential parameters of Table 1 shift towards ideal value but does not cross it even the temperature was increased. Here it is clear from the above analysis that the artefacts that might appear under all other assumptions have been eliminated when the interaction parameters were assumed to be exponential temperature dependent.

4. Conclusion

From the above analysis the following conclusion are drawn:

(a) The Al-Fe and Fe-Si alloys are of ordering and highly interacting in nature.
(b) The artificial miscibility gaps or artefacts appear in the thermo-structural properties of the Al-Fe and Fe-Si alloys at higher temperatures when the interaction parameters are assumed to depend on temperature linearly.

(c) The thermo-structural properties of the Al-Fe and Fe-Si alloys can be explained correctly when the interaction parameters are assumed to be exponentially dependent on temperatures.
(d) The interaction parameters of both of the alloys are exponential temperature dependent.

Disclosure statement

No potential conflict of interest was reported by the authors.

Funding

This work was supported by the University Grants Commission -Nepal.

ORCID

R.K. Gohivar http://orcid.org/0000-0002-6154-7443
S.K. Yadav http://orcid.org/0000-0003-2525-216X
D. Adhikari http://orcid.org/0000-0002-6022-3615

References

[1] Bhatia AB, Singh RN. A quasi-lattice theory compound forming molten alloys. Phys Chem Liq. 1984;13 (3):177–190.
[2] Sommer F. Thermodynamic properties of compound-forming liquid alloys. J Non-Cryst Solids. 1990;7:505–512.
[3] Novakovic R. Thermodynamic, surface properties and microscopic functions of liquid Al-Nb and Nb-Ti alloys. J Non-Cryst Solids. 2010;356(31–32):1593–1598.
[4] Kaptay G, Sytchev J. Thermodynamic properties of phases and the electrochemical synthesis diagram for the Mo-B System - Ukr. Khim Zh. 1999;65:34–41.
[5] Young WH. Structural and thermodynamic properties of NFE liquid metals and binary alloys. Rep Prog Phys. 1992;55(10):1769.
[6] Ruppersberg H, Reiter H. Chemical short-range order in liquid LiPb alloys. J Phys F. 1992;12(7):1311. .
[7] Singh RN. Short-range order and concentration fluctuations in binary molten alloys. Can J Phys. 1987;65 (3):309.
[8] Adhikari D. Disorder in liquid Cu-Pd alloy. Phase Transitions. 2011;84(4):308–314.
[9] Flory PJ. Thermodynamics of high polymer solutions. J Chem Phys. 1942;10(1):51–61.
[10] Jordan AS. A theory of regular associated solution applied to the liquid us curves of the Zn–Te and Cd–Te system. Metall Trans. 1970;1:239–249.
[11] March NH, Alonso JA. Non–monotonic behaviour with concentration of the surface tension of certain binary liquid alloys. Phys Chem Liq. 2008;46(5):522–526.
[12] Bhatia AB, Hargrove WH. Concentration fluctuation and thermodynamic properties of some compound forming binary molten alloys. Phys Rev B. 1974;10(8):3186–3196.
[13] Adhikari D, Singh BP, Jha IS. Structural and energetic asymmetry in liquid Ag-Al alloys. Phys Chem Liq. 2010;48:787–796.
[14] Ansara I, Dinsdale AT, Rand MH. Thermochemical database for light metal alloys, (Cost 507 2). 1998.
[15] Kaptay G. A new equation for the temperature dependence of the excess Gibbs energy of solution phases. Calphad Comput Coupling Phase Diagrams Thermochem. 2004;28(2):115–124. .
[16] George K. The exponential excess Gibbs energy model revisited. Calphad. 2017;56:169.
[17] Redlich O, Kister AT. Algebraic representation of thermodynamic properties and the classification. Ind Eng Chem. 1948;40(2):345–348.
[18] Singh RN, Sommer F. Segregation and immiscibility in liquid binary alloys. Rep Prog Phys. 1977;60 (1):57–150.
[19] Hossain SA, Muneer B, Rizk AH. Corrosion behavior of nanostructure Al-Fe alloy processed by mechanical alloying and high frequency induction heat sintering. Int J Electrochem Sci. 2015;10:3054–3064.
[20] Pavel N, Nová K. Oxidation behavior of Fe–Al, Fe–Si and Fe–Al–Si Intermetallics. Materials (Basel). 2019;12 (11):1748.
[21] Adhikari D, Yadav SK, Jha LN. Thermo-physical properties of Al–Fe melt. J Chinese Adv Mater Soc. 2014;2 (3):149–158.

[22] Adhikar D, Jha IS, Singh BP. Structural asymmetry in liquid Fe – si alloys. Philos Mag. 2010;90(20):2687–2694.
[23] Fuxiao Y, Liu F, Zhao D, et al. Microstructure and mechanical properties of Al-3Fe alloy processed by equal channel angular extrusion. Mat Sci Eng. 2014;63:012079.
[24] Lee IS, Kao PW, Ho NJ. Microstructure and mechanical properties of Al-Fe in situ nanocomposite produced by friction stir processing. Intermetallics. 2008;16(9):1104.
[25] Kaloshkin SD, Tcherdyntsev VV, Tomilin IA, et al. Composed phases and microhardness of aluminium-rich aluminium-iron alloys obtained by rapid quenching, mechanical alloying and high pressure torsion deformation. Mater Trans JIM. 2002;43(8):2031. .
[26] Lucia S, Schneider J, Houbaert Y. High-temperature oxidation of Fe- Si Alloys in the Temperature Range 900-1250°C defect and diffusion forum. Trans Tech Publications Ltd. 2008;273–276:661–666.
[27] Hultgren R, Desai PD, Hawkins DT, et al. Selected values of the thermodynamic properties of binary alloys. OHIO: Metal Park, ASM International; 1973.
[28] Yadav SK, Jha LN, Jha IS, et al. Prediction of thermodynamic and surface properties of Pb -Hg liquid alloys at different temperatures. Philosophical Mag. 2016;96:1909–1925.
[29] Srikanth S, Jacob KT. Volume effects and associations in liquid alloys. Metallurgical Transactions B. 1988;19 (3):465–470.
[30] Lele S, Ramchandrarao P. Estimation of complex concentration in a regular associated solution. Metall Trans B. 1981;12(4):659–666.

Heliyon 7 (2021) e06613

Contents lists available at ScienceDirect

Heliyon

journal homepage: www.cell.com/heliyon

Research article

Study of artifacts in thermodynamic and structural properties of Li–Mg alloy in liquid state using linear and exponential models

R.K. Gohivar [a,b], S.K. Yadav [b], R.P. Koirala [b], D. Adhikari [b,*]

[a] Central Department of Physics, Tribhuvan University, Kritipur, Nepal
[b] Department of Physics, Mahendra Morang Adarsh Multiple Campus, Tribhuvan University, Biratnagar, Nepal

ARTICLE INFO

Keywords:
Li-Mg alloy
R–K polynomial
Exponential parameters
Miscibility gap
High temperature

ABSTRACT

Temperature-dependent interaction parameters of Redlich-Kister (R–K) polynomials for Li–Mg alloy in liquid phase have been optimized using experimental data in the framework of linear and exponential models. These parameters have then been used to compute the thermodynamic properties (excess Gibbs free energy of mixing, enthalpy of mixing and activity) and structural property (concentration fluctuations in the long-wavelength limit) of the alloy at temperatures 1000 K, 1300 K, 1600 K, 1900 K, and 2200 K. The negative values of excess Gibbs free energy of mixing computed using linear T-dependent parameters increases with the rise in the temperature of the system beyond 1000 K while the same physical quantity computed using the exponential T-dependent interaction parameters decreases with the rise in temperatures and does not show any unusual trends up to 2200 K. Similar behavior has been found in the case of other thermodynamic and structural functions. The unusual behavior that appears in the thermodynamic and structural functions computed using linear T-dependent parameters can be eliminated if these functions are computed using exponential T-dependent parameters.

1. Introduction

The coexistence of two distinct liquid phases causes miscibility gaps in the liquid phase of alloys [1, 2]. The miscibility gaps which appear in phase diagrams and thermodynamic functions are termed thermodynamic artifacts. Several researchers [3, 4, 5, 6, 7, 8, 9, 10, 11, 12] have revealed the existence of artificial inverted miscibility gaps in different alloy systems. Kevorkov et al. [3] analyzed published parameters of Feufel [13] and Yan et al. [14] for Mg–Si system and studied the presence of artificial inverted miscibility gaps in the liquid phase at higher temperatures. They then remodeled the system using the data of Yan et al. [14] and computed the phase diagram without the inverted miscibility gaps up to 4273 K. Kaptay [4] explained that the artifacts appear in some alloy systems at high temperature when the coefficients of Redlich-Kister (R–K) polynomials are considered to be linear temperature (T) dependent. The linear T-dependence of interaction parameters are expressed in the form $L_i + a_i + b_i T$ where a_i is the enthalpy term in unit J mol^{-1} and b_i is the entropy term in J mol^{-1} K^{-1}. Following Kaptay, if $a_i < 0$ and $b_2 > 2.R$, then the existence of artifacts is observed. To overcome this, he proposed a model in which the interaction parameters depend exponentially on T called the exponential model. Later Schmidt-Fetzer et al. [7] detected the presence of low-temperature artifact in the phase diagram of Mg–Si system using two exponentially optimized parameters. With this regard, Liang et al. [11] employed the combined linear-exponential T- dependent (LET) interaction parameter in order to remove both high and low T-artifacts of the system. Contrary to Schmidt-Fetzer et al., Kaptay removed both high and low-T artifacts of fifteen different systems by considering four exponential interaction parameters [12]. Furthermore, Kaptay suggested the utility of LET interaction parameters for those systems in which the excess Gibbs free energy changes sign with the temperature. In the present work, we have observed the presence of high T-artifacts in Li–Mg system in the temperature range 1000–2200 K while assuming the interaction parameters to be linear T-dependent.

Lithium–Magnesium based alloys are metallic materials having low densities which are mostly used in aerospace, automotive, portable electronics, etc. [15], among which Li–Mg alloys have extremely lightweight, high mechanical strength, and high stiffness. As a result, they have been assessed by several researchers [16, 17, 18, 19] in the field of metallurgical science. Gasior et al. [16] have optimized coefficients of R–K polynomials for Gibbs energy of mixing for the system using data obtained by electromotive force (emf) method and other experimental

* Corresponding author.
E-mail addresses: adksbdev@yahoo.com, devendra.adhikari@mmamc.tu.edu.np (D. Adhikari).

https://doi.org/10.1016/j.heliyon.2021.e06613
Received 5 July 2020; Received in revised form 22 October 2020; Accepted 24 March 2021

Table 1. Optimized parameters for liquid Li–Mg alloy.

L_i	Linear	Exponential
L_0	-21318 + 2.9 T	-31362 exp (-1.46 × 10^{-4} T)
L_1	7930 - 15.1T	1154251 exp (-1.60 × 10^{-2} T)
L_2	10668–8.9 T	12138 exp (-1.34 × 10^{-3} T)
L_3	-7765 + 7.4 T	-9382 exp (-1.67 × 10^{-3} T)

Table 2. Excess Gibbs free energy of mixing (G_M^{xs}) of liquid Li–Mg alloy at temperatures 1000 K, 1300 K, 1600 K, 1900 K and 2200 K.

X_{Mg}	Excess Gibbs free energy of mixing (G_M^{xs}) in (J/mol)							
	T = 1000K					T = 1300 K		
	Linear fit	Expon. fit	Experimental [25]	Wang et al. [19]	Cost 507 [20]	Linear fit	Expon. fit	Wang et al. [19]
0.1	-2095.23	-1557.95	-2085.82	-1369.21	-466.40	-2336.12	-1515.10	-1426.77
0.2	-3562.91	-2828.97	-3540.46	-2573.13	-801.39	-3797.62	-2738.52	-2701.48
0.3	-4434.11	-3790.56	-4405.72	-3517.11	-1018.03	-4533.01	-3649.81	-3719.74
0.4	-4756.84	-4400.12	-4740.12	-4130.82	-1127.89	-4682.10	-4218.27	-4401.44
0.5	-4596.06	-4611.78	-4598.00	-4368.23	-1141.00	-4376.03	-4413.21	-4690.79
0.6	-4033.70	-4393.37	-4050.42	-4207.57	-1065.87	-3737.25	-4214.18	-4556.28
0.7	-3168.61	-3743.26	-3193.52	-3651.43	-909.50	-2879.53	-3621.17	-3990.71
0.8	-2116.63	-2707.32	-2135.98	-2726.63	-677.35	-1907.93	-2664.87	-3011.16
0.9	-1010.52	-1395.74	-1019.92	-1484.34	-373.38	-918.85	-1416.90	-1659.03

X_{Mg}	Excess Gibbs free energy of mixing (G_M^{xs}) in (J/mol)								
	T = 1600 K			T = 1900 K			T = 2200 K		
	Linear fit	Expon. fit	Wang et al. [19]	Linear fit	Expon. fit	Wang et al. [19]	Linear fit	Expon. fit	Wang et al. [19]
0.1	-2577.0	-1467.9	-1484.3	-2817.9	-1417.9	-1541.9	-3058.8	-1366.3	-1599.4
0.2	-4032.3	-2643.0	-2829.8	-4267.0	-2545.0	-2958.2	-4501.8	-2446.5	-3086.5
0.3	-4631.9	-3508.2	-3922.4	-4730.8	-3367.9	-4125.0	-4829.7	-3230.3	-4327.6
0.4	-4607.4	-4041.8	-4672.1	-4532.6	-3871.3	-4942.7	-4457.9	-3707.0	-5213.3
0.5	-4156.0	-4223.2	-5013.4	-3936.0	-4041.3	-5335.9	-3715.9	-3867.3	-5658.5
0.6	-3440.8	-4039.3	-4905.0	-3144.4	-3869.8	-5253.7	-2847.9	-3706.1	-5602.4
0.7	-2590.4	-3490.9	-4330.0	-2301.3	-3357.4	-4669.3	-2012.3	-3223.9	-5008.6
0.8	-1699.2	-2598.4	-3295.7	-1490.5	-2518.0	-3580.2	-1281.8	-2430.1	-3864.8
0.9	-827.2	-1408.5	-1833.7	-735.5	-1381.9	-2008.4	-643.8	-1344.5	-2183.1

techniques. Jha et al. [18] studied the same system employing a regular associated solution model assuming the favorable complex Li_2Mg and concluded it to be moderately interacting. The phase diagram of Li–Mg alloy shows that there exist three stable liquid phases namely bcc-A2, fcc-A3, and one metastable phase fcc-Al in a liquid solution and two metastable compounds $Al_{12}Mg_{17}$ and AlLi [20]. Braga et al. [17] computed the phase diagram using the reoptimized parameters for the system using the data of Cost 507 [20]. It was found that the computed phase diagram agrees well with the experimental in the composition range $x_{Li} \geq 0.3$ Later, Wang et al. [19] found that there appeared inverse miscibility gap while considering the reassessed parameters of Brag et al. above 973 K. Therefore, they reassessed the system by taking account of experimental data and eliminated inverse miscibility gap and artificial phase relations in Li-rich region which had been appeared in the calculations using parameters from [16, 17] near to its melting temperature. However, it is found that the negative values of excess Gibbs free energy of mixing of the system calculated using parameters of Wang et al. increases with rise in temperature indicating the increase in mixing tendency of the liquid alloy. But the liquid alloys should show ideal mixing behavior at elevated temperatures [21, 22, 23, 24].

In the present work, both the linear and exponential T- dependent interaction parameters have been optimized for the Li–Mg system using experimental data [25]. The excess Gibbs free energy, enthalpy of mixing, activity, and concentration fluctuations in the long-wavelength limit ($S_{cc}(0)$) have been computed using the optimized parameters in the framework of R–K polynomials at different temperatures. Additionally, the presence of artifacts in the thermodynamic as well as structural functions of the system has been detected using the linear T-dependent interaction parameters. These artifacts have been removed by assuming the exponential T-dependent interaction parameters.

2. Formalism

2.1. Thermodynamic properties

Thermodynamic properties like excess Gibbs free energy of mixing (G_M^{xs}), heat of mixing (H_M) and excess entropy of mixing (S_M^{xs}) can be expressed in terms of Redlich-Kister (R–K) polynomials. These three thermodynamic functions can be related in standard form as

$$G_M^{xs} = H_M - TS_M^{xs} \tag{1}$$

The excess entropy of mixing (S_M^{xs}) in terms G_M^{xs} can be given as

$$S_M^{xs} = \frac{-\partial(G_M^{xs})}{\partial T} \tag{2}$$

In the frame work of R–K polynomials, the excess thermodynamic functions (Z^{xs}) for the binary liquid alloys of the type A-B can be expressed in the form [26].

$$Z^{xs} = x_1 x_2 \sum_{i=0}^{n} L_i (x_1 - x_2)^i \tag{3}$$

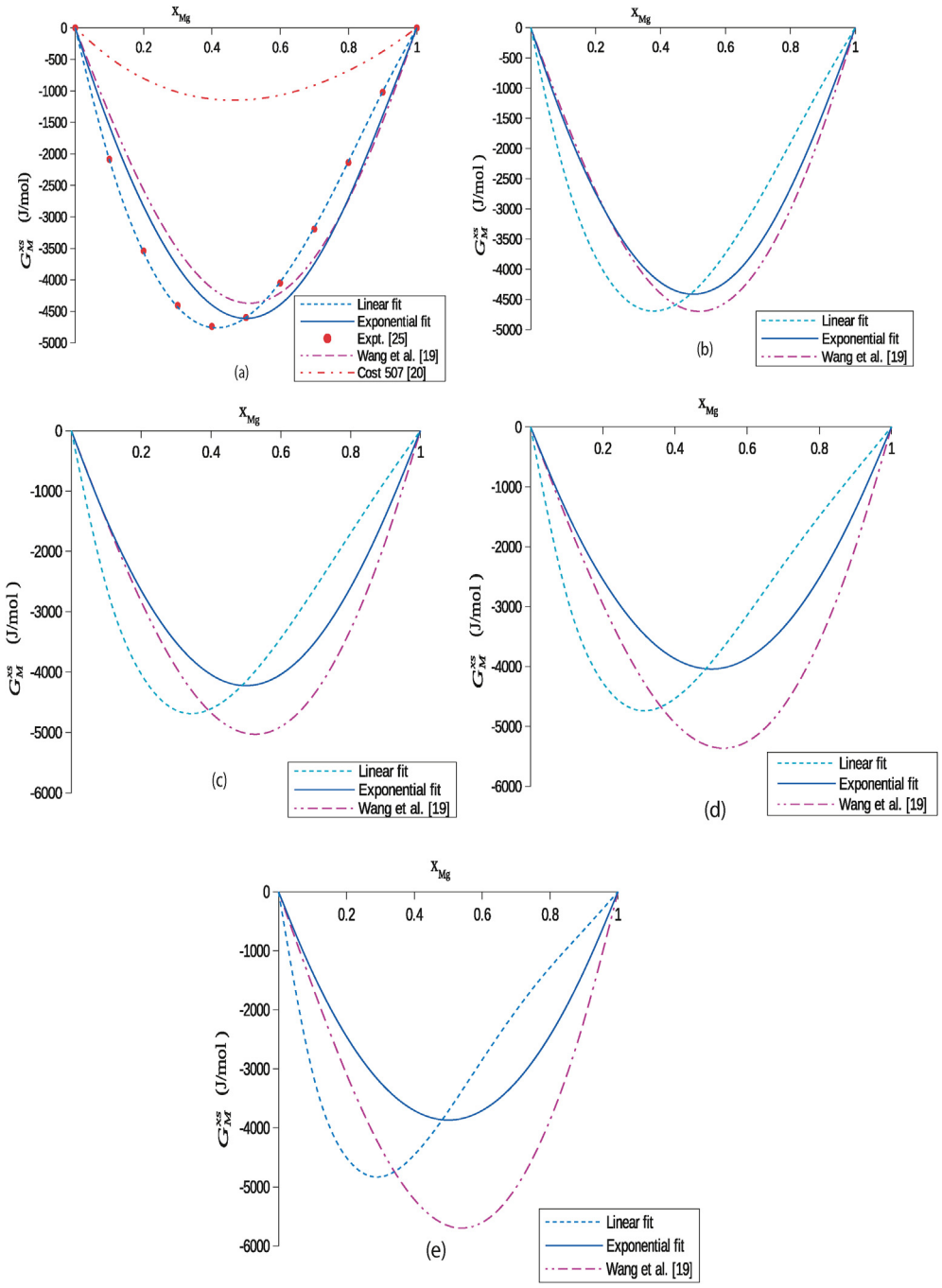

Figure 1. The compositional dependence of the excess Gibbs free energy of mixing (G_M^{xs}) of the liquid Li–Mg alloy at temperatures (a) 1000 K, (b) 1300 K, (c) 1600 K, (d) 1900 K and (e) 2200 K.

where $x_1(x_A = x_{Li})$ and $x_2(x_B = x_{Mg})$ are the concentrations of components A and B of the alloy and L_i are the coefficients of R–K polynomials. Z^{xs} stands for G_M^{xs}, H_M and S_M^{xs}. For G_M^{xs} linear T-dependent parameters L_i be expressed as [7, 11, 12].

$$L_i = a_i - b_i T \tag{4}$$

where a_i and b_i are the parameters associated with the heat of mixing and excess entropy of mixing respectively. Using Eq. (4) in Eq. (3), we get

$$G_M^{xs} = x_1 x_2 \sum_{i=0}^{n} (a_i - b_i T)(x_1 - x_2)^i \tag{5}$$

Now, using Eq. (5) in Eq. (2) and then in Eq. (1), one can obtain the relations for S_M^{xs} and H_M as

$$S_M^{xs} = x_1 x_2 \sum_{i=0}^{n} b_i (x_1 - x_2)^i \tag{6}$$

and

$$H_M = x_1 x_2 \sum_{i=0}^{n} a_i (x_1 - x_2)^i \tag{7}$$

Following, Kaptay [4], Li in terms of exponential T-dependent interaction parameters can be given as

Table 3. Enthalpy of mixing (H_M) of liquid Li–Mg alloy 1000 K, 1300 K, 1600 K, 1900 K and 2200 K.

X_{Mg}	Enthalpy of mixing (H_M) in (J/mol)							
	T = 1000 K				Expon. fit			
	Linear fit	Expon. fit	Experimental [25]	Wang et al. [19]	T = 1300K	T = 1600K	T = 1900K	T = 2200K
0.1	-1091.0	-1424.2	-1091.0	-1177.4	-1318.8	-1207.4	-1095.0	-985.3
0.2	-2303.5	-2539.8	-2340.8	-2145.3	-2333.3	-2124.8	-1920.9	-1725.9
0.3	-3556.6	-3326.0	-3582.3	-2841.7	-3036.2	-2754.9	-2486.5	-2233.3
0.4	-4648.2	-3786.0	-4648.2	-3228.8	-3441.4	-3116.2	-2810.8	-2525.1
0.5	-5329.5	-3935.2	-5362.9	-3293.0	-3571.5	-3231.9	-2914.9	-2619.1
0.6	-5379.7	-3790.3	-5379.7	-3045.2	-3446.2	-3120.3	-2814.0	-2527.5
0.7	-4680.1	-3357.5	-4606.4	-2520.5	-3069.9	-2784.0	-2509.4	-2250.3
0.8	-3289.4	-2621.3	-3201.9	-1778.2	-2419.9	-2199.6	-1979.8	-1769.7
0.9	-1517.3	-1533.2	-1517.3	-902.0	-1434.3	-1307.1	-1173.4	-1043.7

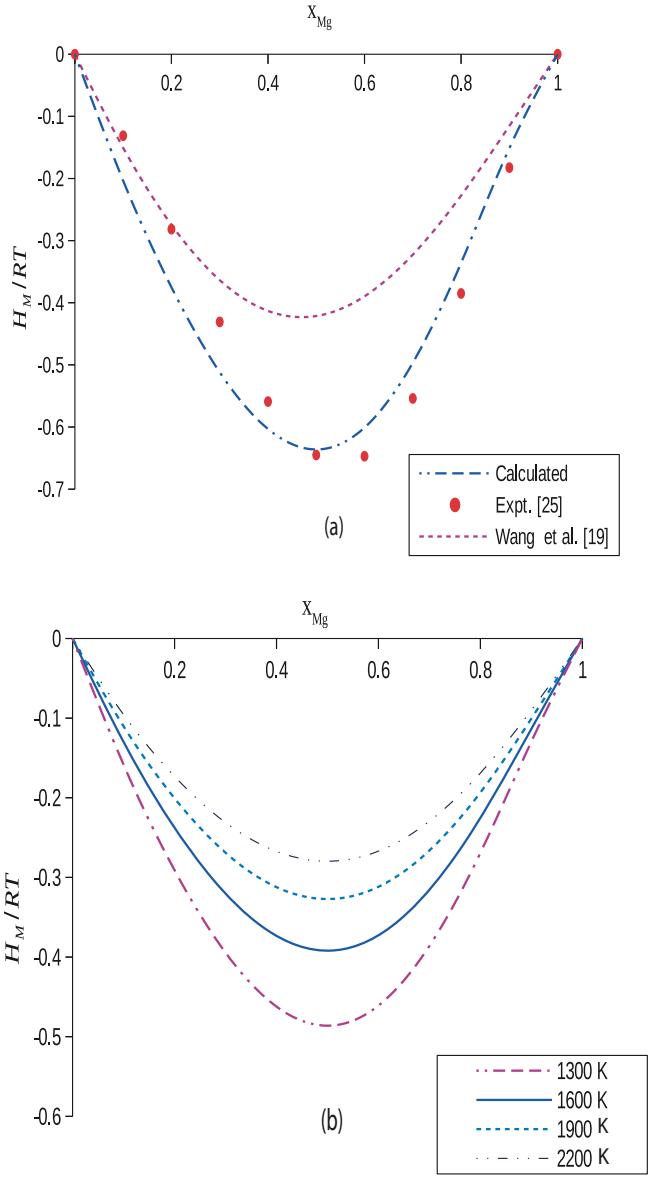

Figure 2. The compositional dependence of the enthalpy of mixing (H_M) of liquid the Li–Mg alloy at (a) 1000 K and (b) 1300 K–2200 K.

$$L_i = h_i exp\left(\frac{-T}{\tau_i}\right) \tag{8}$$

where h_i and τ_i are exponential parameters which are to be optimized. Similarly, using Eqs. (5), (6), (7) and (8) can be transformed as

$$G_M^{xs} = x_1 x_2 \sum_{i=0}^{n} h_i exp\left(\frac{-T}{\tau_i}\right)(x_1 - x_2)^i \tag{9}$$

$$S_M^{xs} = x_1 x_2 \sum_{i=0}^{n} \left(\frac{1}{\tau_i}\right) h_i exp\left(\frac{-T}{\tau_i}\right)(x_1 - x_2)^i \tag{10}$$

and

$$H_M = x_1 x_2 \sum_{i=0}^{n} \left(1 + \frac{T}{\tau_i}\right) h_i exp\left(\frac{-T}{\tau_i}\right)(x_1 - x_2)^i \tag{11}$$

Activity is an important thermodynamic property of the liquid alloy which are directly computed from the experimental measurements. It provides an immediate insight of the mixing tendency of the system. The activity of components A and B of the liquid alloy can be related to G_μ^{xs} as

$$a_\mu = x_\mu exp\left(\frac{G_\mu^{xs}}{RT}\right) \tag{12}$$

where μ= 1, 2 for components A and B and G_μ^{xs} are partial excess Gibbs free energy of components A and B of the alloy which can further be expressed as [27].

$$G_\mu^{xs} = G^{xs} + \sum_{j=1}^{2} (\delta_\mu{}^j - x_j) \frac{\partial G_M^{xs}}{\partial x_j} \tag{13}$$

2.2. Structural properties

It is well known fact that the liquid alloys are disorder systems having no long-range interactions. Therefore, the knowledge of the local arrangements of the atoms of the liquid mixture is mandatory to understand the energetic of the initial melt. The extent of local ordering of the atoms can be studied and explained in terms of concentration fluctuations in long-wavelength limit ($S_{cc}(0)$). The standard relation for $S_{cc}(0)$ in terms of excess free energy of mixing can be given as [28].

$$S_{cc}(0) = RT\left[\frac{\partial^2 G_M^{xs}}{\partial x_1^2}\right]^{-1} \tag{14}$$

Table 4. Activities of components of liquid Li–Mg alloy at temperatures 1000 K, 1300 K, 1600 K, 1900 K and 2200 K.

X_{Mg}	Activities							
	T = 1000 K							
	Linear fit		Expon. fit		Experimental [25]		Wang et al. [19]	
	a_{Li}	a_{Mg}	a_{Li}	a_{Mg}	a_{Li}	a_{Mg}	a_{Li}	a_{Mg}
0.1	0.866	0.012	0.885	0.018	0.865	0.012	0.893	0.021
0.2	0.690	0.043	0.746	0.048	0.689	0.043	0.763	0.052
0.3	0.510	0.107	0.591	0.097	0.509	0.107	0.609	0.101
0.4	0.353	0.213	0.432	0.174	0.353	0.213	0.449	0.178
0.5	0.232	0.357	0.287	0.287	0.232	0.356	0.303	0.289
0.6	0.146	0.521	0.172	0.437	0.146	0.521	0.186	0.430
0.7	0.090	0.678	0.093	0.608	0.090	0.679	0.103	0.591
0.8	0.053	0.808	0.046	0.771	0.053	0.808	0.050	0.750
0.9	0.027	0.909	0.019	0.900	0.027	0.908	0.019	0.889
Activities								
T = 1300 K							T = 1600 K	
Linear fit		Expon. fit		Wang et al. [19]			Linear fit	
a_{Li}	a_{Mg}	a_{Li}	a_{Mg}	a_{Li}	a_{Mg}		a_{Li}	a_{Mg}
0.864	0.016	0.888	0.028	0.895	0.028		0.863	0.019
0.686	0.061	0.757	0.070	0.773	0.066		0.683	0.075
0.509	0.150	0.614	0.132	0.630	0.122		0.508	0.185
0.362	0.283	0.469	0.218	0.479	0.202		0.368	0.338
0.254	0.437	0.332	0.332	0.336	0.312		0.270	0.496
0.179	0.584	0.217	0.471	0.216	0.448		0.203	0.627
0.126	0.706	0.129	0.622	0.125	0.600		0.156	0.724
0.084	0.808	0.068	0.769	0.063	0.752		0.112	0.807
0.044	0.902	0.028	0.895	0.024	0.888		0.059	0.898

T = 1600 K					
Expon. fit		Wang et al. [19]			
a_{Li}	a_{Mg}	a_{Li}	a_{Mg}		
0.890	0.037	0.897	0.034		
0.765	0.089	0.779	0.077		
0.630	0.159	0.643	0.137		
0.493	0.251	0.499	0.219		
0.364	0.364	0.359	0.328		
0.250	0.495	0.237	0.460		
0.157	0.634	0.142	0.607		
0.087	0.771	0.073	0.754		
0.037	0.894	0.028	0.888		

T = 1900 K						T = 2200 K					
Linear fit		Expon. fit		Wang et al. [19]		Linear fit		Expon. fit		Wang et al. [19]	
a_{Li}	a_{Mg}	a_{Li}	a_{Mg}	a_{Li}	a_{Mg}	a_{Li}	a_{Mg}	a_{Li}	a_{Mg}	a_{Li}	a_{Mg}
0.863	0.022	0.892	0.044	0.898	0.039	0.862	0.024	0.893	0.051	0.898	0.042
0.681	0.087	0.771	0.104	0.783	0.085	0.680	0.097	0.775	0.116	0.786	0.092
0.507	0.213	0.642	0.180	0.653	0.148	0.507	0.237	0.651	0.197	0.660	0.157
0.372	0.381	0.512	0.275	0.513	0.232	0.375	0.417	0.525	0.294	0.523	0.241
0.281	0.541	0.387	0.387	0.375	0.339	0.289	0.577	0.405	0.405	0.388	0.347
0.222	0.658	0.275	0.512	0.253	0.468	0.236	0.682	0.294	0.526	0.265	0.474
0.180	0.737	0.179	0.644	0.154	0.611	0.200	0.746	0.197	0.652	0.164	0.614
0.136	0.807	0.103	0.774	0.081	0.755	0.157	0.807	0.116	0.777	0.087	0.756
0.073	0.895	0.044	0.894	0.032	0.888	0.085	0.893	0.051	0.894	0.034	0.888

Using Eq. (3) in Eq. (13), we get

$$S_{cc}(0) = RT\Big[-2L_0 + (-12x_1+6)L_1 + \big(-48x_1^2+48x_1-10\big)L_2 + \big(-160x_1^3+240x_1^2-108x_1+14\big)L_3 + \frac{RT}{x_1(1-x_1)}\Big]^{-1} \quad (15)$$

and ideal value of concentration fluctuations in long-wavelength limit is $S_{cc}^{id}(0) = x_1x_2$

The experimental values of $S_{cc}(0)$ can also be calculated using activity of components of binary liquid alloy [22, 29] as

$$S_{cc}(0) = (1-x_i)a_i\left[\frac{\partial a_i}{\partial x_i}\right]^{-1} \quad (16)$$

Here liquid A-B alloy stands for liquid Li–Mg alloy.

3. Results and discussion

The experimental data of enthalpy of mixing and excess entropy of mixing for liquid Li–Mg alloy [25] were used to optimize the linear T-dependent interaction parameters of R–K polynomials for excess Gibbs free energy of mixing using Eqs. (5), (6), and (7). The optimized linear parameters were then used to obtain exponential T-dependent interaction parameters using Eqs. (8), (9), (10), and (11). The optimized linear and exponential interaction parameters are presented in Table 1.

The excess Gibbs free energy of mixing (G_M^{xs}) of the liquid alloy has been computed at temperatures 1000 K, 1300 K, 1600 K, 1900 K and 2200 K using Eqs. (5) and (9) with the help of the optimized parameters and listed in Table 2. The values so obtained have been compared with the available literature and experimental data (Figure 1(a–e)). The values of G_M^{xs} computed using the linear parameters of this work are in excellent agreement with the experimental results. But the values so obtained

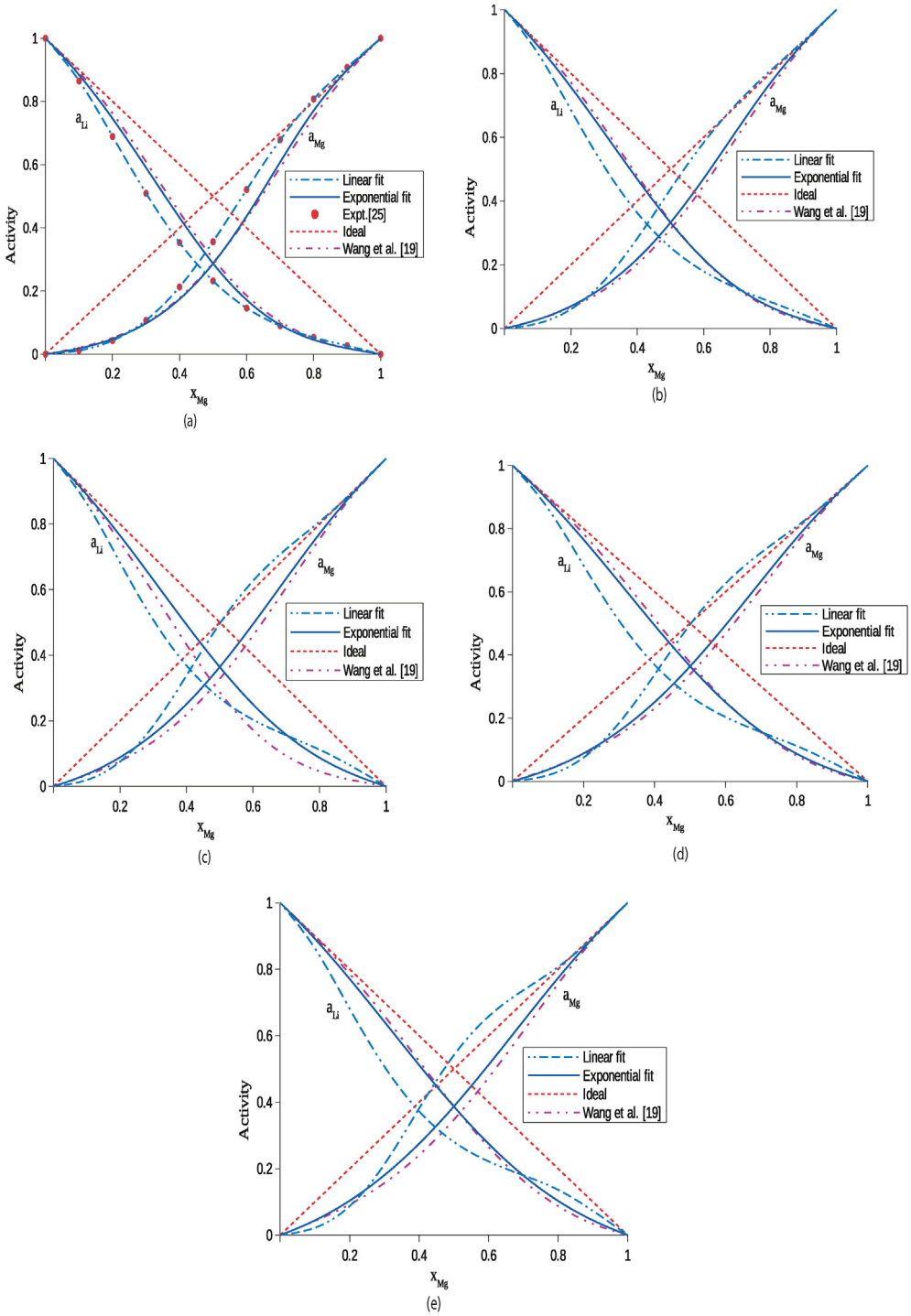

Figure 3. Activities of components Li and Mg of the liquid Li–Mg alloy at temperatures (a) 1000 K, (b) 1300 K, (c) 1600 K, (d) 1900 K and (e) 2200 K.

using exponential parameters slightly deviate from experimental results [25] and its variation is similar to the work of Wang et al. [19]. The computed values of G_M^{xs} using parameters of Cost 507 [20] are much less than the experimental and the present work results (Figure 1(a)). The values of G_M^{xs} obtained using linear parameter of this work decrease rapidly with the rise in temperature of the system in Mg-rich region (Figure 1(c), (d)) showing the presence of inverse miscibility gap at higher temperatures while the values computed using the exponential parameter changes smoothly at all concentrations. The negative values of excess Gibbs free energy of mixing using parameters of Wang et al. [19] increases with the rise in the temperature of the system beyond 1000 K (Figure 1(a)–(e)). This result contradicts with the predictions of other researchers that the liquid alloys must show ideal behavior with respect to mixing tendency at elevated temperatures [9, 10, 11]. When the same physical quantity is computed using the exponential T-dependent interaction parameters, it decreases with the rise in temperatures and does not show any unusual trends or so-called artifacts up to 2200 K.

The enthalpy of mixing (H_M) of the liquid Li–Mg alloy has been computed at 1000 K using Eqs. (7) and (11) with the aid of the exponential T-dependent parameters and listed in Table 3. The theoretical and experimental values as the function of concentration are in considerable agreement (Figure 2(a)). But H_M computed using the parameters of Wang

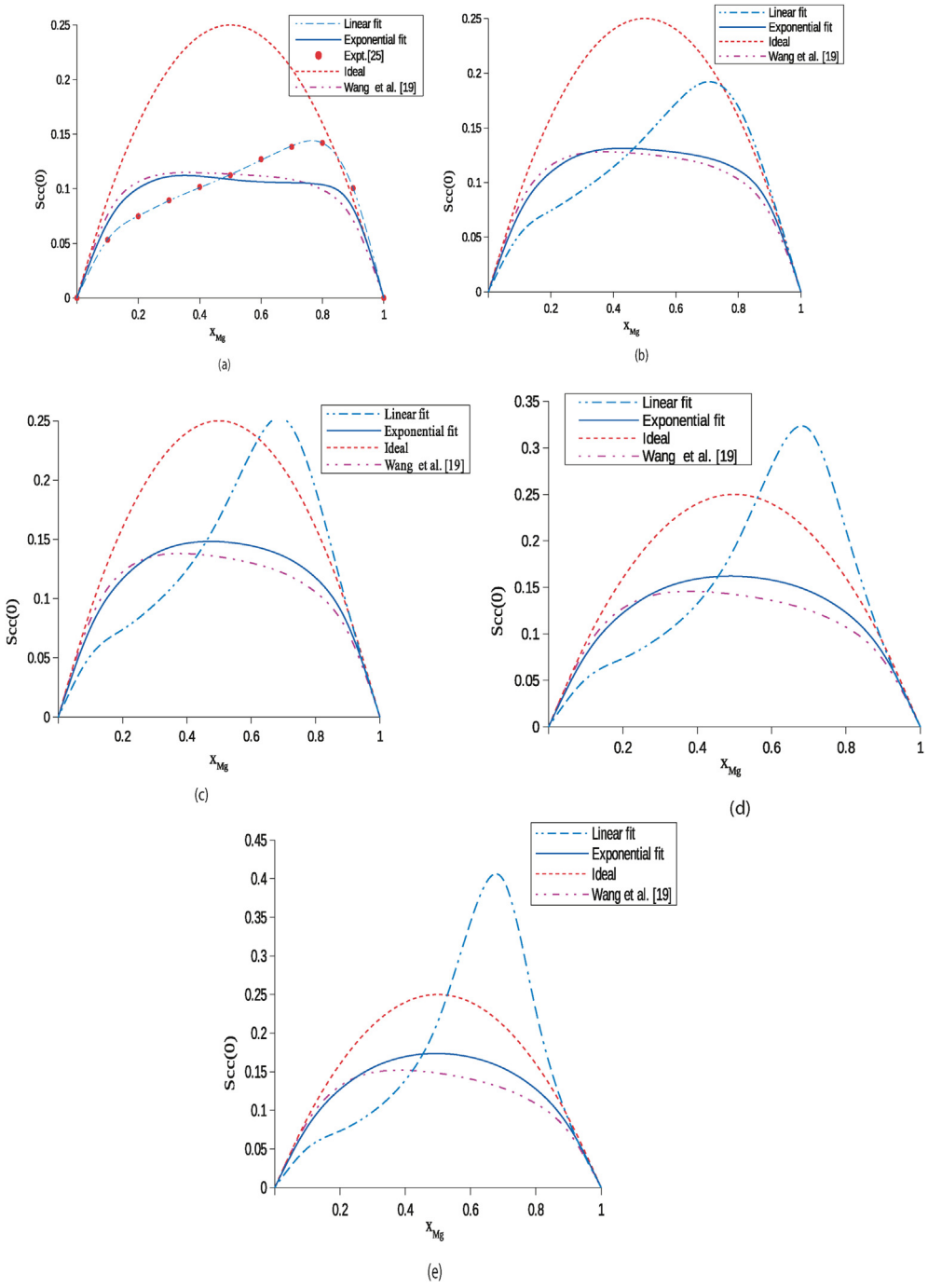

Figure 4. Concentration fluctuations in long-wavelength limit ($S_{CC}(0)$) of the liquid Li–Mg alloy at temperatures (a) 1000 K, (b) 1300 K, (c) 1600 K, (d) 1900 K and (e) 2200 K.

et al. [19], differ significantly with the results of the present work as well as experimental values (Figure 2(a)). Further, the enthalpy of mixing (H_M) of the liquid Li–Mg alloy has also been computed at temperatures 1300 K, 1600 K, 1900 K and 2200 K following a similar procedure as above. The computed negative values of H_M gradually decreases with the increase in the temperature of the system beyond 1000 K (Figure 2(b)). The present theoretical investigations thus predict that the compound forming tendency of the considered system gradually decreases with the rise in its temperatures. These findings further support the results predicted by the excess free energy of mixing in the previous section of the work and are in accordance with other researchers [21, 22, 23, 24] too. These results correspond to the reliability and fruitfulness of exponential T-dependent optimized parameters of this work.

Activities of the components Li and Mg of the system have been computed using optimized parameters in Eq. (12) and listed in Table 4 in the above-mentioned temperature range. The values so computed using the exponential parameters of this work and parameters of Wang et al. are in a good agreement and show negative deviations from ideal values (Raoult's law) at 1000 K (Figure 3 (a)). Moreover, both the experimental values and values calculated using exponential parameters are in well harmonic. When the temperature of the liquid alloy is gradually increased, the activities calculated using exponential parameters gradually move toward ideal value revealing the decrease in the mixing tendency (Figure 3(a)–(e)). These predictions further support the results of excess free energy of mixing and enthalpy of mixing presented in the earlier sections of the work. The activity of Mg calculated using linear T-

Table 5. Concentration fluctuations in long-wavelength limit ($S_{cc}(0)$) of liquid Li–Mg alloy at temperatures 1000 K, 1300 K, 1600 K, 1900 K and 2200 K.

X_{Mg}	Concentration fluctuations in long-wavelength limit ($S_{cc}(0)$)									
	T = 1000 K				T = 1300 K			T = 1600 K		
	Linear fit	Expon. fit	Experimental [25]	Wang et al. [19]	Linear fit	Expon. fit	Wang et al. [19]	Linear fit	Expon. fit	Wang et al. [19]
0.1	0.0535	0.0688	0.0533	0.0762	0.0524	0.0725	0.0798	0.0517	0.0752	0.0822
0.2	0.0751	0.1005	0.0749	0.1064	0.0743	0.1095	0.1157	0.0738	0.1166	0.1224
0.3	0.0891	0.1112	0.0894	0.1142	0.0927	0.1260	0.1267	0.0951	0.1378	0.1360
0.4	0.1010	0.1115	0.1016	0.1147	0.1142	0.1311	0.1279	0.1244	0.1466	0.1379
0.5	0.1130	0.1087	0.1124	0.1135	0.1414	0.1305	0.1259	0.1677	0.1481	0.1352
0.6	0.1262	0.1063	0.1271	0.1118	0.1724	0.1276	0.1223	0.2235	0.1445	0.1300
0.7	0.1393	0.1056	0.1385	0.1085	0.1922	0.1226	0.1161	0.2520	0.1358	0.1215
0.8	0.1420	0.1037	0.1421	0.0991	0.1692	0.1113	0.1029	0.1923	0.1176	0.1055
0.9	0.1005	0.0818	0.1006	0.0712	0.0947	0.0786	0.0716	0.0913	0.0783	0.0718

Concentration fluctuations in long-wavelength limit ($S_{cc}(0)$)					
T = 1900 K			T = 2200 K		
Linear fit	Expon. fit	Wang et al. [19]	Linear fit	Expon. fit	Wang et al. [19]
0.0513	0.0772	0.0839	0.0510	0.0789	0.0852
0.0735	0.1223	0.1275	0.0733	0.1271	0.1315
0.0969	0.1474	0.1432	0.0982	0.1552	0.1489
0.1324	0.1592	0.1456	0.1390	0.1696	0.1518
0.1922	0.1621	0.1424	0.2150	0.1736	0.1481
0.2803	0.1580	0.1359	0.3440	0.1688	0.1405
0.3202	0.1462	0.1255	0.3987	0.1545	0.1285
0.2120	0.1229	0.1073	0.2291	0.1274	0.1087
0.0892	0.0789	0.0720	0.0877	0.0790	0.0721

dependent parameters exceeds the ideal value at higher temperatures beyond 1000 K indicating the presence of unusual trend (Figure 4(b)–(e)). These unusual trends, however, have been removed considering the exponential T-dependent parameters. Hence, it can be stated that at higher temperatures, the thermodynamic functions depend exponentially on temperature rather than linear.

In structural properties, concentration fluctuations in long-wavelength limit ($S_{cc}(0)$) has been established as an important tool to study and explain the hetero or homo-coordinating nature of the liquid alloys. At a given concentration and temperature, if $S_{CC}(0) < S_{CC}^{id}(0)$, then it indicates the hetero-coordinating or ordering nature and if $S_{CC}(0) > S_{CC}^{id}(0)$, then it corresponds to the homo-coordinating or segregating nature of the liquid system. The theoretical, ideal and observed values of $S_{CC}(0)$ at 1000 K have been computed using optimized parameters in Eqs. (14), (15) and (16) and depicted in Table 5. Both the computed values of $S_{CC}(0)$ using the exponential T-dependent parameters are in reasonable agreement and less than the ideal value indicating the ordering nature of the system at 1000 K (Figure 4(a)). But the values computed using linear T-dependent parameters exceeds ideal values in the concentration range $x_{Mg} > 0.9$ indicating the segregating tendency of the alloy (Figure 4(a)) and can be termed as unusual trend. Likewise, Singh et al. [30] had revealed the appearance of the narrow miscibility gap in the liquid phase of Li–Mg alloy in region of 18–30 at % of Li at 830 K. They had further calculated $S_{cc}(0)$ from data of neutron diffraction measurement at 695 K, 830 K and 887 K by using quasi-chemical expression (exponential parameters) in which no miscibility gap was found to appear which supports the findings of this work.

The theoretical values of $S_{CC}(0)$ have been computed at higher temperatures in the range 1300–2200 K employing the similar procedure as discussed above (Figure 4(b)–(e)). At higher temperatures, the values computed using linear parameters exceed ideal value but those computed using exponential parameters are found to be less than ideal values at all concentrations. These findings further correspond that the thermodynamic functions depend exponentially on temperature at higher temperatures. Additionally, the computed values of $S_{CC}(0)$ using the exponential parameters gradually move towards ideal values with an increase in temperature of the alloy supporting the results predicted by thermodynamic functions.

4. Conclusions

The theoretical investigation predicts the appearance of artifacts in the thermodynamic and structural properties of liquid Li–Mg alloy at higher temperatures when the parameters are assumed to be linear T-dependent. When the same thermodynamic and structural properties are calculated using exponential T-dependent parameters, the above discrepancies have been removed. Therefore, it can be concluded that at higher temperatures, the interaction parameters depend exponentially on temperature for liquid alloys. Moreover, the thermodynamic and structural properties of the preferred liquid alloy show ideal mixing tendency at higher temperatures.

Declarations

Author contribution statement

R. K. Gohivar: Conceived and designed the experiments; Performed the experiments; Wrote the paper.

S. K. Yadav, R. P. Koirala: Analyzed and interpreted the data; Wrote the paper.

D. Adhikari: Conceived and designed the experiments; Contributed reagents, materials, analysis tools or data.

Funding statement

R K Gohivar was supported by RMC, MMAMC, TU (2020).

Data availability statement

Data included in article/supp. material/referenced in article.

Declaration of interests statement

The authors declare no conflict of interest.

Additional information

No additional information is available for this paper.

References

[1] N. Derimow, R. Abbaschian, Liquid phase separation in high-entropy alloys-a review, Entropy 20 (2018) 11.
[2] L. Bo, S. Li, L. Wang, D. Wu, M. Zuo, D. Zhao, Liquid-liquid phase separation and solidification behavior of Al55Bi36Cu9 monotectic alloy with different cooling rates, Results Phys. 8 (2018) 1086–1091.
[3] D. Kevorkov, R. Schmid-Fetzer, F. Zhang, Phase equilibria and thermodynamics of the Mg-Si-Li system and remodeling of the Mg-Si system, J. Phase Equilibria Diffus. 25 (2004) 140–151.
[4] G. Kaptay, A new equation for the temperature dependence of the excess Gibbs energy of solution phases, Calphad Comput. Coupling Phase Diagrams Thermochem. 28 (2004) 115.
[5] R. Schmid-Fetzer, A. Janz, J. Gröbner, M. Ohno, Aspects of quality assurance in a thermodynamic Mg alloy database, Adv. Eng. Mater. 7 (2005) 1142–1149.
[6] J. Nakano, D.V. Malakhov, S. Yamaguchi, G.R. Purdy, A full thermodynamic optimization of the Zn-Fe-Al system within the 420-500 °C temperature range, Calphad Comput, Coupling Phase Diagrams Thermochem. 31 (2007) 125–140.
[7] R. Schmid-Fetzer, D. Andersson, P.Y. Chevalier, L. Elenod, O. Fabrichnaya, U.R. Kattner, B. Sundman, C. Wang, A. Watson, L. Zabdyr, M. Zinkevich, Assessment techniques , database design and software facilities for thermodynamics and diffusion, Calphad Comput. Coupling Phase Diagrams Thermochem. 31 (2007) 38.
[8] X. Yuan, W. Sun, Y. Du, D. Zhao, H. Yang, Thermodynamic modeling of the Mg-Si system with the Kaptay equation for the excess Gibbs energy of the liquid phase, CALPHAD Comput. Coupling Phase Diagrams Thermochem. 33 (2009) 673.
[9] Y. Tang, X. Yuan, Y. Du, W. Xiong, Thermodynamic modeling of the Fe – Zn system using exponential temperature dependence for the excess Gibbs energy, J. Min. Met. Sect. B-Metall 47 (2011) 1.
[10] Y. Tang, Y. Du, L. Zhang, X. Yuan, G. Kaptay, Thermodynamic description of the Al-Mg-Si system using a new formulation for the temperature dependence of the excess Gibbs energy, Thermochim. Acta 527 (2012) 131.
[11] S. Liang, P. Wang, R. Schmid-Fetzer, Inherently consistent temperature function for interaction parameters demonstrated for the Mg – Si assessment, CALPHAD Comput, Coupling Phase Diagrams Thermochem 54 (2016) 82.
[12] G. Kaptay, The exponential excess Gibbs energy model revisited, Calphad Comput. Coupling Phase Diagrams Thermochem. 56 (2017) 169.
[13] H. Feufel, T. Godecke, H. Lukas, F. Sommer, Investigation of the Al-Mg-Si system by experiments and thermodynamic calculations, J. Alloys Compd. 247 (1997) 31–42.
[14] X. Yan, F. Zhang, Y.A. Chang, A thermodynamic analysis of the Mg-Si system, Basic Appl. Res. 21 (2000) 379–384.
[15] R. Wu1, Y. Yan, G. Wang, L.E. Murr, W. Han, Z. Zhang, M. Zhang, Recent progress in magnesium-lithium alloys, Int. Mater. Rev. 60 (2015) 65.
[16] W. Gasior, Z. Moser, W. Zakulski, G. Schwitzgebel, Thermodynamic studies and the phase diagram of the Li-Mg system, Metall. Mater. Trans. A 27A (1996) 2419.
[17] M.H. Braga, L.F. Malheiros, M. Hämäläinen, The Cu-Li-Mg system at room temperature, Thermochim. Act 344 (2000) 47.
[18] I.S. Jha, D. Adhikari, J. Kumar, B.P. Singh, Anomaly in mixing properties of lithium-magnesium liquid alloy, Phase Transitions 84 (2011) 1075.
[19] P. Wang, Y. Du, S. Liu, Thermodynamic optimization of the Li-Mg and Al-Li-Mg systems, Calphad Comput, Coupling Phase Diagrams Thermochem. 35 (2011) 523.
[20] I. Ansara, A.T. Dinsdale, M.H. Rand, Thermochemical database for light metal alloys, Cost 507 (1998) 2.
[21] G. Kaptay, The exponential excess Gibbs energy model revisited, Calphad Comput. Coupling Phase Diagrams Thermochem. 56 (2017) 169.
[22] S.K. Yadav, L.N. Jha, I.S. Jha, B.P. Singh, R.P. Koirala, D. Adhikari, Prediction of thermodynamic and surface properties of Pb-Hg liquid alloys at different temperatures, Philos. Mag. 96 (2016) 1909–1925.
[23] S.K. Yadav, L.N. Jha, D. Adhikari, Modeling equations to predict the mixing behaviours of Al-Fe liquid alloy at different temperatures, Bibechana 15 (2018) 60–69.
[24] S.K. Yadav, U. Mehta, R.K. Gohivar, A. Dhungana, R.P. Koirala, D. Adhikari, Reassessments of thermo-physical properties of Si-Ti melt at different temperatures, Bibechana 17 (2020) 146–155.
[25] K.K. Hultgren, R. Desai, P.D. Hawkins, D.T. Gleiser, M. Kelley, Selected Values of Thermodynamic Properties of Binary Alloy, Met. Park. Ohio ASM., 1973.
[26] O. Redlich, A.T. Kister, Algebraic representation of thermodynamic properties and the classification, Ind. Eng. Chem. 40 (1948) 345.
[27] X. Ding, P. Fan, W. Wang, Thermodynamic calculation for alloy systems, Metall. Mater. Trans. B 30 (1999) 7–8.
[28] A.B. Bhatia, D.E. Thornton, Structural aspects of the electrical resistivity of binary alloys, Phys. Rev. B 2 (8) (1970) 3004–3012.
[29] R.N. Singh, D.K. Pandey, S. Sinha, N.R. Mitra, P.L. Srivastava, Thermodynamic properties of molten Li-Mg alloy, Physica 145B (1987) 358.

Physica B 610 (2021) 412941

Contents lists available at ScienceDirect

Physica B: Physics of Condensed Matter

journal homepage: http://www.elsevier.com/locate/physb

Study of excess free energy of mixing and heat of mixing of liquid ternary Al–Li–Zn alloy by assessing the thermodynamic properties of sub-binary alloys

R.K. Gohivar [a,b], S.K. Yadav [b], R.P. Koirala [b], D. Adhikari [b,*]

[a] Central Department of Physics, Tribhuvan University, Kirtipur, Nepal
[b] Department of Physics, Mahendra Morang Adarsh Multiple Campus, Tribhuvan University, Biratnagar, Nepal

ARTICLE INFO

Keywords:
Al–Li–Zn system
Exponential interaction parameter
Inverted miscibility gap
Excess Gibbs free energy of mixing
Enthalpy of mixing

ABSTRACT

The exponential temperature-dependent interaction parameters of the Redlich-Kister (R–K) polynomial for the binary sub-systems of the liquid Al–Li–Zn ternary alloy were optimized using available literature data. The ternary interaction terms of the Redlich-Kister-Maggianu (R–K–M) polynomial were then optimized in order to determine the excess Gibbs free energy of mixing (G_M^{xs}) and the enthalpy of mixing (H_M) of the system. These functions for the liquid ternary alloys were also computed at temperatures of 973 K, 1273 K and 1573 K. The calculated inverted miscibility gap that appeared in G_M^{xs} while using the linear temperature-dependent interaction parameters was suppressed in this work by the assumption of the interaction parameters to be exponential temperature dependent. The enthalpy of mixing of the alloy so calculated was found to be in good agreement with the available experimental data.

1. Introduction

The construction materials in many industrial applications are mostly metal alloys. In particular applications, such as in aerospace engineering works and vehicle parts manufacturing, there is a high demand for suitable lightweight materials. The addition of light elements in alloys makes material light by lowering its density. Mechanical properties like stiffness, elastic strength, heat treatment as well as the electrical properties of the light material should be appropriate for the specific usage. In the process of manufacturing vehicles and other articles and during their operations, these materials have to withstand high temperatures. Therefore, the development of lightweight materials required for various applications is of great interest in the field of materials science and engineering. Experimental as well as theoretical research works are equally important in the development of materials for specific applications. In the vast world of metallurgy, Lithium-containing Aluminum alloys have been mostly investigated due to their large mechanical strength and light weight. Al–Li based alloys are very important for structural materials. The liquid ternary Al–Li–Zn alloy is one of such Al–Li-based alloy that has been previously taken in several experimental and theoretical studies [1–9].

Kim and Sommer performed experimental work to measure the enthalpy of mixing (H_M) for the Al–Li–Zn system in the temperature range 729–955 K using the high-temperature calorimeter method [1]. Furthermore, they calculated the parameters on the basis of the association solution model using the previous experimental data and found that the calculated enthalpy of mixing deviated from the observed values without considering the ternary interaction term. Guo et al. critically assessed many solution phases, stable compounds and intermetallic compounds of sub-binary and ternary Al–Li–Zn systems to describe the thermodynamic of the ternary system using the CALPHAD technique [2]. The temperature dependent ternary interaction parameters of Redlich-Kister-Muggianu polynomial for liquid phases of the system were optimized using experimental data of enthalpy of mixing from Ref. [1]. Trybula et al. [3] also optimized the temperature-dependent ternary interaction parameters of the liquid Al–Li–Zn systems by using experimental data of partial excess Gibbs free energy of Li from electromotive force measurement and thermodynamic interaction parameters of sub-binary Al–Li, Li–Zn and Al–Zn systems, respectively from Refs. [4–6]. They computed the excess Gibbs free energy mixing, excess entropy of mixing and enthalpy of mixing of the ternary liquid system using ternary interaction parameters and thermodynamic parameters of sub-binary systems at three cross-sections of x_{Al}: x_{Zn} at 3, 1 and 0.136 and compared them with the results obtained

* Corresponding author.
E-mail addresses: adksbdev@yahoo.com, devendra.adhikari@mmamc.tu.edu.np (D. Adhikari).

https://doi.org/10.1016/j.physb.2021.412941
Received 28 November 2020; Received in revised form 8 February 2021; Accepted 26 February 2021
Available online 2 March 2021
0921-4526/

using ternary interaction parameters from Ref. [2]. The experimental measurements of enthalpy of mixing of Al–Li and Al–Li–Zn systems were carried out by Debski and Terlicka [7] using the Setaram MHTC 96 Line Evo calorimeter, where the discrepancy in value of H_M was reported due to errors in the measurement or optimization procedure adopted. The integral enthalpy of mixing of $(Al_{0.5}-Zn_{0.5})_{(1-x)}-Li_x$ at 851 K was reported to be in good agreement with the values in Refs. [2,3,8] but differed from the value in Ref. [1]. Gasior et al. [9] carried out two experimental works using calorimetric and emf methods to study the integral enthalpy of mixing and partial excess Gibbs free energy of the liquid Al–Li–Zn alloy. The temperature-dependent ternary interaction parameters were calculated using the experimental data of enthalpy of mixing and partial Gibbs energy and also taking into account the literature values of the two functions [9]. Further, they reported that there appeared a remarkable deviation between the experimental values obtained from the two techniques.

For the assessment of the thermodynamic properties of the binary as well as ternary systems, most often linear temperature-dependent interaction parameters are used. When the computed values of these functions are extrapolated at higher temperatures, unusual behaviors often appears which are termed as inverted miscibility gaps [10–12]. In order to solve the problem, exponential temperature-dependent parameters proposed by Kaptay [13] were used by several researchers [14–19]. The exponential model was further modified by combining the linear and exponential temperature-dependent interaction parameters for the re-stabilization of the solidus phases of more complex systems [20,21].

In the present work, we intend to describe the thermodynamic properties of liquid Al–Li–Zn alloys at higher temperatures, such as 973 K, 1273 K and 1573 K using exponential temperature-dependent interaction parameters. The necessary theoretical formulation is presented in Section 2 and the results and discussion are outlined in Section 3 and the conclusion in Section 4.

2. Theoretical basis

Among the thermodynamic functions, the excess Gibbs free energy of mixing of alloys (G_M^{xs}) is the most basic function and it can be calculated using different models. For a binary A-B alloy, G_M^{xs} can be calculated from the Redlich-Kister (R–K) polynomial using the following expression [22].

$$G_M^{xs} = x_A x_B \sum_{i=0}^{n} L_i (x_A - x_B)^i \tag{1}$$

where x_A and x_B are the respective mole fractions of the components A and B and L_i represents the temperature-dependent interaction parameters for the given alloy. The parameters may depend either linearly or exponentially on temperature. The linear temperature-dependent interaction parameters are expressed as

$$L_i = a_i + b_i T \tag{2}$$

where a_i and b_i are constants which contribute respectively to the enthalpy of mixing (H_M) and excess entropy of mixing (S_M^{xs}) of the system. Following Kaptay, the exponential temperature-dependent interaction parameters can be given as [13].

$$L_i = h_i exp\left(\frac{-T}{\tau_i}\right) \tag{3}$$

where h_i and τ_i contribute respectively to the enthalpy of mixing and excess entropy of mixing of the system.

The excess free energy of mixing of the ternary A–B–C systems can be calculated on the basis of the Redlich–Kister–Muggianu (R-K-M) model. According this model, G_M^{xs} is computed using the following analytical expression [23].

$$G_M^{xs} = x_A x_B \sum_{i=0}^{n} L_i^{AB}(x_A - x_B)^i + x_B x_C \sum_{i=0}^{n} L_i^{BC}(x_B - x_C)^i + x_C x_A \sum_{i=0}^{n} L_i^{CA}(x_C - x_A)^i + x_A x_B x_C\left(x_A L_0^{ABC} + x_B L_1^{ABC} + x_C L_2^{ABC}\right) \tag{4}$$

where L_i^{AB}, L_i^{BC} and L_i^{CA} are the interaction parameters for the liquid binary A–B, B–C and C–A systems respectively and L_0^{ABC}, L_1^{ABC} and L_2^{ABC} are the ternary interaction parameters for the liquid alloy.

The asymmetric model formulated by Toop [24] to calculate the thermodynamic function of the liquid ternary alloy is expressed as

$$G_M^{xs} = \frac{x_B}{1-x_A} G_{AB}^{xs}(x_A; 1-x_A) + (x_B + x_C)^2 G_{BC}^{xs}\left(\frac{x_B}{x_B + x_C}; \frac{x_C}{x_B + x_C}\right) + \frac{x_C}{1-x_A} G_{AC}^{xs}(x_A; 1-x_A) \tag{5}$$

The asymmetrical behavior of the excess Gibbs free energy or enthalpy of mixing of sub-binary systems determines the first position of the component in the A–B–C ternary alloy in the Toop model. The enthalpy of mixing of the binary and ternary liquid alloys can be determined theoretically from the following most general expression

$$H_M = G_M^{xs} - T\frac{\partial G_M^{xs}}{\partial T} \tag{6}$$

The temperature-dependent interaction parameters for H_M can be obtained using Eq. (3) in Eq. (1) then in Eq. (6) as follows

$$L_i = \left(1 + \frac{T}{\tau_i}\right) h_i exp\left(\frac{-T}{\tau_i}\right) \tag{7}$$

Using Eq. (7) in Eq. (1) one can obtain the analytic expression for the enthalpy of mixing of the binary A-B liquid system in the following form [16].

$$H_M = x_A x_B \sum \left(1 + \frac{T}{\tau_i}\right) h_i exp\left(\frac{-T}{\tau_i}\right)(x_A - x_B)^i \tag{8}$$

The H_M of the liquid ternary system is calculated using the enthalpy of mixing of the sub-binary systems from Eq. (8) and the necessary ternary interaction parameters from Eq. (7) in Eqs. (4) and (5) for the respective models.

3. Results and discussion

In order to explain the thermodynamic functions of the liquid ternary Al–Li–Zn alloy at preferred higher temperatures, the exponential interaction parameters for the three liquid sub-binary Al–Li, Li–Zn and Zn–Al systems as well as the liquid ternary system were optimized. The exponential parameters of the Al–Li liquid alloy were taken from Ref. [25]. For the liquid Li–Zn and Zn–Al alloys, the respective linear temperature-dependent interaction parameters from Refs. [5,6] were used in Eqs. (2) and (3) to optimize the exponential parameters for the respective systems. The exponential ternary interaction parameters for the liquid Al–Li–Zn system were optimized using the linear temperature-dependent interaction parameters of Ref. [3]. The optimized temperature-dependent parameters for the sub-binary systems and the ternary Al–Li–Zn liquid alloys are presented in Table 1.

The excess Gibbs free energies of mixing of the sub-binary systems of the Al–Li–Zn system were computed using Eq. (1) and the interaction parameters from Table 1 at temperatures 973 K and 1573 K and are plotted in Fig. 1(a–c). A consistency was observed between the values of G_M^{xs} for the binary systems computed using the exponential and linear parameters of Table 1 at a temperature of 973 K (Fig. 1(a–c)). The inverted miscibility gap was depicted in the calculated values of G_M^{xs} in the concentration range 0.6–1.0 of Li for liquid Li–Zn alloy at 1573 K while using the linear temperature-dependent interaction parameters of Ref. [5]. The linear-temperature dependent interaction parameters are expressed as $L_i = a_i + b_i T$, where i = 0–4 and a_i (in unit $Jmol^{-1}$) are the

Table 1
Interaction parameters of sub-binary and ternary systems.

System	Linear interaction parameters		Exponential interaction parameters	
Al–Li	$L_0 = -44200 + 20.6T$	Ref. [4]	$L_0 = -61954.01 \exp(-9.85 \times 10^{-4}T)$	Ref. [25]
	$L_1 = 13{,}600\text{-}5.3T$		$L_1 = 22608.02 \exp(-7.97 \times 10^{-4}T)$	
	$L_2 = 14{,}200$		$L_2 = 44253.179 \exp(-1.57 \times 10^{-3}T)$	
	$L_3 = -12100$		$L_3 = -20589.38 \exp(-3.13 \times 10^{-4}T)$	
	$L_4 = -7100$			
Li–Zn	$L_0 = -45258.6 + 26.3677\ T$	Ref. [5]	$L_0 = -56461.95 \exp(-10.645 \times 10^{-3}T)$	This work
	$L_1 = 22887.2\text{–}4.1921\ T$		$L_1 = 23168.75 \exp(-21.35 \times 10^{-5}T)$	
	$L_2 = -4552.6 + 4.0715T$		$L_2 = -13536.88 \exp(-29.62 \times 10^{-4}T)$	
Al–Zn	$L_0 = 10466.6\text{–}3.39259\ T$	Ref. [6]	$L_0 = 11564.55 \exp(-5.545 \times 10^{-4}T)$	This work
Al–Li–Zn	$L_0 = 7700\text{-}52\ T$	Ref. [3]	$L_0 = -11624.75 \exp(13.78 \times 10^{-4}T)$	This work
	$L_1 = -112{,}500\text{-}4T$		$L_1 = -112554.56 \exp(3.44 \times 10^{-5}T)$	
	$L_2 = 29{,}000\text{-}14T$		$L_2 = 35296.44 \exp(-8.56 \times 10^{-4}T)$	

contribution due to the enthalpy of mixing term and b_i (in unit $Jmol^{-1}K^{-1}$) are contribution due to the excess entropy of mixing term. One of the condition for the appearance of the inverted miscibility gaps in the calculated results of the excess Gibbs free energy of mixing is b_0-$b_2 > 2R$ [26], where R is the real gas constant in unit $Jmol^{-1}K^{-1}$. The optimized values of b_0 and b_2 mentioned in Ref. [5] are 26.3677 J $mol^{-1}K^{-1}$ and 4.0715 J $mol^{-1}K^{-1}$ respectively and hence b_0-b_2 = 22.2962>2R which satisfies the condition for the appearance of the inverted miscibility gap in the present work. This inverted miscibility gap was suppressed significantly by using the exponential fitting parameters of this work (Fig. 1(b)).

In order to employ Toop model, an asymmetric element is to be chosen for the computation of the thermodynamic functions. For the purpose, the excess Gibbs free energy of mixing for the sub-binary systems were plotted. It can be observed that the values of G_M^{xs} were found to be negative for both Al–Li and Li– Zn alloys and positive for Zn–Al alloy (Fig. 1(a–c)). Therefore, the component (Li) was chosen at the first position in the Al–Li–Zn system. The G_M^{xs} of the ternary system was computed using Eq. (4) and the linear parameters of Table 1 in ratio x_{Al}: x_{Zn} equal to 3:1, 1:1, 0.136:1 at temperatures of 973 K, 1273 K and 1573 K and the values so obtained are plotted in Fig. 2(a–c).

The G_M^{xs} for the ternary Al–Li–Zn system was also computed using the R–K–M polynomial and the linear parameters of Table 1 in Eq. (4). It was observed that with the increase in the temperature, the values of G_M^{xs} were found to be more positive toward the Li-rich region (Fig. 2(a–c)). A small positive value was noticed in the Li-rich region in the ratio x_{Al}: x_{Zn} equal to 1:1 and 0.136:1 at 1273 K. This unusual behavior was identified as an inverted miscibility gap (Fig. 2(a and b)). The miscibility gap also appeared at temperature 1573 K (Fig. 2(a–c)) which gradually becomes prominent in the ratio 0.136:1 of x_{Al}: x_{Zn} in the concentration range 0.6–1.0 of Li-component. This gap was found to increase with the increase in the concentration of Al and resembles with that of the sub-binary systems.

The value of G_M^{xs} was further computed using the optimized exponential parameters of this work (Table 1) at 973 K, 1273 K and 1573 K. The computed value of G_M^{xs} at 1573 K was found to have small positive value at $x_{Li} = 0.9$ in the ratio 0.136:1 of x_{Al}: x_{Zn}. The inverted miscibility gap in G_M^{xs} that appeared while using the linear interaction parameters was suppressed noticeably by using the exponential interaction parameters (Fig. 2(a–c)).

The enthalpy of mixing (H_M) of the liquid ternary alloy was

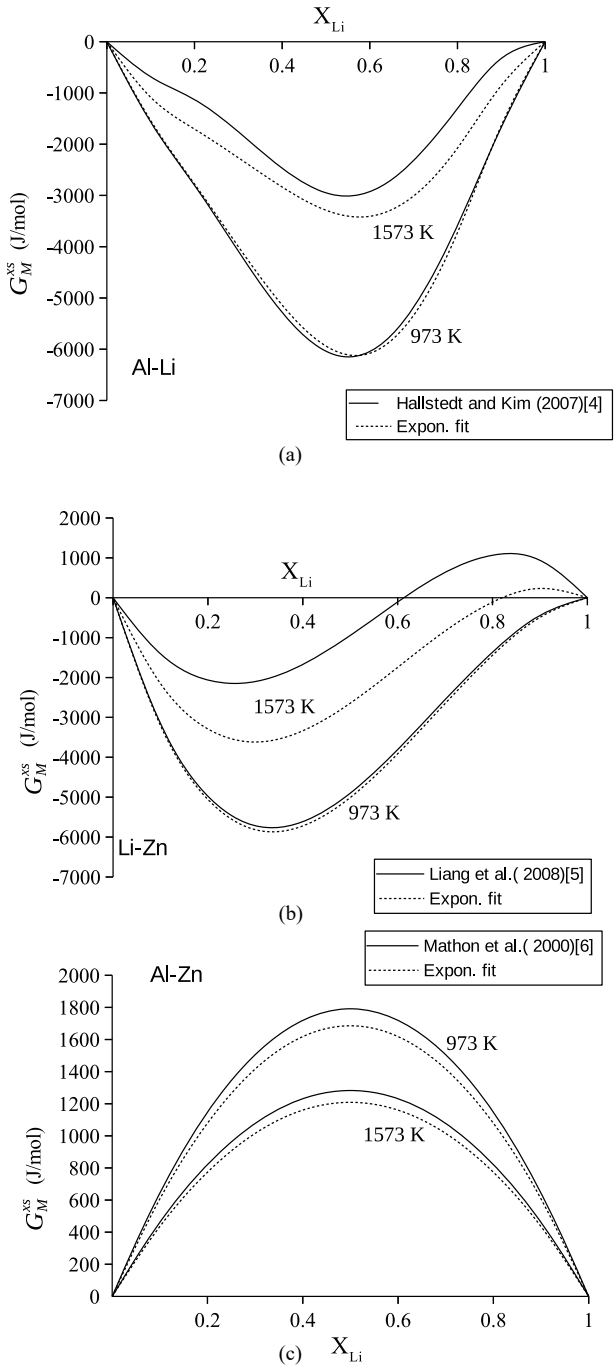

Fig. 1. The compositional dependence of excess Gibbs free energy of mixing (G_M^{xs}) for the liquid sub-binary systems of the liquid Al–Li–Zn alloy at different temperatures. (a) Al–Li system, (b) Li–Zn system and (c) Al–Zn system.

computed using Eqs. (4) and (5) respectively in the frame work of R–K–M polynomial and Toop model with the aid of the exponential temperature-dependent parameters in Table 1. The value was obtained in the ratio x_{Al}: x_{Li} = 3:1 at 995 K, x_{Al}: x_{Zn} = 1:1 at 951 K, and x_{Al}: x_{Zn} = 7:3 at 883 K. The result for H_M at 951 K was found to be in well agreement with the available experimental data [1] and the theoretical data [8] (Fig. 3(a)). Moreover, the results of this work and experimental data from Ref. [1] at 951 K and data from Ref. [3] at 973 K were also compared in the plot of Fig. 3(b). It was found that the results obtained using R–K–M polynomial and Toop model were in close agreement and they differ by a maximum value of 1.4 kJ/mol from the data of Trybula et al. [3]. The results of the present work were in fair agreement with

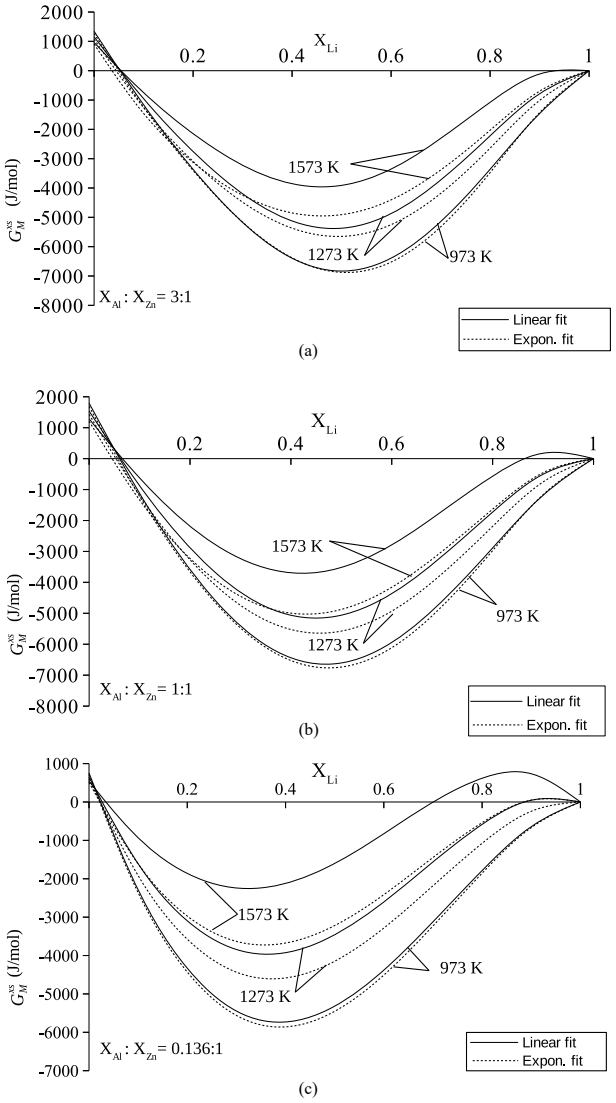

Fig. 2. The compositional dependence of the excess Gibbs free energy of mixing (G_M^{xs}) for the liquid ternary Al–Li–Zn system at different cross-sections and temperatures. (a) x_{Al}:x_{Zn} = 3:1, (b) x_{Al}:x_{Zn} = 1:1 and (c) x_{Al}:x_{Zn} = 0.136:1.

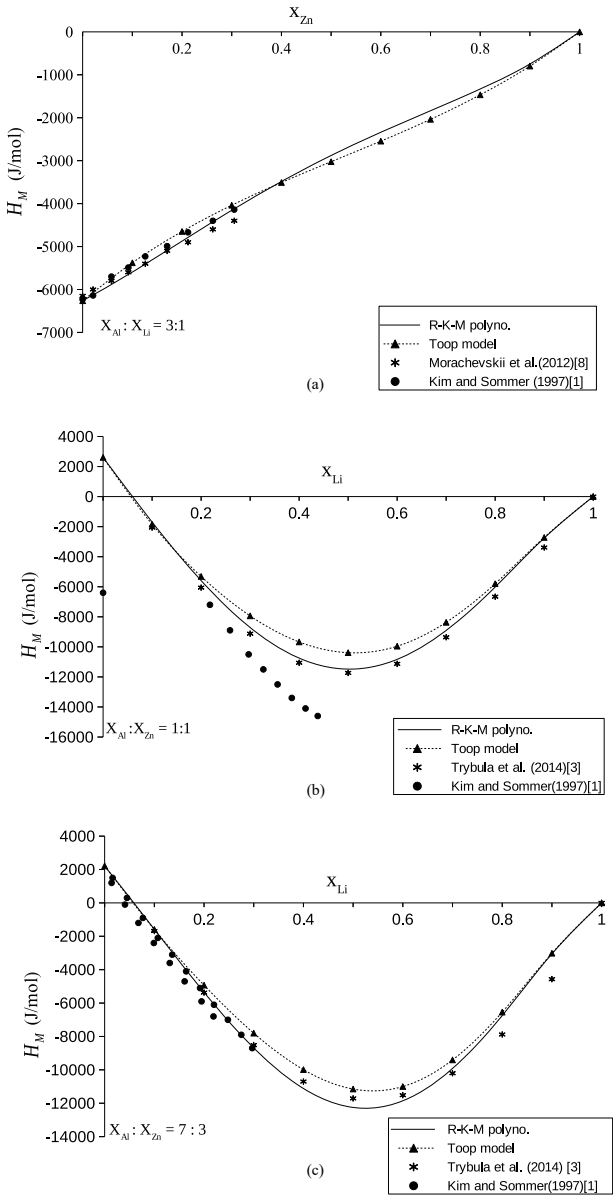

Fig. 3. The compositional dependence of the enthalpy of mixing (H_M) of the liquid Al–Li–Zn ternary system at different temperatures and cross-sections. (a) x_{Al}:x_{Li} = 3:1, (b) x_{Al}:x_{Zn} = 1:1 and (c) x_{Al}:x_{Zn} = 7:3.

data of Kim and Sommer [1]. Finally, the results for H_M at temperature 883 K and x_{Al}: x_{Zn} = 7:3 were compared with Kim and Sommer [1] and the experimental data of Trybula et al. [3] at 973 K and x_{Al}: x_{Zn} = 3:1 in Fig. 3(c). The calculated results were found to be in well agreement with both experimental data of Refs. [1,3].

4. Conclusion

The inverted miscibility gap was observed in the computed values of G_M^{xs} in the sub-binary Li– Zn system as well as in the liquid Al–Li–Zn ternary system at 1573 K in Li- rich region while using the linear-temperature dependent interaction parameters. It was further revealed that the calculated miscibility gap of the ternary system gradually increased with decrease in concentration of Al. But these inverted gaps of the binary and the ternary were suppressed using the optimized exponential parameters. Further, the enthalpy of mixing (H_M) of the ternary system calculated at different temperatures using the exponential parameters were found to be in good agreement with the experimental results. The theoretical investigations of the present work predicted that the interaction parameters depend exponentially on temperature rather than linear at preferred higher temperature range.

Credit authors statement

R.K. Gohivar: Investigation, Formal analysis, Writing – original draft Writing; S.K. Yadav: Validation, Review and Editing; R.P. Koirala: Methodology, Review and Editing; D. Adhikari: Conceptualization, Supervision, Funding acquisition.

Declaration of competing interest

The authors declare that they have no known competing financial interests or personal relationships that could have appeared to influence the work reported in this paper.

References

[1] Y.B. Kim, F. Sommer, Calorimetric measurement of liquid Aluminium-Lithium-Zinc alloys, Thermochim. Acta 291 (1997) 27–34.
[2] C. Guo, Y. Liang, C. Li, Z. Du, Thermodynamic description of the Al–Li–Zn system, Calphad 35 (2011) 54–65.

[3] M. Trybula, P. Fima, W. Gasior, Thermodynamic properties of liquid Al–Li–Zn alloys determined from electromotive force measurement, Thermochim. Acta 588 (2014) 16–21.
[4] B. Hallstedt, O. Kim, Thermodynamic assessment of the Al–Li system, Int. J. Math. Res. 98 (2007) 961–969.
[5] Y. Liang, Z. Du, C. Guo, C. Li, Thermodynamic modeling of the Li–Zn system, J. Alloy. Comp. 455 (2008) 236–242.
[6] M. Mathon, K. Jardet, E. Aragon, P. Satre, A. Sebaoun, Al-Ga-Zn system, Reassessments of the three binary systems and discussion on possible estimations and on optimisation of the ternary system, Calphad 24 (2000) 253–284.
[7] A. Debski, S. Terlicka, Calorimetric measurements of liquid (Al+ Li+ Zn) alloys, J. Chem. Thermodyn. 92 (2016) 91–96.
[8] A.G. Morachevskii, T.V. Butukhanova, E.N. Val'Kovskaya, Thermodynamic analysis of liquid alloys of the system aluminum-lithium-zinc, Russ. J. Appl. Chem. 85 (2012) 1955–1958.
[9] W. Gasior, A. Debski, S. Terlicka, Calorimetric and electromotive force measurements of Al-Li-Zn liquid solutions, J. Phase Equilibria Diffus. 37 (2016) 481–490.
[10] R. Schmid-Fetzer, A. Janz, J. Gröbner, M. Ohno, Aspects of quality assurance in a thermodynamic Mg alloy database, Adv. Eng. Mater. 7 (2005) 1142–1149.
[11] T. Balakumar, M. Medraj, Thermodynamic modeling of the Mg–Al–Sb system, Calphad 29 (2005) 24–36.
[12] Y. Tang, Y. Du, L. Zhang, X. Yuan, G. Kaptay, Thermodynamic description of the Al–Mg–Si system using a new formulation for the temperature dependence of the excess Gibbs energy, Thermochim. Acta 527 (2012) 131–142.
[13] G. Kaptay, A new equation for the temperature dependence of the excess Gibbs energy of solution phases, Calphad 28 (2004) 115–124.
[14] R. Arroyave, Z. Liu, Thermodynamic modelling of the Zn–Zr system, Calphad 30 (2006) 1–13.
[15] R. Schmid-Fetzer, D. Andersson, P.Y. Chevalier, L. Eleno, O. Fabrichnaya, U. R. Kattner, B. Sundmann, C. Wang, A. Watson, L. Zabdyr, M. Zinkevich, Assessment techniques, database design and software facilities for thermodynamics and diffusion, Calphad 31 (2007) 38–52.
[16] X. Yuan, W. Sun, Y. Du, D. Zhao, H. Yang, Thermodynamic modeling of the Mg–Si system with the kaptay equation for the excess Gibbs energy of the liquid phase, Calphad 33 (2009) 673–678.
[17] Y. Tang, X. Yuan, Y. Du, W. Xiong, Thermodynamic modeling of the Fe-Zn system using exponential temperature dependence for the excess Gibbs energy, J. Min. and Metall B 47 (2011) 1–10.
[18] S. Wang, Y. Du, Y. Peng, P. Zhou, X. Yuan, S. Liu, A thermodynamic assessment of the Li-Ge system, J. Phase Equilibria Diffus. 39 (3) (2018) 315–323.
[19] R.K. Gohivar, S.K. Yadav, R.P. Koirala, D. Adhikari, Artifacts in Al–Mn liquid alloy, Phys. B Condens. Matter 595 (2020) 412348.
[20] S.M. Liang, P. Wang, R. Schmid-Fetzer, Inherently consistent temperature function for interaction parameters demonstrated for the Mg–Si assessment, Calphad 54 (2016) 82–96.
[21] G. Kaptay, The exponential excess Gibbs energy model revisited, Calphad 56 (2017) 169–184.
[22] O. Redlich, A.T. Kister, Algebraic representation of thermodynamic properties and the classification of solutions, Ind. Eng. Chem. 40 (1948) 345–348.
[23] N. Chakraborti, H.L. Lukas, Thermodynamic optimization of the Mg-Al-Si phase diagram, Calphad 16 (1992) 79–86.
[24] D. Manasijevic, D. Zivkovic, Z. Zivkovic, Prediction of the thermodynamic properties for the Ga–Sb–Pb ternary system, Calphad 27 (2003) 361–366.
[25] R.K. Gohivar, S.K. Yadav, R.P. Koirala, G.K. Shrestha, D. Adhikari, Temperature dependence of interaction parameters for Al–Li liquid alloy, Philos. Mag. A 101 (2020) 179–192.
[26] T. Fu, Y. Du, Z. Zheng, Y. Peng, B. Jin, Y. Liu, C. Du, S. Liu, C. Shi, J. Wang, An effective algorithm to identify the miscibility gap in a binary substitutional solution phase, J. Min. and Metall B 56 (2020) 183–191.

BIBECHANA
ISSN 2091-0762 (Print), 2382-5340 (Online)
Journal homepage: http://nepjol.info/index.php/BIBECHANA
Publisher: Department of Physics, Mahendra Morang A.M. Campus, TU, Biratnagar, Nepal

Exponential Temperature-Dependent Parameters for Thermodynamic and Structural Properties of Al-Ti MeltR.K.

Gohivar [a, b*], S.K. Yadav[b], R.P. Koirala[b], D. Adhikari[b]

[a] Central Department of Physics, Tribhuvan University, Kirtipur, Kathmandu, Nepal
[b] Department of Physics, M.M.A.M. Campus, T.U., Biratnagar, Nepal
*Email: ramesh.gohibar@mmamc.tu.edu.np

Article Information:
Received: April 08, 2021
Accepted: October 30, 2021

Keywords:
Thermo-structural properties
Al-Ti melt
Exponential T-dependent parameters
Artifacts
R-K polynomials

ABSTRACT

Thermodynamic and structural properties of Al-Ti melt have been estimated in the framework of Redlich-Kister (R-K) polynomial using linear temperature-dependent (T-dependent) interaction parameters above melting temperatures. These calculations show the existence of the artificial inverted miscibility gaps (artifacts) at temperatures 2000 K, 2500 K, and 2700 K. Therefore, interaction parameters are assumed to vary exponentially with temperature and have been optimised for excess free energy of mixing. The artifacts do not appear in the calculation of these properties of the concerned alloy when these optimized parameters are used.

DOI: https://doi.org/10.3126/bibechana.v19i1-2.46392

1. Introduction

The fabrication of materials for their various applications at high temperatures is one of the major tasks for the researcher in the field of material and metallurgical science. Such high-temperature materials are used as exhaust valves and turbine blades in aerospace and automotive vehicles. Titanium-based alloys are most often preferred as high-temperature materials. Moreover, the AlTi-based alloys have lightweight as well as high strength. Therefore, complete knowledge of Al-Ti alloys is mandatory and hence several researchers so far have studied the phase diagram of this system [1–9].

The experimental value of enthalpy of Al was used to calculate the enthalpy of Ti using Gibbs-Duhem

relation which were used to compute the enthalpy of mixing of liquid Al-Ti alloy at 2000 K [1]. Kattner et al. [2]. analyzed the phases of stoichiometric compounds, the disordered solution phases and the ordered intermetallic compounds, and optimised the thermodynamic functions of the Al-Ti system. Maeda et al. [3] studied the activity of the system at 2073 K and found that the observed values showed negative deviation from the Raoult's law throughout the entire concentration of Al. Zhang et al. [4] analyzed the Al-Ti system by taking nine phases and calculated excess Gibbs free energy of mixing of disordered solution phases using a generalized bond energy model. Witusiewicz et al. [7] modeled Gibbs free energy of mixing of all phases of the system using computer-based software PARROT optimizer of Thermo-Calc and optimised the thermodynamic parameters of the Al-Ti system. Sudavtsova and Podoprigora [8] used an isoperibolic calorimeter to determine the enthalpy of mixing of the liquid alloy at temperatures 1770 ± 5K and 1790 ± 5 K and concluded that these values are temperature-dependent. Egry et al. [9] measured the thermo-physical properties of the Al-Ti-based ternary system and compared them with the corresponding values calculated from the optimised parameters of the system of Ref. [7]. Novakovic et al. [10] used quasi-chemical approximation to study the surface, dynamic and structural properties of the liquid Al-Ti alloy at 1973 K and predicted that Al segregates on the surface phase of the solution throughout the entire concentration range. Their result showed that the theoretical value of concentration fluctuations in the long-wavelength limit was found to be greater than the corresponding ideal values at very low concentration of Ti $(x_{Ti} \leq 0.15)$ indicating the segregating tendency of the system in the constrained concentration range [11-13].

In this work, R-K polynomial has been used to study the thermodynamic and structural properties of liquid alloy by using the linear temperature interaction parameters. On extrapolating these values at higher temperatures, the artificial inverted miscibility gaps appeared [14-18]. With this regard, the exponential interaction parameters have been optimised and the thermodynamic and structural properties of the system have been recomputed at elevated temperatures, such as 1500 K, 2000 K, 2500 K and 2700 K in order to remove the inverted miscibility gaps.

The necessary mathematical formulation is presented in the Section 2, the results and discussion are presented in the Section 3 and the conclusions are outlined in the Section 4.

2. FORMULATION

The thermodynamic properties like excess free energy of mixing (G_M^{xs}), enthalpy of mixing (H_M), and the activity of components of binary liquid alloy can be determined by using coefficients of R-K polynomial. These coefficients are called the interaction parameters of the system and are considered to be temperature-dependent. The linear temperature-dependent form of the interaction parameters can be given as

$$L_i = a_i + b_i T \tag{1}$$

where a_i and b_i are parameters associated with the enthalpy of mixing and excess entropy of mixing respectively. Likewise, the exponential temperature-dependent terms of the interaction parameters are expressed as [19]

$$L_i = h_i \exp(\frac{-T}{\tau_i}) \tag{2}$$

where h_i and τ_i are constant parameters which are to be optimised for the preferred alloy. In the framework of R-K polynomial, the excess free energy of mixing (G_M^{xs}) of the liquid alloy is expressed [20]

$$G_M^{xs} = x_{Al} x_{Ti} \sum_{i=0}^{3} L_i (x_{Al} - x_{Ti})^i \tag{3}$$

where x_{Al} and x_{Ti} are concentrations of the components Al and Ti of the liquid Al-Ti alloy. Using Equations (2) in Equation (3), one can obtain

$$G_M^{xs} = x_{Al}\, x_{Ti} \sum_{i=0}^{3} h_i \exp\left(-\frac{T}{\tau_i}\right) (x_{Al} - x_{Ti})^i \tag{4}$$

The general expression relating the excess free energy of mixing, enthalpy of mixing (H_M) and excess entropy of mixing (S_M^{xs}) is

$$H_M = G_M^{xs} + TS_M^{xs} \quad (5)$$

The excess entropy of mixing can be calculated in terms of (S_M^{xs}) given as

$$S_M^{xs} = \frac{-\partial G_M^{xs}}{\partial T} \quad (6)$$

Using linear parameters and exponential parameters from Equations (1) and (2) in Equations (3), (6) and finally in Equation (5) then respective expressions for enthalpy of mixing (H_M) are

$$H_M = x_{Al}x_{Ti}\sum_{i=0}^{3} a_i(x_{Al} - x_{Ti})^i \quad (7a)$$

and

$$H_M = x_{Al}x_{Ti}\sum_{i=0}^{3}(1 + \frac{T}{\tau_i})\, h_i \exp(\frac{-T}{\tau_i})(x_{Al} - x_{Ti})^i \quad (7b)$$

The partial excess free energy of the components Al and Ti of liquid Al-Ti alloy can be computed using the following relation

$$G_{Al}^{xs} = x_{Ti}^2 \sum_{i=0}^{3} L_i[(1+2i)x_{Al} - x_{Ti}](x_{Al} - x_{Ti})^{i-1}$$

and

$$G_{Ti}^{xs} = x_{AL}^2 \sum_{i=0}^{3} L_i[x_{Al} - x_{Ti}(1+2i)](x_{Al} - x_{Ti})^{i-1} \quad (8)$$

The activities of the components Al and Ti are calculated using the values from Equations (8) then

$$a_{Al} = x_{Al}\exp(\frac{G_{Al}^{xs}}{RT}) \text{ and}$$
$$a_{Ti} = x_{Ti}\exp\left(\frac{G_{Ti}^{xs}}{RT}\right) \quad (9)$$

The structural property of the liquid alloy system can be analyzed by computing concentration fluctuations in the long-wavelength $S_{cc}(0)$ limit . Following Bhatia and Singh, the expression for $S_{cc}(0)$terms of excess free energy of mixing can be given as [21]

$$S_{cc}(0) = RT(\frac{\partial^2 G_M}{\partial x_k^2})^{-1} \quad (10)$$

where k = Al or Ti and

$$G_M = G_M^{xs} + RT(x_{Al}\ln x_{Al} + x_{Ti}\ln x_{Ti})$$

Using above relation and Equation (3) in Equation (10), then $S_{cc}(0)$ is expressed as

$$S_{cc}(0) = RT[-2L_0 + (-12x_{Al} + 6)L_1 + (-48x_{Al}^2 + 48x_{Al} - 10)L_2 + (-160x_{Al}^3 + 240x_{Al}^2 - 108x_{Al} + 14)L_3 + \frac{RT}{x_{Al}(1-x_{Al})}]^{-1} \quad (11)$$

The ideal value of $S_{cc}(0)$ is calculated using the relation $S_{cc}^{id}(0) = x_{Al}(1 - x_{Al})$

3. Results and Discussion

In present work, we aim to study the thermodynamic and structural properties of the Al-Ti liquid alloy at elevated temperatures. When these properties were calculated using linear temperature-dependent interaction parameters of the R-K polynomial, there appeared unusual trends. Therefore, the interaction parameters of the system were re-optimised assuming the interaction parameters to be exponential temperature-dependent. For the purpose, the linear parameters were taken from the work of Witusiewicz et al. [7] and the exponential parameters were optimised using Equations (1) and (2), and are presented in the Table 1. The excess free energy of mixing (G_M^{xs}) was computed at temperatures 1500 K, 2000 K, 2500 K and 2700 K using Equation (3) with the aid of the exponential parameters and the linear parameters of Zhang et al. [4], Witusiewicz et al. [7] and Cost 507 [5] (Table1). The compositional dependence of the values so obtained are plotted in Figs. 1(a-d).

Table 1. Interaction parameters for the excess free energy of mixing of Al-Ti liquid alloy

Reference	Thermodynamic interaction parameters [J/mol]
Cost 507 [5]	L_0 = -108250+38T L_1 = -6000+5T, L_3 =15000
This work	L_0 = -134188.7 exp (-5.677x10^{-4} T), L_1 = -4343504.6 exp (-7.01x10^{-3} T), L_3=41482.8 exp (-6.85x10^{-4} T)
Zhang et al. [4]	L_0=-111811.4+34.199T, L_1=9746.9+7.69T
Witusiewicz et al. [7]	L_0 = -118048+41.972T, L_1 =-23613+19.704T, L_2 =34757-13.844T

At temperature 1500 K, all the computed values of G_M^{xs} were found to be in good agreement with each other at lower concentration of Ti whereas the values obtained using the parameters of Zhang et al. differed from the rest at higher concentration of Ti. With the increase in temperatures, the results obtained using the linear parameters showed pronounced wavy natures at lower concentrations of Ti (Figs. 1(b-d)). These types of variations in (G_M^{xs}) is not in accordance with the general trends. It is an indication of the appearance of an artificial inverted miscibility gap. But this artificial inverted miscibility gap has been removed using the exponential parameters.

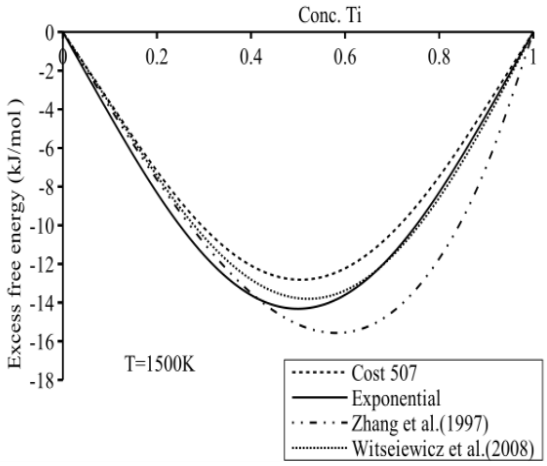

1(a)

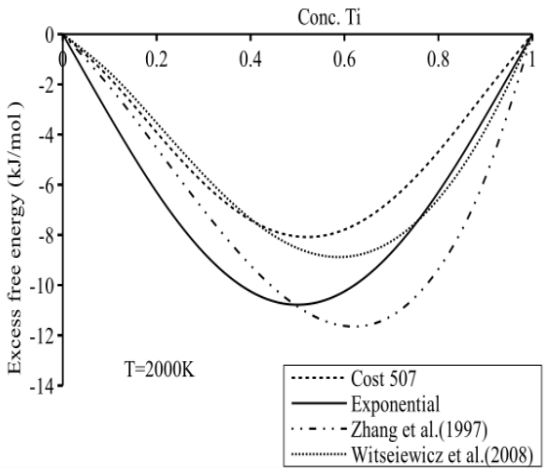

1(b)

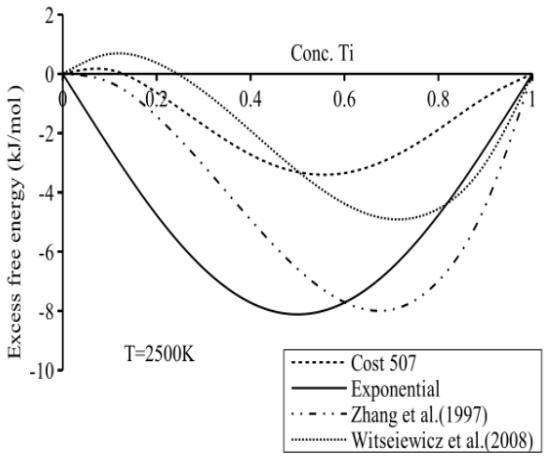

1(c)

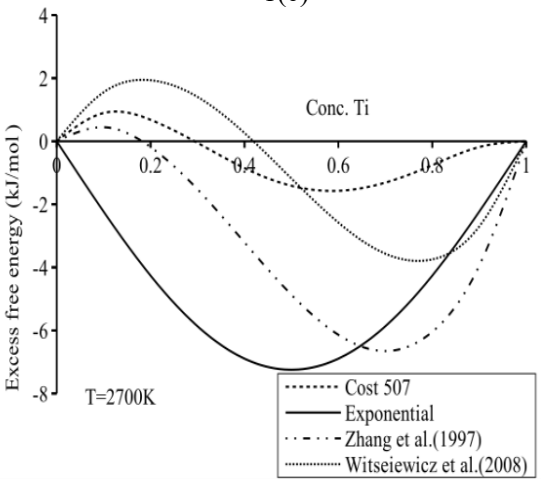

1(d)

Figs. 1(a-d): The compositional dependence of the excess free energy of mixing of the liquid Al-Ti alloy at different temperatures.

The enthalpy of mixing(H_M)of the liquid alloy were computed using Equation (7a) and the temperature independent terms of the linear parameters of Table 1.

The temperature-dependent (H_M) was computed using Equation (7b) and the exponential parameters of Table 1. The compositional dependence of H_M so computed values is compared in Fig. (2).

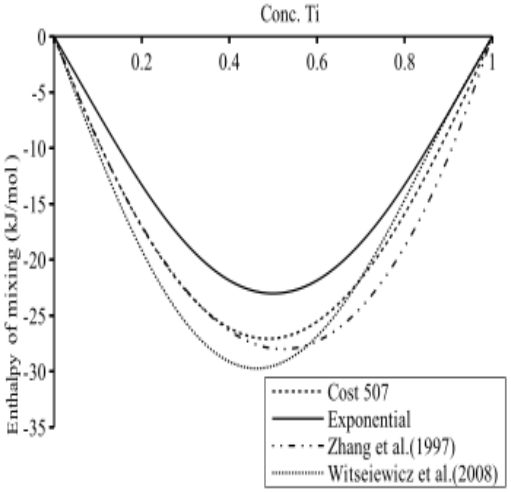

Fig. 2: Enthalpy of mixing of the liquid Al-Ti alloy versus concentration of Ti at 2000 K.

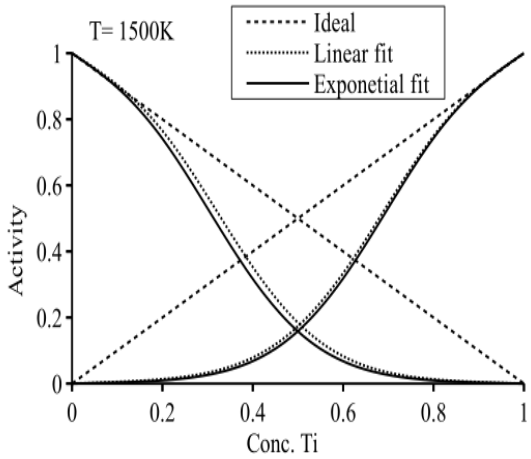

3(a)

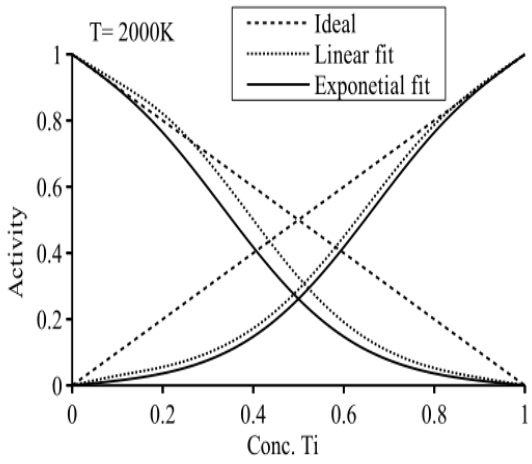

3(b)

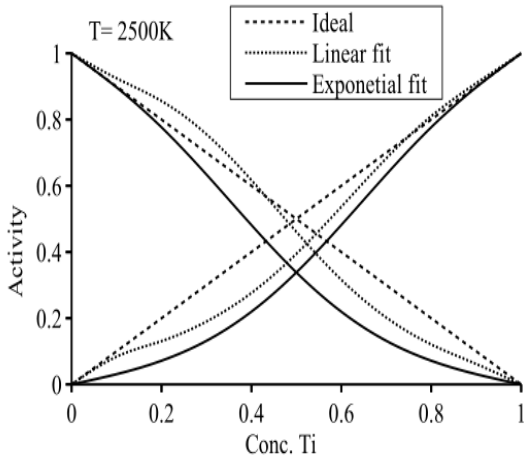

3(c)

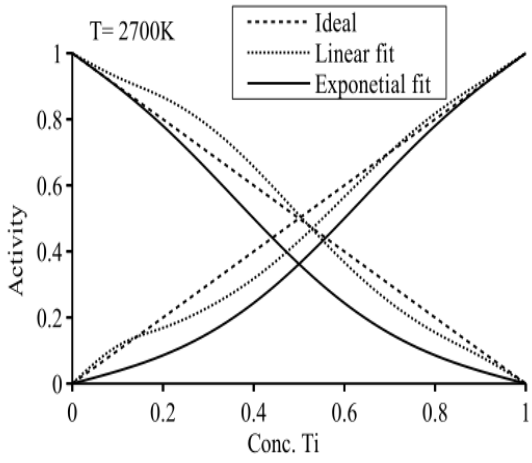

3(d)

Figs. 3(a-d): Activity of the components of the liquid Al-Ti alloy versus concentration of Ti at different temperatures.

The compositional dependence of the computed values of the activities of components Al and Ti are plotted in Figs. 3(a-d). They found to be in well agreement at temperature 1500K (Fig. 3(a)). With the increase in temperature of the system, it is observed that the activity of Al computed using linear parameters shows negative deviation from Raoult's law at lower concentrations of Ti. Generally, the activity shifts towards ideal values with an increase in temperatures. In this work, this general trend is observed when exponential parameters are used.

The study of structural properties like concentration fluctuation in long-wavelength limit (S_{cc} (0)) gives information about the arrangement of the atoms in the initial melt. Moreover, the positive or negative deviations of *Scc*(0) with respect to its ideal value ($S_{cc}^{id}(0)$) gives information about the nature of local arrangements of atoms, such as for $S_{cc}(0) > S_{cc}^{id}(0)$segregating or homo-coordination behaviour is expected and for $S_{cc}(0) < S_{cc}^{id}(0)$ compound forming or hetero-coordination tendency is expected.

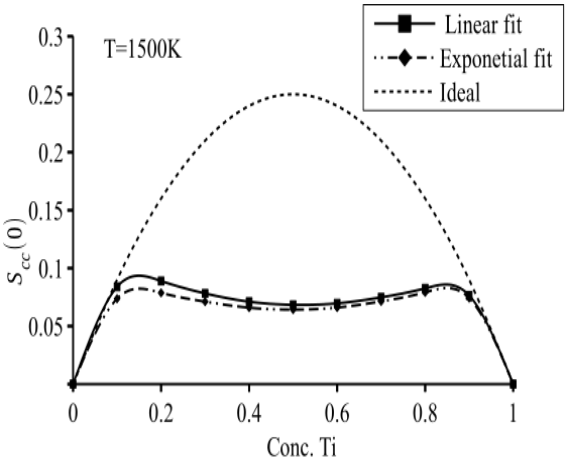

4(a)

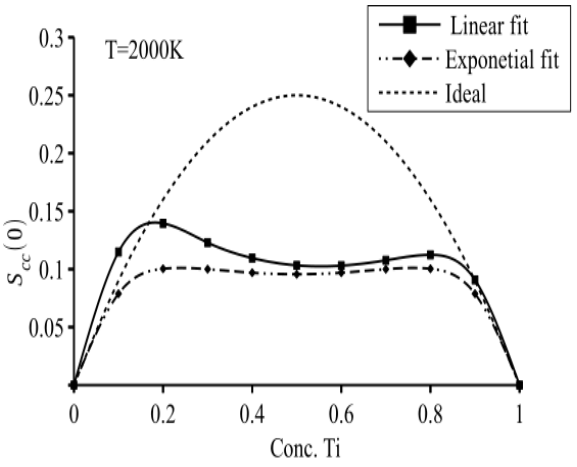

4(b)

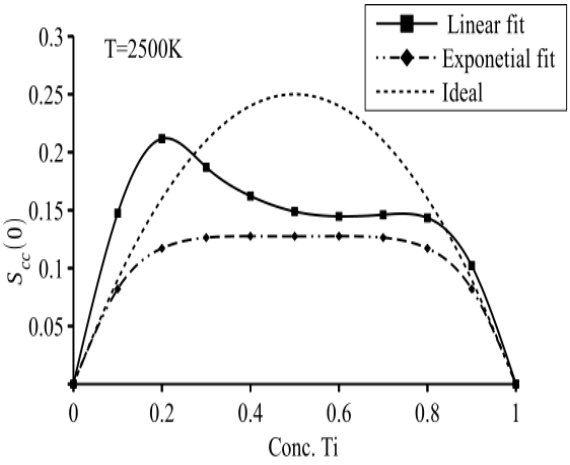

4(c)

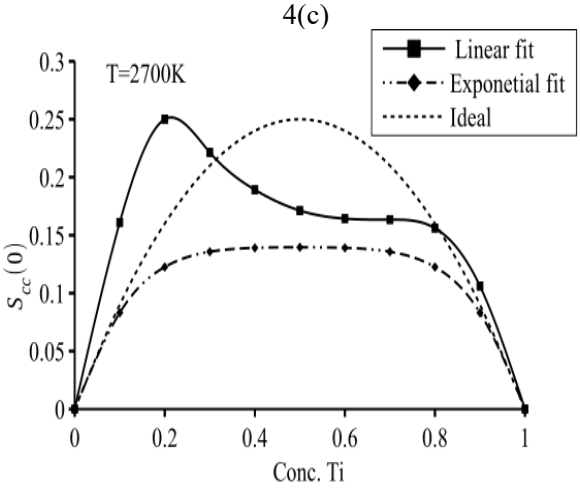

4(d)

Figs. 4(a-d): The compositional dependence of the concentration fluctuations in long-wavelength limit

(S_{cc} (0)) of liquid Al-Ti alloy at different temperatures.

The values of $S_{cc}(0)$ have been computed using Equation (11) with the aid of the linear parameter and exponential parameters from Table 1 and are plotted in Figs. 4(a-d). It is observed that the computed values of $S_{cc}(0)$ at temperature 1500 K are in good agreement. Generally, it is observed that the computed value of $S_{cc}(0)$ gradually shifts toward the ideal value with the increase in the temperature of the liquid alloys [22]. But in the present work, it is observed that the computed values of $S_{cc}(0)$ using the linear parameters shifts beyond respective ideal values at the low concentrations of Ti (Figs. 1(b-d)) with the increase in the temperature of the system. The variation of $S_{cc}(0)$ beyond the ideal value can be termed as the appearance of the artificial miscibility gap. However, the presence of such trend has been removed by using the exponential temperature-dependence parameters at high temperatures. Therefore, it can be concluded that the exponential temperature-dependent parameters of the interaction energy parameters well explain the thermodynamic and structural properties of the liquid Al-Ti system at preferred higher temperatures.

4. Conclusion

The linear as well as exponential temperature-dependent interaction parameters were used in the frame work of R-K polynomial to compute the thermodynamic and structural properties of liquid Al-Ti alloy at constrained higher temperature range, 1500-2700 K. The artificial inverted miscibility gaps (artifacts) appeared in the computed thermodynamic properties (G_M^{xs}) and activity and structural property (S_{cc} (0)) at higher temperatures, such as 2000 K, 2500 K, and 2700 K when the interaction parameters were assumed to be linear temperature-dependent. But these gaps were found to be removed when the interaction parameters were assumed to be exponential temperature-dependent. The present study predicts that the thermo-structural properties of the system are well explained by the exponential parameters at considered higher temperature range.

Acknowledgment

We are grateful to the Central Department of Physics, Tribhuvan University, Kathmandu, Nepal for the research facilities.

References

[1]P. D. Desai, Thermodynamic Properties of Selected Binary Aluminum Alloy Systems, J. Phys. Chem.Ref.Data.16(1987)109-124. https://doi.org/10.1063/1.555788.

[2]U. R. Kattner, J. Lin, Y. A. Chang, Thermodynamic Assessment and Calculation of the Ti-AI System, Metall Trans. A. 23 (1992) 2081-2090. https://doi.org/10.1007/BF02646001.

[3]M. Maeda, T. Kiwake, K. Shibuya, T. Ikeda, Activity of aluminum in molten Ti-Al alloys, Mat Sci and Eng.A.240(1997)276-280. https://doi.org/10.1016/S0921- 5093(97)00593-5.

[4]F. Zhang, S. L. Chen, Y. A. Chang, U. R. Kattner, A thermodynamic description of the Ti-Al system, Intermetallics.5(1997)471-482. https://doi.org/10.1016/S0966-9795(97)00030-7

[5]I. Ansara, A. T. Dinsdale, M. H. Rand, Thermochemical Database for Light Metal Alloys. 2 (1998).

[6]Y. Fujita, H. Mitsui, K. Ishikawa, R. Kainuma, K. Ishida, Phase equilibria in the Ti-Al binary system, Acta.Mater.48(2000). https://doi.org/10.1016/S1359-6454(00)00118-X

[7]V. T. Witusiewicz, A. A. Bondar, U. Hecht, S. Rex, T. Y. Velikanova, The Al-B-Nb-Ti system III. Thermodynamic re-evaluation of the constituent binary system Al - Ti, J. of Alloys and Compd. 465 (2008)64-77. https://doi.org/10.1016/j.jallcom.2007.10.061

[8]V. S. Sudavtsova and N. V. Podoprigora, Thermodynamic properties of melts in Al-TI (Zr, Hf) binary systems, Powder Metall. Met. Ceram. 48 (2009) 83-87. https://doi.org/10.1007/s11106-009-9091-1

[9]I. Egry, D. Holland-Moritz, R. Novakovic, E. Ricci, R. Wunderlich, N. Sobczak, Thermo -physical properties of liquid AlTi-based alloys, Int. J. Thermophys.31(2010)949-965. https://doi.org/10.1007 /s10765-010-0704-1

[10]R. Novakovic, D. Giuranno, E. Ricci, A. Tuissi, R. Wunderlich, H.-J. Fecht, I. Egry, Surface, dynamic and structural properties of liquid Al-Ti

alloys, Appl. Surf. Sci. 258 (2012) 3269- 3275. https://doi.org /10.1016/j.apsusc.2011.11.080
[11]S. K. Yadav, L.N. Jha, D. Adhikari, segregating to ordering transformation in In - Sn melt, Phy. Chem.Liq.53(2015)37-41.
https://doi.org/10.1080/00319104.2014.999337
[12]S. K. Yadav, L. N. Jha, D. Adhikari, Thermodynamic and structural properties of Bi-based liquid alloys, Phys. B: Phys. Condens. Matter.475(2015)40-47.
https://doi.org/10.101/j.physb.2015.06.015
[13]S. K. Yadav, L. N. Jha, D. Adhikari, Thermodynamic and structural behaviour of Tl-Na liquid alloy, Bibechana.12(2014)20-29.
http://dx.doi.org/10.3126/bibechana.v12i0.11784
[14]R. Schmid-Fetzer, D. Andersson, P.Y. Chevalier, L. Eleno, O. Fabrichnaya, U.R. Kattner, B. Sundman, C. Wang, A. Watson, L. Zabdyr, and M. Zinkevich, Assessment techniques, data base design and software facilities for thermodynamics and diffusion, Calphad Comput. Coupling Phase Diagrams Thermochem. 31 (2007) 38-52.
https://doi.org/10.1016/j.calphad.2006.02.007
[15]X. Yuan, W. Sun, Y. Du, D. Zhao, H. Yang, Thermodynamic modeling of the Mg-Si system with the Kaptay equation for the excess Gibbs energy of the liquid phase, CALPHAD Comput. Coupling Phase Diagrams Thermochem. 33(2009)673-678.
https://doi.org/10.1016/j.calphad.2009.08.004
[16]Y. Tang, Y. Du, L. Zhang, X. Yuan, G. Kaptay, Thermodynamic description of the Al-Mg-Si system using a new formulation for the temperature dependence of the excess Gibbs energy, Thermochim.Acta.527(2012)131-142.
https://doi.org/10.1016/j.tca.2011.10.017
[17]S. Liang, P. Wang, R. Schmid-Fetzer, Inherently consistent temperature function for interaction parameters demonstrated for the Mg-Si assessment, CALPHAD Comput. Coupling Phase Diagrams Thermochem.54(2016)82-96.
https://doi.org/10.1016/.calphad.2016.06.003
[18]R. K. Gohivar, S. K. Yadav, R. P. Koirala, G. K. Shrestha, D. Adhikari, the Temperature dependence of interaction parameters for Al-Li liquid alloy, Philos. Mag. 121 (2021) 179-192.
https://doi.org /10.1080/14786435.2020.1825858.
[19]G. Kaptay, A new equation for the temperature dependence of the excess Gibbs energy of solution phases, Calphad Comput. Coupling Phase Diagrams Thermochem. 28 (2004)115-124.
https://doi.org/ 10.1016/j.calphad.2004.08.005.
[20]O. Redlich, A. T. Kister, Algebraic representation of thermodynamic properties and the classification, Ind.Eng.Chem.40(1948)345-348.
https://doi.org/10.1021/ie50458a036.
[21]A. B. Bhatia, R. N. Singh, A Quasi-lattice Theory for Compound Forming Molten Alloys, Phys. Chem. Liq.13(1984)177-190.
https://doi.org/10.1080/00319108408080778.
[22]G. Kaptay, On the tendency of solutions to tend toward ideal solutions at high temperatures, Metall. Mater. Trans. A Phys. Metall. Mater. Sci. 43 (2012) 531-543.https://doi.org/10.1007/s11661-011-0902-x.

ICC 2019

3rd International Conference on Condensed Matter & Applied Physics

Organized By: Department of Physics, Govt. Engineering College, Bikaner

Paper ID : A-0084

Certificate

This is to certify that

Mr. Ramesh Kumar Gohivar

of

Tribhuvan University

has participated in 3rd International Conference on Condensed Matter & Applied Physics (ICC 2019) organized by Govt. Engineering College, Bikaner during Oct. 14-15, 2019 and presented a paper entitled

Removal of Thermodynamic Miscibility Gap in Al-Fe-Si Liquid Alloy at High Temperature

15 October 2019
Bikaner

(Dr. M. S. Shekhawat)
Convener

St. Xavier's College

Maitighar, Kathmandu, Nepal

Department of Physics

This e-certificate of appreciation is awarded to **Mr. Ramesh Kumar Gohivar**, of

Central Department of Physics, Kritipur, Nepal

for poster presentation On the title "***Exponential temperature dependent Parameters for thermodynamics and structural properties of AL-TI metal***"

in the

"International Conference on Material Science and Characterization Technology (ICMSCT)"

held on **September 26-28, 2021**

Mr. Drabindra Pandit Head, Department of Physics	Fr. Dr. Augustine Thomas, S.J. Principal St. Xavier's College	Prof. Dr. Bhim Prasad Subedi Chairperson, University Grants Commission Nepal

Nepal Physical Society

Ghantaghar, Kathmandu

Certificate of Participation

This certificate is awarded to

Mr. Ramesh Kumar Gohivar from

MMAMC, TU, Biratnagar for his successful participation in

NPS School of Computing - 2020

Conducted from July 4, 2020 to January 31, 2021.

Prof. Dr. Narayan Prasad Chapagain	Dr. Sunil Babu Shrestha	Dr. Dibakar Sigdel
President	Chief Guest	Instructor
Nepal Physical Society	Vice – Chancellor, NAST	Data Scientist, UCLA, USA

February 6, 2021

This is to Certify that

MR. RAMESH KUMAR GOHIVAR

has Successfully Completed

Workshop on Research Writing and Publishing

July 8 – 9, 2020

Organized by

Nepal Physical Society

Province - 1

Prof. Dr. Binil Aryal	**Prof. Dr. Devendra Adhikari**	**Prof. Dr. Narayan P. Chapagain**
Chief Guest / Head CDP	*President / Facilitator*	*Special Guest / President, NPS*
T.U., Nepal	Nepal Physical Society	
	Province - 1	